Haris S. Chrysikopoulos

Clinical MR Imaging and Physics

A Tutorial

Springer

Haris S. Chrysikopoulos

Clinical MR Imaging and Physics

Haris S. Chrysikopoulos

Clinical MR Imaging and Physics

A Tutorial

Springer

Haris S. Chrysikopoulos, MD
EuroDiagnosis Imaging Center
8th Parodos Ioannou Theotoki
49100 Corfu
Greece
E mail: xx.kerkyra@hotmail.com

ISBN 978-3-540-77999-5 e-ISBN 978-3-540-78023-6
DOI 10.1007/978-3-540-78023-6

Library of Congress Control Number: 2008939383

Cover design: Frido Steinen-Broo, eStudio Calamar, Spain
Reproduction, typesetting and production: le-tex publishing services oHG, Leipzig, Germany

Printed on acid-free paper

9 8 7 6 5 4 3 2 1

springer.com

Prologue

Το λακωνίζειν εστί φιλοσοφείν[1]

To laconizein esti philosophein

This text was written for all health care professionals who would like a concise introduction to magnetic resonance imaging (MRI). The author's intention is to provide a tutorial-like presentation with emphasis on the underlying physics. Practical considerations, which are useful for routine clinical work, are distilled in the last chapter.

The phenomena of MR are varied, complex, and interrelated. The number of MR techniques, methods, and clinical applications is ever increasing. Thus, any presentation of sufficient detail runs the risk of "overwhelming" the reader. To overcome this danger, I sought a minimalistic approach, both in content and in form. Where applicable, concepts have been simplified and several topics have been omitted or underrepresented (such as artifacts, contrast agents, etc.). Most of the cases presented have been proven by surgery/histopathology or are based on compelling clinical, laboratory, and radiologic data. A few cases, without solid proof, have been labeled with the most likely (presumptive) diagnosis. Most of the illustrations were obtained using a 1.0 T system.

Interested readers should consult standard sources for integrated and detailed exposure to the physics, techniques, and applications of MR and a treatise on the various diseases (Amirsys various; Atlas 2001; Berquist 2005; Fischbein et al. 2000; Haacke 1999; Hashemi et al. 2004; McRobbie et al. 2003; Mitchell and Cohen 2004; Ros et al. 2006; Runge 2005; Sprawls 1987; Weishaupt et al. 2006; Westbrook 2002; Yock 2002).

I am grateful to J. Andreou, MD, PhD (Clinical Associate Professor of Radiology) for his continuous guidance and support. I am obliged to N. Gourtsoyiannis, MD, PhD (Professor of Radiology) for his enthusiasm with regard to this book and for his help in making it materialize.

I would like to thank several colleagues for their comments and advice about the physics part of the text: M. Crowley, PhD (Instructor in Radiology), D. Goussis, PhD (Associate Professor of Engineering), M. Gunn, MD (Associate Professor of Radiology), J. Nikolakopoulos, MSc, N. Papanikolaou, PhD (Research Associate in Radiology), S.S. Sagel, MD (Professor of Radiology), K.C. Spigos, MD, and L.B. Talner, MD (Professor of Radiology). N. Gatsoulis, MD, PhD and G. Iliadis, MD helped me considerably with the preparation of several of the illustrations.

I would like to acknowledge my colleague A. Vlachos, MD and all the staff at "Eurodiagnosis" for their support during this project.

During the editing of the book I had the pleasure of working closely with Mrs. W. McHugh of Springer publishing, Ms. A. Strohbach of le-tex publishing services and Ms. P. Francis. I would like to thank them for their time, patience and valuable comments.

Kerkyra, June 2008

[1] "Behaving like Lakon (ancient Spartan) is an exercise in philosophy." The Spartans were disciplined by a simple and austere way of life. The above adage usually refers to their succinct manner of speaking.

Contents

Introduction

Keywords

- Spin
- Electromagnetic radiation
- Resonance
- Nucleus
- Hydrogen
- Proton

Certain atomic nuclei possess inherent magnetic properties called spin, and can interact with electromagnetic (EM) radiation[1] through a process called resonance. When such nuclei absorb EM energy they proceed to an excited, unstable configuration. Upon return to equilibrium, the excess energy is released, producing the MR signal. These processes are not random, but obey predefined rules.

The simplest nucleus is that of hydrogen (H), consisting of only one particle, a proton. Because of its abundance in humans and its strong MR signal, H is the most useful nucleus for clinical MRI. Thus, for our purposes, MRI refers to MRI of hydrogen, and for practical purposes the terms proton, spin, nucleus, and hydrogen can be used interchangeably.

Let us summarize the MRI procedure. The patient is placed in a magnetic field and becomes temporarily magnetized. Resonance is achieved through the application of specific pulses of EM radiation, which is absorbed by the patient. Subsequently, the excess energy is liberated and measured. The captured signal is processed by a computer and converted to a gray scale (MR) image.

Why do we need to place the patient in a magnet? Because the earth's magnetic field is too weak to be clinically useful; it varies from 0.3–0.7 Gauss (G). Current clinical MR systems operate at low, mid or high field strength ranging from 0.1 to 3.0 Tesla (T), where 1 T = 10,000 G.

The atoms are composed of nuclei and electrons, and the nuclei consist of a variable number of protons and neutrons. Only nuclei with unpaired proton(s) are magnetically active, such as the isotopes H1, carbon 13, sodium 23, and phosphorus 31.

[1] The term EM radiation is equivalent to EM wave(s) and EM field(s).

Resonance 1

Keywords

- Resonance
- Energy
- Matter
- Oscillation
- Frequency

Resonance is the coordinated coupling of energy (stimulus) to matter (system), resulting in the smooth, rhythmic motion of matter according to its inherent oscillation dynamics.

The stimulus is the driving force that initiates and sustains the motion of the system. It can consist of various forms of energy, such as mechanical, sound or electromagnetic, that exist in a wave-like form.

The system must be capable of recurrent, to-and-fro motion around a resting point. The number of repetitions per unit of time of this type of motion (oscillation) is called frequency, expressed in cycles per second or Hertz. Each system has an intrinsic oscillation or resonance frequency, determined by its physical and chemical make-up.

It follows that the ease of oscillation of the system depends on the frequency of application of the stimulus.

In the case of magnetic resonance (MR), the stimulus is electromagnetic radiation and the system is a group of protons that oscillate between two discrete energy levels. Resonance is accomplished only if the frequency of the radiation matches the natural oscillation frequency of the protons. In such cases, there is efficient transfer of energy, i.e., rapid and without losses (as heat).

2 Electromagnetic Fields

Keywords

- Magnetic field
- Dipole
- Vector
- Vector amplitude and phase

Magnetism and electricity are interrelated phenomena: a moving electrical charge creates a magnetic field. The reverse is also true: a magnetic field that varies in time induces the flow of electric current.

The protons carry a positive electric charge and spin around their axis; thus, the protons generate a local magnetic field and behave as magnetic dipoles (Fig. 1). The magnetic dipoles are vector quantities defined by two parameters: the strength or amplitude of their magnetic field and their orientation or phase, i.e., the direction of their (north–south pole) axis.

The graphic representation of such a vector, called a magnetic dipole moment (μ), is displayed in Fig. 2.

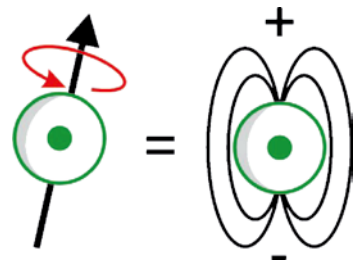

Fig. 1 The protons as microscopic magnets. The positive electric charge of the spinning proton generates a magnetic field

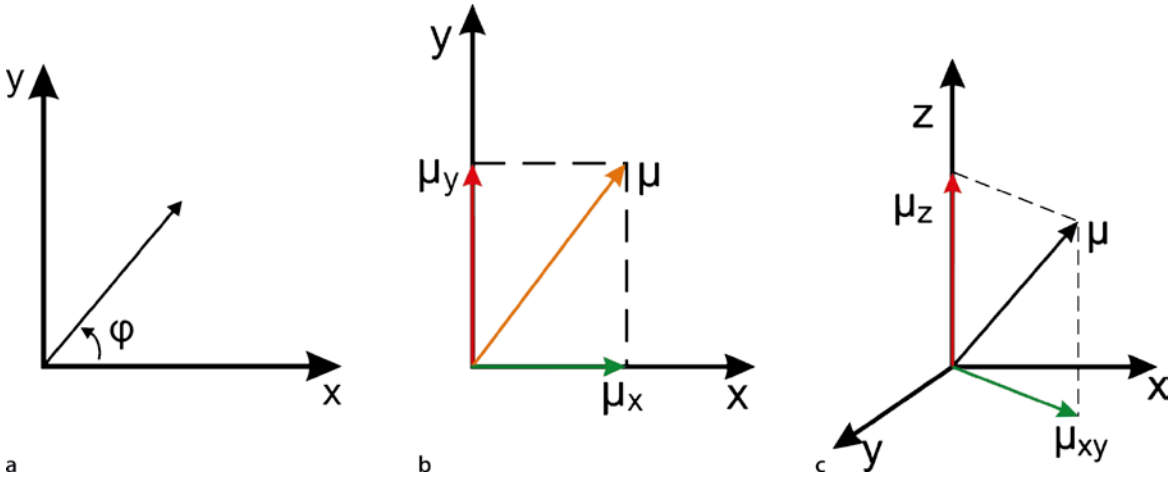

Fig. 2a–c Magnetization vectors. **a** The magnetic dipoles can be depicted as vectors placed in a coordinate system. The vector size or amplitude is indicated by its length. The direction or phase is indicated by the angle subtended by the vector and the x-axis (φ). **b** Each vector can be analyzed in two components, or projections (x- and y-axes). **c** The concept of vector analysis can be extended into 3D space

Macroscopic Magnetization 3

Keywords

- Macroscopic or bulk magnetization (vector)
- Equilibrium

Each tissue is composed of innumerable magnetization vectors (μ) that are distributed in all possible orientations in space; thus, the net macroscopic magnetization vector (M) is zero (Fig. 3a).

When subjected to the force of a strong and constant (static) magnetic field (B), the patient acquires a total macroscopic magnetization (M) parallel to the magnetic field B (Fig. 3b).

The process is not instantaneous, but orderly and biphasic. A rapid upstroke is followed by a slow approach to a plateau (Fig. 4). This specific relation of the amplitude (or size) of macroscopic M with time is exponential and will be explored in Chap. 6.

The appearance of macroscopic magnetization M is explained by quantum mechanics, the branch of physics that describes the behavior of elementary particles. The orientation of the microscopic vectors, μ, is restricted to one of two possibilities: either parallel or antiparallel to B, corresponding to lower and higher energy states respectively. The microscopic μ favor the more stable state so that a slight excess stays parallel to B. It follows that the collective or bulk magnetization, M, is also aligned parallel to B (Fig. 5).

To summarize, the application of a magnetic field, B, drives the patient to a final state (equilibrium or steady state) with a measurable magnetization vector parallel to B.

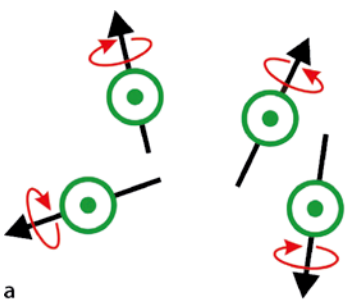

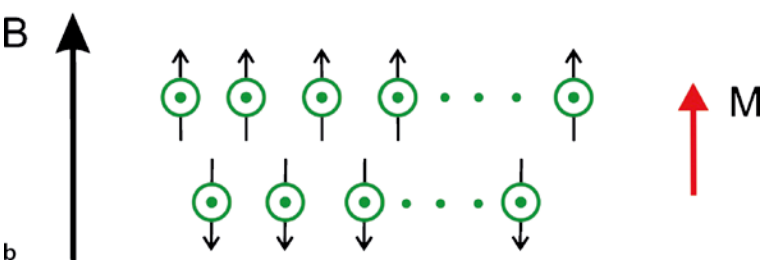

Fig. 3a,b Macroscopic magnetization (M) of tissues

a Natural state. The earth's magnetic field is too weak to influence the random orientation of the microscopic μ; thus, the vector sum, or macroscopic M, is zero

b Following the application of a strong constant external field B. The spins are forced to one of (only) two orientations: in the same direction as B, or opposing it. Since the more stable configuration is preferred, the net vector M is also parallel to B

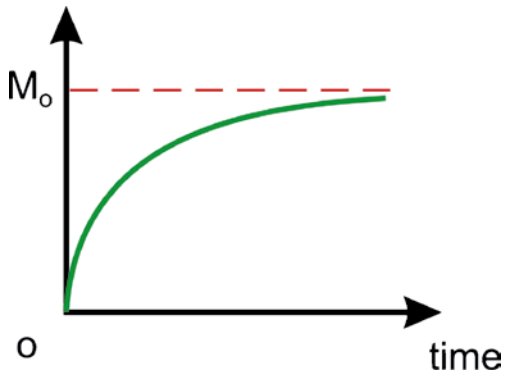

Fig. 4 Magnetization of a tissue in a static magnetic field. After application of a static magnetic field the tissue develops magnetization in an exponential fashion, up to a plateau (M_0)

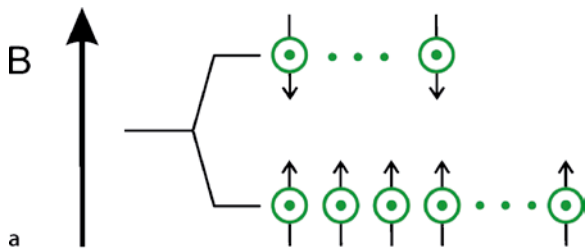

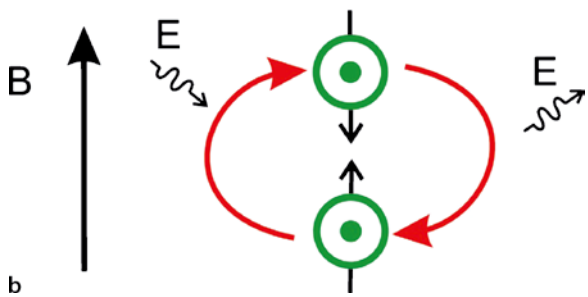

Fig. 5a,b Quantum mechanical explanation of bulk M

a After application of an external field B only two energy states are permitted, either parallel or antiparallel to B

b Bidirectional transition of spins is possible only through absorption or emission of energy, both at the resonant frequency

Macroscopic Magnetization Revisited 4

Keywords

- Rotation
- Precession
- Vector components
- Larmor frequency
- Gyromagnetic ratio

The discussion in the preceding chapter is an approximation of the true state of affairs. We will now introduce the concept of rotation of the magnetization vectors.

All spins within a static magnetic field B are asked to align parallel or antiparallel to the B-axis. In reality (because of random motion, collisions and inertia), the spins do not fall on the B-axis, but rotate (or precess) around it (Fig. 6).

To aid our understanding we can "break up" the vectors μ into two components: along the B-axis (by convention the z-axis) and in the xy plane, called μ_z and μ_{xy} respectively (Fig. 6). The same holds true for the macroscopic magnetization M (M_z, M_{xy}).

M_z/μ_z can be positive or negative and M_{xy}/μ_{xy} can rotate clockwise or counterclockwise around the z-axis.

In the absence of extrinsic forces in the xy plane the individual vectors μ_{xy} are distributed randomly and their sum cancels them out (thus $M_{xy} = 0$, Fig. 6).

The angular speed or rotation frequency of the vector μ or M (ω, in cycles/s or Hertz) is proportional to the strength of the static field B in a linear manner, expressed by the Larmor equation: $\omega = \gamma B$.

Thus, each nuclear species has a unique resonant frequency, for any value of B. Reversing this statement, we realize that we can "isolate" the nuclear species of our choice and investigate it without interference from nearby "unwanted" nuclei. Selective excitation and interrogation of spins is accomplished through irradiation at the appropriate frequency, the resonant or Larmor frequency.

The Larmor relation is of fundamental importance and we will encounter it multiple times in subsequent chapters (T1/T2 relaxation curves, gradients, image formation, selective fat suppression).

The constant γ is called the gyromagnetic ratio and it is characteristic to each spin. The exact resonance frequency of any spin depends on its local microenvironment. For example, the water protons resonate at 63.9 MHz (megahertz) at 1.5 T, whereas the lipid protons resonate at a slightly lower frequency, 220 Hz less. This difference of 220 Hz is called the chemical shift of protons in water vs lipids.

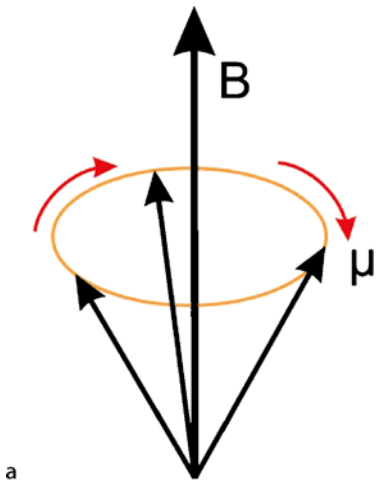

a

Fig. 6a–c Precession of magnetization vectors

a μ/M precesses (rotates) around B at the Larmor frequency, describing a cone

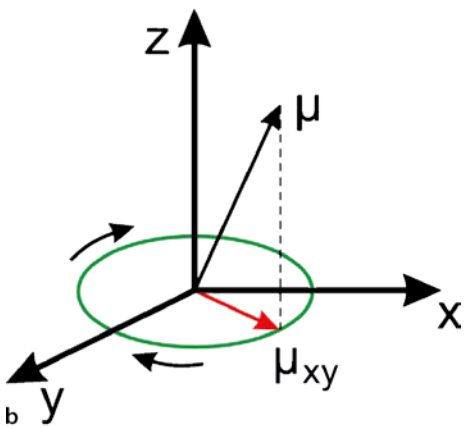

b

b μ/M can be analyzed in two components – one along the z-axis, and one rotating in the xy plane

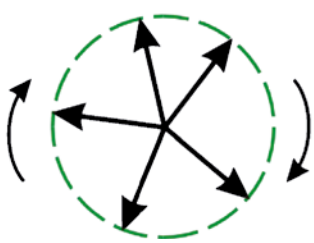

c

c Looking "down" at the xy plane or transverse plane. The transverse components of μ are in random positions and $M_{xy} = 0$

Excitation Phenomena 5

Keywords

- Excitation
- Energy pulses
- Longitudinal and transverse magnetization
- Phase coherence

At this point we are ready for the MR experiment. Inside the magnet bore the patient acquires temporary magnetization, M (called longitudinal magnetization), under the influence of the static field B. However, the magnetization vector M cannot be measured directly; thus, in order to investigate the patient we need to disturb the steady state and to observe the course of M as it returns to equilibrium.

How can we perturb the magnetic equilibrium of the patient? We add energy in short bursts at the appropriate frequency to induce resonance. These pulses[1] (β) are superimposed on the static field B and deflect the bulk magnetization M away from the lon-

[1] These waves are short-lived magnetic fields that rotate in the xy plane (around the z-axis) at the proton Larmor frequency and they command the spins to move in synchrony or in phase (in the xy plane). Since these pulses fall within the radio wave energy spectrum they are called radiofrequency (RF) pulses. In theory, these pulses can be of a single value, but in practice they host a narrow or broad range (bandwidth) of values.

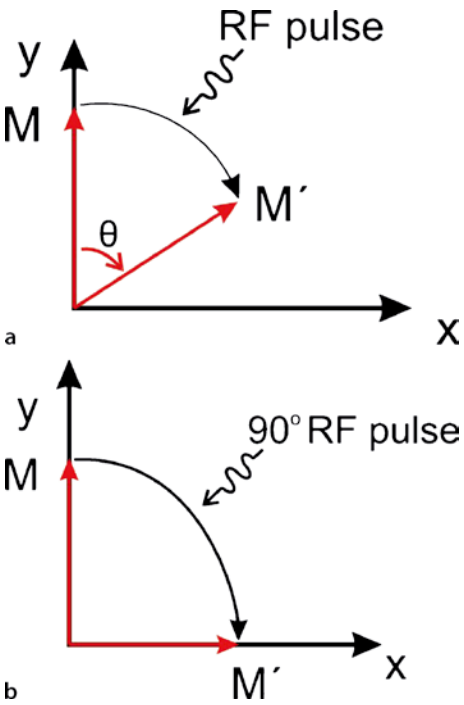

Fig. 7a,b Excitation. The radiofrequency (RF) pulse displaces M away from the z-axis. The value of theta is adjusted by the strength and duration of the RF pulse

a Flip angle < 90°

b Flip angle = 90°

gitudinal (z) axis by angle theta (flip angle, θ, Figs. 7, 8). Once the magnetization vector M leaves the z-axis, a transverse component (M_{xy}) appears, the value of which depends on θ. Thus, resonance has two effects: excitation of the spins through absorption of energy and induction of the phase coherence of the spins, with the appearance of transverse magnetization. We will first consider the simplest case, $\theta = 90^0$, in which the bulk magnetization vector M is transferred entirely onto the xy plane. In this case M_z is nulled and M_{xy} acquires the value of M_z (M_0). In other words, the value of M_{xy} equals the value of M_z just before the excitation pulse. Therefore, we can measure M_z indirectly through quantification of M_{xy}. As a matter of fact, M_{xy} is the MR signal that we record with a receiver coil or antenna. The frequency of the received signal is thus identical to the Larmor frequency of the resonating spins (or the M_{xy} precession frequency).

In summary, we have witnessed two steady states of the bulk magnetization M, in the longitudinal axis and in the transverse plane, which occur before and during the excitation pulse respectively. The transformation of the steady states is possible only in one direction, from the longitudinal axis to the transverse plane.

In the next two chapters, we will scrutinize two unstable conditions that take place upon cessation of the excitatory pulses: the process of return of both M_z and M_{xy} to the state prior to excitation (also called relaxation of M_z and M_{xy}).

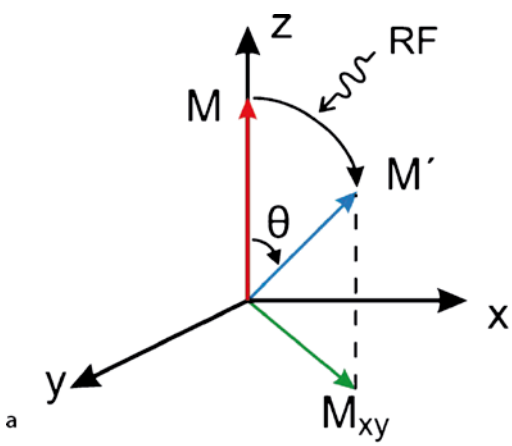

a

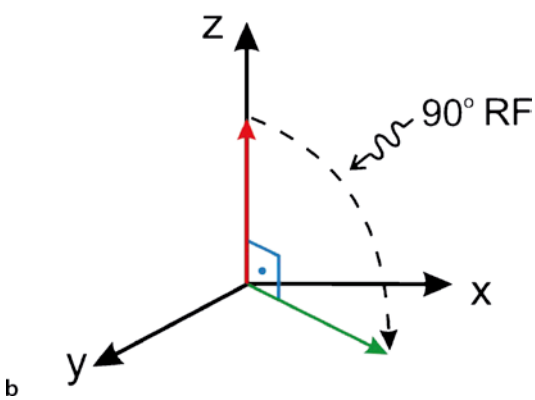

b

Fig. 8a,b 3D representation of Fig. 7. As soon as the RF pulse is withdrawn the spins are free to return to equilibrium (relax), which means that M_z will regrow to M_0 and M_{xy} will diminish to zero

a Flip angle < 90°. M gains a projection on the xy plane

b Flip angle = 90°. As long as the 90° pulse remains active, M is kept in the xy plane rotating at the Larmor frequency (around the z-axis)

T1 Relaxation (Longitudinal or Spin-Lattice Relaxation)

6

Keywords

- Longitudinal or spin-lattice relaxation
- T1 rate
- T1 contrast

This type of relaxation results in the restoration of longitudinal magnetization (M_z), as there is a transfer of energy from the spins to their environment (lattice). The 90° pulses (β) keep the entire bulk magnetization M on the xy plane, i.e., $M_z = 0$. When the β pulse is withdrawn, the magnetization vector M begins its course toward equilibrium with gradual growth along the z-axis toward the value M_0 (Fig. 9).

The measure of the rate of growth of M_z is called T1 and it is characteristic to each tissue. If we wait one T1 interval, M_z recovers 63% of its maximal value (M_0). After two, three, or five T1 periods the corresponding numbers are 87%, 95%, and 99%. Thus, we accept that M_z of any tissue has reached full strength after a time period equal to 3T1. The maximum value of M_z is proportional to the number of spins per voxel (proton or spin density). The T1 rates depend on the strength of the main static field B, are in the order of milliseconds, and representative values are listed in Table 1.

Tissue separation based on T1 "fingerprints" is called T1 contrast, and the corresponding images are called T1-weighted (w; Fig. 10).

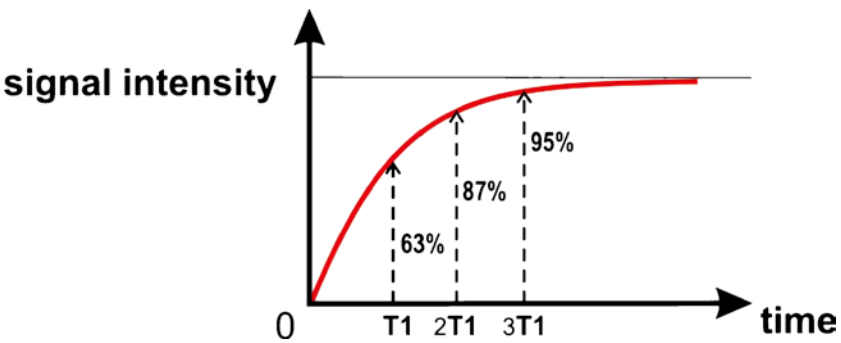

Fig. 9 T1 or longitudinal or spin lattice relaxation. To fully describe the T1 curve we need a starting point, an end point, and the rate of change. In the case of θ = 90°, Mz is nulled and the starting point is 0. The end point, or maximum magnetization (M_0), depends on the number of protons in the voxel. The rate of change is indicated by the time constant T1

Table 1 Approximate T1 values (ms) of several tissues for B = 1.5 T

Fat	260	
Liver	500	
Muscle	870	
Brain WM	780	WM: white matter
Brain GM	920	GM: gray matter
CSF	2500	CSF: cerebrospinal fluid

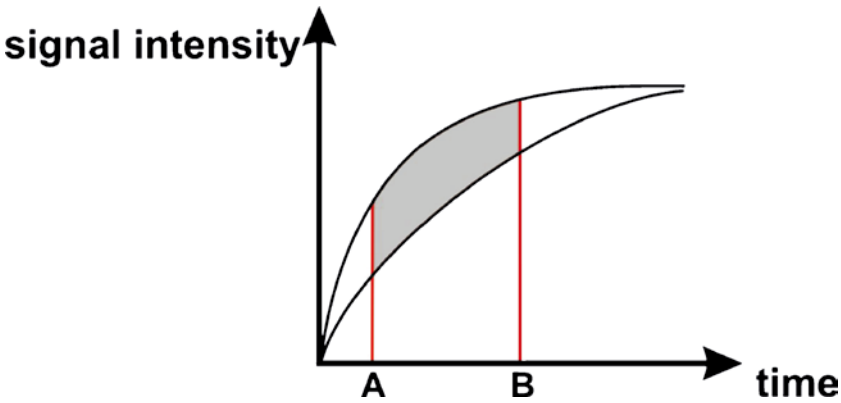

Fig. 10 T1 contrast. Consider two tissues of approximately equal spin density, but different T1 rates. The curves approach each other at both ends. In between, there is a time window (*A*–*B*) of T1 contrast with clear demarcation of the two tissues

T2 Relaxation (Transverse or Spin–Spin Relaxation) 7

Keywords

- Transverse or spin–spin relaxation
- T2 rate
- T2 contrast

The T2 process results in complete loss of transverse magnetization (M_{xy}) due to phase dispersion in the xy plane. The explanation is as follows: complex forces develop between dipoles moving in close proximity of each other, altering the local magnetic profiles. Thus, numerous sites develop slightly positive or negative deviations from the nominal strength of the main field B. Since the Larmor frequency follows the apparent value of B, there is a spread of the precession rates of the spins, around the nominal value. After a short time the microscopic spins (μ) move apart like a fan, and occupy random orientations (Fig. 11).

Thus, M_{xy} decays in an exponential manner with a rate, called T2, that is specific to each tissue. After one T2 period, M_{xy} has lost 63% of its initial value. We can consider T2 to be the ability of the tissue to "sustain" its signal (Fig. 12). T2, like T1, is measured in milliseconds and representative values are listed in Table 2. T2, unlike T1, is not influenced by the static field B.

Tissue separation based on T2 "fingerprints" is called T2 contrast and the corresponding images are called T2-weighted (w; Fig. 13).

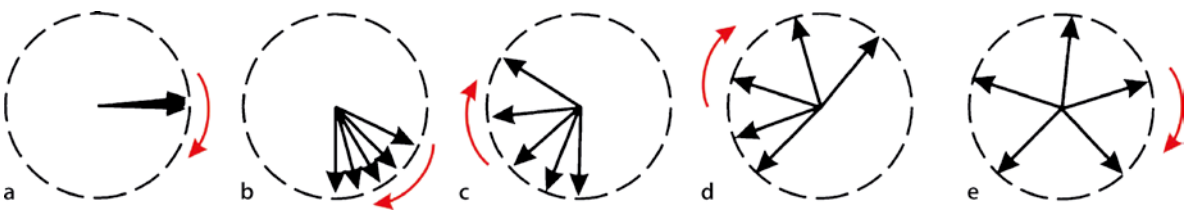

Fig. 11a–e Transverse relaxation. **a** For the entire duration of the pulse β, all μ point in the same direction, i.e., they have the same phase (**a**), while they rotate around the z-axis; thus, M_{xy}, the vector sum of μ, has its greatest possible value (M_0). When b is revoked, there is a progressive loss of phase coherence of μ with a steady decline of M_{xy} to 0 (**b–e**)

Table 2 Approximate T2 values (ms) of various tissues

Fat	85
Liver	45
Muscle	50
Brain white matter	90
Brain gray matter	100
CSF	250

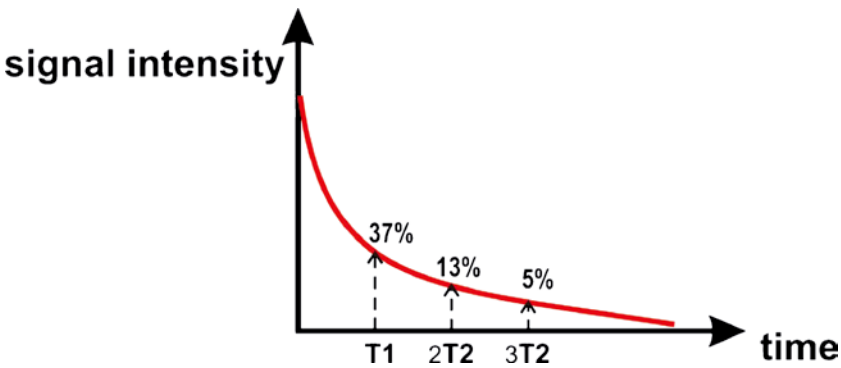

Fig. 12 T2 relaxation curve. Exponential decay of M_{xy} with time constant T2

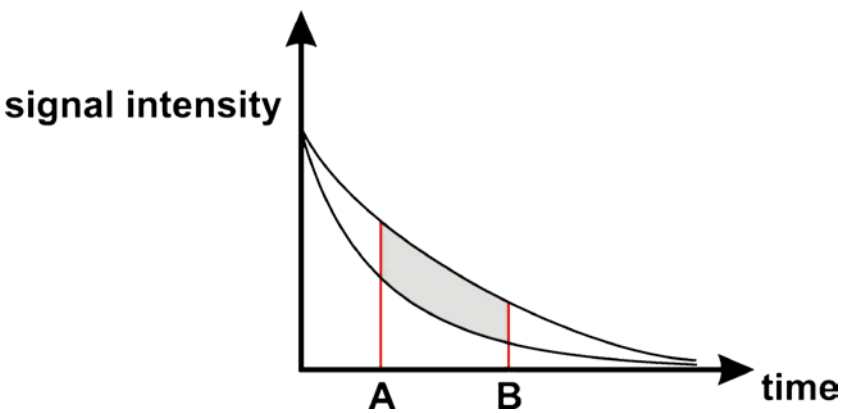

Fig. 13 T2 contrast. Consider two tissues of approximately equal spin density, but different T2 rates. Differentiation is not possible at the beginning. As time elapses the curves diverge with increasing separation of the two tissues. If we wait too long, the signal intensity drops significantly and the entire image becomes dark and "grainy" (noisy). We can easily define a window (*A*–*B*) of useful T2 contrast

Magnetic Substrates of T1 Relaxation 8

Keywords

- Local magnetic fields
- Larmor frequency
- Hydration layer

The stimulated spins want to return to the ground state; they can, upon liberation of the excess energy they carry. They only need to find an appropriate partner to accept the energy load. What we have now is a potential resonance pair: the excited spins are the energy source and their chemical surroundings (lattice) can serve as the receiver.

The magnetic properties of the lattice depend upon its physicochemical signature: the regularity and homogeneity of structure, the strength of bonding, and the freedom of motion of its constituents (translation, vibration, rotation; Fig. 14). These characteristics dictate the appearance, strength, and persistence of the magnetic fields in each niche of the lattice.

When the fluctuations of these local fields (on the average) are close to the Larmor frequency of the excited spins, then resonance becomes possible. In this case, we speak of efficient or quick T1 relaxation, resulting in a short T1 constant of the lattice (tissue or tissue component). Molecular motion that is either too fast or too slow presents a conflict between the average local field fluctuations and the Larmor frequency of protons. The result is delayed T1 interactions and thus long T1 rates.

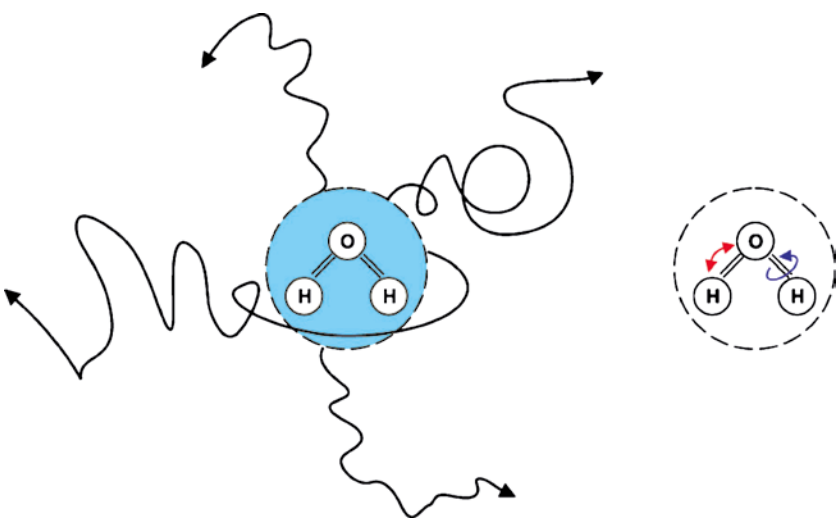

Fig. 14 Schematic representation of water that is free to exercise all types of molecular motion: translation, tumbling, rotation, vibration

Let us consider some examples of how the lattice consistency affects the T1 rates. Solid and rigid frameworks (e.g., collagen) severely restrict motion (Fig. 15a), well below the requirements for efficient T1 relaxation. Thus, we predict long T1 values. The loose lattice of pure liquids (e.g., water) allows very rapid motion, exceeding the limits of efficient T1 resonance (Fig. 15b). Water, therefore, has a long T1 value. We can introduce obstacles to the translation of water, through the addition of biologic macromolecules, e.g., proteins. Via electrostatic effects the macromolecules "capture" a thin film of water (hydration layer) retarding their motion. The slowed speed of the hydration layer facilitates T1 relaxation with shortening of the T1 rate of the solution (Fig. 15c). Examples include cysts complicated by hemorrhage or infection. Lipid macromolecules have a very short T1 value, because they happen to possess the appropriate size and mobility for rapid T1 relaxation (Fig. 15d).

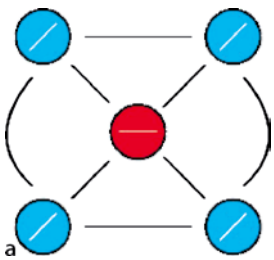

a

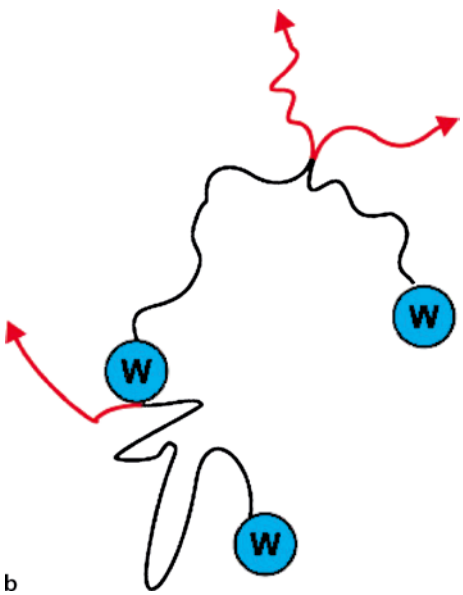

b

Fig. 15a–d Magnetic substrates of T1 relaxation

a Simplified depiction of a crystal lattice. Very strong chemical and electrostatic bonds forbid any significant motion

b Schematic representation of the rapid and free translational motion of water

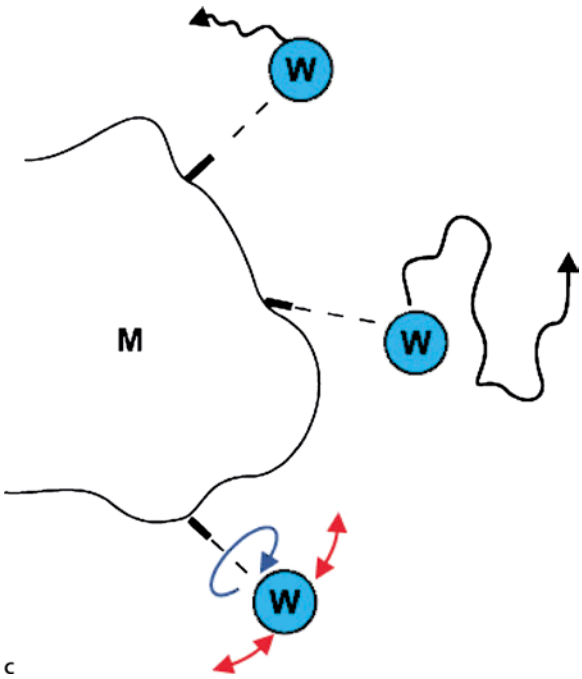

c

c Hydration layer. In aqueous solutions weak electrostatic interactions develop between water and macromolecules. Thus, a thin film of water slows down and is forced to stay close to the macromolecules

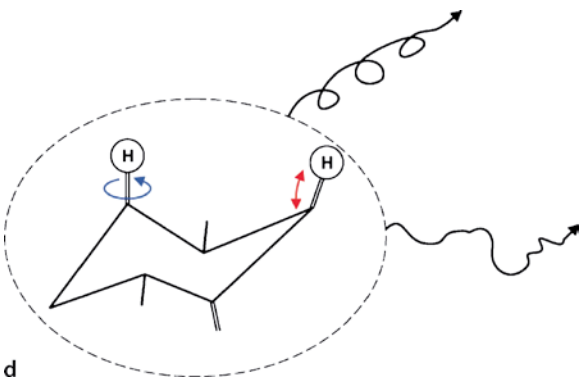

d

d Simplified sketch of a lipid molecule with motional freedom intermediate to free water (**b**) and crystalline cages (**a**)

9 Magnetic Substrates of T2 Relaxation

Keywords

- Dephasing
- Free vs restricted motion of protons

In T2 relaxation there is a loss of phase coherence. Let us examine what conditions promote or resist dephasing.

We will start with the simplest case, which is pure water, with free and rapid motion. The spins do not "stand" in any place very long; thus, any interactions are too short-lived to provoke significant changes (Fig. 16a). These transient perturbations, averaged over time, look like a smooth and shallow variation of the external magnetic field. Thus, dephasing is slow and the T2 of water is extended, approaching its T1 value. At the other end of the spectrum are compact and rigid structures that leave little "room" for any type of motion (Fig. 16b). These dipoles are very close to each other and essentially become "anchored" in space. Therefore, they cannot avoid the magnetic burden of their neighbors and undergo rapid dephasing (short T2). Such examples are collagenous structures (tendons and ligaments), which appear dark on all pulse sequences.

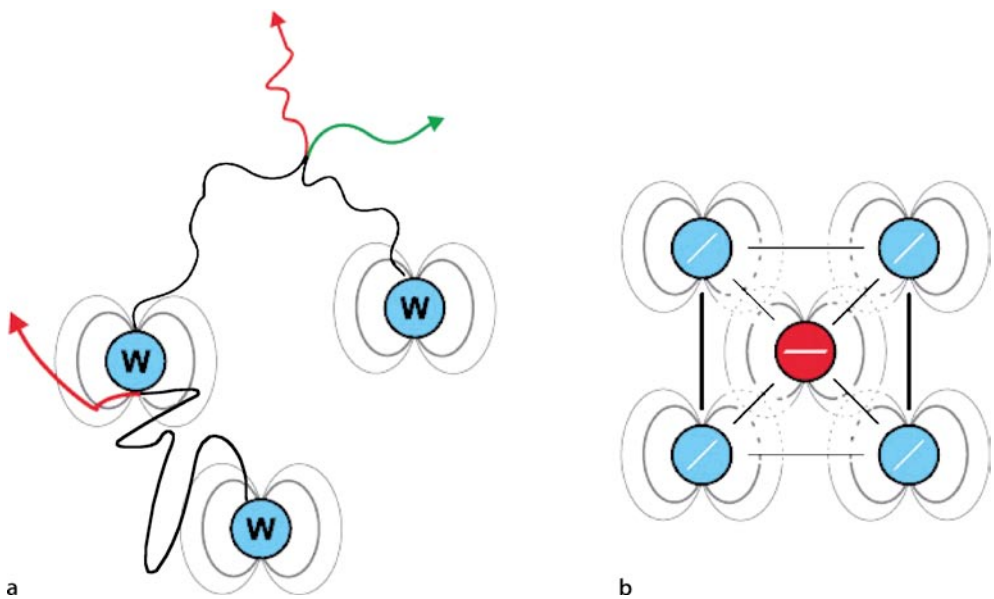

Fig. 16a,b Magnetic substrates of T2 relaxation. **a** Water as the prototype tissue with long T2 relaxation. Most of the time the water molecules are far away from each other and their magnetic fields undergo only transient perturbations. Thus, phase coherence is maintained for a relatively long time. **b** A solid, rigid crystalline conformation as the prototype structure with rapid T2 relaxation. The continuous overlap of the local magnetic fields results in a distorted magnetic environment that cannot sustain phase coherence

Proton (Spin) Density Contrast 10

Keywords

› Proton density or spin density contrast

So far we have studied in detail two fundamental magnetic properties of tissues, namely the T1 and T2 relaxation rates. We will now consider another tissue variable that can influence the strength of the final MR signal, specifically the proton (or spin) density, i.e., the number of protons per unit of tissue. This number depends on the exact chemical make-up of each tissue and determines the maximum signal that each tissue can produce, represented by the plateau of the T1 curve (Fig. 9). Differences in proton density (PD) afford tissue discrimination called PD contrast (Fig. 17). The corresponding images are called PD-weighted images.

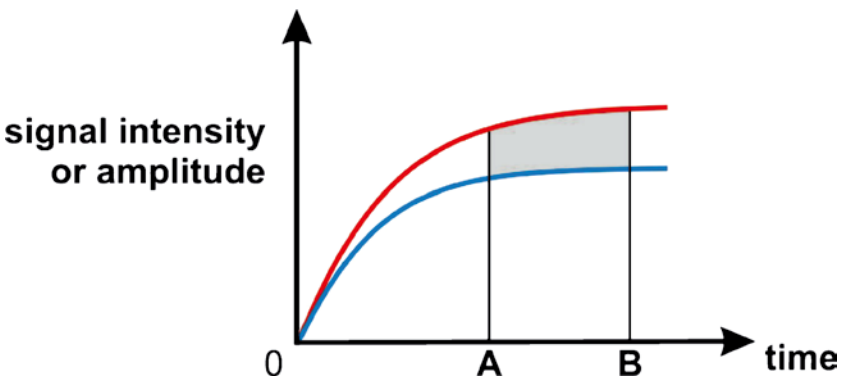

Fig. 17 Proton density contrast. Consider two tissues with similar T1 rates, but different proton densities. Tissue differentiation is not possible at the beginning of the T1 relaxation curves. After we enter the plateau of the curves it is easy to separate the two tissues

11 Partial Saturation

Keywords

- Repetition time (TR)
- Partial saturation

Let us examine the effect of multiple 90° pulses spaced at equal time intervals, called TR or repetition time (Fig. 18). If TR > 3T1 (long TR), the tissue is given plenty of time to regain full strength of its longitudinal magnetization (M_0). If TR < T1 (short TR), tissue M_z stops very short of M_0, and is forced to a new steady state called partial saturation.

Thus, the final value M' of longitudinal magnetization depends on both T1 and spin density, and the relative contribution (weight) of each is determined by TR.

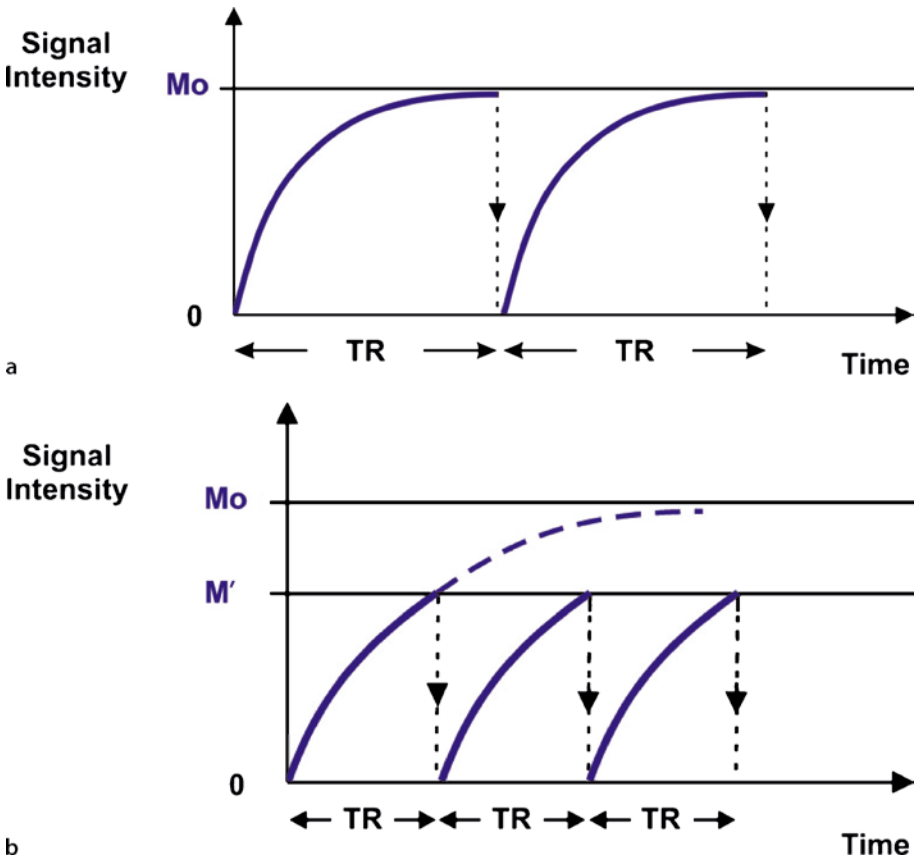

Fig. 18a,b Longitudinal magnetization as a function of TR. Every TR period a 90° excitation pulse is applied

a Long TR (TR > 3T1). M_z is allowed to reach the maximum value

b Short TR (TR < T1). The T1 ascent is interrupted on the rapid phase of the upstroke, and M_z recovers to a small fraction of M_0

Free Induction Decay 12

Keywords

- Free induction decay
- T2* rate
- Inhomogeneity of the static magnetic field

The raw MR signal, before computer processing, is called free induction decay (FID) and is generated by the transverse component of magnetization, M_{xy} (see Chap. 5). Since M_{xy} rotates in the xy plane, it is an oscillating magnetic field, and as such it induces the flow of electric current in a coil. Thus, through a coil or antenna the MR signal is transformed into an electric signal that describes a sinusoidal time course with rapid damping (Fig. 19).

The envelope of the FID peaks is an exponential curve with a constant T2* that is shorter than expected, i.e., T2* is shorter than T2. This discrepancy is explained as follows. The strength of the static magnetic field B is not uniform across space, due to the technical constraints of the MR machinery. The flaws of B are small on an absolute scale, but seem large for the tiny spins and influence the spin precession rates.

So, there are two causes of proton dephasing: intrinsic, due to spin–spin interactions (see Chap. 7), and extrinsic, due to the inhomogeneity of the static field B. Thus, with our antenna we measure the T2* variable, which represents the composite decay constant of M_{xy}. However, we are interested in the T2 value, which is an intrinsic property of each tissue, independent of the static magnetic field B. Therefore, we have to figure out a way to extract the T2 rate from the measurement of T2*. The answer is given in the next chapter.

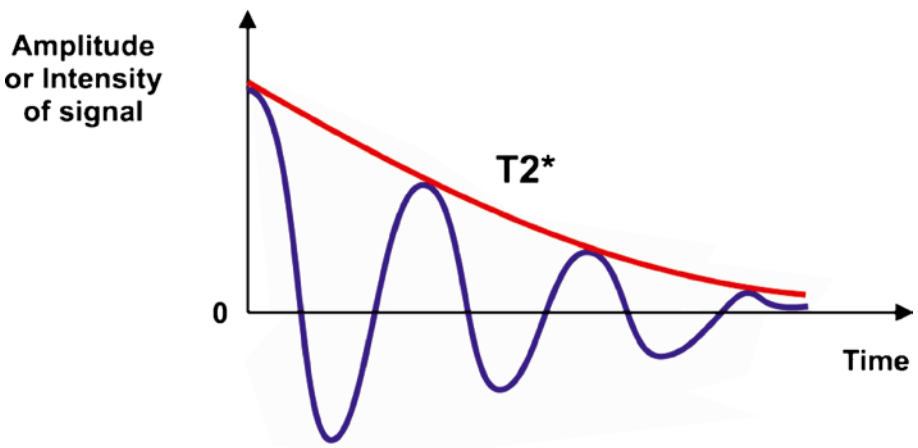

Fig. 19 Free induction decay (FID). The FID course is an exponential decay with rapid damping and T2* rate

13 Spin Echo

Keywords

- Echo
- Spin echo
- Time to echo

We have seen that variations in the external field B contribute to dephasing of the dipoles. These extrinsic variations are constant in time and space and can therefore be neutralized. All we have to do is reverse the direction of spin precession, without affecting the precession rate. This is accomplished with an RF pulse of 180°, called the refocusing pulse. After the activation of such a pulse all spins are instantaneously shifted into mirror-image positions with respect to the z-axis (Fig. 20). This way the advancing spins are placed "behind" the slow ones. The fast spins still move fast, and the slow ones still move slowly. Since the relative speed is preserved, the fast spins "catch up" with the slow ones and the macroscopic magnetization M_{xy} reappears as a signal, called the spin echo. The time between the excitation pulse and the peak of the echo is called the time to echo, or TE. The refocusing pulses can be repeated several times, generating a train of echoes. However, we cannot cancel the effects of random events (due to spin–spin dephasing). Thus, each successive echo is of lower intensity than the previous one; if we draw an envelope along the peaks of the echoes we reconstitute the T2 curve (Fig. 21).

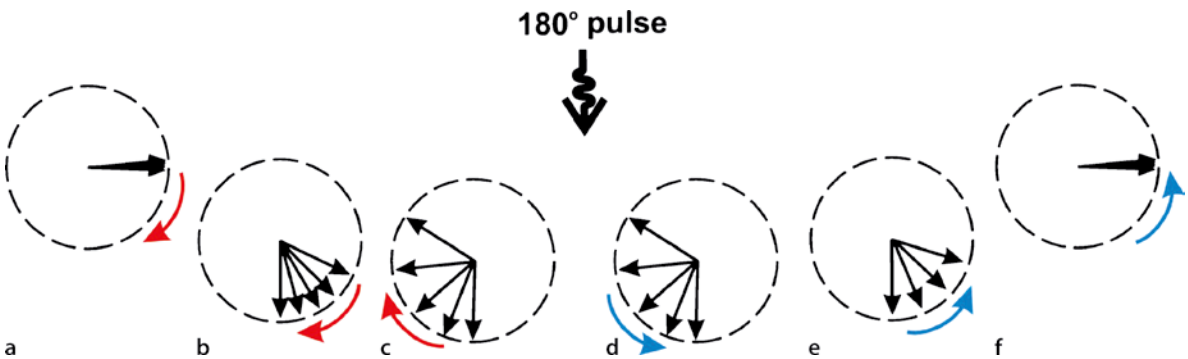

Fig. 20a–f Spin echo. **a–c** After termination of the 90° pulse there is progressive loss of phase coherence. At a specified time T we deliver a refocusing pulse that reverses the phase of the spins. **d–f** Since the relative speed is not altered, the spins converge to coherence at time TE (**f**)

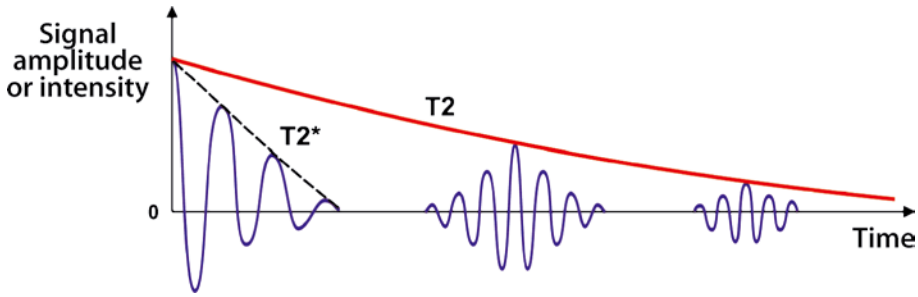

Fig. 21 T2 envelope. The initial (FID) signal is succeeded by multiple spin echoes. The smooth curve uniting the peaks defines the T2 trajectory

14 Integration of T1, T2, and Proton Density Phenomena

Keywords

- T1 weighting
- Proton density weighting
- T2 weighting

T1 and T2 relaxation occur simultaneously, so it is appropriate to combine the two curves (Fig. 22). The initial point of the T2 curve can occur anywhere on the T1 ascent. Thus, the final value of the signal is a mixture of spin density and both T1 and T2 relaxation mechanisms. The relative contribution (weight) of the above factors is modified by TR and TE, which determine the high and the low points that we reach on the T1 and T2 curves respectively.

Improper selection of parameters can result in signal overlap with low or no tissue contrast (Fig. 23). Thus, how do we choose the appropriate time for measurements? The answer depends on the type of contrast we want (Fig. 24).

If we want to extract T1 information, we use a window in the "upstroke" of the T1 curve by keeping TR short, and we "stop" the T2 curve early (short TE), in order to suppress T2 contamination.

For proton density (PD) contrast, we let the T1 curve "run" all the way (i.e., extend TR as much as feasible[1]) and we restrain TE, in order to minimize T2 impurities.

If we want to emphasize T2 variations, we start in the range of PD (long TR) so as to escape from the T1 influence, and we wait for the T2 curve to "run" its course (long TE).

A short TR value is considered to be less than 750 ms and a short TE less than 25 ms. A long TR should exceed 2,000 ms and a long TE is over 80 ms.

---

[1] Ideally TR should be about three times the T1 of the tissue.

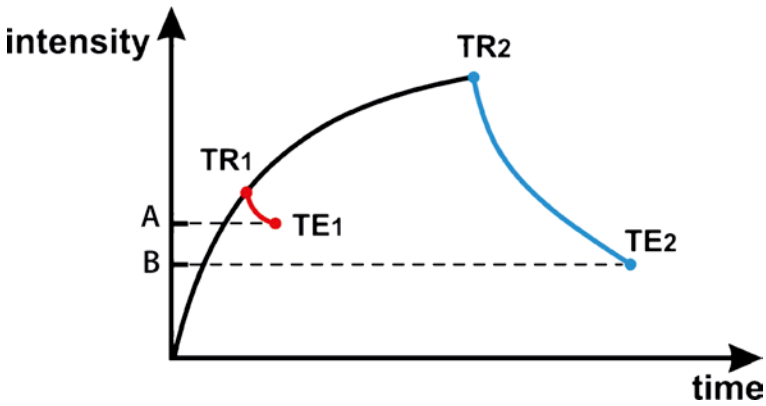

Fig. 22 Composite curve of signal intensity (SI). **A** Final signal intensity with TR1/TE1. **B** Final signal intensity with TR2/TE2

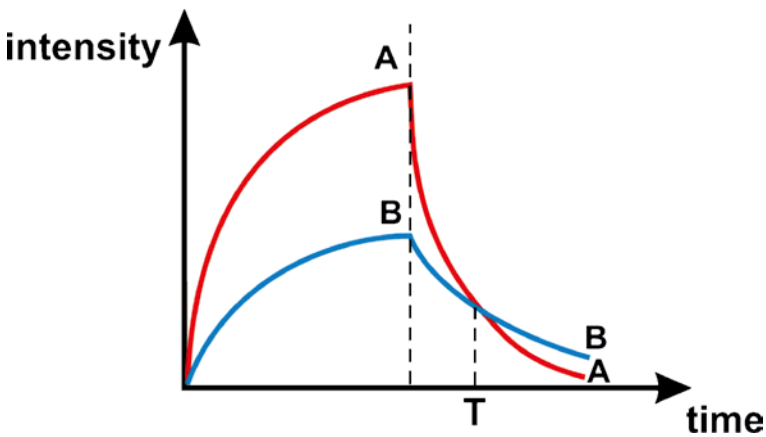

Fig. 23 Tissue overlap. Tissue *A* has a short T1/short T2 and tissue *B* has a long T1/long T2, with a crossover of signal at time T

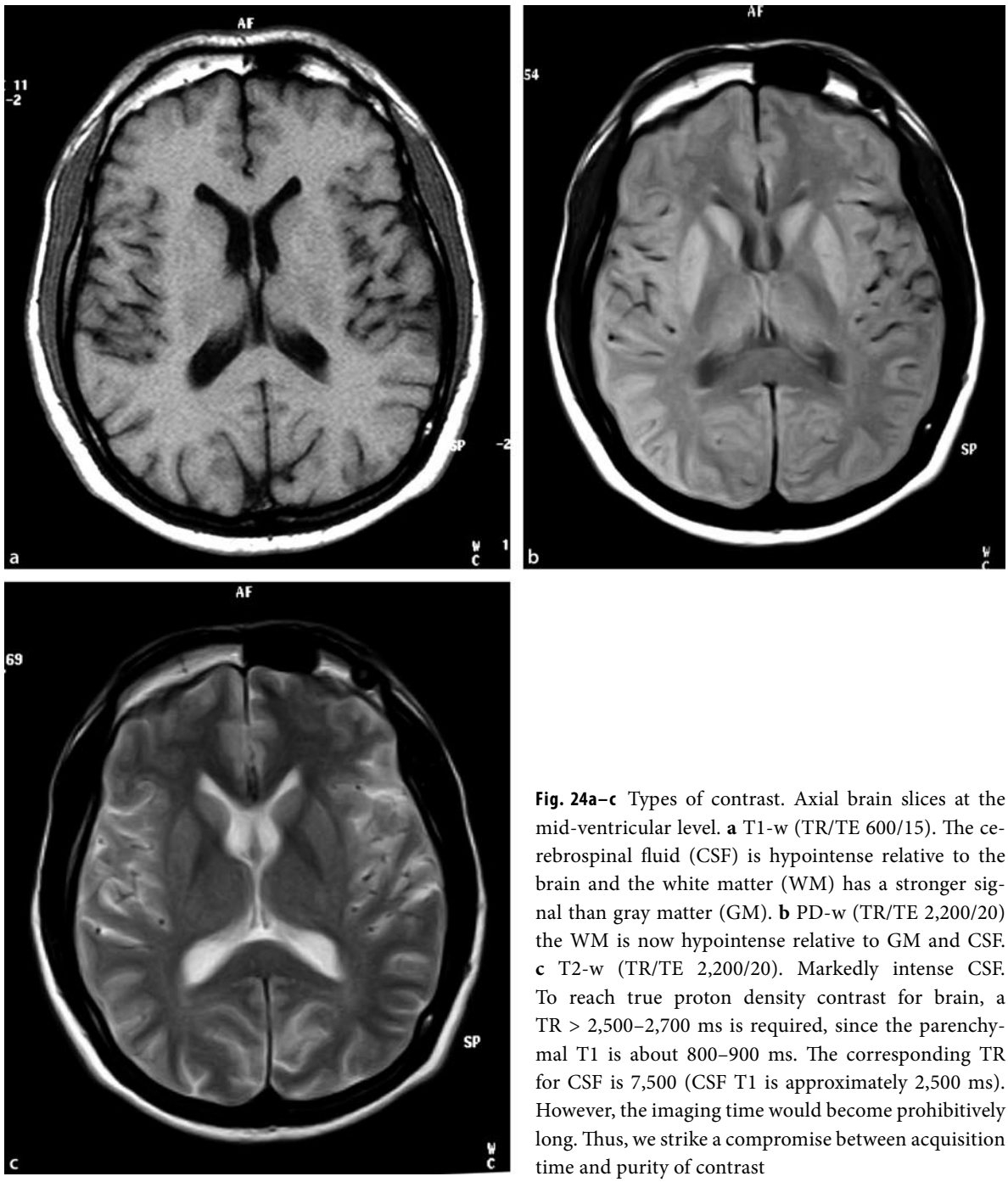

Fig. 24a–c Types of contrast. Axial brain slices at the mid-ventricular level. **a** T1-w (TR/TE 600/15). The cerebrospinal fluid (CSF) is hypointense relative to the brain and the white matter (WM) has a stronger signal than gray matter (GM). **b** PD-w (TR/TE 2,200/20) the WM is now hypointense relative to GM and CSF. **c** T2-w (TR/TE 2,200/20). Markedly intense CSF. To reach true proton density contrast for brain, a TR > 2,500–2,700 ms is required, since the parenchymal T1 is about 800–900 ms. The corresponding TR for CSF is 7,500 (CSF T1 is approximately 2,500 ms). However, the imaging time would become prohibitively long. Thus, we strike a compromise between acquisition time and purity of contrast

Inversion Recovery 15

Keywords

- Inversion
- Inversion recovery
- Time to inversion
- STIR
- FLAIR

We now proceed to the situation of θ = 180°, in which M_z is inverted ($M_z = -M_0$; Fig. 25). We still have to turn Mz in the xy plane through a 90° pulse and then collect the echo through a 180° pulse. This sequence is called inversion recovery (IR); it simply incorporates an inversion pulse in front of the standard SE sequence. The new variable, called inversion time (TI), is the delay between the inversion and the excitation pulses. Thus, the familiar T1 curve is modified two-fold: it is "stretched" to twice the (vertical) distance as before, and it has to cross the zero (null) point (Fig. 26).

The added complexity affords two advantages: greater latitude in T1 contrast (Fig. 27), and the ability to "eliminate" normal tissues that may obscure pathology. If the 90° pulse is transmitted at the null point of the "unwanted" tissue, that tissue will return no signal (Fig. 28). In this way, the lesion stands out "bright" against a muted background (Figs. 29, 30).

The two most commonly used IR sequences are: STIR (short tau inversion recovery), used for suppression of fatty tissues, and FLAIR (fluid attenuated inversion recovery), used for suppression of CSF and CSF-like lesions, e.g., arachnoid cysts (Figs. 29, 30).

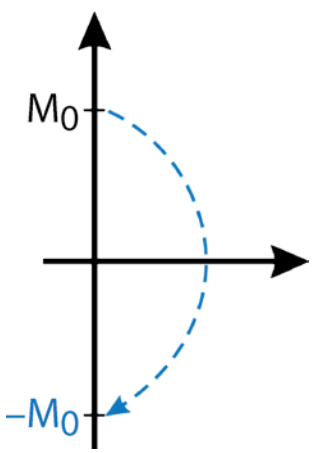

Fig. 25 Inversion recovery (IR) pulse. M is rotated 180°, below the *x*-axis, to negative values

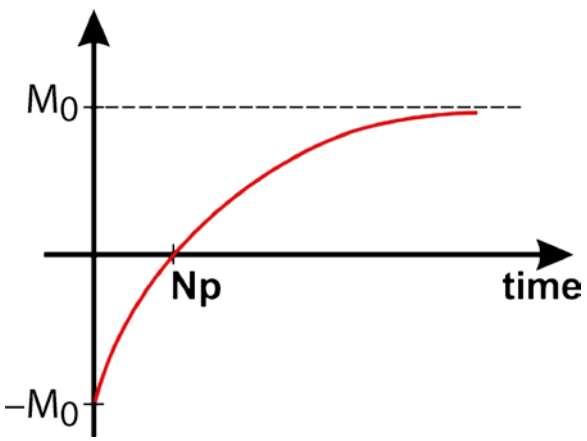

Fig. 26 Inversion recovery (IR) curve. The ascending relaxation curve crosses the null point (zero) at time Np

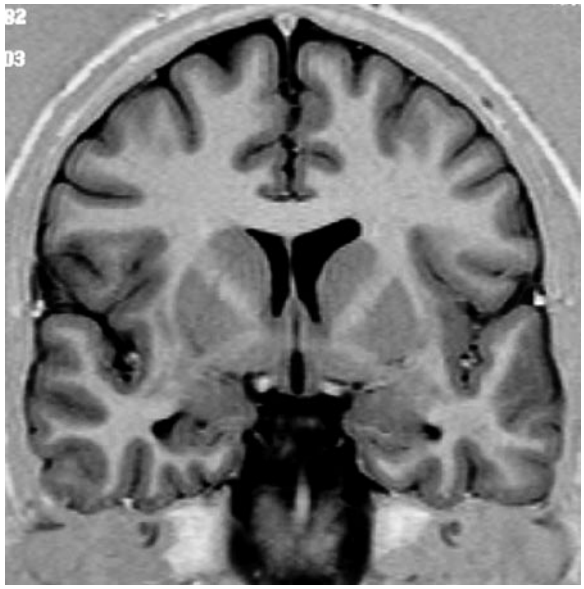

Fig. 27 T1-w IR coronal brain slice (TR/TI/TE: 7,000/350/60). Excellent gray–white separation

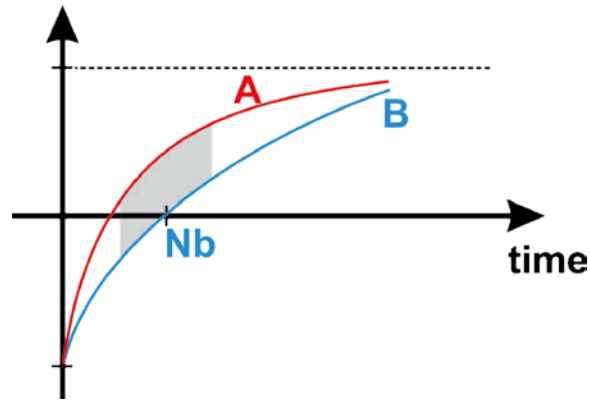

Fig. 28 Tissue contrast through IR. Consider two tissues, *A* and *B*, with their inversion recovery curves as shown. If we sample the MR signal around the null point of *B*, then we maximize the contrast between *A* and *B*

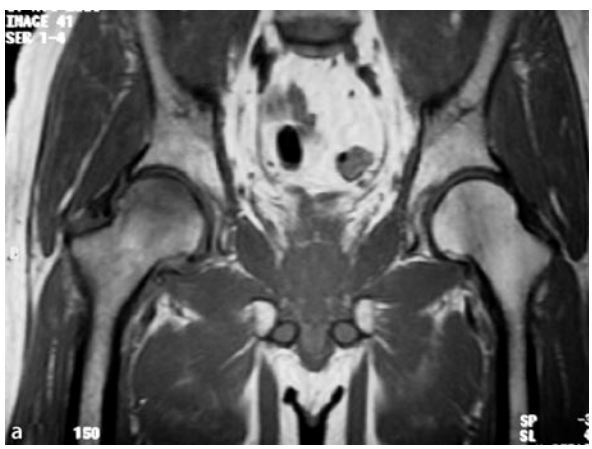

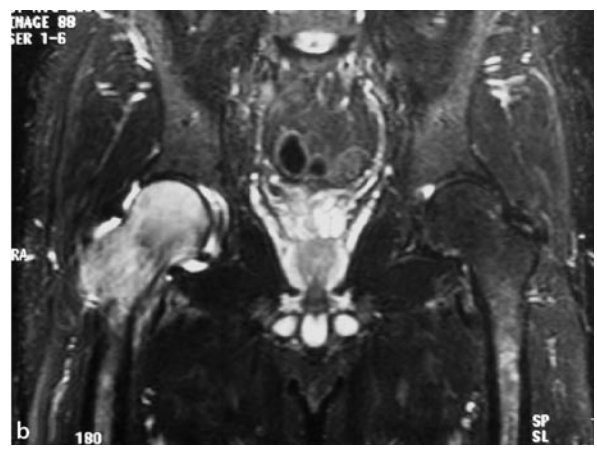

Fig. 29a,b Transient osteoporosis of the right femur in a 43-year-old. **a** T1-w image (TR/TE: 700/12). **b** Short tau (TI) inversion recovery (STIR; TR/TI/TE: 4,000/140/60). The bone marrow edema appears hypointense in **a** and hyperintense in **b**. By their nature, STIR sequences are excellent at tracing and highlighting structures – lesions of low T1 – high T2 relaxation rates, e.g., fluids, edema, inflammation, and "watery" tumors

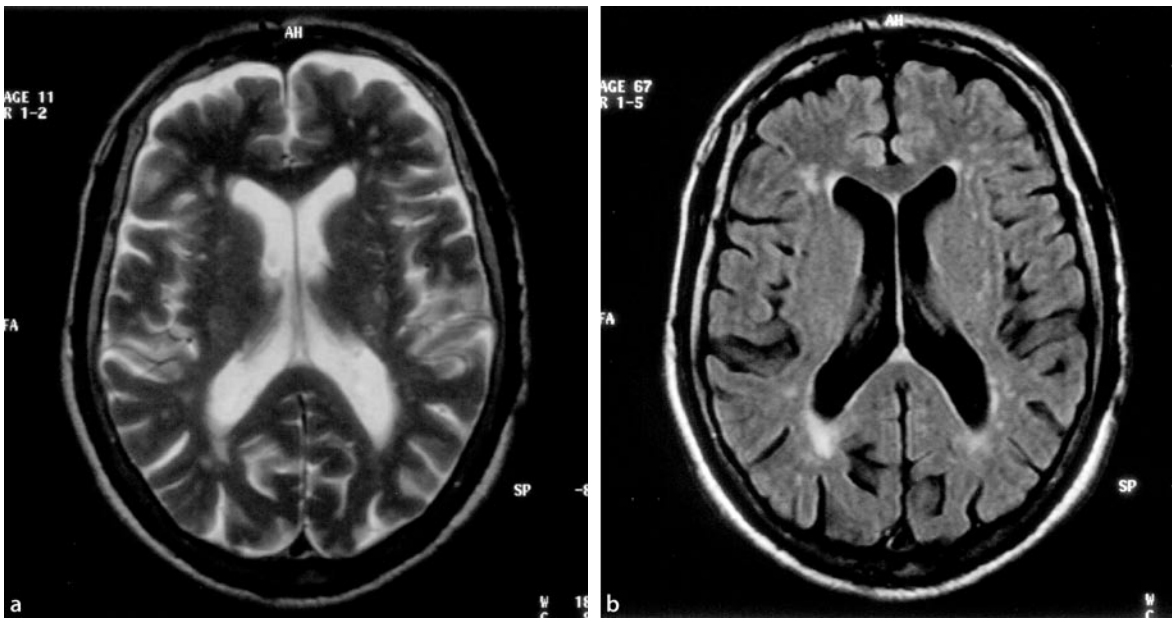

Fig. 30a,b Periventricular small vessel ischemic disease in a 67-year-old. **a** T2-w image (TR/TE: 4465/120). **b** Fluid attenuated inversion recovery (FLAIR; TR/TI/TE: 7500/2243/105). Axial brain slices at a high ventricular level. The hyperintense subependymal lesions are more conspicuous after suppression of the CSF

16 Image Formation – Fourier Transform – Gradients

Keywords

- Encoding
- Gradient
- Fourier transform
- Slice select
- Phase encoding
- Frequency encoding

The construction of an image entails the assignment of an intensity value (brightness) to each unit of the image (voxel). Our raw data are contained in the FID curve, which comprises overt information about amplitude (intensity) and frequency and covert information about phase (Fig. 31). However, spatial knowledge is "lost" since the signals from the individual voxels have merged into a composite FID wave. Somehow, we need to recover positional information. Now is the time to revisit the Larmor principle: there is a one-to-one correspondence between the proton resonance frequency and the strength of the static field B. So, if we force B to grow in a smooth and continuous manner along a line, then we spread the resonance frequencies, and each voxel along that line is tied to a unique frequency. Thus, the frequency of the received signal betrays the position of the voxel in question.

The last step in the deciphering process is the Fourier transform (FT). The FT is a mathematical algorithm, through which we can deconvolute the FID signal from a function of amplitude vs time to a function of amplitude vs frequency (Fig. 32).

In theory, we can complete encoding of the position through manipulation of the frequency in three dimensions. In practice, however, the most efficient way of carrying out spatial encoding is through frequency in two directions and through a phase in the third axis.

The way to distort B in an orderly, temporal, and spatial sequence is through gradients, which are weak static magnetic fields[1]. The gradients are superimposed on the main magnetic field B for brief periods (Figs. 33, 34). Their action is to create a smooth, linear variation (gradation) of B along a specified axis.

First, we divide the patient into chunks with the slice select gradient. Since the excitation and refocusing pulses can be slice-selective, the MR signal in a specific time window can be traced to a specific slice (we excite a slice, sample the echoes we want, then proceed to another slice, and so on). Next, we apply the phase encoding or preparation gradient in order to impart phase shifts in one axis of the selected slice. The last gradient, in the remaining direction, is activated during formation of the echo and spreads the frequencies of the emitted signal. This gradient is naturally called the frequency encoding, or readout gradient.

---

[1] In contrast to RF pulses, which are rotating magnetic fields that induce resonance.

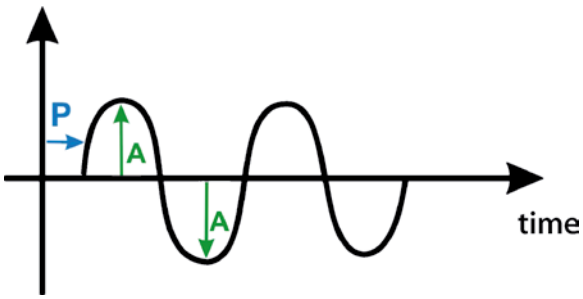

Fig. 31 Description of sinusoidal waves in two cycles of a pure sinusoidal wave. Amplitude (*A*) is the maximum positive or negative excursion from the *x*-axis. The distance between peaks is one cycle. Frequency is the number of cycles per second. Phase (*P*) is the horizontal distance (of each point of the wave) from the *y*-axis

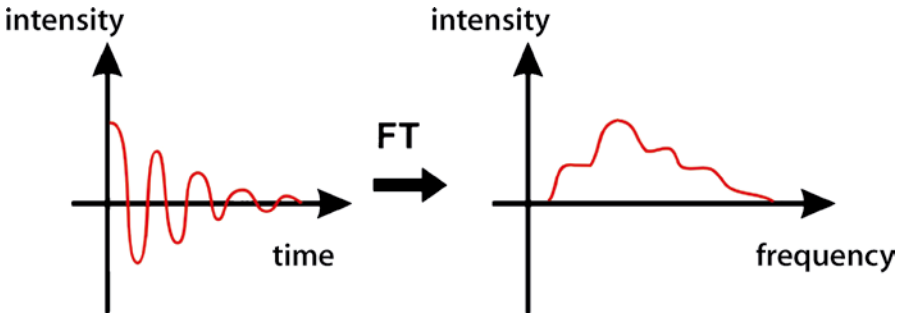

Fig. 32 Fourier transform (FT). Through a mathematical algorithm (FT) we can "translate" the FID to a simple correspondence of SI to frequency. Reminder: there is a spread of values around the central Larmor frequency, due to variations in *B* about its nominal value

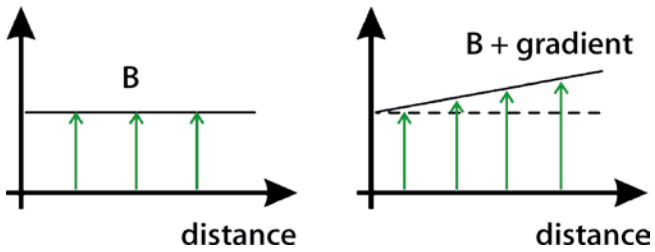

Fig. 33 Magnetic field gradients. The addition of a gradient modifies the magnitude of the external field in a linear manner across a specified axis

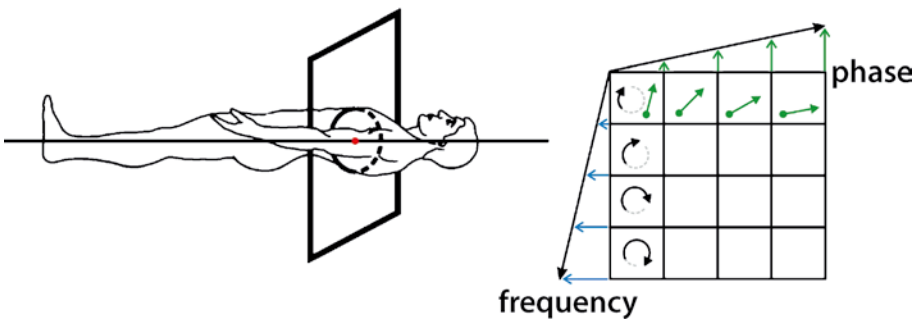

Fig. 34 Slice select, frequency, and phase encoding gradients. The first gradient isolates a slice of tissue for selective excitation/interrogation. The second and third gradients produce linear transitions of phase and frequency respectively

Frequency is a scalar quantity with specific, absolute values. Thus, it can be manipulated and measured with ease. Phase is more difficult to handle. It can attain positive or negative values with overlap for each completed cycle (i.e., a phase value φ is indistinguishable from φ + 360°). Fortunately, the individual, precise numbers are not as important as the relative values (phase offsets or phase shifts).

Phase shifts modulate the composite MR signal according to the rules of constructive and destructive interference (Fig. 35). Therefore, phase information is encrypted in the amplitude of the MR signal. A single MR measurement is equivalent to a single and limited view of the object of interest. The more views we get, the more accurate the reconstruction of the object (Fig. 36), with the drawback of a longer acquisition time. To create multiple views we repeat the entire TR process, each time with a different value (step) of the phase encoding gradient (Fig. 37).

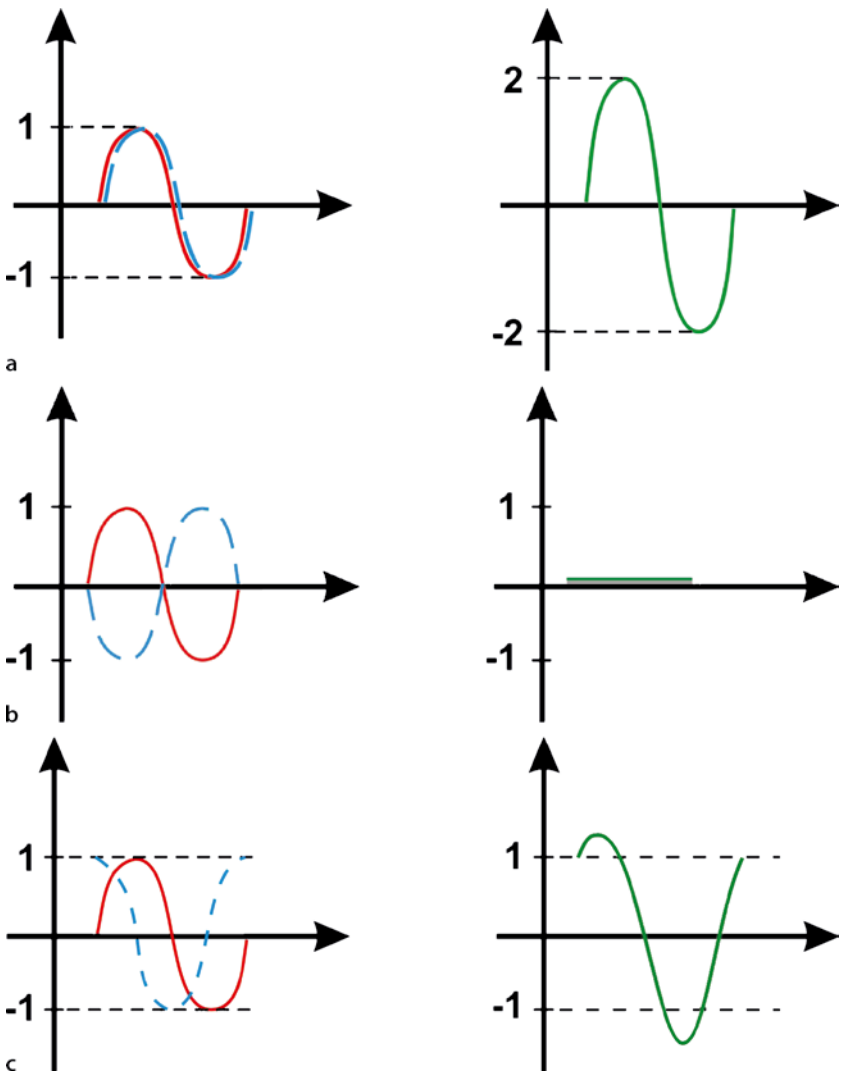

Fig. 35a–c Phase shifts and MR signal

a Completely in-phase. Composite wave with doubled amplitude

b Completely out-of-phase. Composite wave has 0 amplitude (complete cancellation)

c 90° out-of-phase. Composite wave with slightly enhanced amplitude

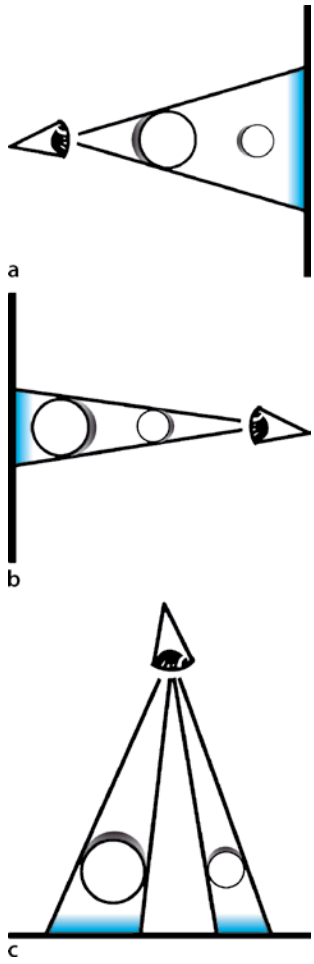

Fig. 36a–c Reconstruction of a target consisting of two unequal, closely apposed circles

Point of view **a**: the small circle is "lost" in the shadow of the large one. Thus, the projection of the object is inaccurate, composed of a single line

Point of view **b**: the two shadows are aligned and again appear as a single line

Point of view **c**: each circle casts its own shadow. Thus, from this point of view, we realize the dual nature of the target

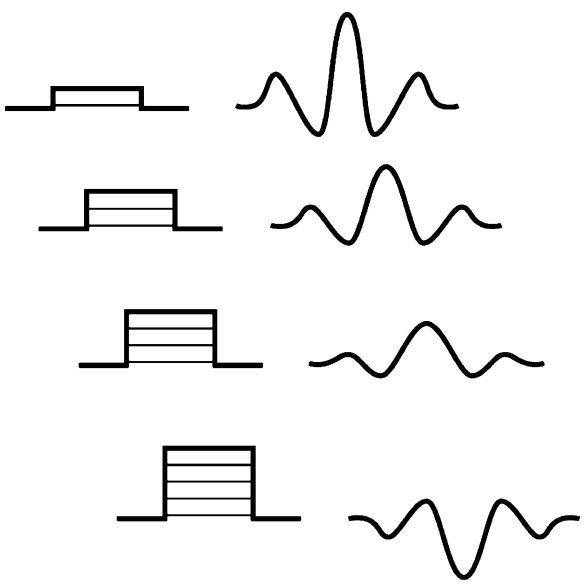

Fig. 37 Hypothetical series of MR signals with progressive step-up of the phase encoding gradient strength

17 Gradient Echo Imaging

Keywords

- Partial flip angle
- Gradient echo
- Magnetic susceptibility

Spin echo imaging suffers from long acquisition times, especially for T2 weighting. Hence, there is a need for rapid alternatives. Since imaging time is linearly related to TR, one would be tempted to compress TR for time savings. This action (everything else held constant) poses two problems: low overall signal and poor tissue contrast, since we slide leftward on the T1 curve (Fig. 38). The ingenious solution is to disengage tissue saturation and tissue contrast from the influence of TR, using excitation pulses (θ) less than 90° (partial flip angle). In this way, only a fraction of the longitudinal magnetization M_z is converted to transverse magnetization M_{xy}. A considerable portion of the macroscopic vector M is kept on the z-axis (at all times), available for successive TR cycles. A new steady state is reached, equivalent to a rightward shift of the starting point of the T1 curve, away from 0 (Fig. 39). To get a signal, we need an echo, as in SE imaging. Thus, we need a new method of realigning the spins. This time, spin refocusing is performed with gradients instead of 180° RF pulses. Specifically, we use a scheme with two lobes, of opposite polarity (Fig. 40). The initial (dephasing) limb forces the spins to move apart and the rephasing lobe brings them together, forming an echo, called a gradient echo (GE). The second lobe negates only the dephasing effects induced by the initial lobe. Thus, the decay rate is the T2* that incorporates both the intrinsic spin–spin interactions and the constant inhomogeneities of B (see Chap. 12).

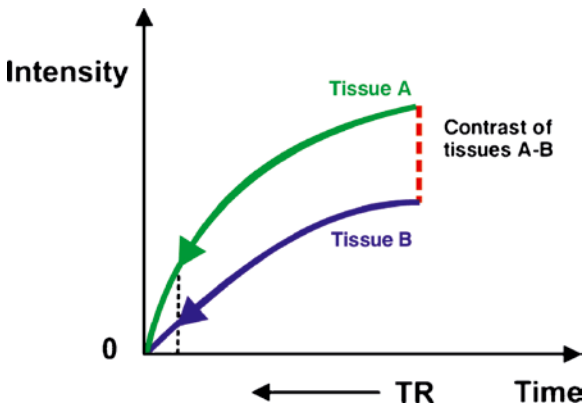

Fig. 38 Standard T1 curve. A very short TR drives the T1 curve to low contrast and low signal

In GE imaging, contrast is largely manipulated through the flip angle, θ (Figs. 41–43). Large values (70–90°) coupled with short TE (5–10 ms) result in T1-w images. A small flip angle (10–30°) disturbs M_z to a small degree; thus, M_z remains close to M_0, in the territory of spin density contrast. If we combine small θ with long TE (20–35 ms) we obtain T2*-w images. We are reminded that T2* is much shorter than T2, necessitating the use of abbreviated TE values in GE compared with SE sequences.

We will now discuss two special cases of GE imaging, arising when we prescribe very short TR values. When TR approaches the T2 rate of the tissue,

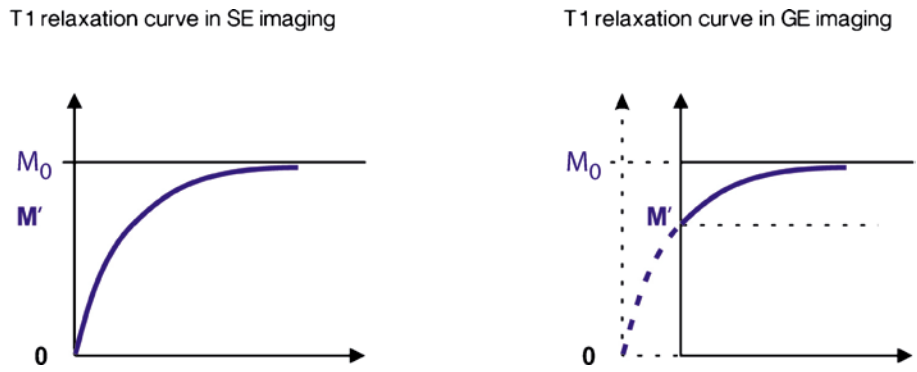

Fig. 39 New steady state in gradient echo (GE) imaging. In GE imaging, M_z does not fall to 0. Instead, T1 relaxation starts at M', shifted rightward compared with SE sequences

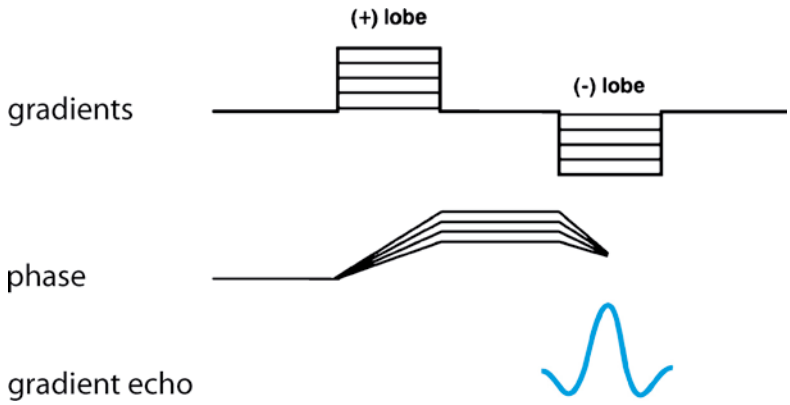

Fig. 40 Gradient echo

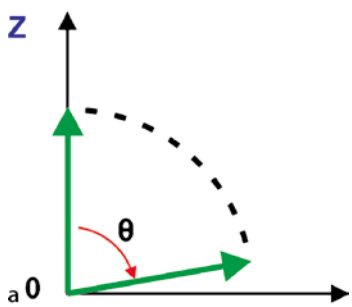

Fig. 41a,b Contrast in GE imaging

a Large θ – most of M is rotated away from the z-axis

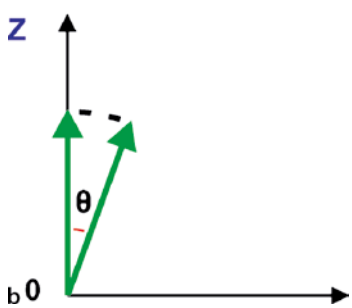

b Small θ – most of M remains faithful to the z-axis

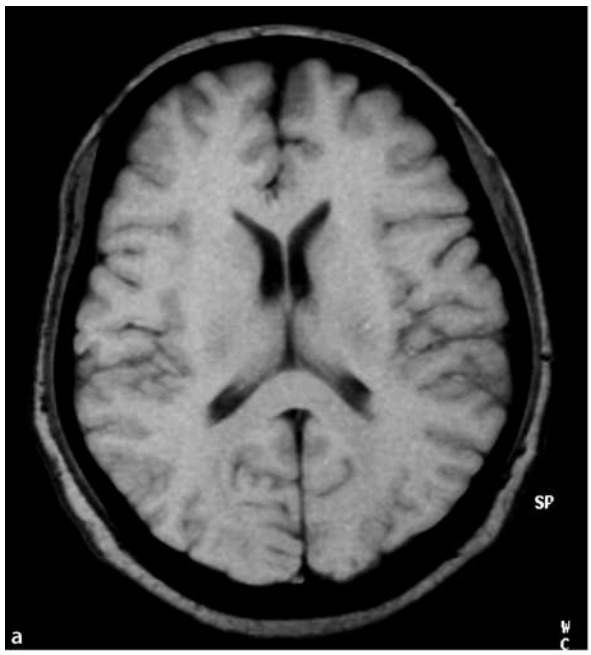

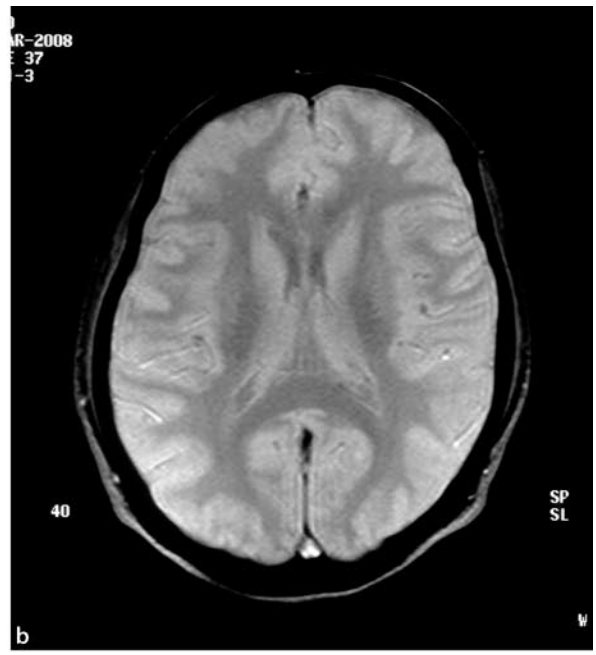

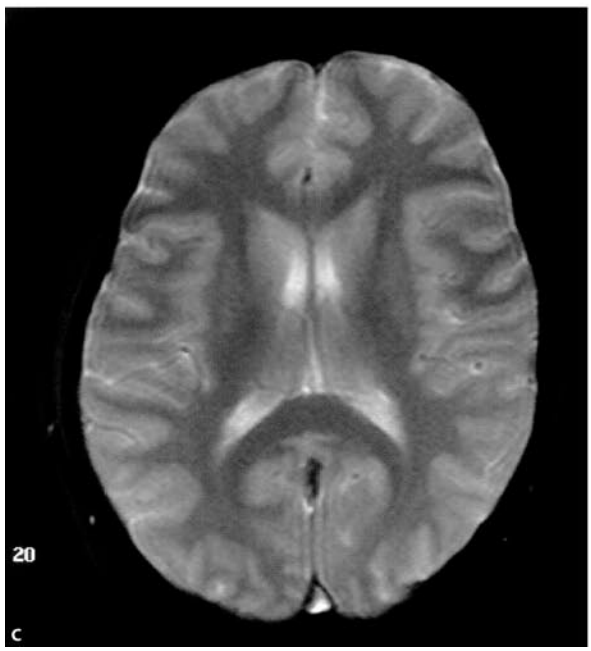

Fig. 42a–c Examples of contrast in GE imaging. **a** T1-w: TR/TE: 450/12/90°; **b** PD-w: 740/15/40°, **c** T2-w:740/35/20°. Note similarity to corresponding SE sequences (Fig. 24)

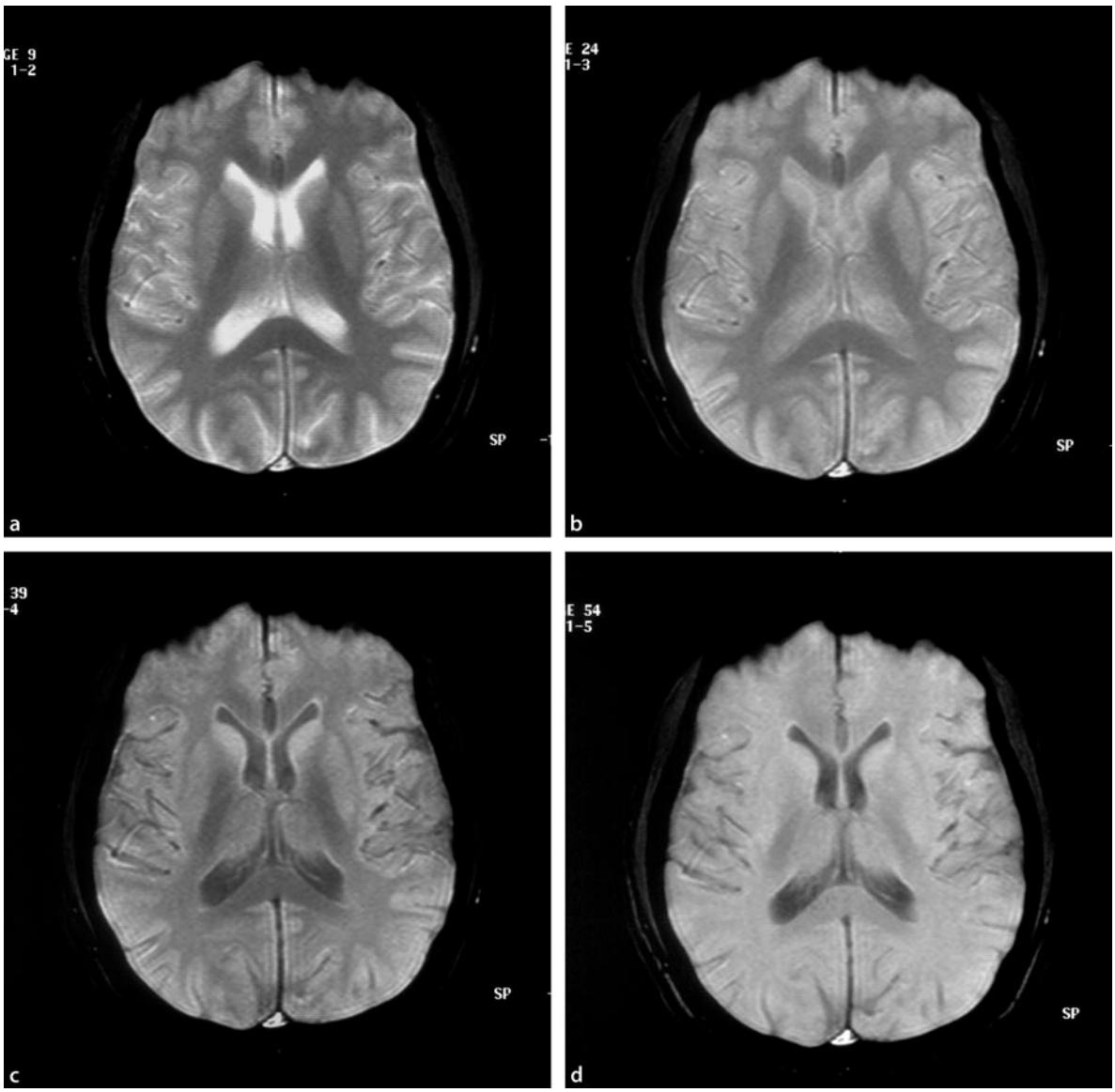

Fig. 43a–d Contrast in the gradient echo image through the manipulation of θ. Axial brain images at the same level, with the same TR/TE 700/25 and different θ, in increments of 20°:20° in **a**, 40° in **b**, 60° in **c** and 80° in **d**. Note the moderate T2 weighting in **a** despite the short TR/TE combination; this is due to the small flip angle (20°). The other images demonstrate the profound effect of flip angle upon tissue contrast. As we proceed to 80°, we move from T2 weighting to proton density and then to T1 weighting

a new excitation cycle starts before completion of the ongoing T2 decay. Thus, the new echo falls upon the residual echo of the prior TR cycle. Now we have two options: either to destroy the signal residue (after we collect the echo) or to amplify and combine the two signals. In the first case we speak of spoiled GE imaging, because we spoil or dephase any residual transverse magnetization before we embark on a fresh TR cycle. The type of contrast we get is similar to the generic GE sequences that we discussed in the preceding paragraph, independent of TR (Fig. 43). In the second situation we speak of steady-state GE imaging. Additional gradients protect the combined transverse magnetization and keep it constant (in a steady state) throughout the MR cycle. The benefit is a strong signal with significant T2 weight (Fig. 44).

Magnetic susceptibility is the reaction of any material upon exposure to an exogenous magnetic field (B). A local microscopic field, B, develops in the vicinity of the material[1], either in parallel or contrary to the main magnetic field B. In either case there is local perturbation that macroscopically looks like inhomogeneity of the main field B. These distortions become intense upon abrupt transitions in magnetic properties, setting up rapid dephasing. Examples include parenchymal tissues vs calcium or iron (in hemoglobin). Such interfaces appear as areas of low or absent signal that seem to grow with TE prolongation. This phenomenon, called "blooming," or magnetic susceptibility artifact, is much more pronounced in GE than in SE sequences (Fig. 45). This property establishes GE imaging as the preferred MR method for detecting hemorrhage (or its byproducts) and calcium.

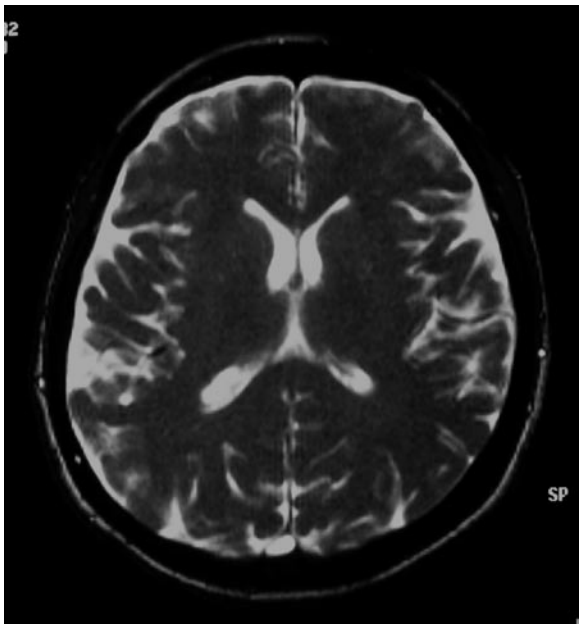

Fig. 44 Steady-state gradient echo image. Axial brain slice with TR/TE/θ: 10.2/4.7/70°. Note heavy T2 weighting despite very short TR (10.2) and very short TE (4.7)

Other major applications of GE imaging are: abdominal and chest scanning, combined with breath-holding in order to avoid artifacts from respiratory motion (Fig. 46), and cardiovascular imaging including MR angiography (MRA). The topics of blood flow and MRA are presented in Chaps. 29 and 30.

[1] Most human tissues are diamagnetic, opposing the external field B. A small number of substances reinforce the nominal B field and are called paramagnetic (e.g., gadolinium). Some compounds are ferromagnetic and become permanent magnets (e.g., iron).

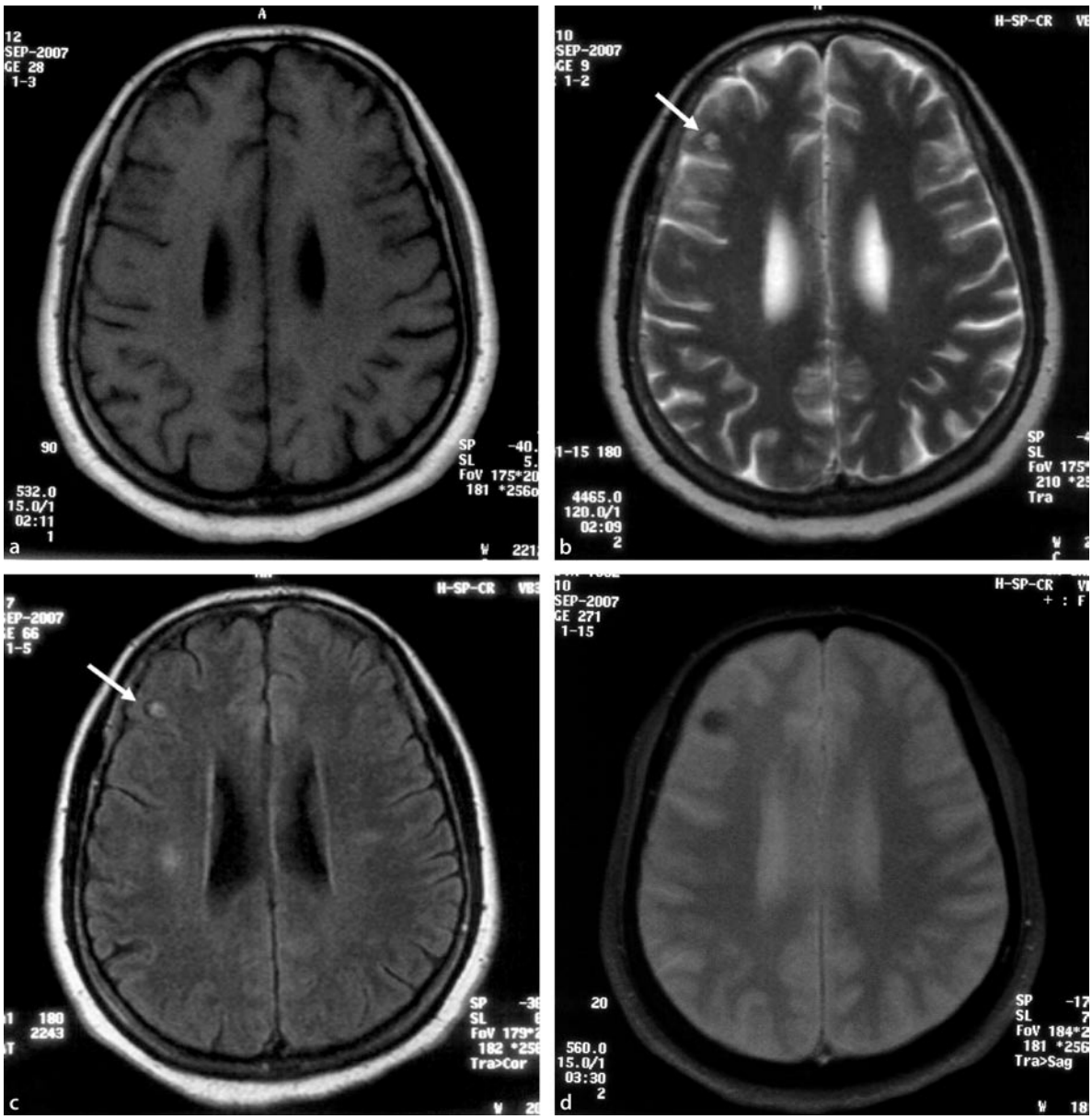

Fig. 45a–e Magnetic susceptibility artifact. Cavernoma in a 55-year-old with focal seizures. Axial **a** T1-w SE (532/15), **b** T2-w TSE (4,465/120), **c** FLAIR (7,500/2243/105), **d** PDw GE (560/15/20°) and **e** T2-w GE (560/35/20°) images. **a** Without abnormalities. **b** and **c** reveal a small hyperintense focus (0.7 cm) in the right frontal lobe (*arrows*). In **c** the outer margin appears as a thin hypointense rim. **e** *see next page*

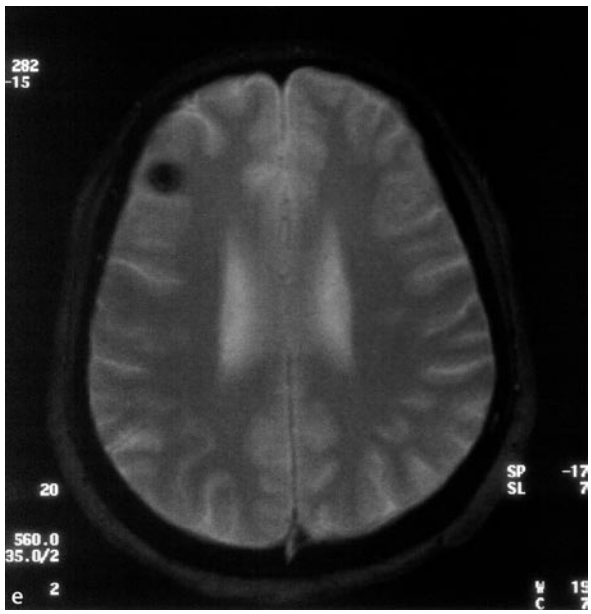

Fig. 45a–e *(continued)* In **d** and **e** the entire lesion turns "dark". Note artifactual increase in size with only a slight prolongation in TE, from 15–35 ms. Also, observe the apparent magnification of the lesion on the gradient echo compared with the spin echo images. These "blooming" phenomena are due to the hemosiderin content of the cavernoma

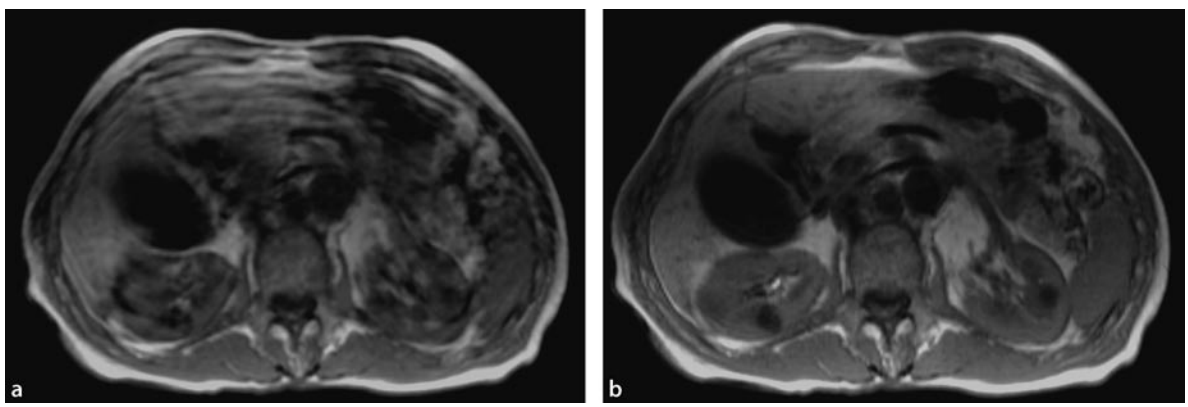

Fig. 46a,b Abdominal scanning with breath-holding. The same T1-w GE sequence (TR/TE/θ: 116/6/70°) was performed twice: **a** without and **b** with breath holding (acquisition time 17 s). Image degradation in **a** is due to respiratory motion artifact

Pulse Sequences 18

Keywords

- Pulse sequence
- Graphic display

A pulse sequence is a specific arrangement of RF bursts, gradients, and the intervening "silent" time delays. We can use symbols to represent each component of a pulse sequence (Fig. 47).

There are two major classes of pulse sequences, since there are two major ways of refocusing the echo MR signal: with RF pulses (spin echo), or with gradients (gradient echo).

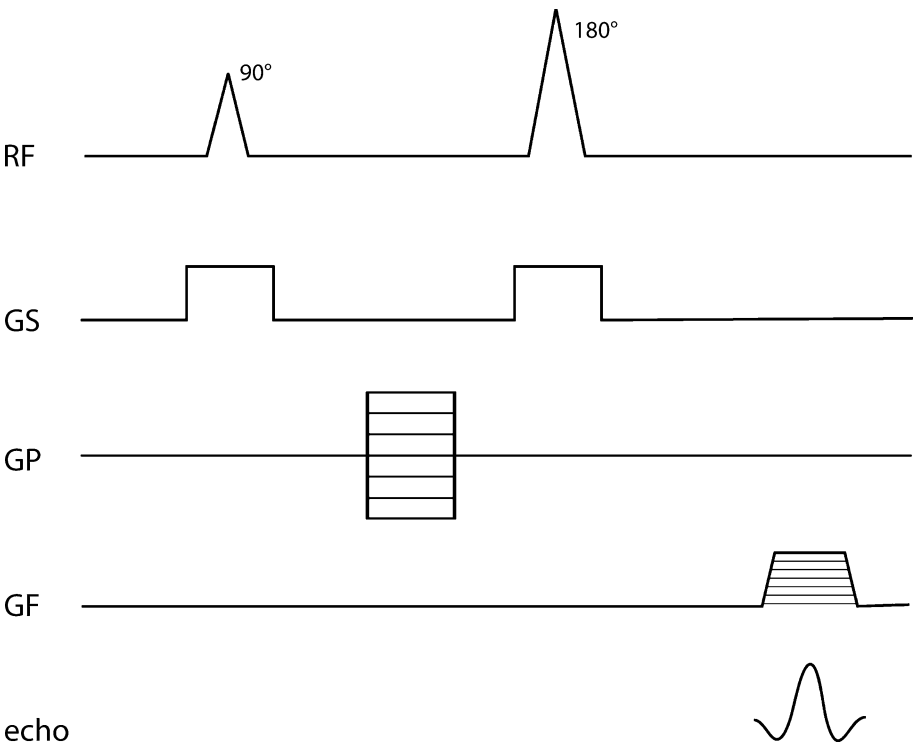

Fig. 47 Spin echo pulse sequence, graphic representation (one cycle). RF = RF pulse, GS = slice selection gradient, GP = phase encoding gradient (one value per TR cycle), GF = frequency encoding gradient, echo = spin echo

19 Fast or Turbo Spin Echo Imaging

Keywords

› Multiple spin echoes per TR cycle

Fast spin echo, or turbo spin echo (FSE or TSE), imaging is an evolution of the conventional spin echo (CSE) technique we have been discussing so far. The innovation of TSE is that it accelerates the echo acquisition without altering the excitation limb. Specifically, multiple echoes are generated per TR cycle, each one with a different value of the phase encoding gradient (Fig. 48). All echoes contribute to the contrast in the image, despite the fact that they are shifted in time and phase with respect to each other.[1] The relative weighting of each echo depends on the time distance between them (echo spacing) and the number of echoes (echo train length or turbo factor). Even though it is not intuitive, we can arrange the data in such a way as to produce the desired type of contrast (T1-w, PD-w or T2-w; Fig. 49). We can also conjugate the TSE principle to STIR and FLAIR, creating rapid sequences for fat or CSF suppression. The time saving in TSE is proportional to the turbo factor and is maximal for long TE sequences. The misbehavior of TSE sequences needs to be mentioned: the blurring of tissue edges with short/moderate TE values (Fig. 49) and the persistent hyperintensity of fat, even in heavily T2-w images (Figs. 49, 50).

There is also a class of very fast or ultrafast sequences with a variety of acronyms such as HASTE, GRASE, and EPI. Discussion of these is beyond the scope of this book.

[1] In contrast to CSE, in which we generate only one phase view per TR cycle, and all phase views are collected at the same echo time. In TSE we cannot speak of a true echo time, but of an effective echo time.

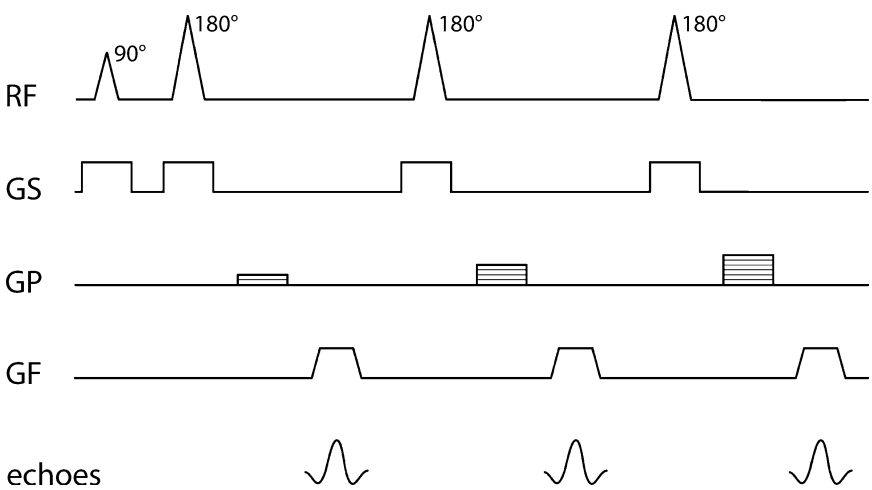

Fig. 48 Graphic representation of a TSE sequence, with three echoes in this example: RF = RF pulse, GS = slice selection gradient, GP = phase encoding gradient, GF = frequency encoding gradient, echoes = spin echoes

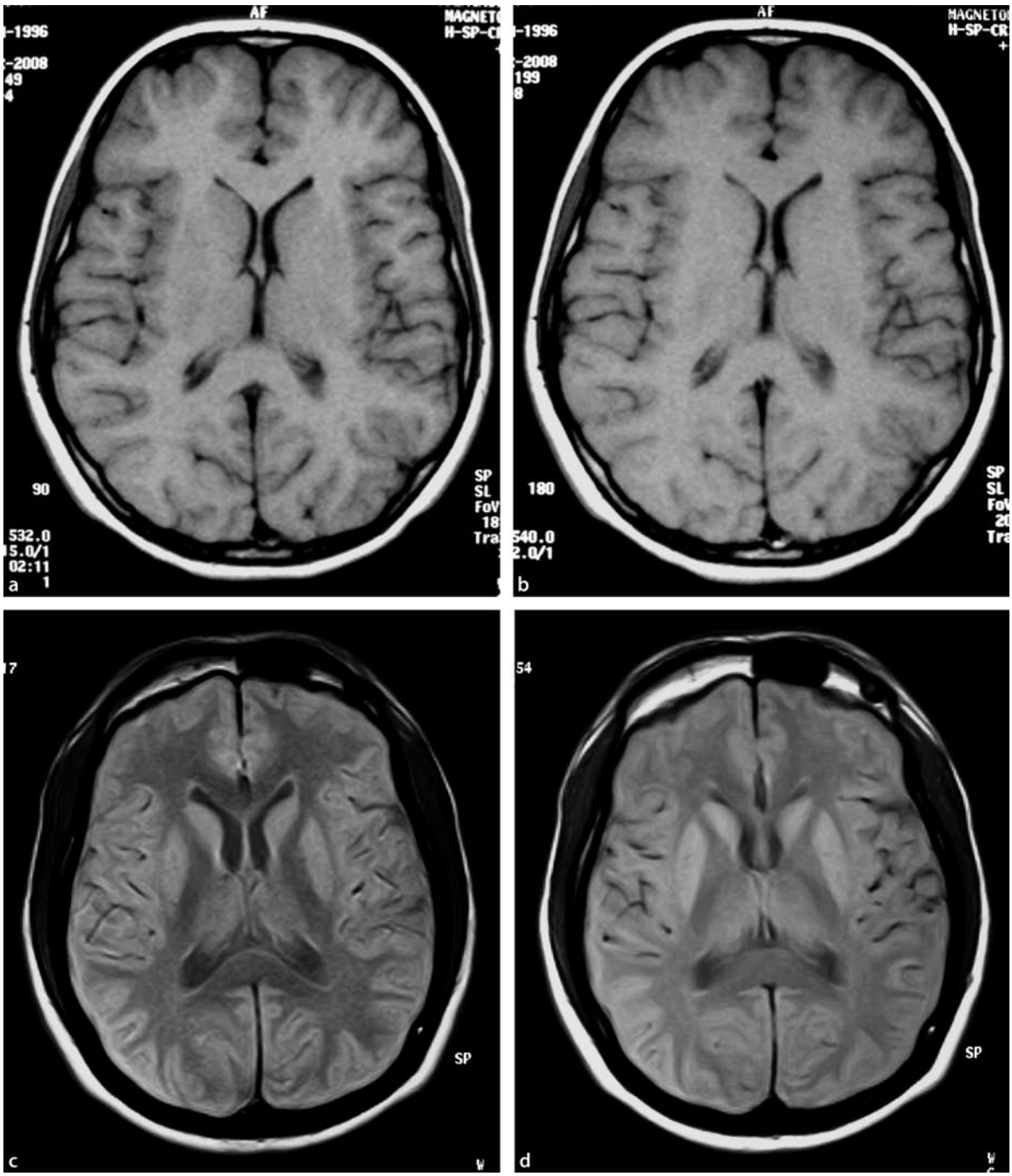

Fig. 49a–f Conventional SE vs TSE: side-by side-comparison. **a** T1-w SE (532/15), **b** T1-w TSE (540/12). Blunted gray-white differentiation and blurring of ventricular margins in **b**. **c** PD-w SE (2,200/20). **d** PD-w TSE (2,200/22). Diminished contrast between cortex and subcortical white matter, blurring of ventricular borders, and relative hyperintensity of CSF in **d**. **e**,**f** *(see next page)*

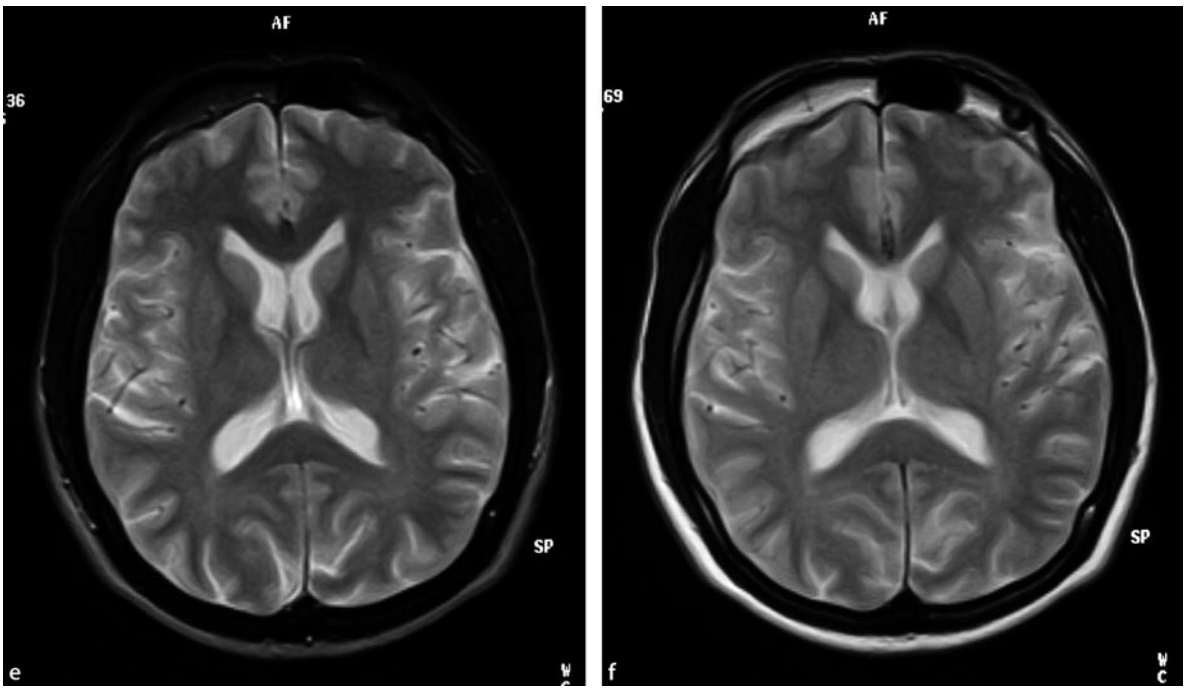

Fig. 49a–f *(continued)* **e** T2-w SE (2,200/80). **f** T2-w TSE (2,200/90). The obvious difference is the hyperintensity of marrow of the frontal bones in **f**. The ventricle–parenchyma interface is not as sharp in **f** as it is in **e**. The relative hyperintensity of gray matter in **f** is a subtle difference between the two images

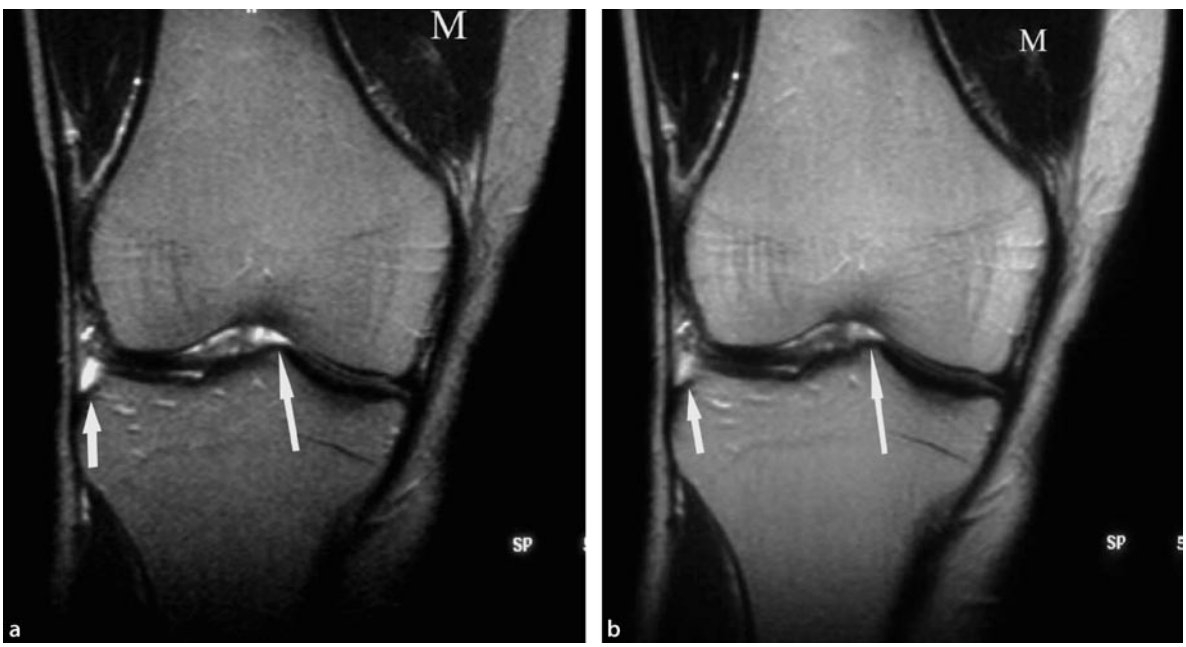

Fig. 50a,b Hyperintensity of fat in T2-w TSE sequences. A 46-year-old healthy volunteer undergoing MRI of the knee. **a** Coronal SE (2,800/90) and **b** TSE (2,800/96) images with the same slice thickness and spatial resolution. Compare the marrow and subcutaneous fat with the musculature (*M*) and with a normal quantity of joint fluid (*arrows*). The signal intensity of fat in **b** is obviously higher than that in **a**

Selective Fat Suppression 20

Keywords

- Selective fat suppression
- Fluid-sensitive sequences

Fat is a regular inhabitant of many body compartments and organs. It has high T1 and intermediate T2 signal intensity. Its presence may hinder the assessment of lesions in T2-w and of contrast enhancement in T1-w images. Thus, in many situations it would be advantageous to "eliminate" fat. We have already encountered a fat suppression method, STIR (Chap. 15). This method is not specific to fat suppression, since it inverts the longitudinal magnetization of all contents of a given slice. Thus, any tissue or process with a short T1 will be suppressed, including gadolinium enhancement and some hematomas. Selective fat suppression (SFS) relies on the Larmor principle: the precession frequencies of water protons and fat protons do not coincide, because of different local magnetic environments. Therefore, it is possible to eliminate fat and create water "weighted" images, preferably in a SE or TSE fashion (Fig. 51). Both T1-w SFS and T2-w SFS sequences are valuable. The major clinical applications of T1-w SFS are the differentiation of fatty from hemorrhagic lesions (Figs. 52, 53) and the confident demonstration of gadolinium contrast enhancement within fatty tissues (e.g., orbit, bone marrow). T2-w SFS is used to uncover or confirm edema/infiltration of fatty tissues or to highlight small amounts of fluid abutting fatty structures. This need becomes pressing in TSE imaging in which fat stays hyperintense and can obscure edema or fluid or infiltrative lesions (Figs. 54, 55).

Successful SFS requires enhanced homogeneity of the main magnetic field, B. Failure or breakdown of the homogeneity[1] of B results in poor or non-uniform SFS. In these cases, STIR becomes our reliable "water"-sensitive sequence (Fig. 56).

Selective fat suppression PD-w and T2-w sequences enjoy a stronger signal and higher spatial resolution than STIR (given the same scan time).

A by-product of T2-w SFS sequences is fluid-"weighted" images that resemble myelograms, cholangiograms, and urograms (Figs. 57, 58). We can highlight stationary fluids if we combine heavy T2 weighting with fat suppression. For a "fluid" effect, elimination of fat is mandatory in regions that contain a large amount of fat (e.g., abdomen, pelvis, spine). With prolonged TE we "burn" out the signal of the solid organs and reinforce the signal of the fluids.

---

[1] The reasons may be intrinsic to the patient or may be technical, related to the magnet. Examples of the former include asymmetric anatomy due to unilateral postoperative changes and abrupt changes in magnetic susceptibility, e.g., at the skull base, close to air-filled paranasal sinuses or close to a metallic foreign body.

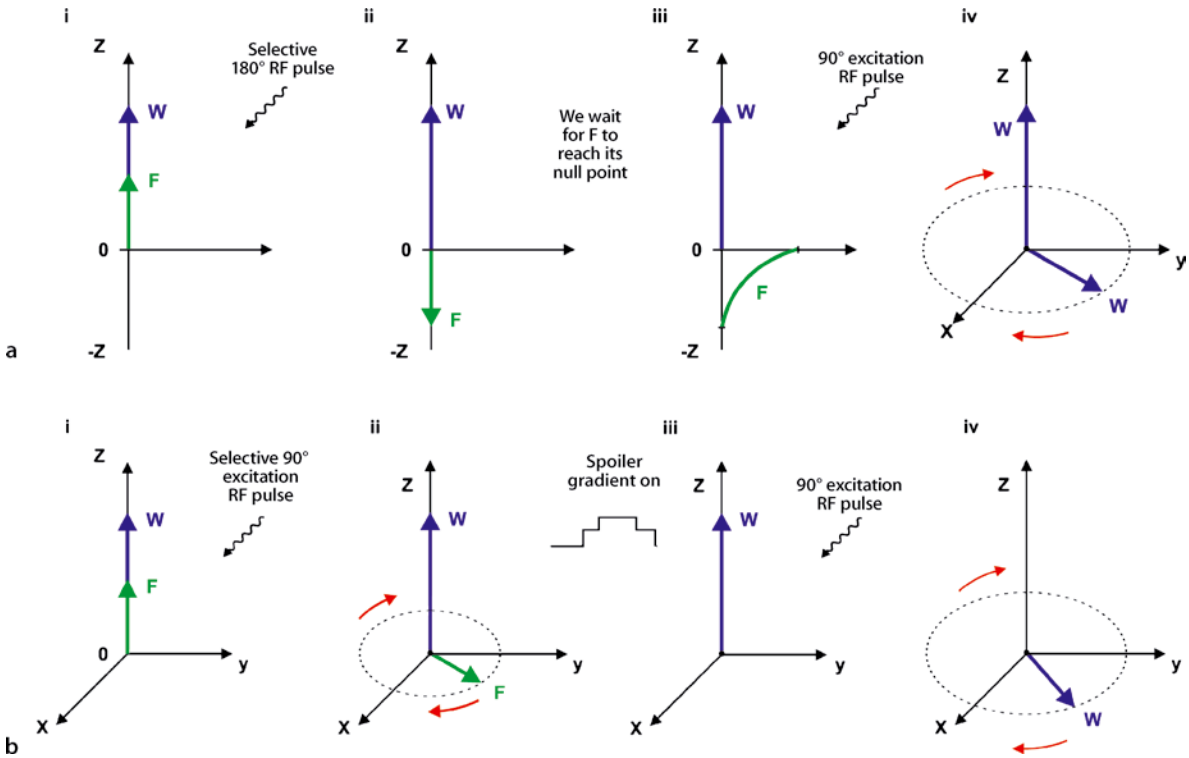

Fig. 51 Selective fat suppression. First, we want to disable the longitudinal magnetization of fat. Then we can proceed as usual with spin echo sequences (conventional or turbo). **a** Spectral presaturation with inversion recovery (SPIR). Through a selective180° pulse we invert the magnetization of fat protons and we wait until they reach their null point. Then we start our familiar spin echo sequence, because momentarily the fat protons cannot react to any excitatory pulses. Thus, only water protons show up in the images, the situation being similar to STIR (Chap. 15). **b** Selective excitation with spoiling. With a selective 90° pulse we tip the longitudinal magnetization of fat onto the xy plane and then destroy it with a spoiler gradient. Thus, only water protons are available for the upcoming pulses and only water protons give off signal

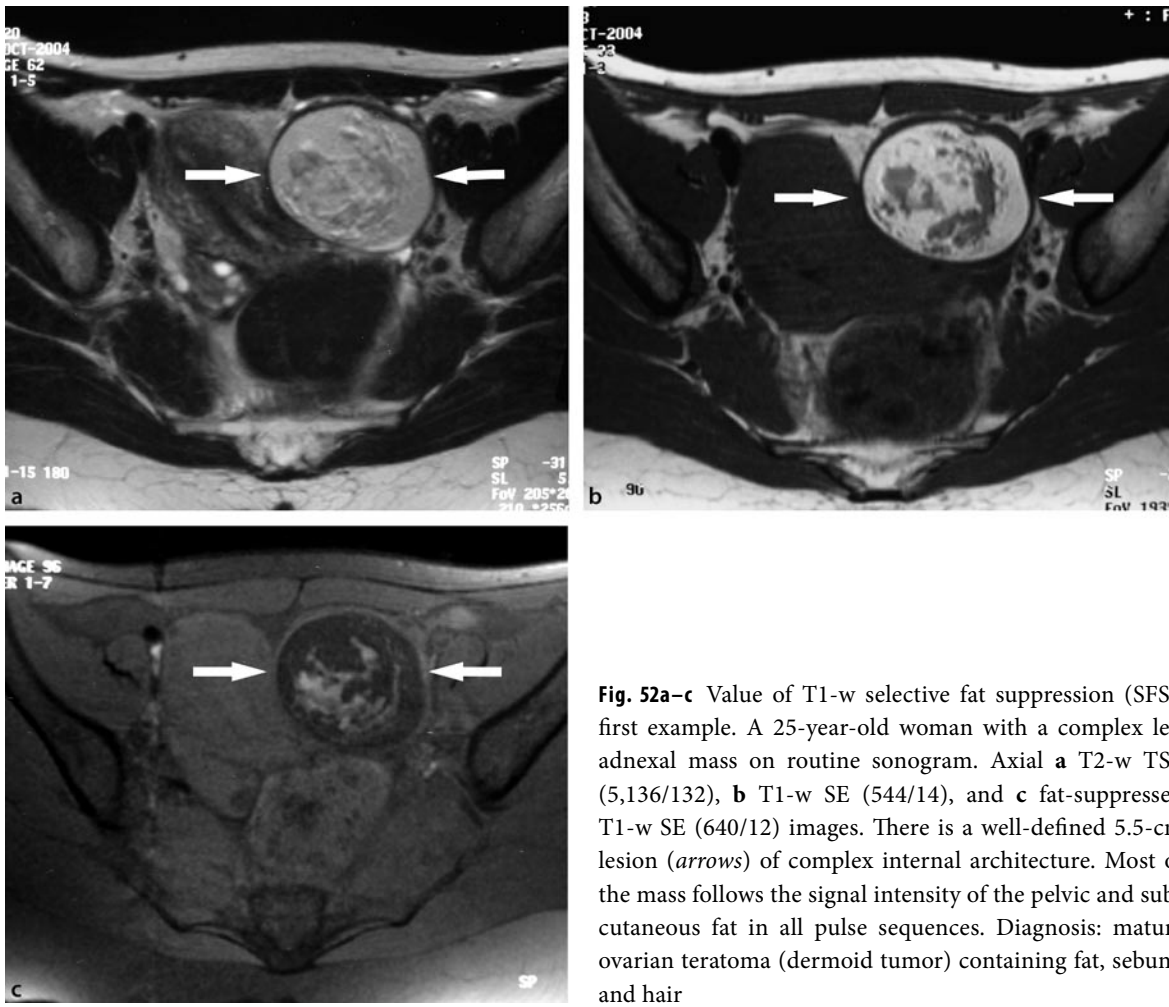

Fig. 52a–c Value of T1-w selective fat suppression (SFS): first example. A 25-year-old woman with a complex left adnexal mass on routine sonogram. Axial **a** T2-w TSE (5,136/132), **b** T1-w SE (544/14), and **c** fat-suppressed T1-w SE (640/12) images. There is a well-defined 5.5-cm lesion (*arrows*) of complex internal architecture. Most of the mass follows the signal intensity of the pelvic and subcutaneous fat in all pulse sequences. Diagnosis: mature ovarian teratoma (dermoid tumor) containing fat, sebum, and hair

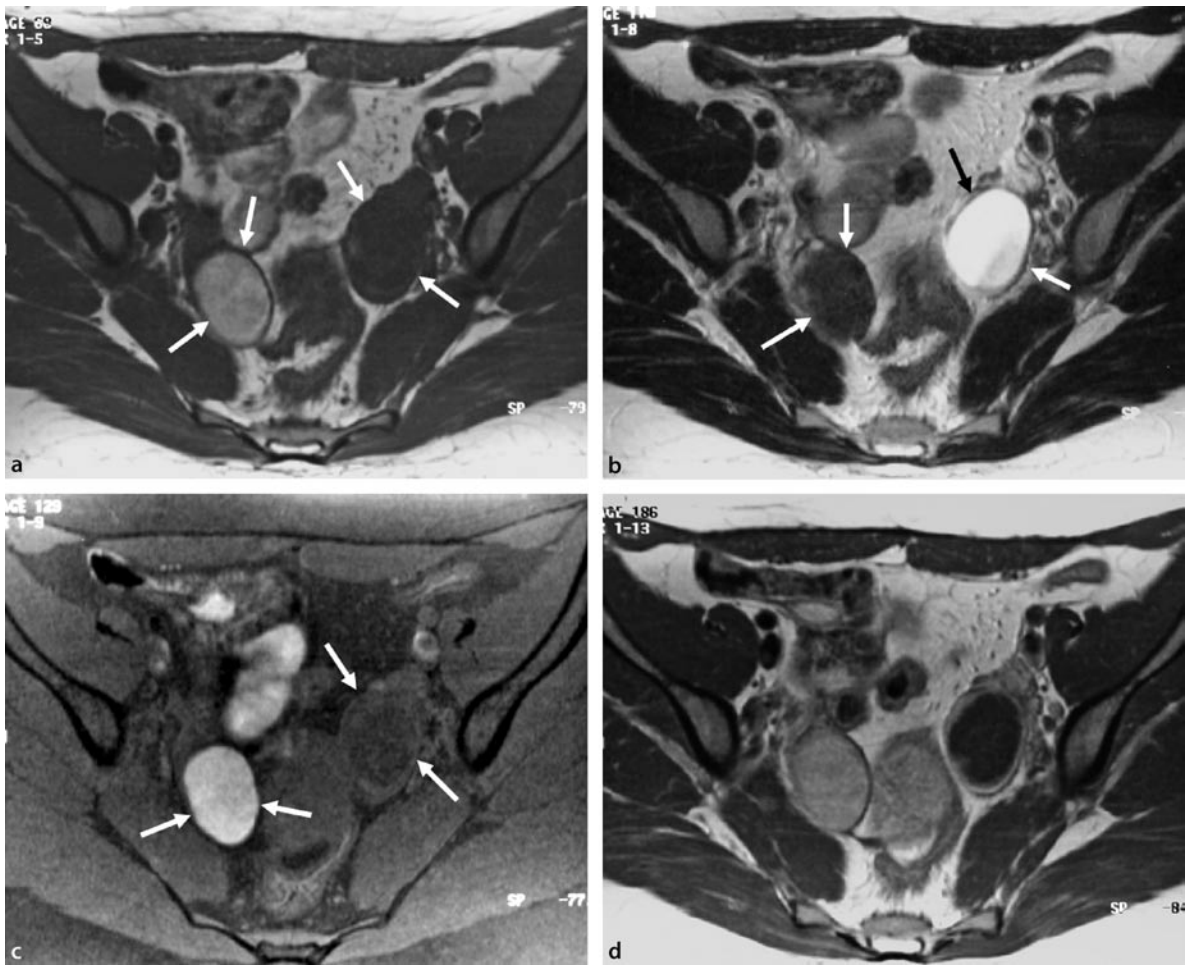

Fig. 53a–d Value of T1-w SFS: second example. A 30-year-old woman with dysmenorrhea. Transaxial **a** T1-w TSE (690/20), **b** T2-w TSE (3,870/112), **c** fat-suppressed T1-w TSE (640/12), and **d** post-contrast T1-w TSE (690/20) slices. Well-defined adnexal masses (3.5 cm in size) are present bilaterally (*arrows*). The right one has intermediate to high T1 and very low T2 signal intensity. It appears very bright after fat saturation. The left lesion is moving in the opposite direction in all pulse sequences. Note the peripheral (rim) enhancement, which is more obvious on the left-hand side. Careful comparison of **a** with **d** reveals subtle enhancement of the right-sided lesion along its anterior and right lateral margins. Diagnosis: endometriomas (hemorrhagic cysts)

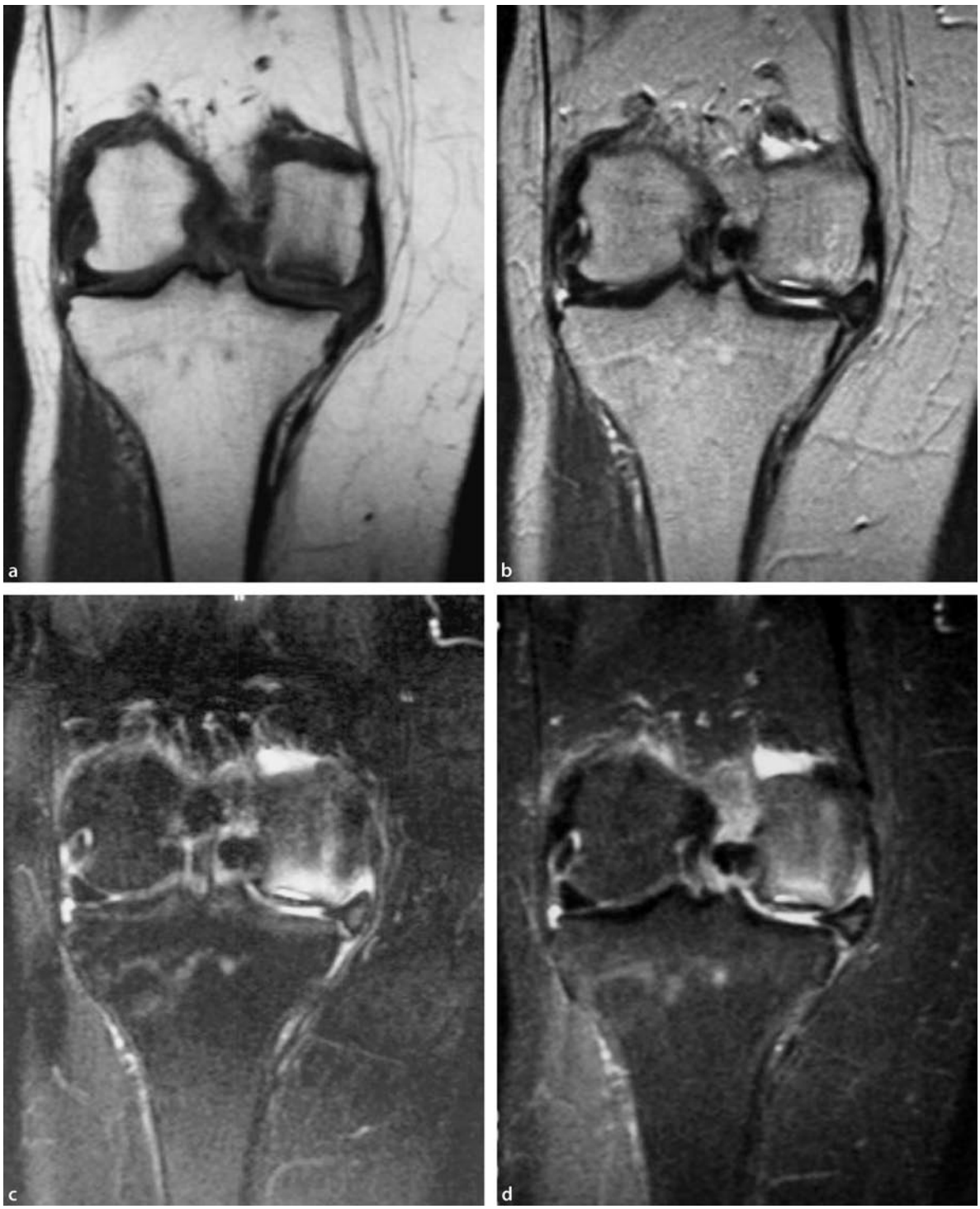

Fig. 54a–d A pitfall of T2-w TSE due to the hyperintensity of fat: bone marrow edema pattern. Avascular necrosis of the medial femoral condyle in a 60-year-old woman. Coronal **a** T1-w SE (475/15), **b** T2-w TSE (3,500/96), **c** fat-suppressed T2-w TSE (3,500/96), and **d** STIR (4,465/TI 120/30) images. The edema of the subchondral marrow is obscured in the T2-w TSE, but is obvious in the other images, especially in **c** and **d**. In this particular example, the STIR and fat-suppressed T2-w images are diagnostically equivalent

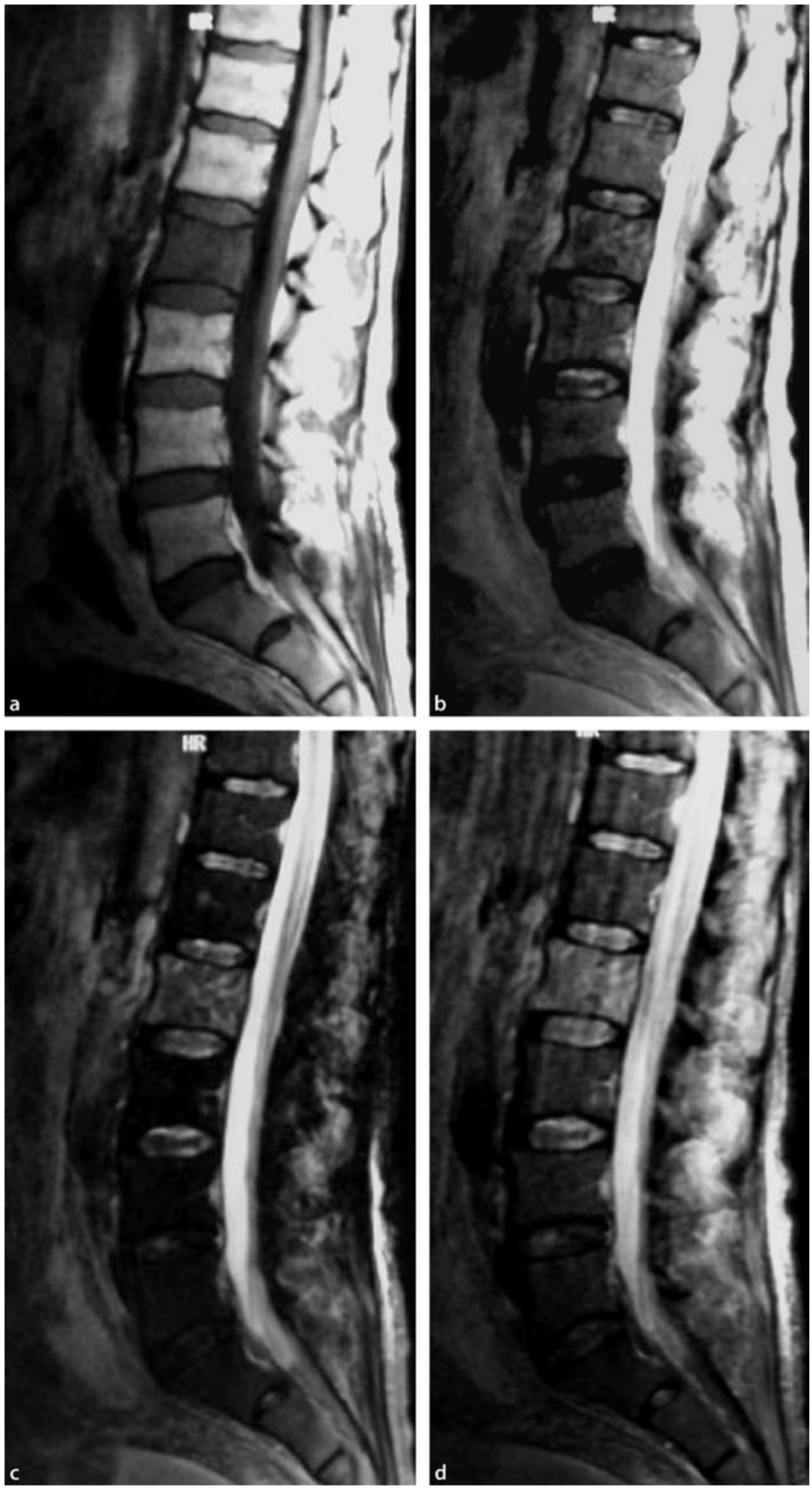

Fig. 55a–d A pitfall of the T2-w TSE method due to the hyperintensity of fat: neoplasia. Spine metastasis in a 67-year-old man with hepatocellular carcinoma. Sagittal **a** T1-w TSE (700/12), **b** T2-w TSE (4,324/112), **c** fat-suppressed T2-w TSE (4,502/112), and **d** STIR (4,000/TI 120/30) images of the lumbar spine. There is complete infiltration of the L2 vertebral body. This finding, however, is not evident in **b** because the fatty marrow is nearly isointense to the metastasis. The lesion is "unmasked" by fat suppression, in **c** and **d**. Note that the lesion is more conspicuous in STIR than in **c**, despite an unfavorable large difference in TE (30 vs 112 ms). On a computed tomography scan the metastasis was of mixed consistency, mostly lytic

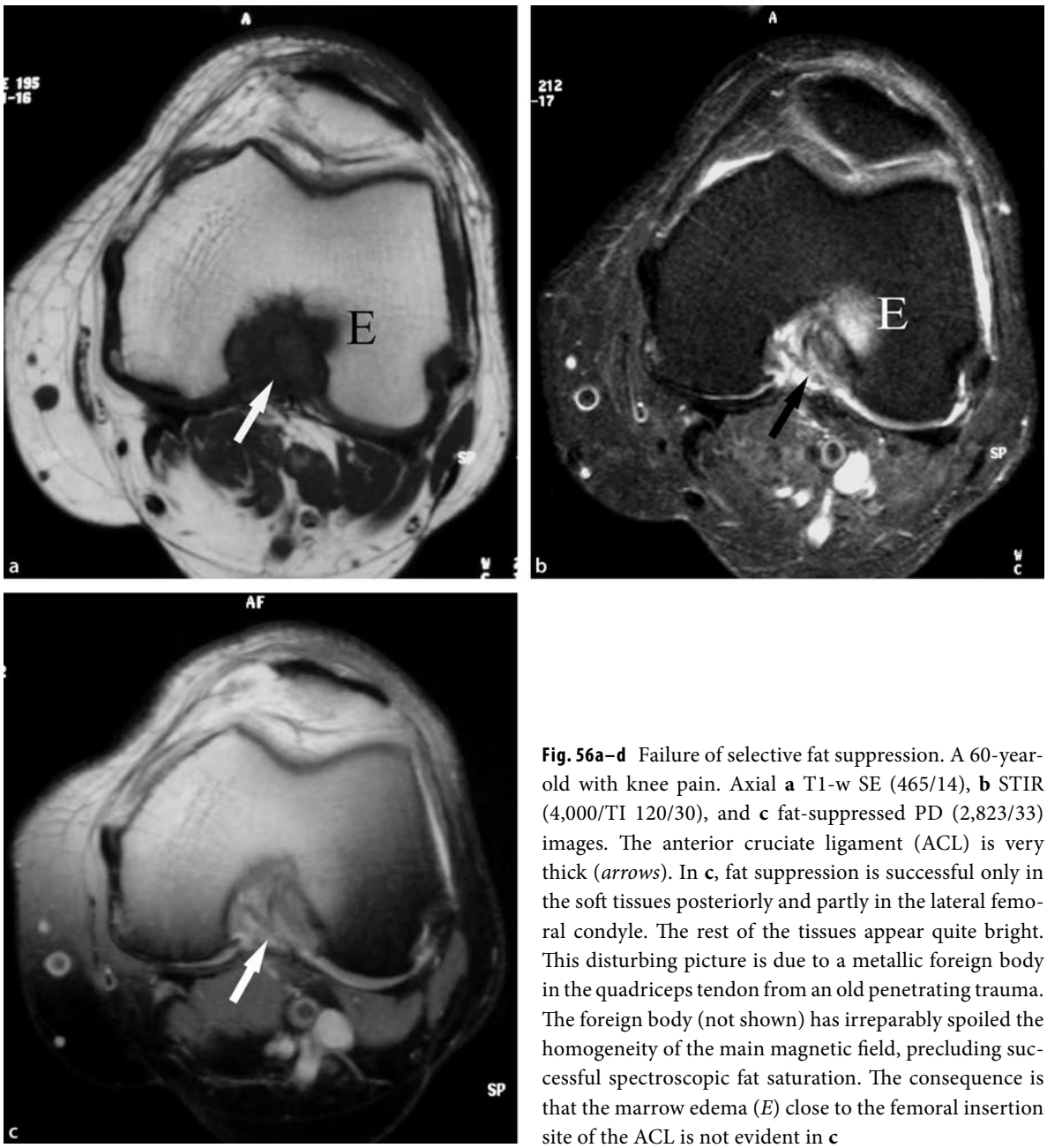

Fig. 56a–d Failure of selective fat suppression. A 60-year-old with knee pain. Axial **a** T1-w SE (465/14), **b** STIR (4,000/TI 120/30), and **c** fat-suppressed PD (2,823/33) images. The anterior cruciate ligament (ACL) is very thick (*arrows*). In **c**, fat suppression is successful only in the soft tissues posteriorly and partly in the lateral femoral condyle. The rest of the tissues appear quite bright. This disturbing picture is due to a metallic foreign body in the quadriceps tendon from an old penetrating trauma. The foreign body (not shown) has irreparably spoiled the homogeneity of the main magnetic field, precluding successful spectroscopic fat saturation. The consequence is that the marrow edema (*E*) close to the femoral insertion site of the ACL is not evident in **c**

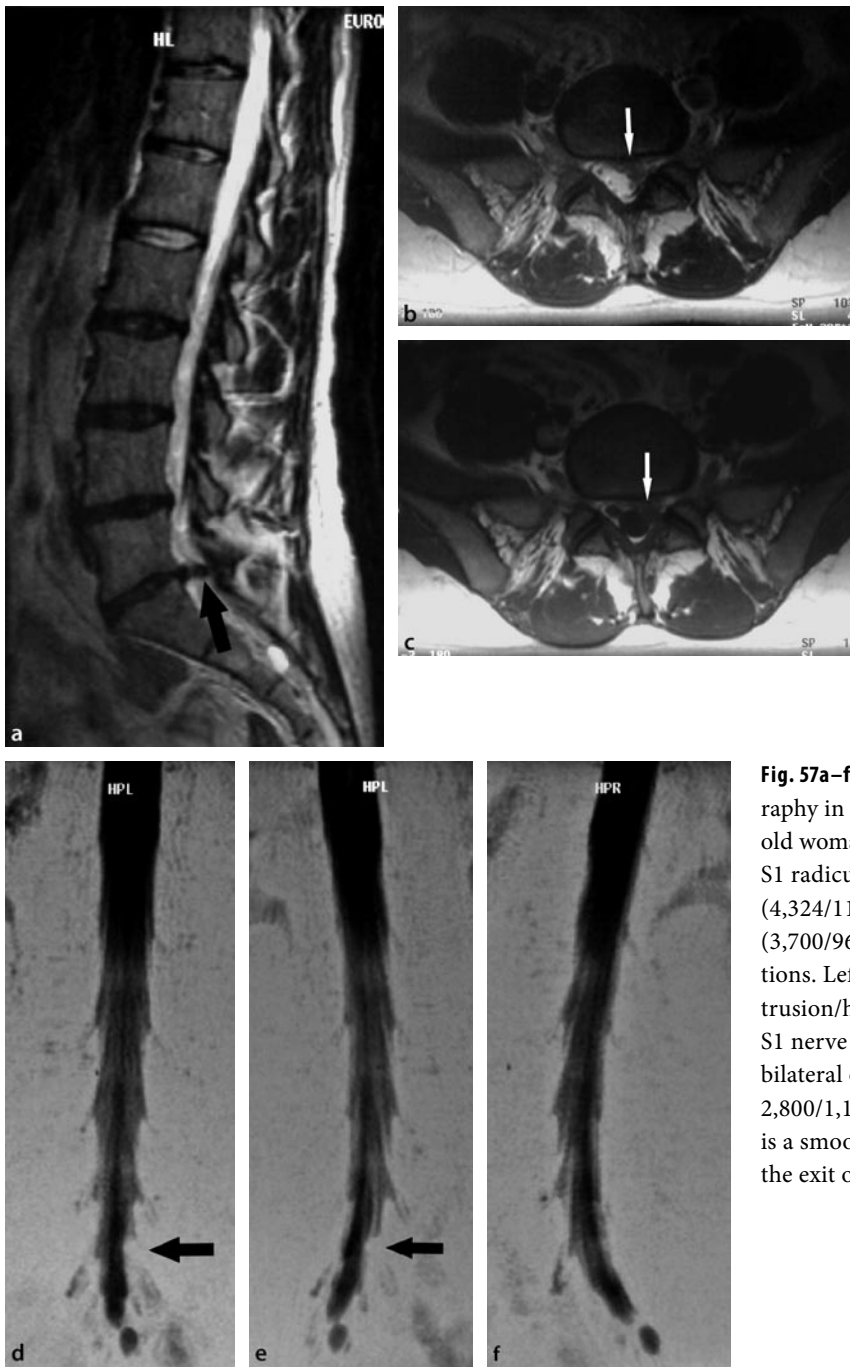

Fig. 57a–f Magnetic resonance myelography in lumbar disk disease. A 32-year-old woman with low back pain and left S1 radiculitis. **a** Parasagittal T2-w TSE (4,324/112), and **b**, **c** axial T2-w TSE (3,700/96) and T1-w TSE (800/12) sections. Left posterolateral L5–S1disk protrusion/hernia compresses the left exiting S1 nerve root (*arrows*). **d–f** Coronal and bilateral oblique MR myelograms (TR/TE 2,800/1,100 with fat suppression). There is a smooth defect of the dural column at the exit of the left S1 root (*arrows*)

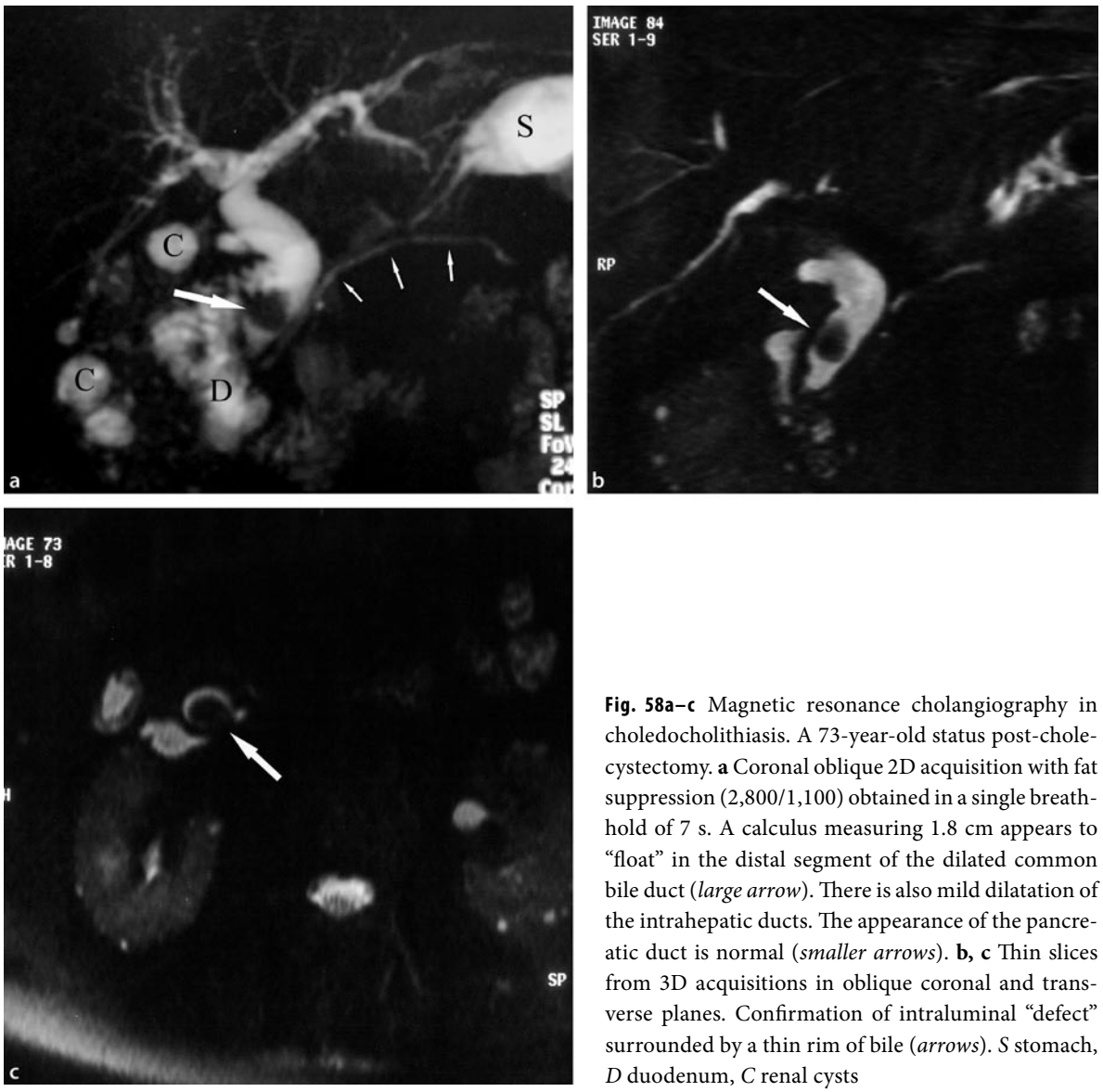

Fig. 58a–c Magnetic resonance cholangiography in choledocholithiasis. A 73-year-old status post-cholecystectomy. **a** Coronal oblique 2D acquisition with fat suppression (2,800/1,100) obtained in a single breath-hold of 7 s. A calculus measuring 1.8 cm appears to "float" in the distal segment of the dilated common bile duct (*large arrow*). There is also mild dilatation of the intrahepatic ducts. The appearance of the pancreatic duct is normal (*smaller arrows*). **b, c** Thin slices from 3D acquisitions in oblique coronal and transverse planes. Confirmation of intraluminal "defect" surrounded by a thin rim of bile (*arrows*). *S* stomach, *D* duodenum, *C* renal cysts

21 Chemical Shift Imaging

Keywords

- Chemical shift
- Protons in water vs lipids

This phenomenon is a direct consequence of the difference in the Larmor frequency between fat and water protons. Let us carry this frequency shift[1] to the transverse plane, where two magnetization vectors precess independently at their own pace. We can predict periodical overlap and opposition of the M_{xy} vectors (in phase and out of phase respectively, Figs. 59, 60). The total signal is the vector sum of the water and lipid contributions. Thus, for the out-of-phase condition there is signal loss over and above that incurred by the T2 process for each proton species. Signal dropout is significant in tissues with approximately an equal number of protons distributed in fat and water. GE sequences are suitable for chemical shift imaging, applied mainly in the abdomen and retroperitoneum (Figs. 61–63).

[1] The frequency shift at 1.5 T is 220 Hz, or 3.5 parts per million

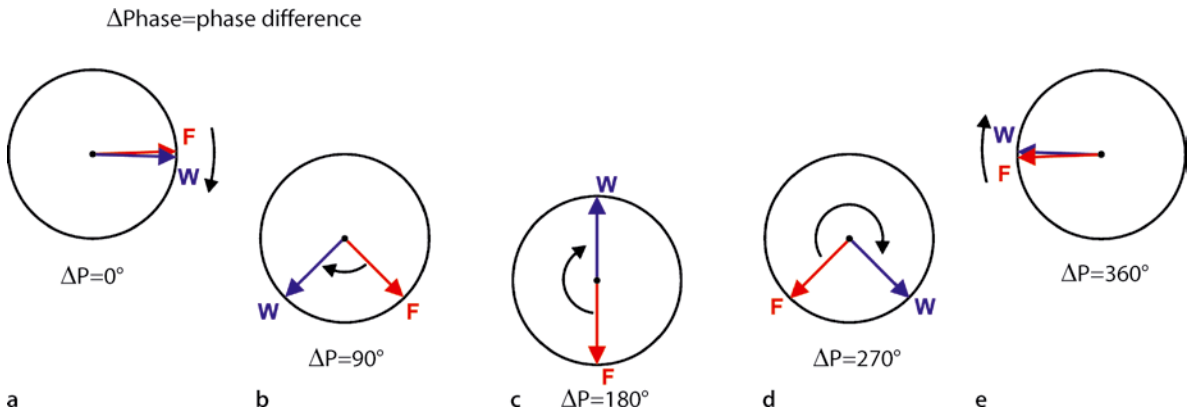

Fig. 59 **a–e** Signal loss due to chemical shift. ΔPhase = phase difference. Both types of protons (water and lipid) are excited simultaneously with a non-selective RF pulse. The transverse magnetization components rotate at their inherent speed. These vectors start in phase, but subsequently diverge and go through repetitive destructive and constructive interference (vector subtraction and addition respectively). The summation vector thus cycles between maxima and minima at regular and specific time intervals

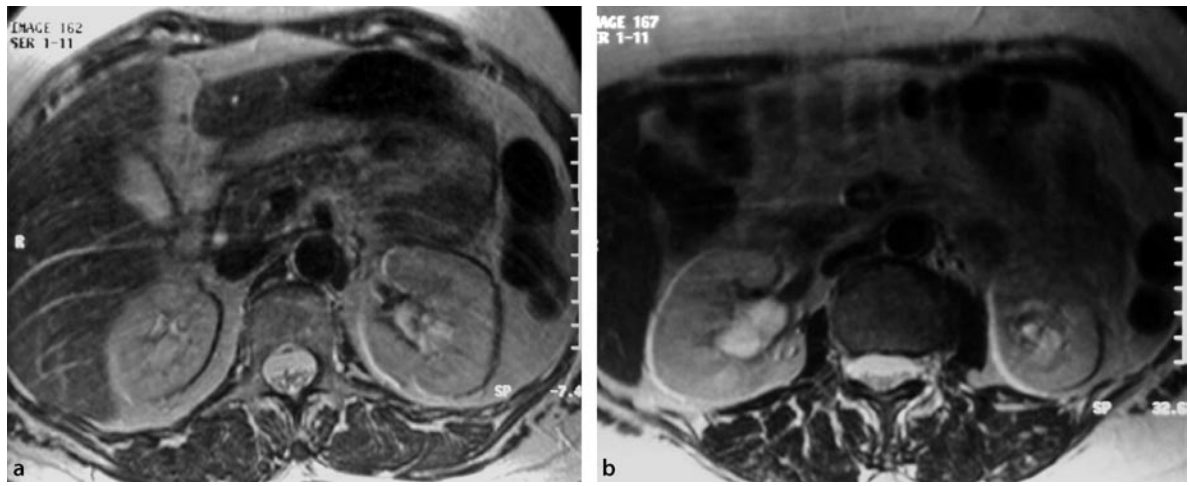

Fig. 60a,b Chemical shift artifact. Normal study of the abdomen. **a**, **b** Axial T2-w TSE (3,400/96) slices. Observe the lateral borders of the kidneys: they appear dark on their left side and bright on their right side. This is due to signal cancellation and addition respectively at interfaces of "watery" vs fatty structures (kidneys vs perirenal fat)

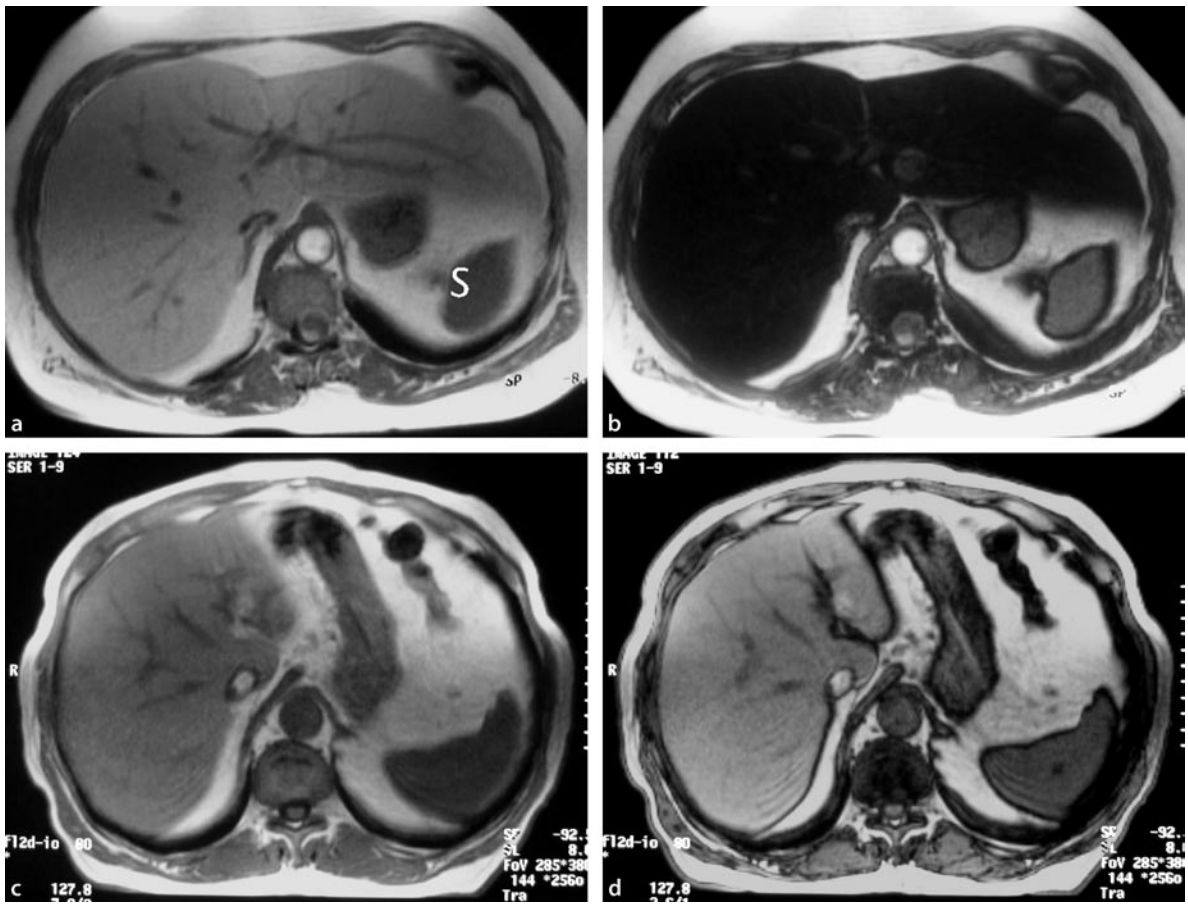

Fig. 61a–d Chemical shift in liver imaging. A 72-year-old woman with elevated liver enzymes. **a** and **b** T1-w GE images in and out of phase respectively (150/3.6; 7.2/80°). Compare the liver with the spleen (*S*). The liver is hyperintense in **a** with a dramatic loss of signal in **b** consistent with marked fatty infiltration. **c**, **d** Compare with normal appearing liver in a healthy 70-year-old. These sequences were obtained with the same parameters as those in **a** and **b**. Note hypointensity and accentuation of the liver–fat and splenic–fat interfaces in **d**. This phenomenon is called the "India ink" artifact

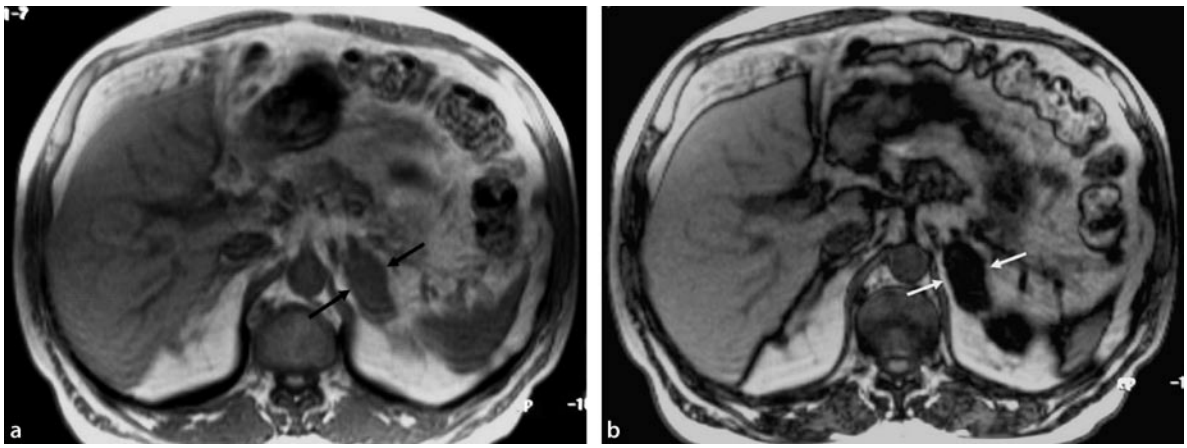

Fig. 62a,b Chemical shift in adrenal imaging: example 1. A 62-year-old with malignant hypertension. **a**, **b** a pair of in- and out-of-phase T1-w GE images (150/3.6; 7.2/80°). There is a well-defined 4.2-cm mass in the left adrenal gland (*arrows*) with marked signal drop in the second echo. Diagnosis: adrenal adenoma (lipid-rich)

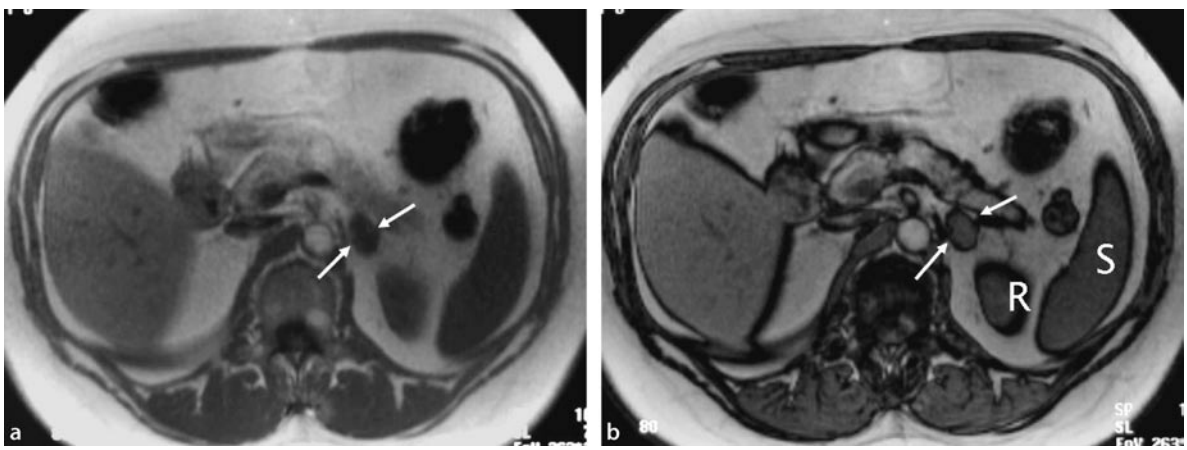

Fig. 63a,b Chemical shift in adrenal imaging: example 2. A 50-year-old with an adrenal tumor discovered incidentally during a CT scan of the lumbar spine. **a, b** A pair of in opposed-phase images (150/3.6; 7.2/80°). An ovoid, 2.3-cm solid mass arises from the left adrenal gland (*arrows*). With respect to signal intensity the mass stays close to the renal cortex and to the spleen in both echoes. Diagnosis: myelolipoma with very low fat content

22 Magnetization Transfer Contrast

Keywords

- Free (bulk) water vs loosely bound or hydration layer
- Transfer of longitudinal magnetization

Water molecules exist either free or loosely attached to macromolecules, the two populations maintaining an equilibrium (Fig. 64). Water in hydration layers is not visible by current MRI due to extremely rapid T2 decay: the emitted signal is so short-lived that current echo times are too long to detect it. Thus, if we affect the magnetization of either pool we will affect the total signal. We can temporarily inactivate the bound fraction with saturation pulses. Some of these water molecules will jump free and displace an equal number of molecules to the bound compartment. The effect is the reduction of active spins in the free pool and thus attenuation of the final signal (Fig. 65).

This type of contrast is called magnetization transfer contrast (MTC), since it results from the exchange of water molecules (and their signal ability) between the free and the bound compartments. It is evident that magnetization transfer (MT) is not applicable to pure tissues such as fat or CSF. Brain white and gray matter differ in their relative water, lipid, and protein content, and thus have different susceptibility to MT pulses (Fig. 66). In routine practice, MTC is used primarily as an additional method of background suppression to "reinforce" either contrast enhancement in T1-w sequences or the blood signal in MR angiography (Figs. 67, 68).

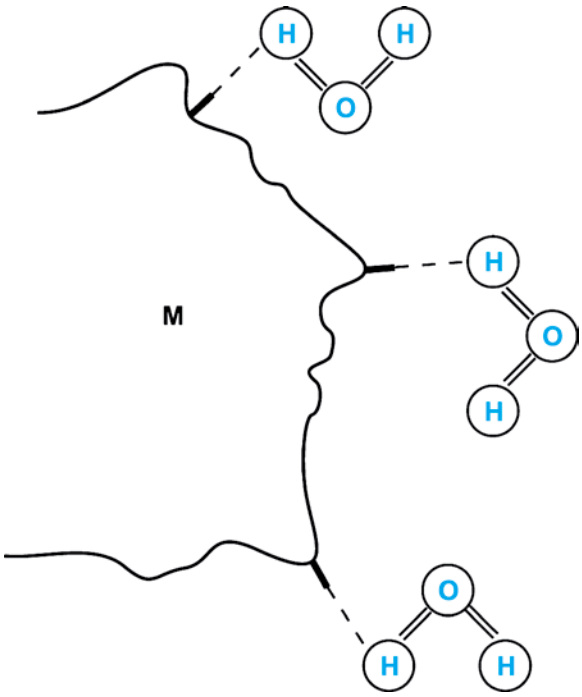

Fig. 64 Hydration layer. Weak electrostatic forces attract water molecules close to the surface of the macromolecules, DNA, and other cellular constituents, forming a water "cloak" of variable thickness (called the hydration layer). The free and bound members can easily trade places, carrying over their current magnetization to the new site

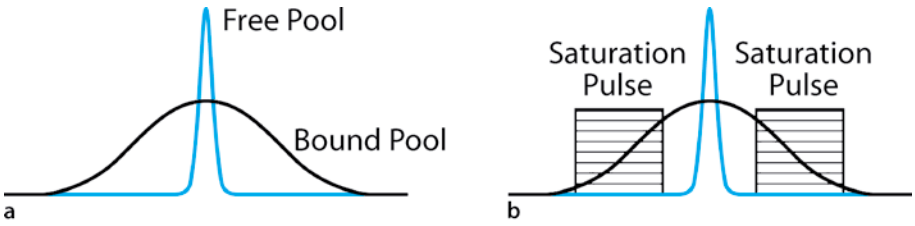

Fig. 65a,b Mechanism of magnetization transfer contrast (MTC). **a** The resonance frequency of free water is a sharp tall spike. The bound pool has a broad distribution around the central peak. **b** With appropriate pulses on either side of the central peak, we affect only the bound component. **c** The result is a reduction of the longitudinal magnetization of the free pool. Thus, the maximum signal of the affected tissue is also reduced

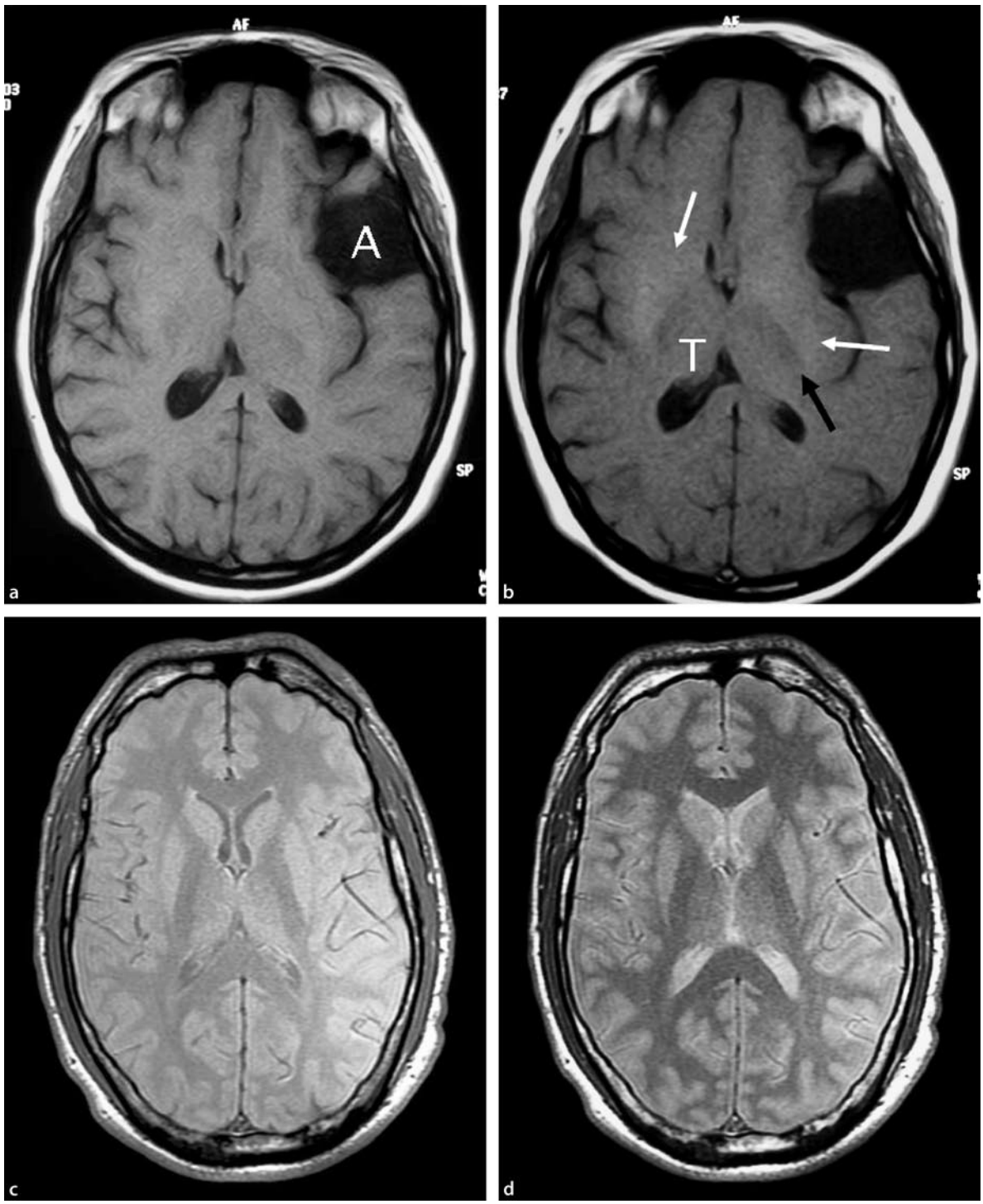
A
T
a
b
c
d

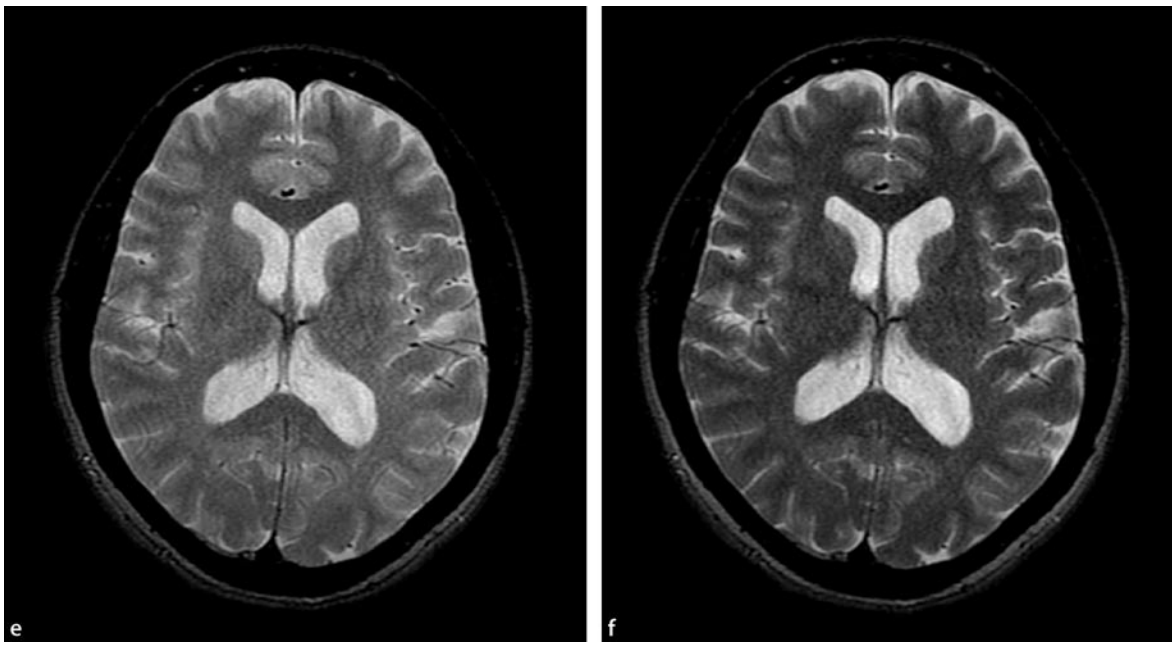

Fig. 66a–f Effect of MT pulses on brain parenchyma. T1-w images from **a** a standard sequence and **b** after application of MT pulses. Spatial resolution, TR and TE (532/15) are the same in **a** and **b**. In **b** note the overall decrease in signal intensity and greater suppression of the white matter: the signal intensity of the white matter and cortical gray matter have become similar in the paramedian frontal areas. Note the hyperintensity of the thalami (*T*) and the basal ganglia (*white arrows*) relative to the internal capsules (*black arrow*). Incidentally, an arachnoid cyst is present in the left temporal area (*A*). **c**, **d** A pair of PD images (TR/TE: 1,750/25) from a healthy volunteer, before and after MT pulses (at 1.5 T). Note relative hyperintensity of CSF and greater suppression of the signal of the white matter after application of MT pulses in **d**. **e**, **f** A pair of T2-w images (TR/TE: 2,500/85) from another patient, before and after MT pulses (at 1.5 T). There is a mild decrease in signal intensity of the white matter in **f**. Slides **c–f** are courtesy of A. Giakoumelos, MPhil, and C. Carounis, GE Medical Systems

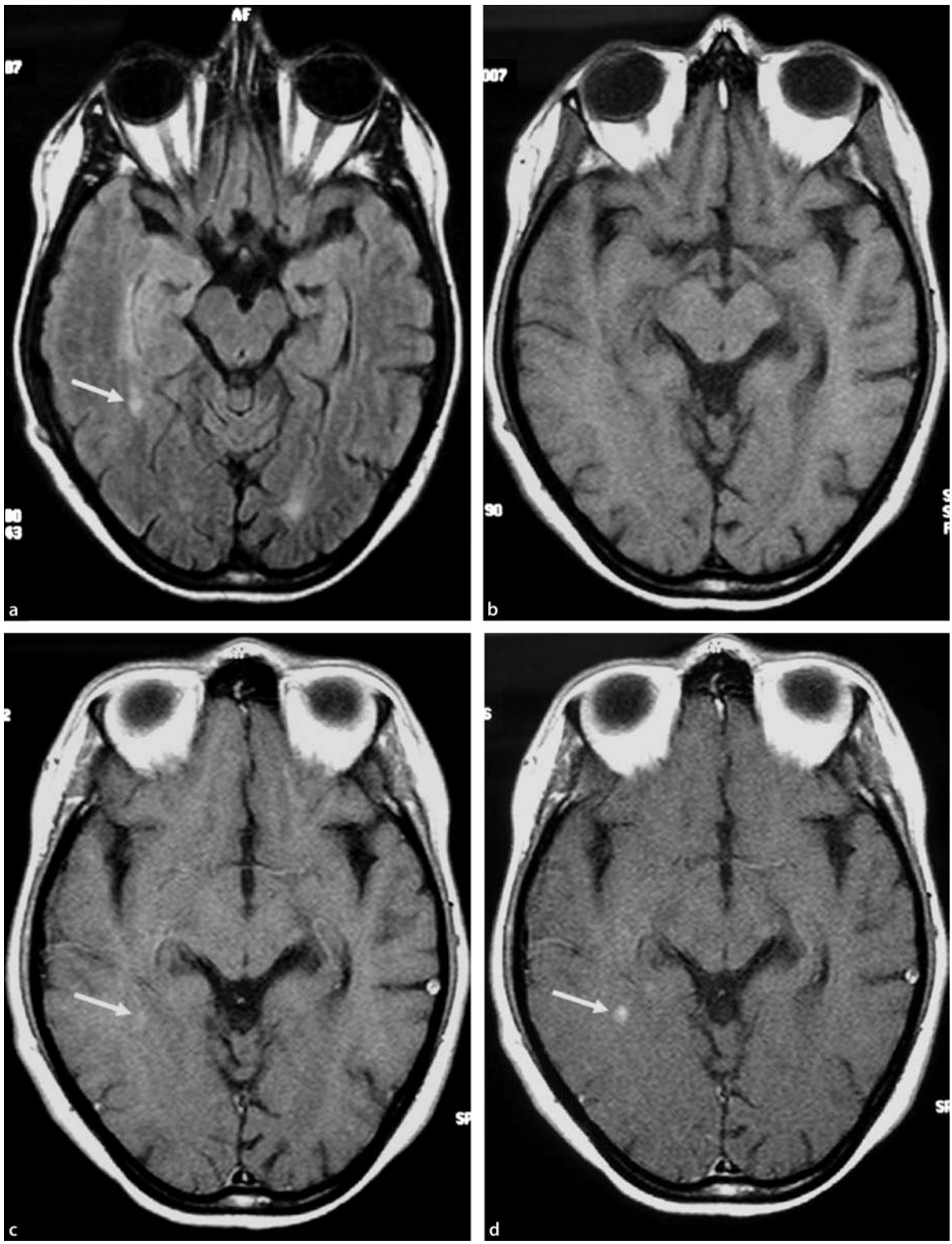
a
b
c
d

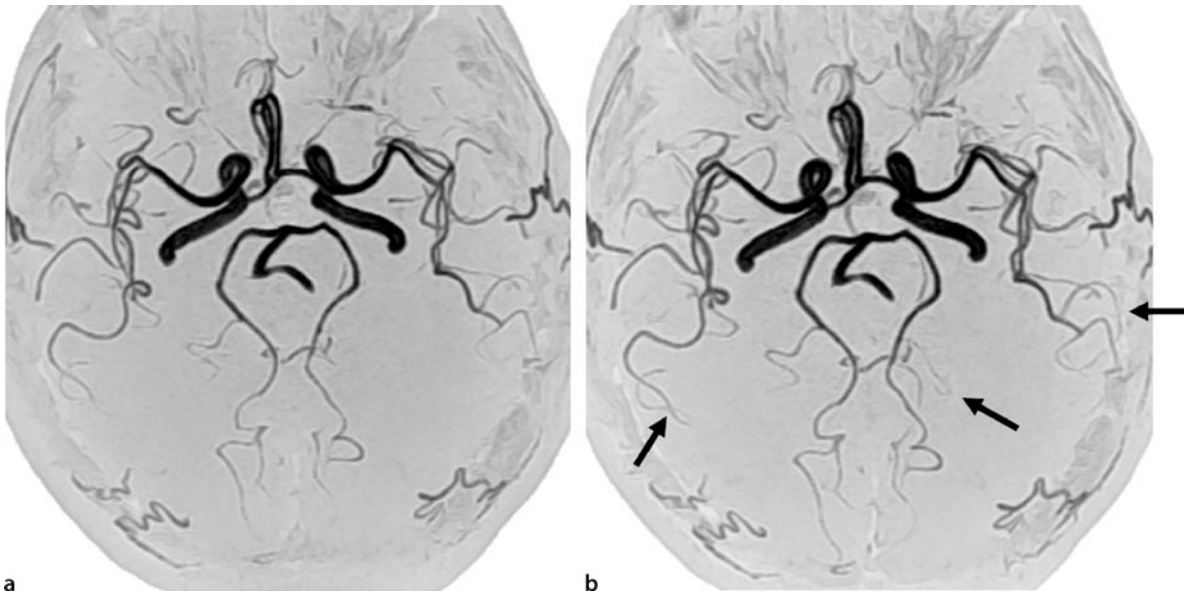

Fig. 68a,b Improvement in inflow MR arteriography (MRA) with MT pulses. Composite (reconstructed) cranial MRA (23/2.7/20°) images in a healthy 40-year-old, **a** without and **b** with MT pulses. In **b** there is better delineation of peripheral branches (*arrows*). Case courtesy of A. Giakoumelos, MPhil, and C. Carounis, GE Medical Systems

◂ **Fig. 67a–d** Value of MT in contrast-enhanced studies. A 38-year-old woman with multiple sclerosis. **a** Axial FLAIR (7,500/TI 2,243/105) and **b** T1-w SE (532/15) images. Following contrast injection, the T1-w sequence was repeated **c** without and **d** with MT pulses (with the same TR/TE and the same spatial resolution). The enhancement of the small plaque close to the temporal horn (*arrows*) is subtle in **c** but definite in **d**

23 Diffusion

Keywords

- Random motion
- Diffusion
- Isotropy
- Anisotropy

So far we have discussed phenomena and MR sequences related to magnetic interactions of spins. We will now consider the effect of molecular (curvi)linear motion on the final echo signal. We distinguish between two types of translational motion, flow and diffusion. Flow is defined as macroscopic motion driven by differences in pressure and will be explored in Chap. 29.

Diffusion is translation on a microscopic scale with frequent changes in direction due to collisions of mobile molecules among themselves or against rigid barriers (e.g., cell wall membranes reinforced with myelin sheaths). Our discussion will be limited to water as the most suitable molecule for clinical MR. Let us consider two water molecules diffusing through a gradient. Soon their paths diverge and they experience slightly different magnetic fields with the corresponding effect upon the precession frequencies and relative phase (Fig. 69). The phase shifts diminish the magnitude of the final echo to a degree that depends on the number, strength and duration of the gradients. These losses occur over and above the phase shifts we have discussed previously (see Chap. 12 on the T2 or T2* decay rate). We can perform two experiments: one with and one without diffusion labeling gradients. If we compare the two echoes we can eliminate the contribution of the stationary spins. In this way we encounter a new type of contrast, called diffusion-weighted, that is independent of T1, T2, and spin density.

If water is free to diffuse in any direction (isotropy), then its random path is contained within a sphere, the radius of which increases with time (Figs. 70, 71). Intracellular water may be constrained by cellular type and geometry. For example, myelinated nerves permit easy diffusion in the longitudinal axis of the fiber and restrict diffusion in any perpendicular direction. Since diffusion may be anisotropic (Fig. 72) we can query the preferred direction of diffusion by activating the appropriate gradients in different axes (Fig. 73). Established uses of diffusion imaging cover all aspects of brain pathology (Figs. 74–76). Perhaps the most important use is in the early detection of ischemic stroke.

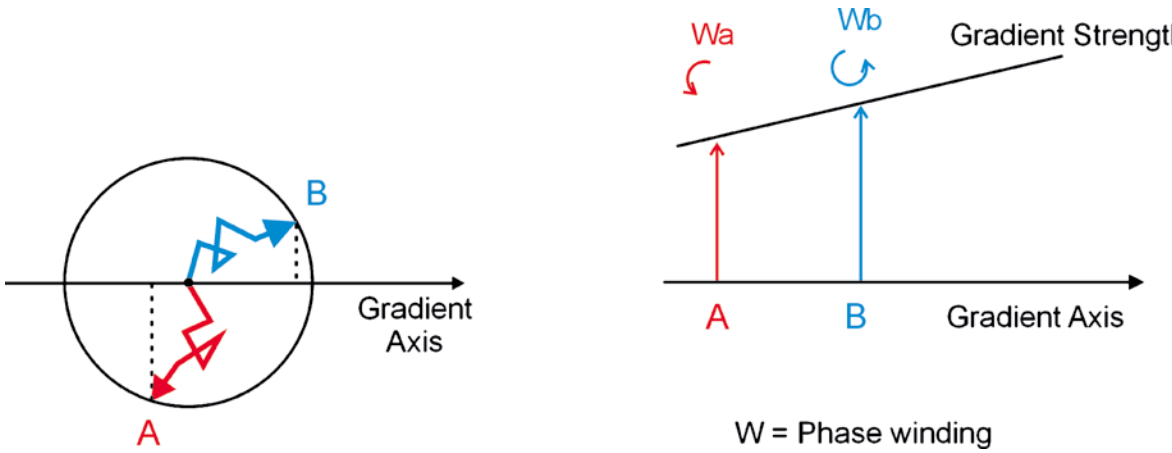

Fig. 69 Diffusion induced signal loss (diffusion weighting). Let us follow two water molecules diffusing through a magnetic gradient, having started at the same point in space and time. Because of random and independent displacement, after time T they are separated by a finite distance along the axis of the gradient and thus undergo unequal phase shifts. The end result is diminution of the final echo due to intravoxel phase dispersion

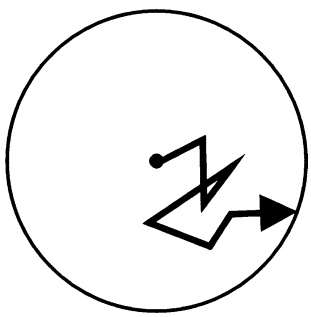

Fig. 70 Free (isotropic) diffusion. In this case all directions of diffusion are likely and the water molecules follow a jagged path. We can predict, however, that after a certain time the water molecules will be at the periphery of a circle. The radius of the circle depends on several parameters, including time

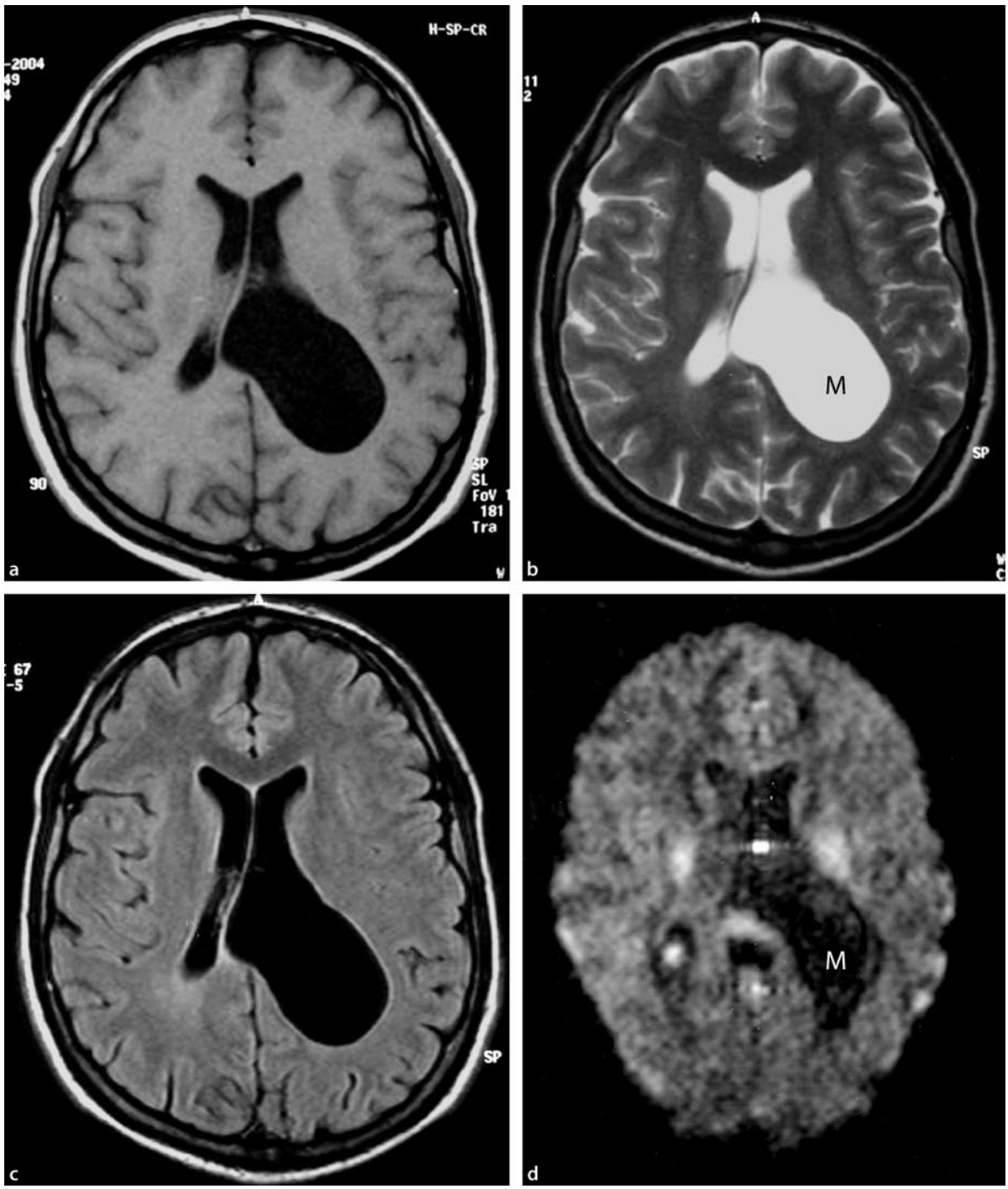

Fig. 71a–e Cerebrospinal fluid spaces as examples of unrestricted diffusion. A 32-year-old man with headaches. Axial **a** T1-w (532/15), **b** T2-w (4,465/120), **c** FLAIR (7,500/2,243/105) and **d** diffusion-weighted images. **e** *see next page*

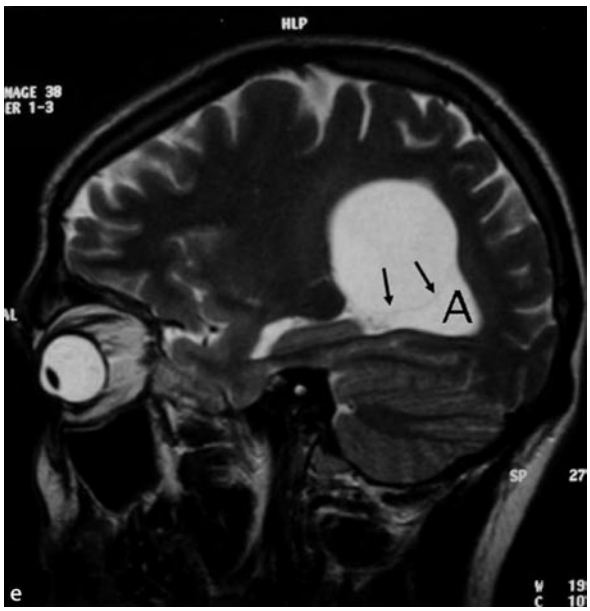

Fig. 71 *(continued)* **e** T2-w slice in a sagittal orientation. The posterior part of the left lateral ventricle is expanded by a mass (*M*) that is isointense to CSF in all pulse sequences. The sagittal image reveals the lower border of the lesion to be a thin, curvilinear septum (*arrows*) convex toward the ventricular atrium (*A*). Diagnosis: intraventricular arachnoid or neuro-epithelial cyst (presumed). The condition was stable at 18 months' follow-up

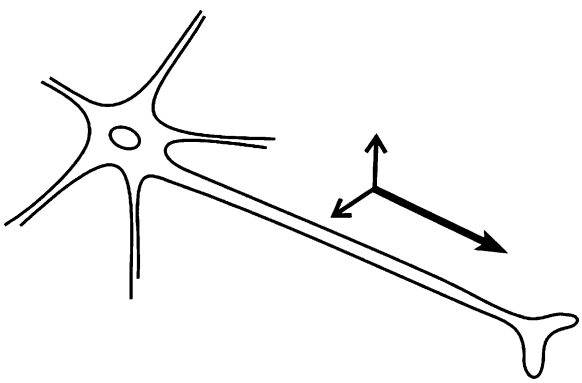

Fig. 72 Anisotropic diffusion. Drawing of a neuron with myelinated processes. Diffusion is rapid along the axon (*large arrow*) and restricted in the other directions (*short arrows*)

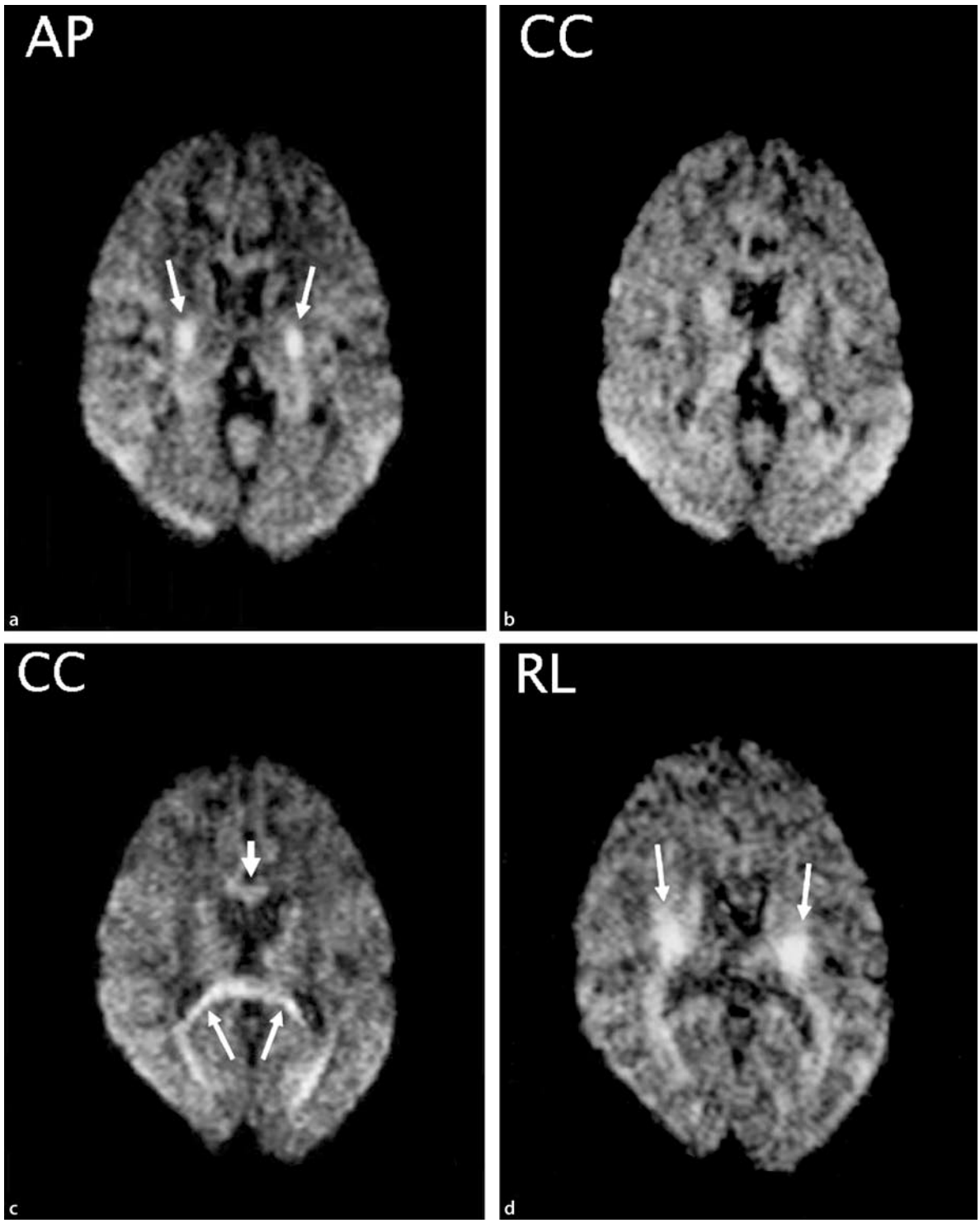

Fig. 73a–d Brain parenchyma as an example of anisotropic diffusion. **a**, **b** Pair of transaxial slices at the level of the thalami. The direction of diffusion encoding is anterior–posterior (AP) in **a** and cranio-caudal (CC) in **b**. **c**, **d** Pair of transaxial slices at the level of the lateral ventricular bodies. Diffusion sensitization is CC in **c** and right–left (RL) in **d**. Major white matter tracts appear "dark" when aligned with the axis of diffusion encoding and "brighten up" when perpendicular to that axis. Note the "highlighting" of the internal capsules in **a** and **d** and of the corpus callosum in **c** (*arrows*). The CSF spaces remain "black" on all images due to unrestricted diffusion in any direction

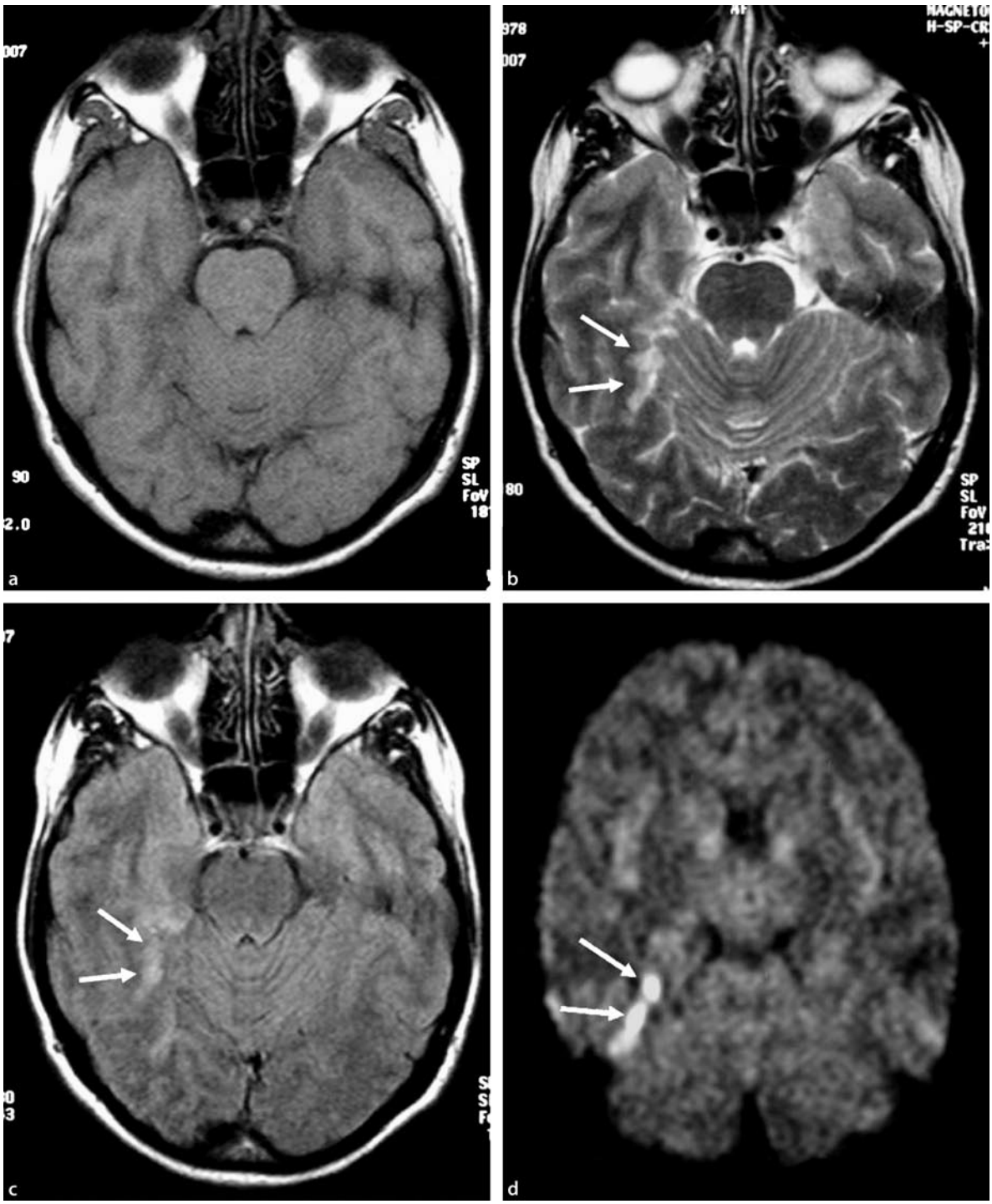

Fig. 74a–d Value of diffusion imaging in acute ischemic cerebral infarction. A 29-year-old female with acute onset of headache, visual disturbance, gait instability, and transient hypesthesia of the left extremities. An MR scan was performed on the third day of the symptoms. Transverse **a** T1-w SE (532/15), **b** T2-w TSE (4,465/120), **c** FLAIR (7,500/2,243/105), and **d** diffusion-weighted images. There is subtle T2 gyriform hyperintensity in the inferomedial aspect of the right temporal lobe (*arrows*). The lesion is very bright in **d** (*arrows*). The patient had additional ischemic lesions ipsilaterally, in the thalamus and posteromedial parietal lobe (not shown), all in the territory of the posterior circulation

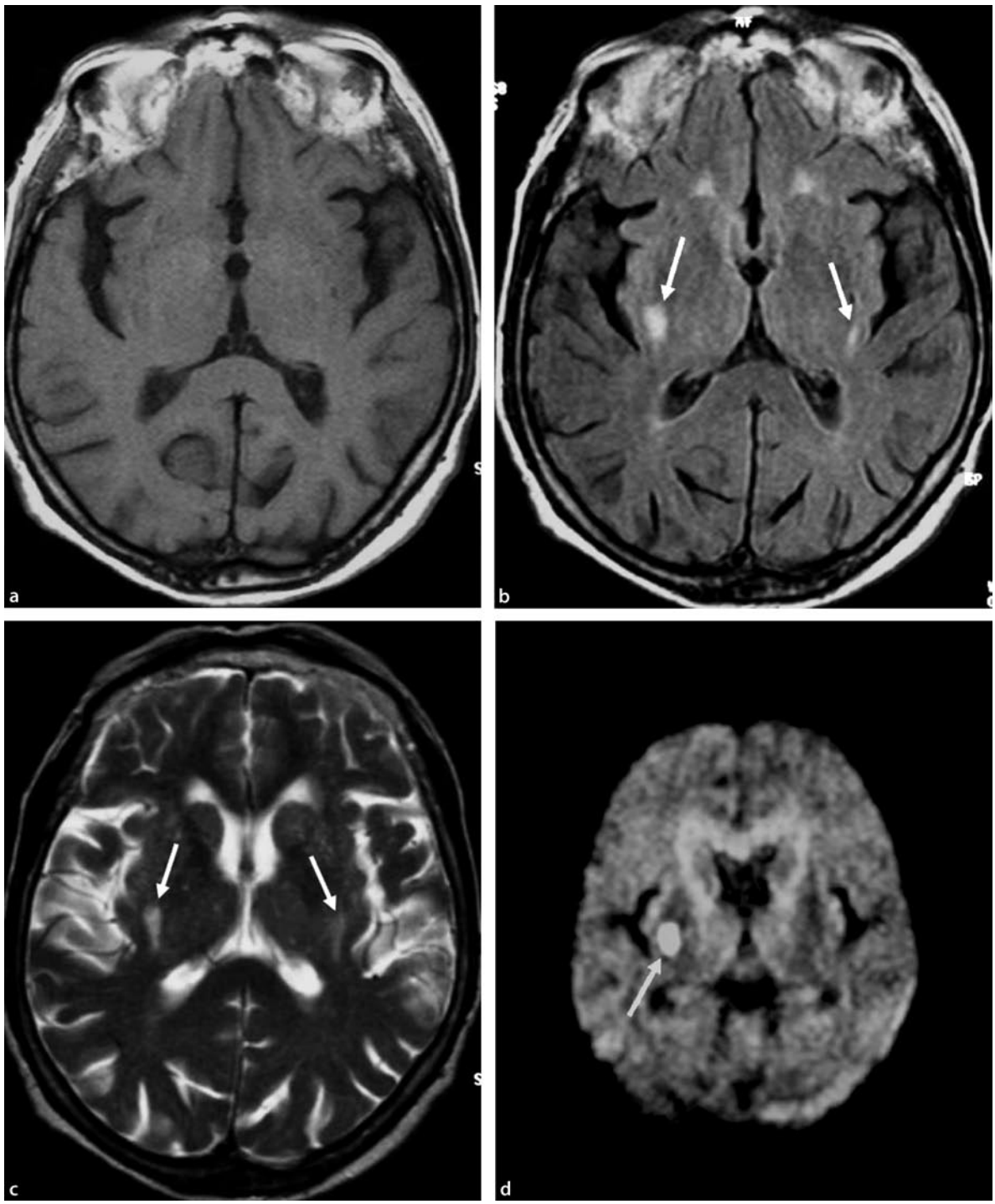

Fig. 75a–d Value of diffusion weighting in cerebral ischemia. A 68-year-old with acute onset of left extremity weakness 4 days prior to the scan. Transverse **a** T1-w SE (532/15), **b** FLAIR (7,500/TI 2,243/105), **c** T2-w TSE (4,465/120), and **d** diffusion-weighted images. Two ischemic foci are placed symmetrically at the dorsal aspect of the lentiform nuclei (*arrows*). Only the right-sided lesion shows up with diffusion sensitization (*single arrow*), correlating with the recent onset of the symptoms

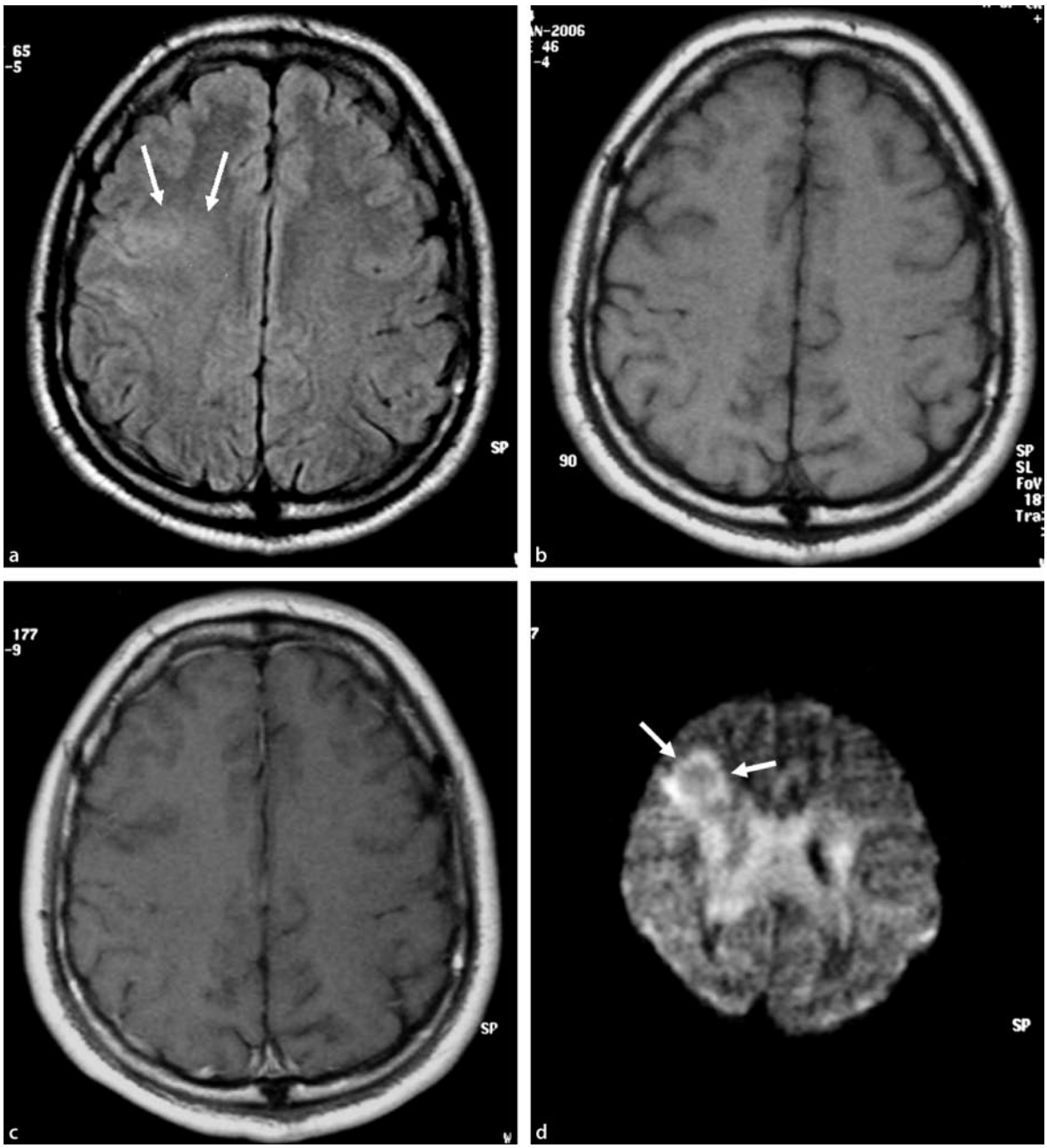

Fig. 76a–d Value of diffusion-weighted imaging: differential diagnosis. A 41-year-old with acute onset of left extremity weakness and alteration of mental status. MR scan obtained on the second day of symptoms. Axial **a** FLAIR (7,500/TI 2,243/105), **b** T1-w SE (532/15), **c** contrast-assisted T1-w, and **d** diffusion-weighted images. Subtle hyperintensity in the right frontal lobe is barely discernible (*arrows*) on FLAIR. No T1 abnormalities either prior to or following contrast administration. The findings so far could be due to early ischemia. However, the last image (obtained with slightly different angulation) reveals a ring-like abnormality in diffusion that is hyperintense (*arrows*) relative to healthy parenchyma. This picture is not consistent with ischemia. One day later the patient developed fever and lumbar puncture revealed mild leukocytosis of the CSF. Final clinical diagnosis: infectious cerebritis. The patient recovered completely within 1 month

24 Artifacts

Keywords

- Misrepresentation
- Distortion
- Obscuration
- Mimics

Artifacts are misrepresentations of the true state of normal or diseased tissues. Artifacts may distort anatomy and mimic or obscure pathology. There are various sources, the most common of which is the patient him- or herself. The artifacts can be traced to one of the following:

1. Faulty generation of data due to magnetic field breakdown (e.g., poor shielding) or due to the malfunction of magnetic gradients or other hardware (Fig. 77)
2. Faulty processing of data due to the malfunction of the Fourier transform algorithm
3. Improper selection of parameters such as small field of view (FOV), small matrix, improper direction of phase or frequency encoding (Fig. 78)
4. The patient because of:
   a) Gross motion due to noncooperation (Fig. 79)
   b) Motion due to physiologic processes such as respiration or flow (Figs. 80–84)
   c) Apposition of structures with a gross difference in water–lipid content (chemical shift, Fig. 85)
   d) Gross difference in magnetic properties of neighboring tissues (magnetic susceptibility, Fig. 45)
   e) Extrinsic factors, such as intravascular contrast agents or metallic prostheses (Fig. 86)

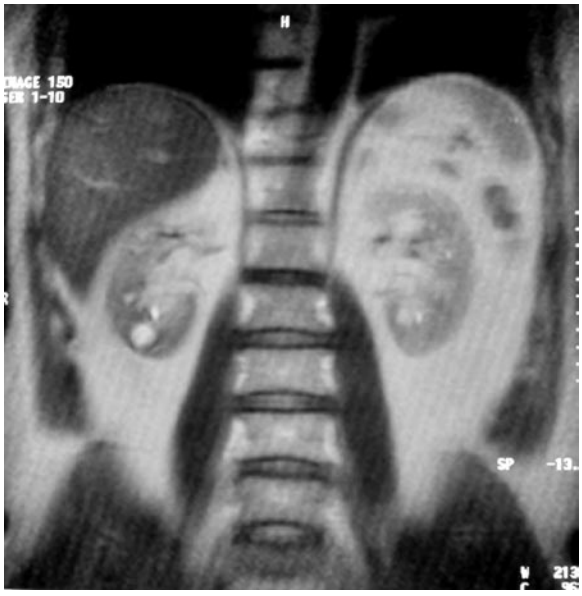

Fig. 77 Example of artifact due to extrinsic factors. Coronal slice through the abdomen from a HASTE (ultrafast T2-w) sequence. Multiple diagonal lines, parallel to each other, cover the entire image in a "corduroy" fashion. This type of artifact occurs when multiple exogenous RF sources interfere with the MR signal. The exogenous RF sources can be personal computers, radio stations – even the scanner's computer

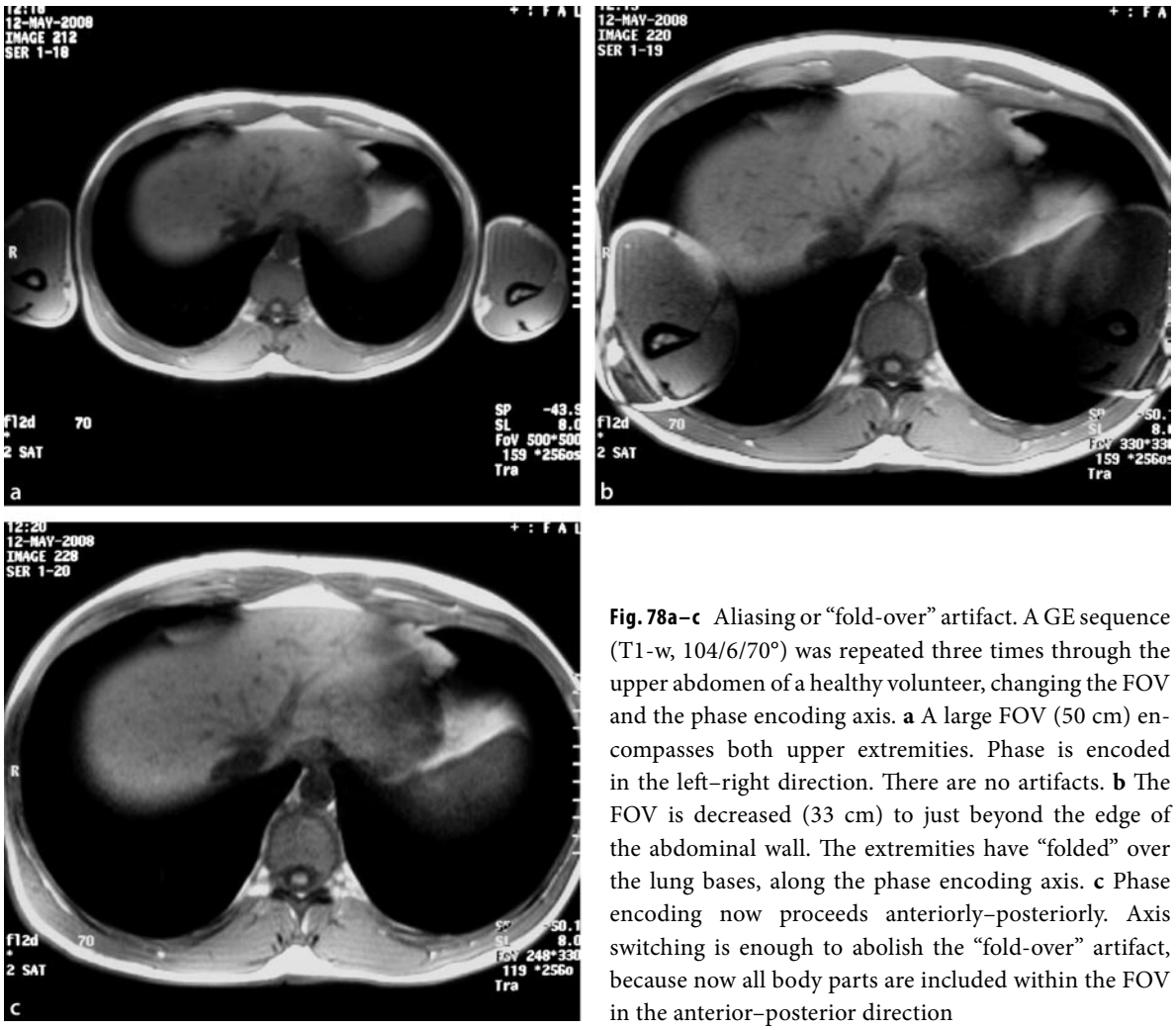

Fig. 78a–c Aliasing or "fold-over" artifact. A GE sequence (T1-w, 104/6/70°) was repeated three times through the upper abdomen of a healthy volunteer, changing the FOV and the phase encoding axis. **a** A large FOV (50 cm) encompasses both upper extremities. Phase is encoded in the left–right direction. There are no artifacts. **b** The FOV is decreased (33 cm) to just beyond the edge of the abdominal wall. The extremities have "folded" over the lung bases, along the phase encoding axis. **c** Phase encoding now proceeds anteriorly–posteriorly. Axis switching is enough to abolish the "fold-over" artifact, because now all body parts are included within the FOV in the anterior–posterior direction

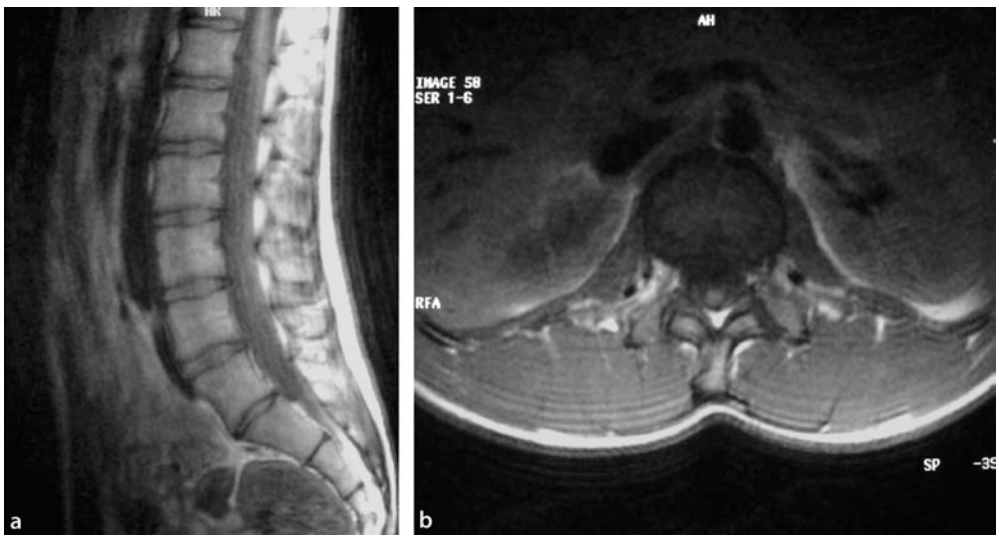

Fig. 79a,b Gross patient motion. **a**, **b** Lumbar spine T1-w study in the sagittal and axial directions respectively. Motion produces blurring of the edges and the images appear out of focus

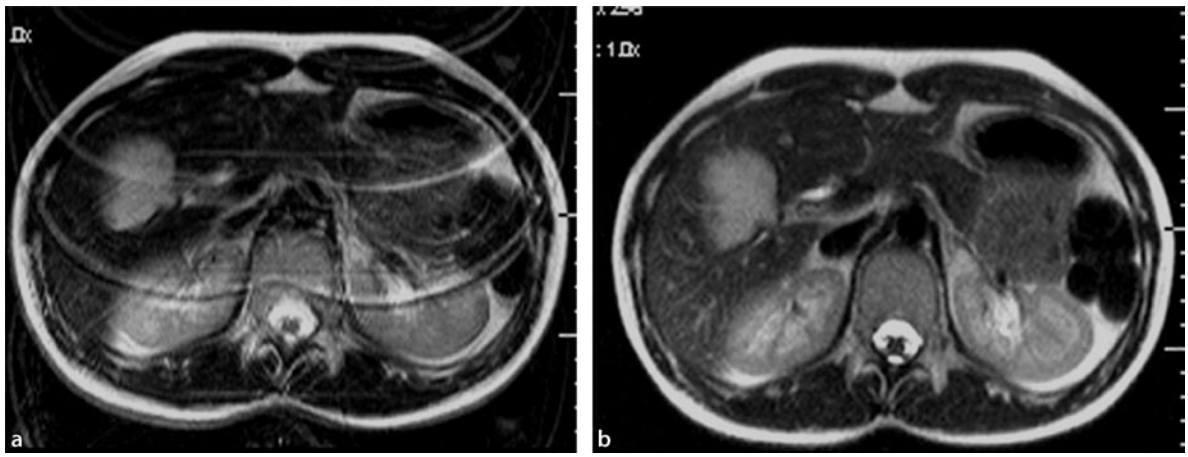

Fig. 80a,b Respiratory motion artifact and respiratory triggering. **a**, **b** T2-w TSE sequence repeated twice through the upper abdomen. In **b** the data were recorded only during the "quiet" phase of respiration, i.e., from end expiration to the beginning of inspiration (of the following cycle). Thus, we avoid the artifact due to motion of the anterior abdominal wall. Since only a fraction of the respiratory cycle is used for data collection, the total scan time is lengthened compared with **a**. Courtesy of N. Papanikolaou, PhD, University of Crete

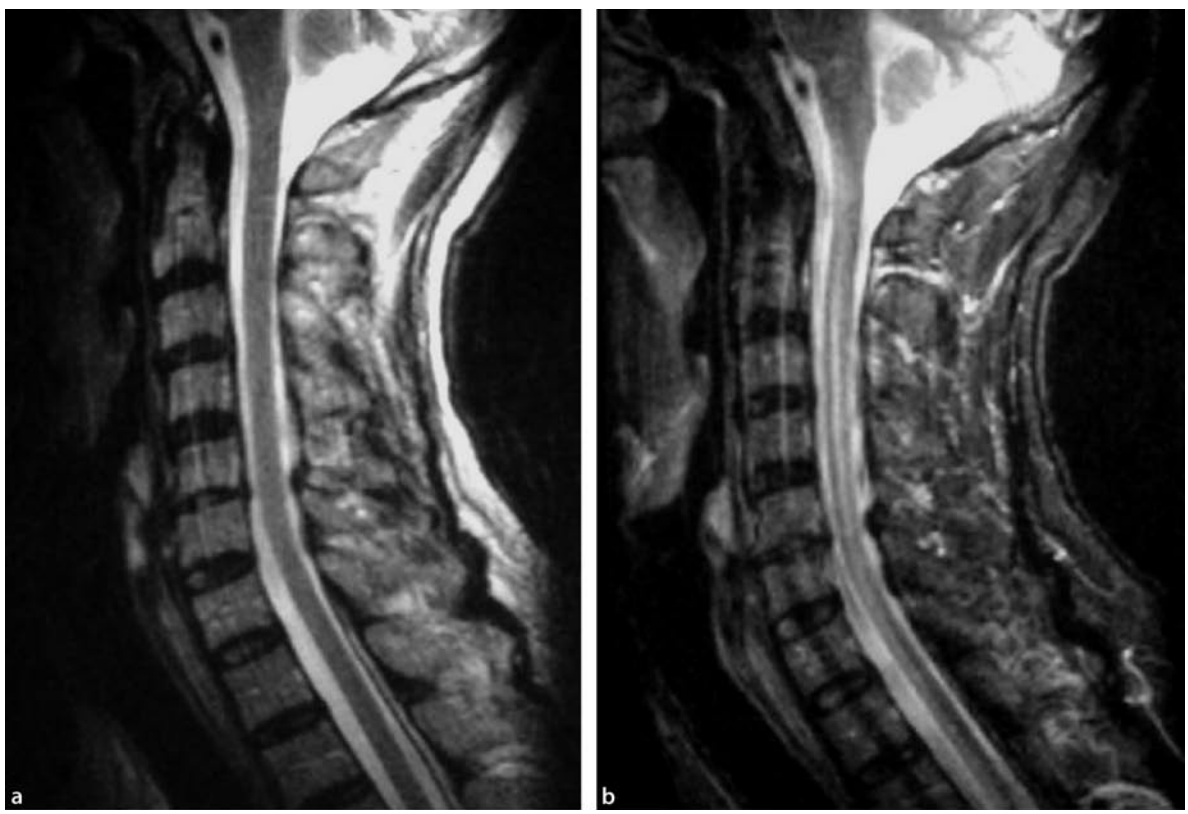

Fig. 81a–c Cerebrospinal fluid flow artifact. Cervical spine MRI study requested in a 65-year-old with radiculopathy without clinical evidence of myelopathy. Sagittal **a** T2-w TSE (4,324/112) and **b** STIR (4,000/120/60) images. **c** *(see next page)*

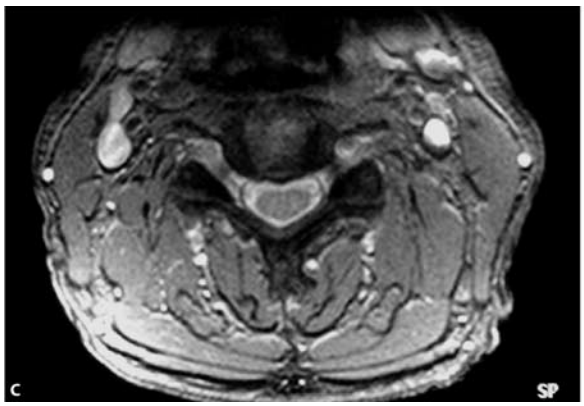

Fig. 81a–c *(continued)* **c** Axial T2*-w (gradient echo 773/23/30°) slice. There is intense artifact in the STIR image, in the form of hyperintense bands through the anterior–posterior dimension. Thus, we are given the false impression of extensive myelopathy. The spinal cord appears normal in **a** and **c**. This artifact is due to the cranio-caudal oscillation of the CSF column, driven by cardiac pulsations, and is much less prominent in **a**

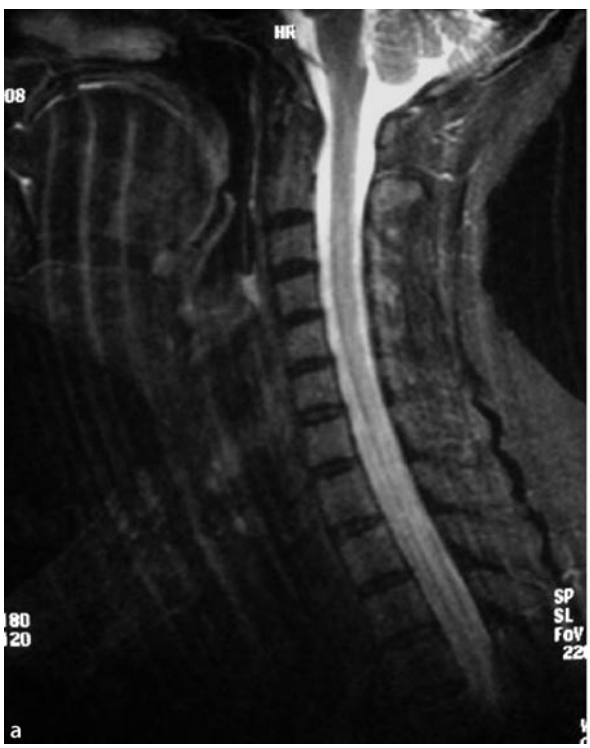

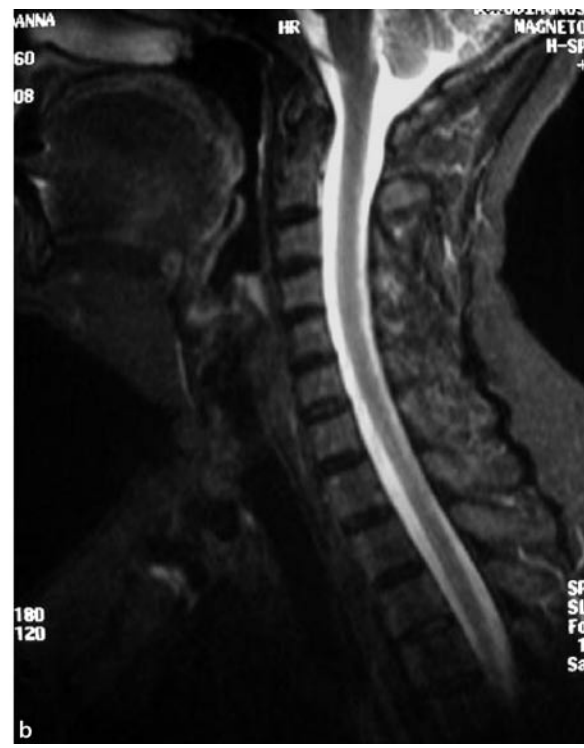

Fig. 82a,b "Obliteration" of CSF flow artifact. **a** STIR mid-sagittal image (4,000/120/60) through the cervical spine. Artifact similar to the prior figure, again in the phase encoding axis. Hyperintense bands replicate the CSF column. **b** The same sequence was repeated, changing only the phase encoding axis (to cranio-caudal). No flow artifact is visible; both cord and CSF appear uniform

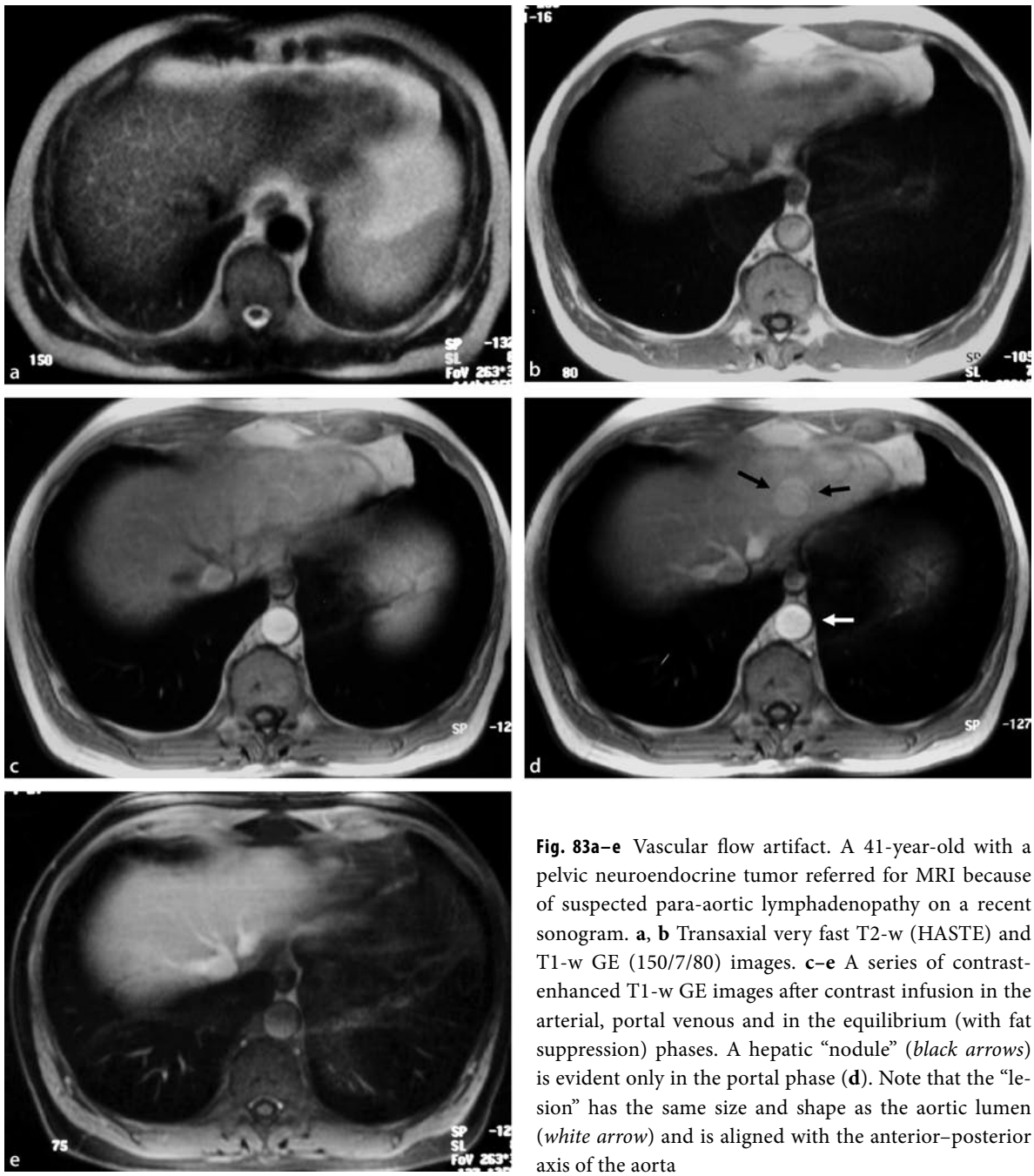

Fig. 83a–e Vascular flow artifact. A 41-year-old with a pelvic neuroendocrine tumor referred for MRI because of suspected para-aortic lymphadenopathy on a recent sonogram. **a**, **b** Transaxial very fast T2-w (HASTE) and T1-w GE (150/7/80) images. **c–e** A series of contrast-enhanced T1-w GE images after contrast infusion in the arterial, portal venous and in the equilibrium (with fat suppression) phases. A hepatic "nodule" (*black arrows*) is evident only in the portal phase (**d**). Note that the "lesion" has the same size and shape as the aortic lumen (*white arrow*) and is aligned with the anterior–posterior axis of the aorta

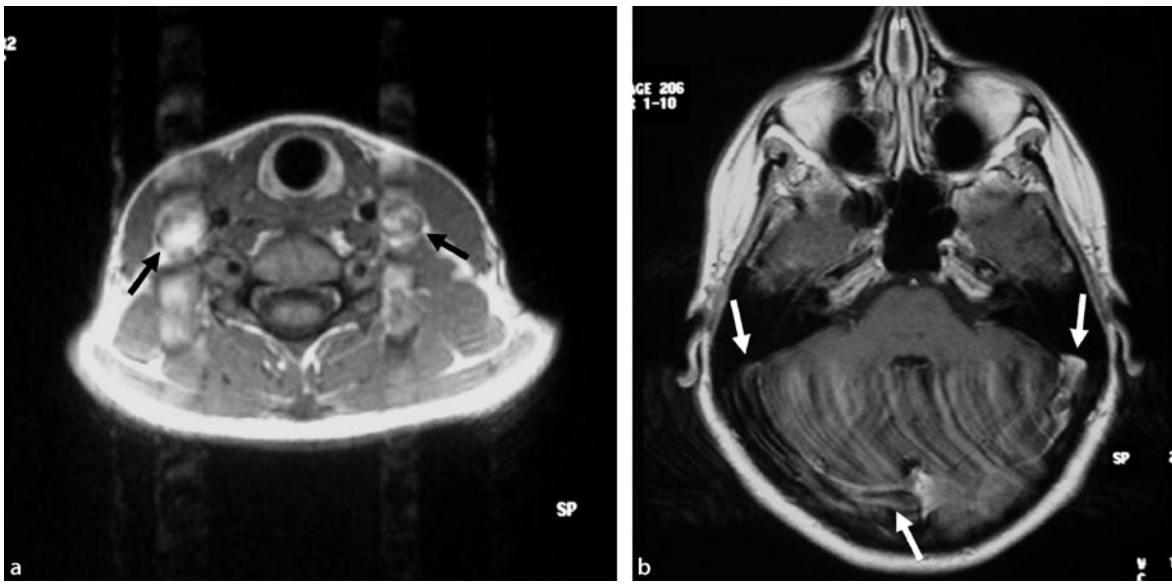

Fig. 84a,b Multiple vascular flow "ghosts." Vascular ghost artifacts may be positive or negative in signal intensity, and single or multiple. When multiple, the ghosts can remain discrete or may overlap with each other. However, they are always in the phase encoding axis, aligned with and replicating the lumen of the causative vessel. **a** Transverse T1-w TSE image (800/12) from a neck study. Multiple vascular replicas in the anterior–posterior direction that propagate beyond the patient. The most obvious ghosts emanate from the jugular veins (*arrows*). No presaturation pulses were employed. The presaturation bands are discussed in Chap. 30 (on MR angiography). **b** Contrast-assisted T1-w SE (532/14) axial brain slice. Numerous ghosts on a left–right axis partly obscure the posterior fossa. Their origins are the transverse and sigmoid venous sinuses (*arrows*)

The artifacts can be reduced or eliminated with appropriate modifications, usually with a time penalty, e. g. repeating the sequence with a larger FOV, or by switching the frequency/phase directions, or through "triggering" (Figs. 78–80).

The artifacts are not always detrimental. It may sound counterintuitive, but some artifacts are very useful:

1. Image distortions due to magnetic susceptibility, chemical shift effects, and vascular ghosts betray the nature of a mass or a pseudomass and allow a specific diagnosis (Figs. 45, 62, 87).
2. Flow voids indicate luminal patency (Fig. 88), hypervascular lesions, or high flow vascular malformations.

The figures have chosen emphasize the artifacts related to flow since these are the most common cause of diagnostic difficulties.

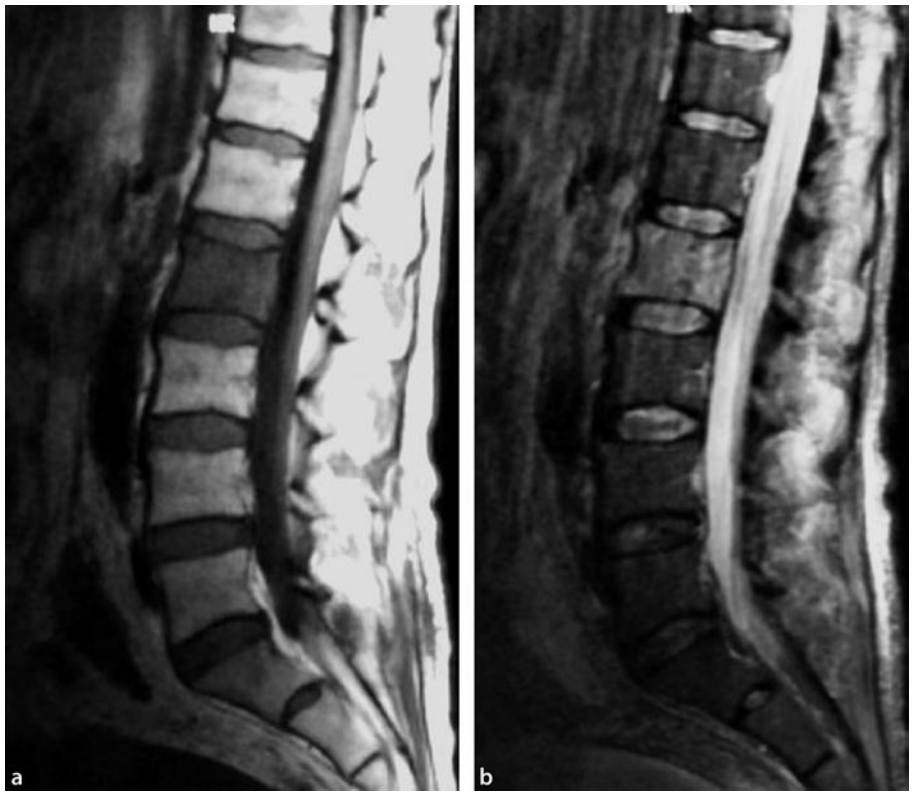

Fig. 85a,b Chemical shift artifact in the spine. Sagittal **a** T1w and **b** STIR views of the lumbar spine in a patient with a metastatic hepatoma to L2 (the same patient as in Fig. 55). **a** The chemical shift artifact occurs in the frequency encoding direction, which is craniocaudally in this case. Note the thickness of the superior and inferior cortical plates. They are unequal in the healthy vertebrae due to summation and cancellation effects at the interface of the fatty marrow and the bony cortex. They are equal in the infiltrated vertebra: since there is no longer fatty marrow, the chemical shift effect cannot take place. **b** STIR suppresses the signal of fatty marrow and thus abolishes the potential for chemical shift. Thus the superior and inferior end plates appear of equal thickness (in all vertebrae, compare to **a**)

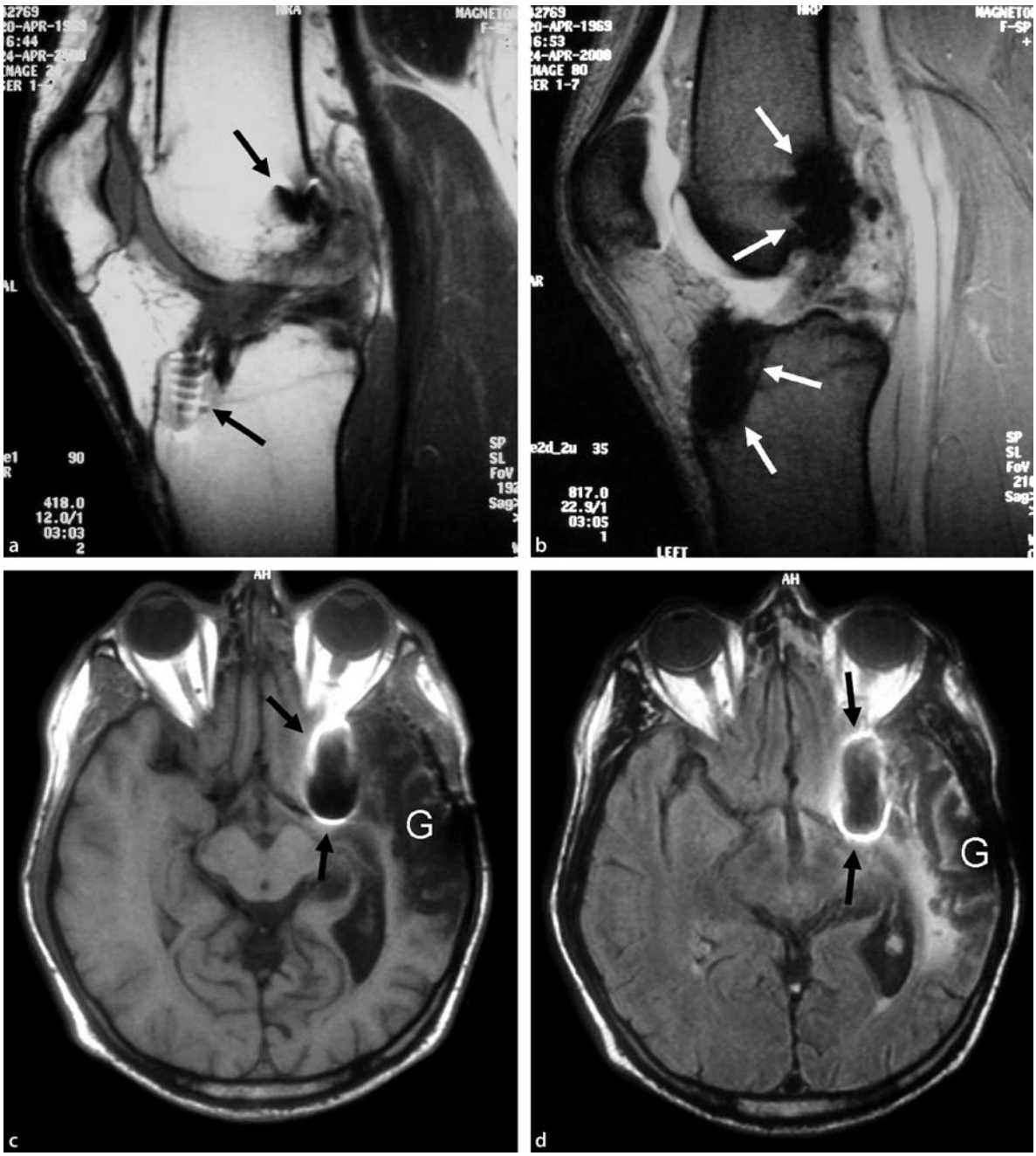

Fig. 86a–d Artifact due to metallic foreign bodies in two different patients. Sagittal **a** T1w SE (418/12) and **b** T2*w GE (817/23/35°) images through the knee of a 32-year-old following reconstruction of the anterior cruciate ligament. The artifacts at the anchor sites of the graft (*arrows*) appear quite extensive in **b**, due to "blooming". Axial **c** T1w SE (532/15) and **d** FLAIR (7500/TI 2243/105) brain images. The patient is status post surgical clipping of a ruptured aneurysm of the left middle cerebral artery (MCA). The metal clip produces an artifact that obscures the left MCA bifurcation: signal void is partly covered by "chalk" white arcs (arrows). Extensive gliosis of the ipsilateral temporal lobe (*G*) is a consequence of the aneurysm rupture (infarction due to vasospasm)

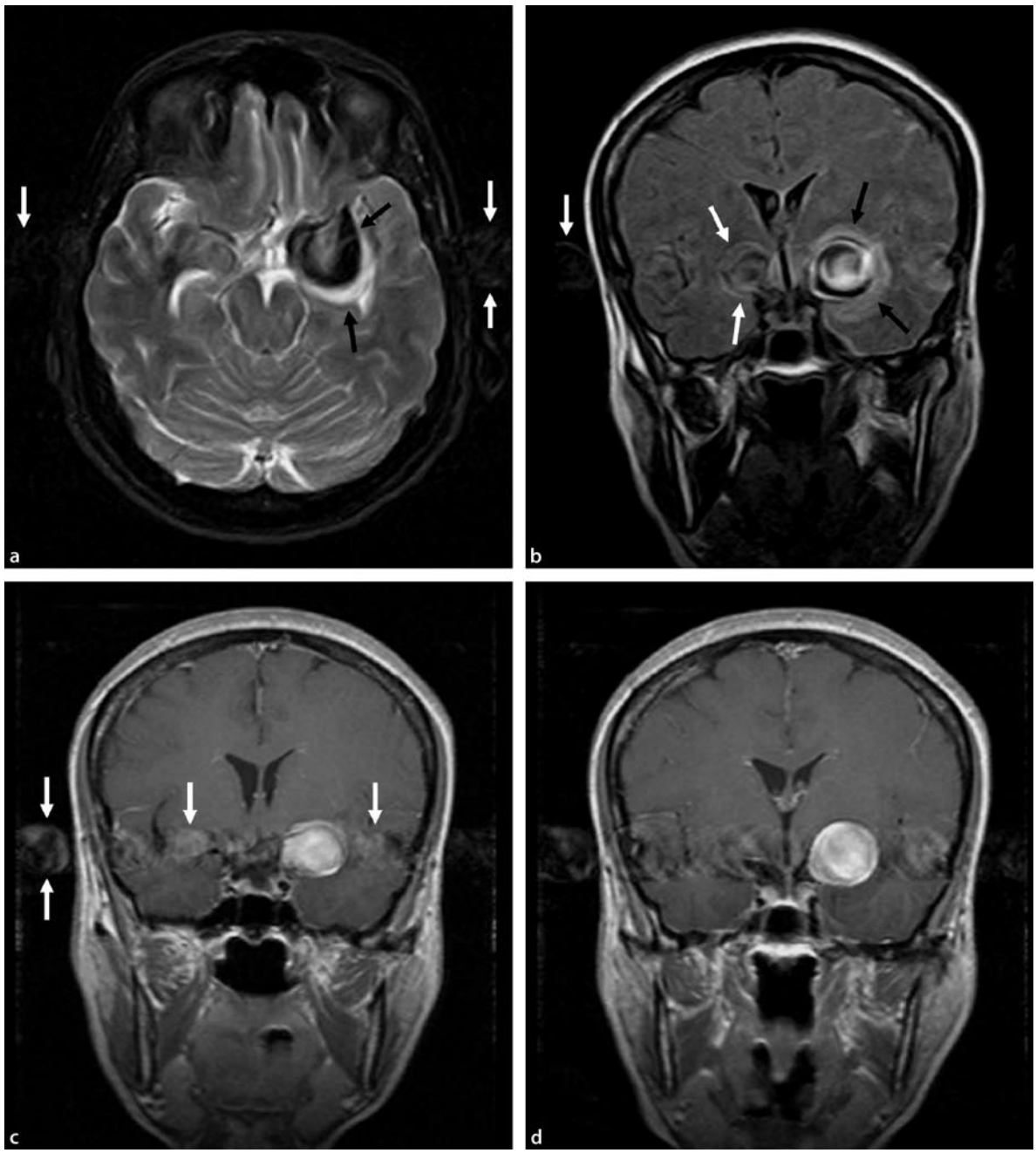

Fig. 87a–d Diagnostic value of the flow artifact. A 62-year-old with headaches. **a** Axial T2w TSE image. **b–d** Coronal FLAIR and post intravenous contrast T1w SE images (from a 1.5 T system). A round mass invaginates into the basal surface of the left cerebrum and is surrounded by a collar of edema (*black arrows*). The borders are smooth and well defined. There is a layered internal appearance with areas of bright signal and areas of signal void. Contrast enhancement is intense and inhomogeneous, forming concentric rings and crescents. A continuous artifact on the left–right axis consists of overlapping "ghosts" of the lesion (*white arrows*) and appears more prominent post contrast. Diagnosis: patent aneurysm of the left carotid bifurcation. Courtesy of A. Roussakis, MD, V. Filippi, MD, and J. Andreou, MD, PhD, "Hygeia" Hospital, Athens, Greece

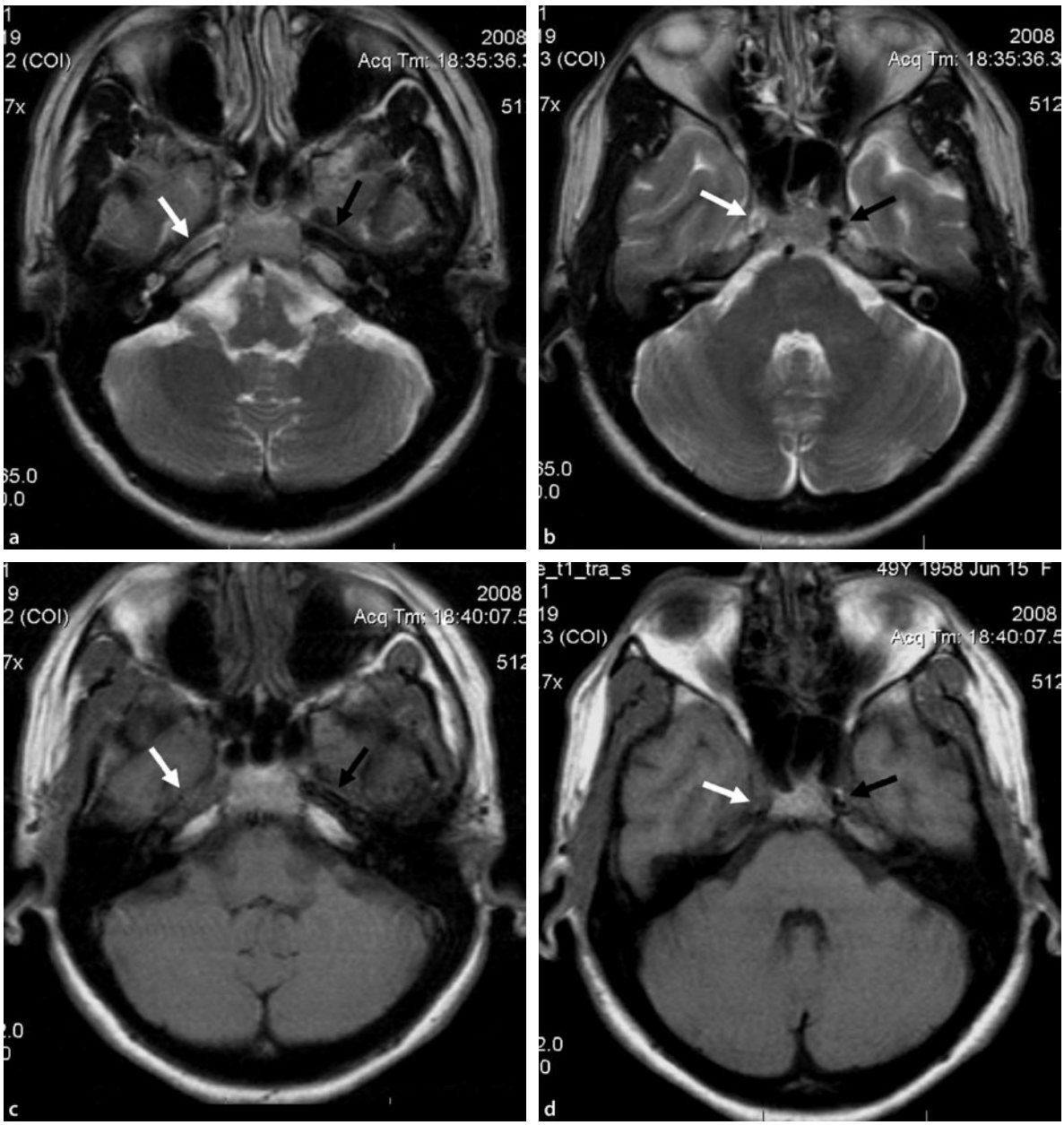

Fig. 88a–g Diagnostic utility of the flow artifact. A 52-year-old with acute ischemic stroke in the right middle cerebral artery territory. **a–d** Axial T2w TSE (4,465/120) and T1w SE (532/15) paired images through the skull base. There is abnormal signal in the course of the right internal carotid (*white arrows*). Compare with the signal void of normal contralateral carotid (*black arrows*). **e–g** *see next page*

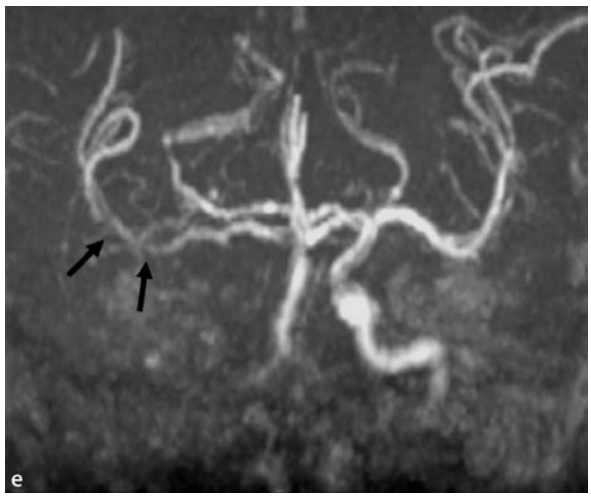

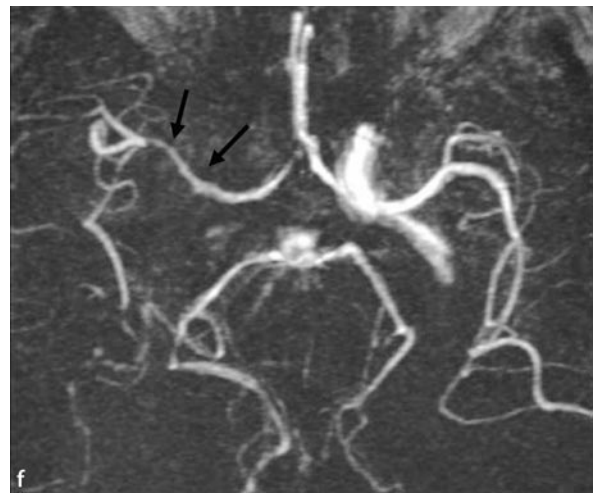

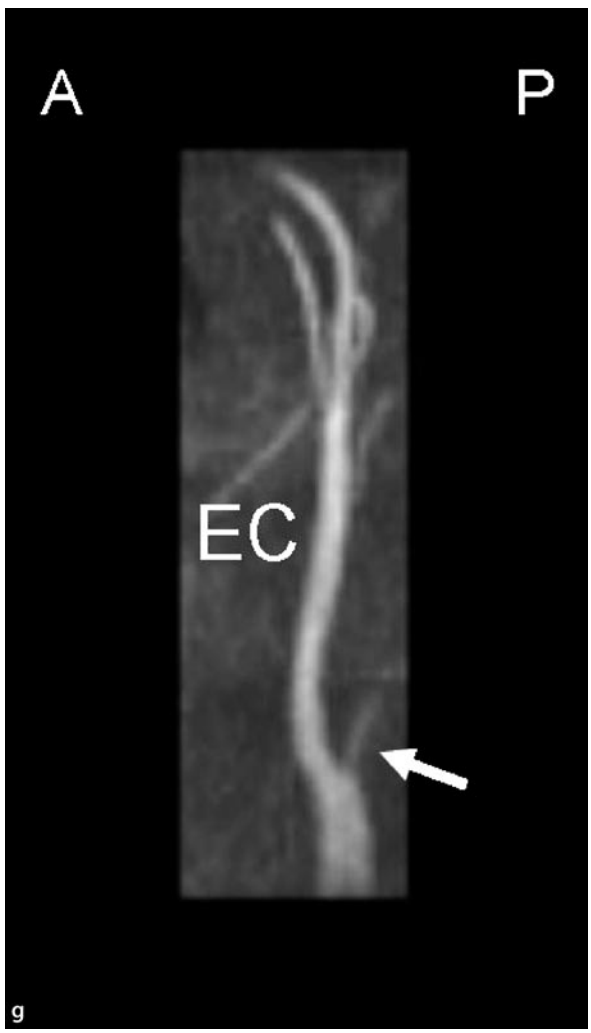

Fig. 88a–g *(continued)* **e**, **f** Coronal and axial reconstructions from a cerebral MR angiogram (3D inflow technique, 37/9.6/20°). No flow is seen in the right internal carotid. The right middle cerebral artery is depicted with diminished flow (*arrows*). **g** "Lateral" reconstructed view from an MR angiogram (3D inflow, 35/10/25°) through the carotid bifurcations. Only a stump of the origin of the internal branch is visualized (*arrow*). *EC* external carotid, *A* anterior, *P* posterior

Noise 25

Keywords

- Random fluctuations
- Signal-to-noise ratio

Thermal energy induces random transitions of spins between the high and low energy states. Changes in the relative spin populations alter temporarily the nominal value of the static magnetic field, B. These random fluctuations of B are called noise, which is inadvertently incorporated in the MR signal. If the overall signal intensity is poor, the noise "shines through" and artifacts become prominent, diminishing diagnostic confidence. The most significant source of noise is the patient. The adequacy of signal is not expressed in absolute terms, but as a ratio, of signal to noise (SNR). The SNR depends on several factors:

1. Machine timing parameters and tissue time constants: TR, TE, T1, T2.
2. The number of spins, which in turn is determined by the intrinsic spin density of the tissues and the voxel size (slice thickness, matrix, and FOV).
3. The number of repetitions of each pulse sequence, termed the number of excitations or signal averaging (NEX/NSA). Increasing the NEX/NSA is not an efficient method of increasing the SNR, since noise is also added with each cycle. Fortunately, the noise is "smeared" on the image, i.e., distributed randomly, even outside the patient. So, with multiple NEX we get an additive effect that is stronger for the signal compared to the noise.

26 Imaging Time

Keywords

- Spatial resolution
- TR
- Signal averaging

The acquisition time of any sequence is directly related to the following:

1. Spatial resolution: specifically the number of phase encoding steps (Chap. 15).
2. TR: only one phase measurement or a limited number of phase steps is feasible per TR cycle[1].
3. Number of repetitions (NEX/NSA).

[1] This is true of conventional and fast sequences, i.e., either spin or gradient echo. It is not true of ultrafast techniques, such as echo planar imaging.

Resolution 27

Keywords

- Field of view
- Matrix
- Pixel
- Voxel

The term "resolution" refers to our ability to distinguish a lesion from its surroundings. In MRI we are dealing with two types of resolution, spatial and contrast[1]. Both are controlled by the operator and they address two important features of any lesion: size and signal intensity (SI). Even a small focus becomes obvious when very "bright" or very "dark."

Let us first look at spatial resolution. Every MR examination produces a large number of slices that are three dimensional objects; their depth or thickness is compressed and "lost" when transferred to the 2D format on film or screen. The other two dimensions of the slice are determined by the field of view (FOV), or the frame that we "draw" around or within the patient. The choice of FOV and slice thickness is related to the size of the object under investigation (e.g., brain, pituitary gland, spinal cord, etc.).

The FOV is divided into boxes by rows and columns that equal the number of frequency and phase encoding steps respectively. The numbers of rows and columns constitute the matrix. The matrix can be square/symmetric (e.g., 256 × 256) or rectangular/asymmetric (e.g., 192 × 256). The boxes are called pixels (picture elements) and their size determines the in-plane resolution. The two dimensions of the pixel are calculated as follows: the FOV divided by the matrix size. When a pixel is multiplied by the slice thickness we get a voxel (volume element), the elementary unit of the image. The smaller the voxel, the greater the spatial resolution (Fig. 89), at the cost of weaker SNR and extended acquisition time. Small voxels have fewer protons and thus lower inherent signal capacity. In order to gather SNR at a given voxel size we need to increase NEX/NSA; the consequence is prolongation of the acquisition time. Spatial resolution also depends upon the mode of excitation: 2D vs 3D (dimensional). In 3D sequences the entire imaging volume is excited at once with the benefit of a much stronger signal compared to individual slices of 2D acquisitions. Thus, the 3D slab can be divided into thin contiguous slices, which in turn can provide useful reconstructions in multiple planes.

In contrast resolution, the resolving power relies on SI differences between lesions and normal tissues. Since there may be an overlap in the magnetic properties, we need multiple pulse sequences for lesion detection and characterization, using T1w and T2w at least. Depending on the clinical picture we may benefit from contrast administration or additional sequences, such as proton density, fat suppression, etc.

[1] In certain angiographic studies we also have to consider temporal resolution.

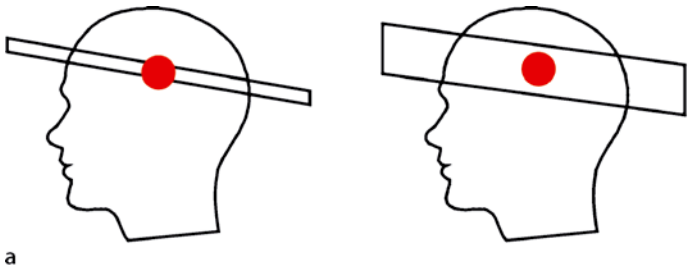

a

a The effect of slice thickness (all else remaining constant): if it is thin, the lesion extends on either side of the slice, in adjacent sections; if it is thick, the lesion is "immersed" in the slice, hidden from easy view

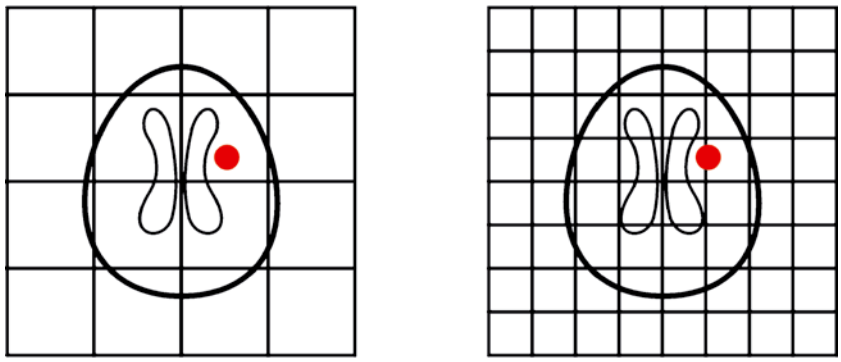

b

b The effect of a small or large matrix (all else remaining constant): it is easy to detect a lesion that occupies a large number of pixels

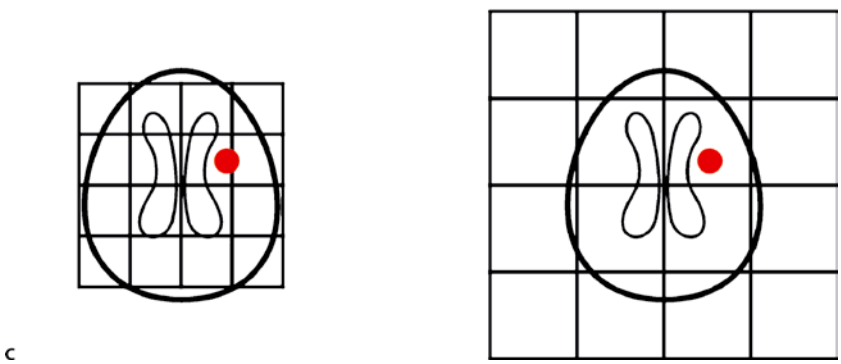

c

c The effect of a small or large FOV (all else remaining constant): a small lesion may get "lost" within a large pixel amidst a background of normal parenchyma

Fig. 89a–c Spatial resolution. The spatial resolution determines the relative size of the object with regard to the patient. Slice thickness, the FOV, and the matrix establish the size of the "frame" limiting the target. The FOV and matrix define the in-plane resolution

Contrast Agents 28

Keywords

- Gadolinium
- Relaxation enhancement or acceleration

There is a variety of MR contrast media, but we will deal exclusively with paramagnetic agents carrying gadolinium (Gd). These compounds are scheduled for intravenous use both in MRI and MRA. Gd is a metal with a very strong magnetic dipole moment facilitating both T1 and T2 relaxation of protons in its immediate vicinity. Simultaneous shortening of T1 and T2 produces conflicting effects. In most tissues T1 exceeds by far T2 and the absolute changes in T1 override the counteraction of T2 shortening. Thus, after Gd infusion it is necessary to obtain T1w sequences and to look for hyperintensity as a sign of contrast accumulation.

Why and when do we use contrast material?

1. Contrast enhancement may unmask "invisible" or "hidden" lesions due to small size, strategic location or isointensity to the parenchyma.
2. We may confirm that a suspicion or a subtle alteration is a true finding.
3. We can differentiate between lesions with similar signal intensities on the plain study, such as granulation tissue vs fluid in the bed of osteochondritis dissecans.
4. We can complete the characterization of a lesion; in other words we can estimate age (e.g., cerebral infarct), assess viability (e.g., possible osteonecrosis; Fig. 90) or grade activity (e.g., inflammatory conditions; Fig. 91).
5. It may help us with our differential diagnosis list, e.g., in cystic vs solid conditions or in establishing the etiology of a condition (Figs. 92, 93).

The use of intravenous contrast in MR angiography is discussed in Chap. 30.

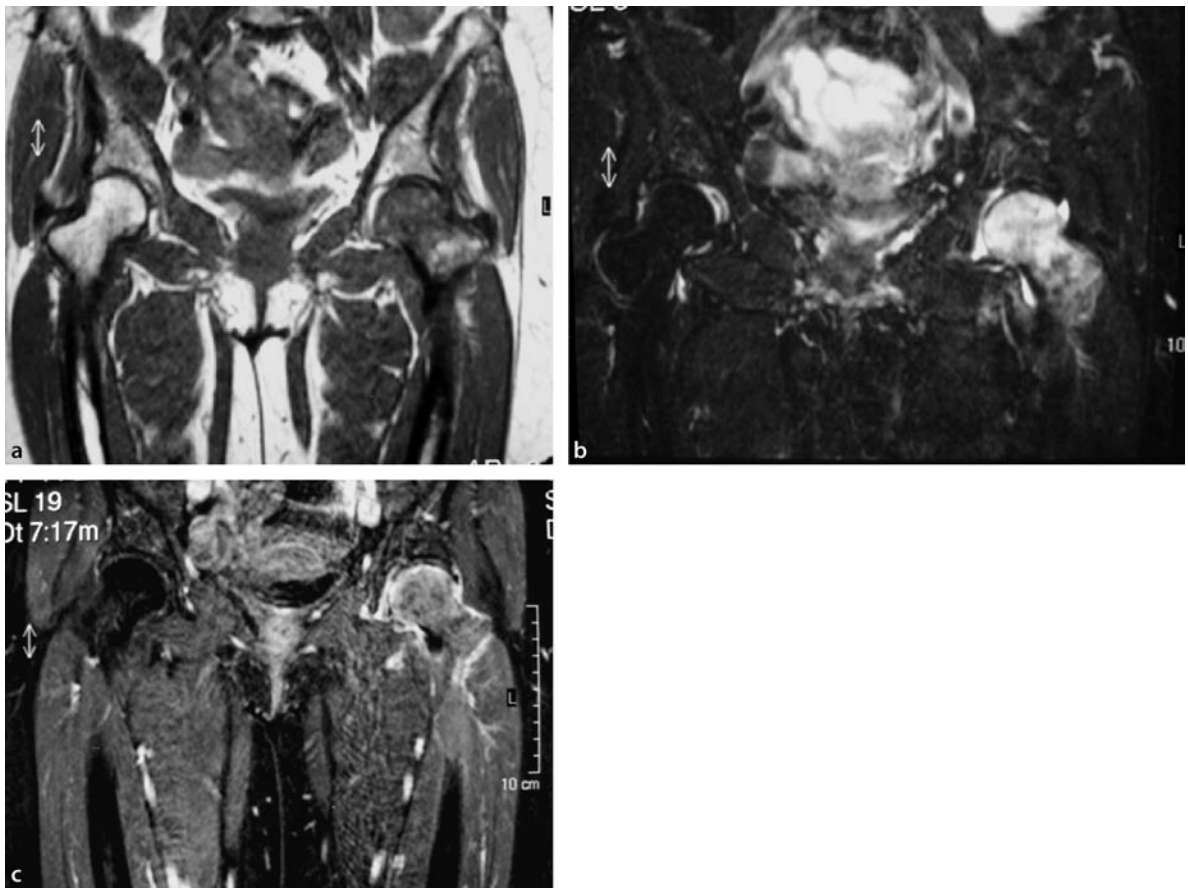

Fig. 90a–c Value of contrast administration: assessment of tissue viability. A 70-year-old woman with progressive hip pain over a 3-month period. Plain radiographs and a CT scan revealed focal osteopenia of the femoral head (not shown). The MR study was performed using a 1.5 T unit. Coronal **a** T1w SE (550/17), **b** fat-suppressed T2w TSE (2,500/110), and **c** contrast-assisted/fat-suppressed T1w gradient echo (3D acquisition 33/4.6/45°) views. There is marked marrow edema throughout the proximal part of the left femur. Free joint fluid is present bilaterally. Contrast uptake in the left femur is diffuse and intense, especially in the immediate subchondral plate. Strong rim enhancement around the affected neck and greater trochanter is due to synovitis. The differential diagnosis was between transient osteoporosis and early avascular necrosis. Immediately after contrast medium injection we see diffuse and intense uptake throughout the lesion, consistent with viable tissue. There was complete resolution of symptoms and the MR abnormalities with conservative treatment over a 7-month period. Final diagnosis: transient osteoporosis

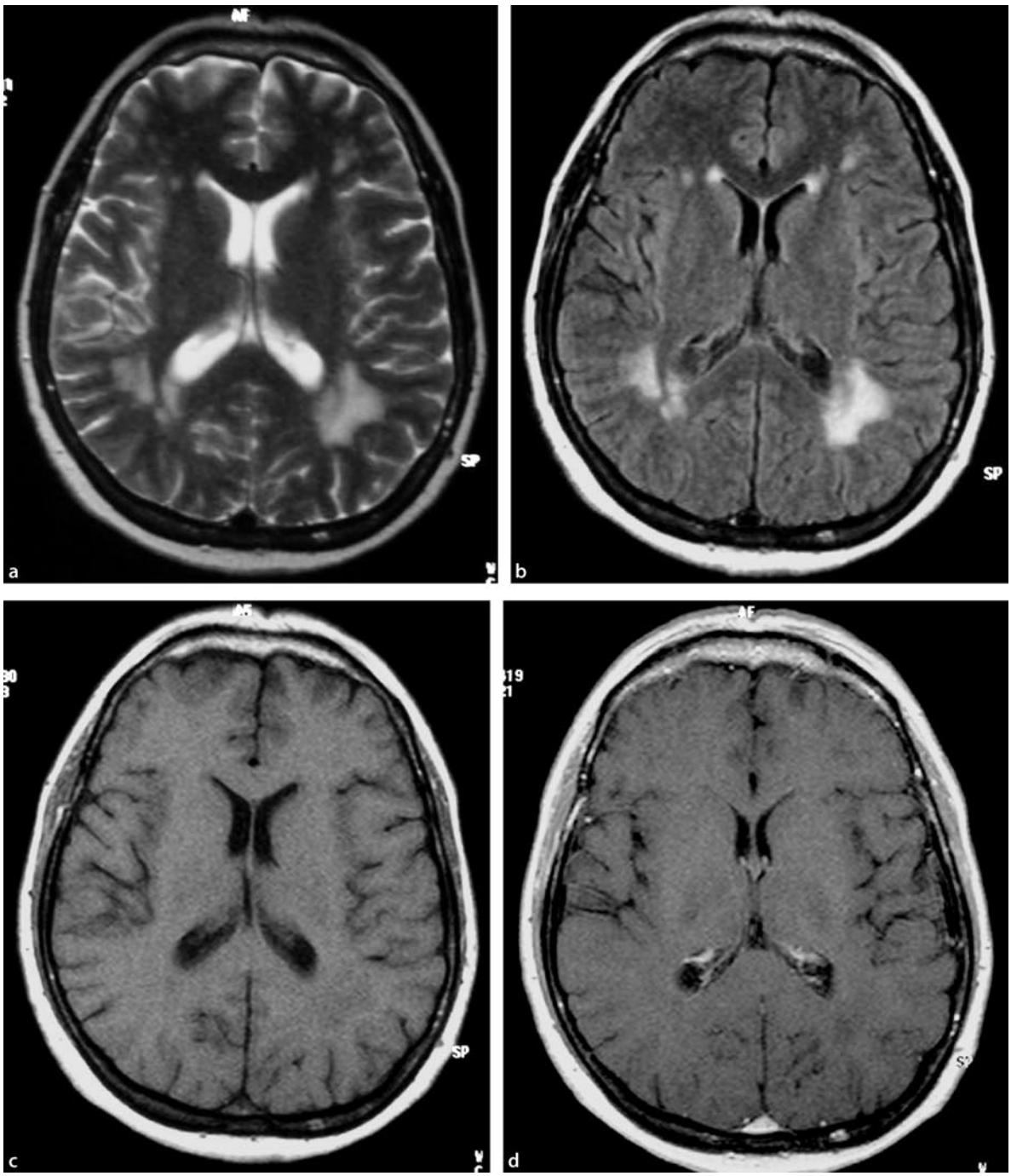

Fig. 91a–d Value of contrast administration: assessment of the activity of inflammatory conditions. A 47-year-old with multiple sensory and motor disturbances. Axial **a** T2w TSE (4,465/120), **b** FLAIR (7,500/TI 2,243/105), **c** plain T1w SE (532/15), and **d** contrast-assisted T1w (532/15) images. Bilateral abnormalities reside in the periventricular zones with elevated T2 signal and well-defined borders. They are barely visible in the T1w sequences. There is no perifocal edema, pressure phenomena or contrast uptake. The outer border (toward the cortex) of the left peritrigonal lesion is scalloped or edema-like. However, note the absence of mass effect given its size and shape. All of the above features count against a diagnosis of infiltrative or active inflammatory/ischemic lesions. Diagnosis: patient with known multiple sclerosis, in remission under strong immunosuppressive therapy

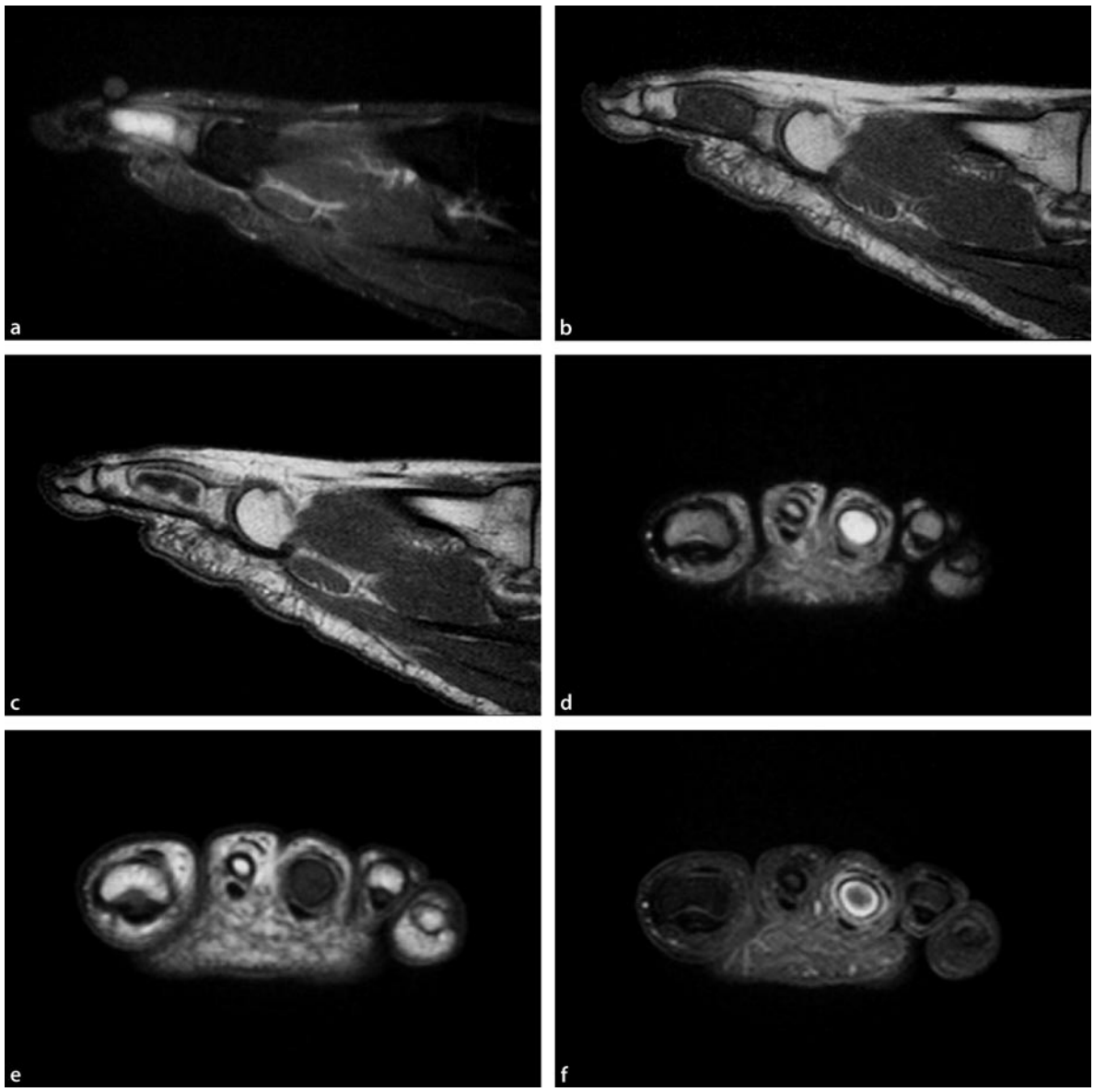

Fig. 92a–f Value of contrast administration: differential diagnosis of cystic vs solid conditions. A 22-year-old woman with pain and swelling of the third toe of the left foot. Sagittal **a** STIR (4,000/TI 120/30), **b** T1w SE (400/12), and **c** contrast-assisted T1w SE views. Coronal **d** T2w TSE (3,000/90), **e** T1w SE (400/12), and **f** fat-suppressed/contrast-enhanced T1w SE (700/20) slices. A homogeneous, low T1 and high T2 signal lesion occupies and expands the medullary cavity of the proximal phalanx of the third toe, sparing the base. Marrow edema in the base of the phalanx shows well in **a**, and is less intense than the "mass". The coronal sections reveal smooth thinning of the cortex. Contrast uptake is intense, limited to the perimeter of the lesion as a thin and complete rim. With fat suppression we also appreciate moderate ring-like enhancement of the periosteal soft tissues. Diagnosis: simple bone cyst

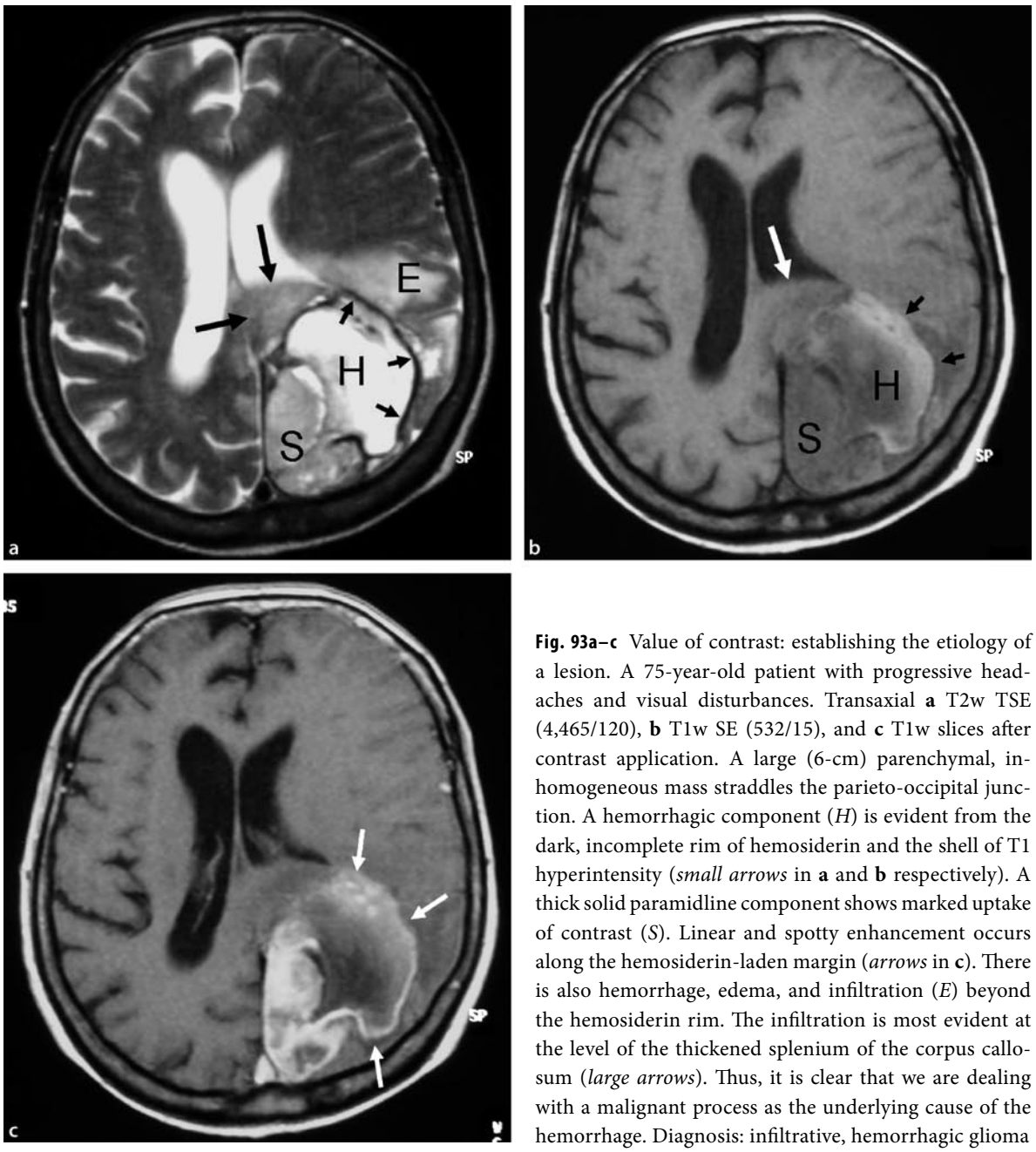

Fig. 93a–c Value of contrast: establishing the etiology of a lesion. A 75-year-old patient with progressive headaches and visual disturbances. Transaxial **a** T2w TSE (4,465/120), **b** T1w SE (532/15), and **c** T1w slices after contrast application. A large (6-cm) parenchymal, inhomogeneous mass straddles the parieto-occipital junction. A hemorrhagic component (*H*) is evident from the dark, incomplete rim of hemosiderin and the shell of T1 hyperintensity (*small arrows* in **a** and **b** respectively). A thick solid paramidline component shows marked uptake of contrast (*S*). Linear and spotty enhancement occurs along the hemosiderin-laden margin (*arrows* in **c**). There is also hemorrhage, edema, and infiltration (*E*) beyond the hemosiderin rim. The infiltration is most evident at the level of the thickened splenium of the corpus callosum (*large arrows*). Thus, it is clear that we are dealing with a malignant process as the underlying cause of the hemorrhage. Diagnosis: infiltrative, hemorrhagic glioma

29 Blood Flow

Keywords

- Time of flight
- Phase shifts

A discussion about flow is a prerequisite for understanding MR angiography. We will concentrate on blood flow, even though the general concepts apply to any fluid, e.g., CSF moving through narrow passages.

Intravascular flow can be quite complex in appearance, depending on vessel characteristics (size, geometry), flow properties (velocity, direction, pulsatility, turbulence), and of course on the type of pulse sequence.

We discern two major classes of successful MR sequences:

1. Those that rely on the travel of the longitudinal magnetization through RF pulses (time of flight)
2. Those that capitalize on the motion of the transverse magnetization though magnetic field gradients (phase shifts)

As an introduction to the topic of time-of-flight or inflow phenomena, we will discuss only the sim-

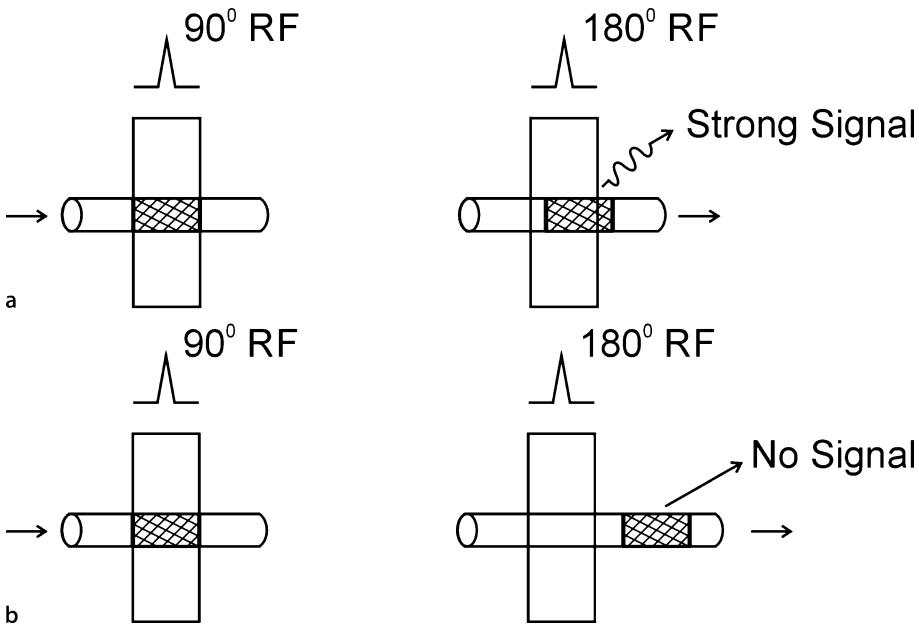

Fig. 94a,b Schematic representation of time-of-flight phenomena.

a Inflow enhancement. *Cross hatched areas*: the flowing spins that perceive the initial excitatory pulse.

b Flow void artifact

plest case: smooth, laminar flow[1] perpendicular to the slice of interest, interrogated with spin echo (SE) techniques. In short TR/short TE SE sequences there is a relatively rapid alternation of the excitatory and refocusing actions, which are slice-selective, i.e., directed at a specific slice. Thus, the stationary tissues of that particular slice are kept in a state of partial saturation.

On the other hand, the inflowing spins, without the burden of prior irradiation, intersect the slice with full magnetization. Their signal intensity depends on the flow velocity. For a certain range of slow velocities most of the moving spins are "caught" within the slice long enough to receive both pulses of a TR cycle. The result is emission of maximum potential signal and "flow" becomes the brightest object in the image. This phenomenon is called "inflow" or "flow-related enhancement" (Figs. 94, 95).

In rapid flow states, the spins have disengaged the slice before the arrival of the refocusing pulse, which is necessary for echo formation. Thus, no signal is elicited from the vessel lumen. This artifact is called the "flow void" or "wash-out" effect and is exploited in the MR angiographic method of "black blood" imaging (Figs. 94, 95).

In the case of phase shift phenomena, sensitivity to flow is afforded by gradients.

Let us first see what happens to the stationary spins. Any phase winding promoted by a gradient is brought back to zero upon reversal of the gradient (Fig. 99, Chap. 17).

On the other hand, motion imparts a phase print that is proportional to flow velocity. Spins relocating between the two gradient lobes are not subjected to mirror image forces and they enjoy a phase slip (Fig. 100). Thus, with the appropriate gradients we

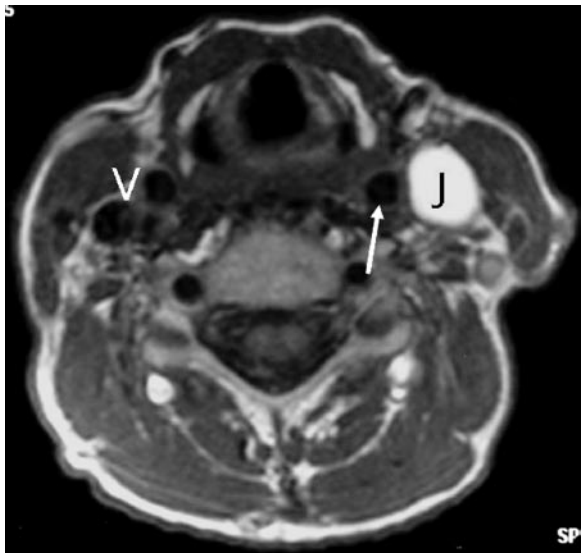

Fig. 95 Magnetic resonance imaging of time-of-flight phenomena. A 72-year-old with neck pain and radiculitis. Transverse T1w TSE (587/12) image from a cervical spine MR scan. The left internal jugular vein (*J*) is large (normal variant). Its signal is bright due to inflow effects*. The left common carotid artery (*arrow*) and the contralateral vessels (*V*) appear "black" due to the signal void phenomenon

* From a single image like this we cannot exclude thrombus in the left internal jugular vein (J). There were no signs of occlusion of J from the rest of the study and there was no clinical evidence of J thrombosis.

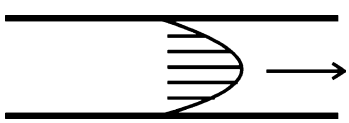

Fig. 96 Laminar flow

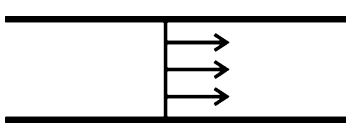

Fig. 97 Plug flow

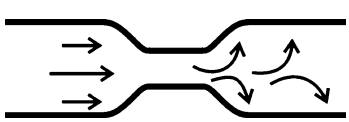

Fig. 98 Turbulent flow

[1] Laminar flow is orderly and its profile looks like a smooth parabolic curve. The velocity peaks in the center of the stream and falls off to zero at the vessel wall (Fig. 96). The two other major types of flow are called plug and turbulent. Plug flow is seen in very small vessels with the front advancing very slowly as a straight line (Fig. 97). Turbulent or disordered flow is characterized by rapid and frequent changes in velocity and direction (Fig. 98). It develops in abrupt bends and in stenoses (Fig. 99).

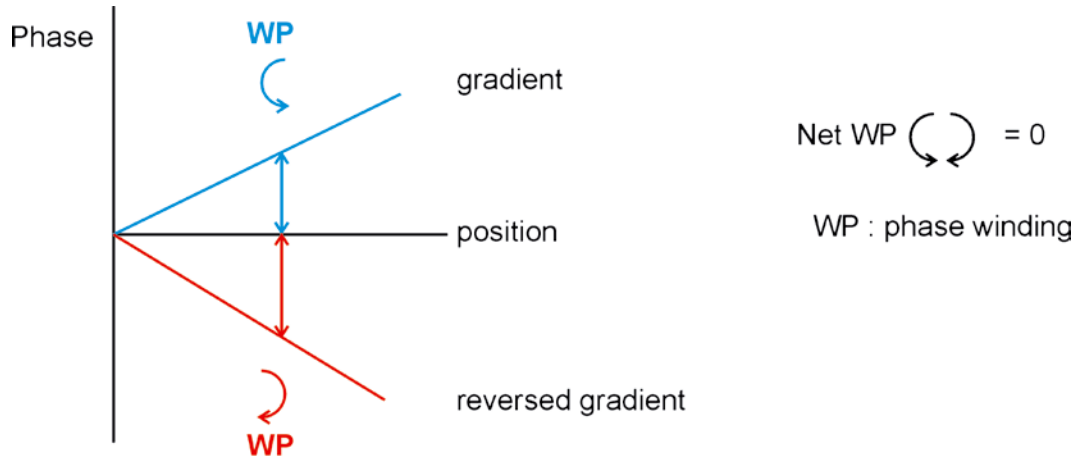

Fig. 99 Phase nulling of immobile tissues. The stationary spins are subjected to forces of the same strength and duration, but of the opposite direction. All phase shifts slips induced by the first gradient are neutralized after the second gradient

can gain qualitative as well as quantitative information about flow.

This situation calls for a double measurement, with and without flow-sensitizing gradients (similar to diffusion weighting). Our purpose is to subtract the two sequences from each other and "eliminate" the immobile tissues.

Any phase residue "belongs" to flow and its magnitude is a complex function of flow velocity. The numbers from the vector subtraction of the phase shifts become meaningful only relative to a reference value, called VENC (velocity encoding).

We can think of VENC as a narrow window: what we see depends on the position of the window. In other words, the brightness of flow depends on the match between the actual flow velocity and the window we have chosen (VENC).

The following discussion is about motion-induced signal loss that occurs in both time-of-flight and phase shift methods. Regardless of the type of flow, spin velocity is not uniform, even within the same voxel. While the spins drift apart along the axis of the magnetic gradient there is progressive phase divergence and thus truncation of the final signal. This type of signal deficit is accelerated in vascular bends, bifurcations, and post-stenotic jets, due to abrupt changes in the magnitude and direction of flow velocity. To counteract these dephasing events we have to employ small voxels and short TEs. Regarding the latter, GE sequences possess a significant advantage over SE methods. GE schemes do not use RF pulses for refocusing the spins, which translates into time savings to echo collection (shorter TE.)

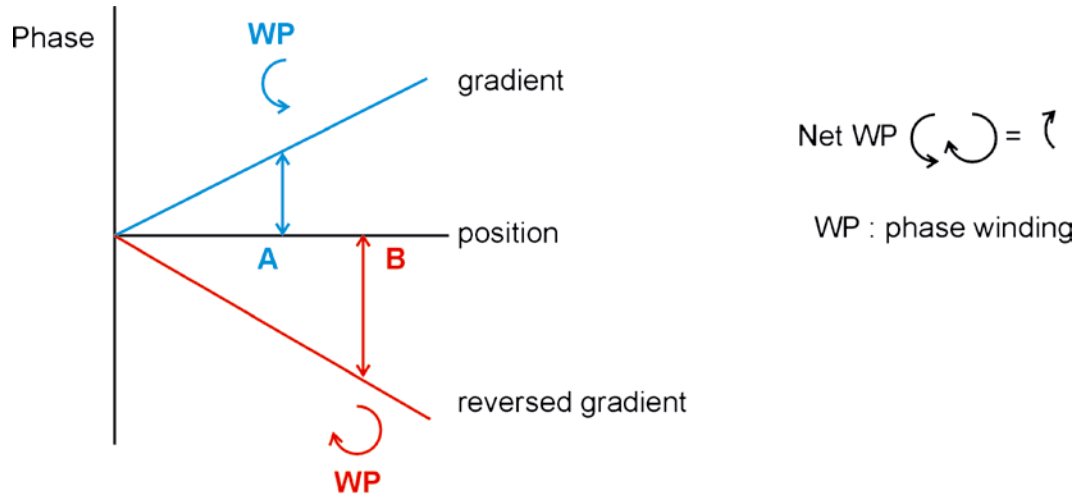

Fig. 100 Phase persistence of flowing spins. Let us follow a spin flowing rightward along a gradient. When it reaches point *A* we reverse the gradient for a finite duration. During this time, the spin has moved to point *B*, experiencing a greater absolute value of the gradient. Thus, in point *B* the phase slip is stronger and reversed than in point *A*. At the end of the bipolar gradient, therefore, the flowing spins have acquired a phase tag. The progression or regression of phase depends on the "initial" and "final" location of the spins relative to the two lobes of the gradient. Thus, the phase residue of the flowing spins is proportional to the flow velocity. Please be reminded that we cannot rectify the dissipation of signal due to inhomogeneities of the static field B or due to the T2 decay process, whether the spins are moving or stationary

30 MR Angiography

Keywords

- Time of flight (inflow)
- Phase contrast
- Contrast-enhanced MRA

Magnetic resonance angiography examinations are technically demanding, since they require high resolution in a relatively short time. There are three major classes of MRA: time-of-flight, phase contrast, and contrast-enhanced.

In time-of-flight (TOF) MRA, both "black" and "bright" blood techniques are available, each with relative merits (Figs. 101, 102). We will concentrate on "bright" blood MRA.

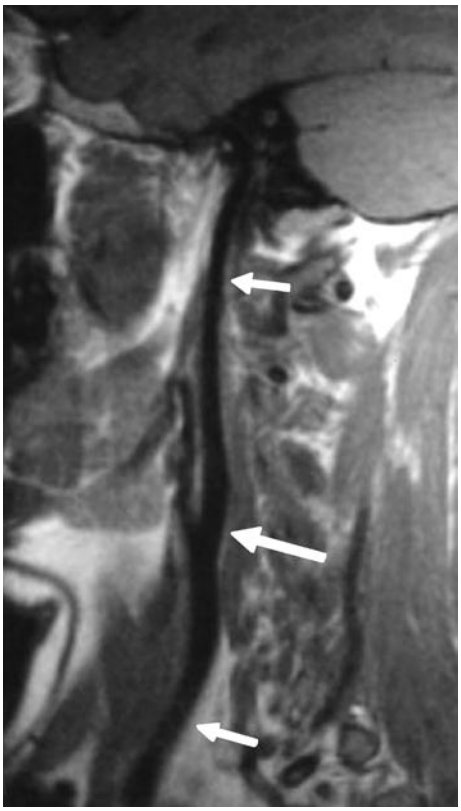

Fig. 101 Black blood MRA. 27 year old underwent MR study because of neck pain and radiculopathy. Lateral T1w TSE section (640/12): the right common and internal carotid arteries fortuitously are "caught" in a straight course to the skull base (the *arrow* points to the bulb). The proximal external carotid is also seen

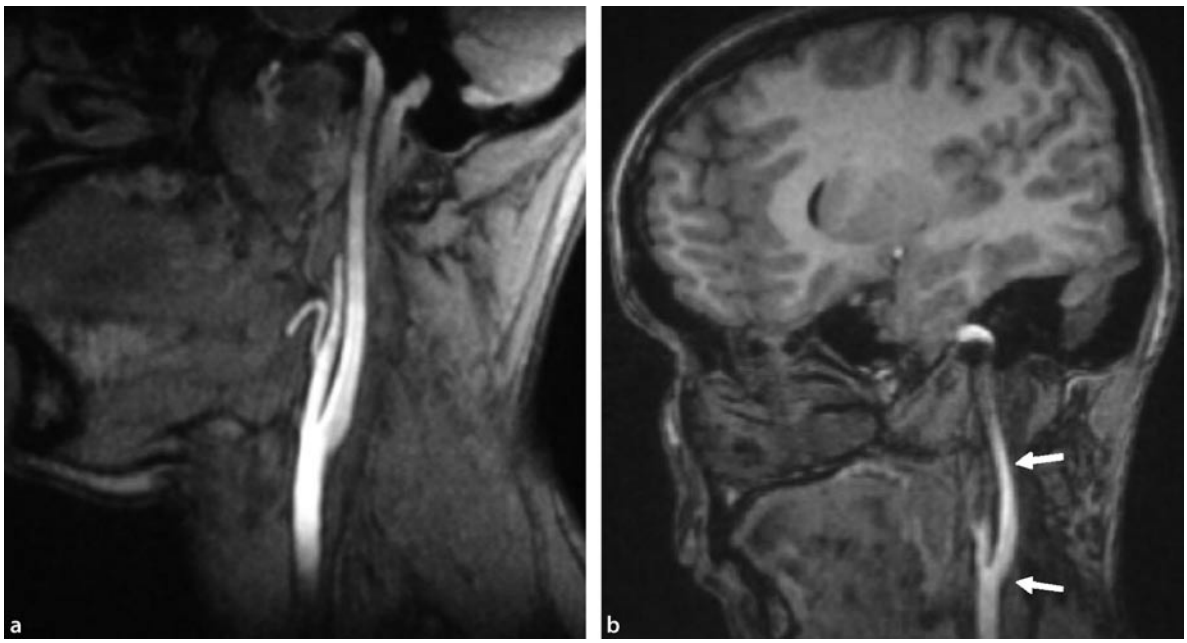

Fig. 102a,b Bright blood MRA. **a** Thin slice (source image) from a 3D sagittal acquisition (36/10/20°). Flow in the carotid system appears bright with excellent depiction of the lumen against a partially suppressed background. **b** Oblique lateral reconstruction from a 3D T1w gradient echo sequence of the brain. The carotid appears bright (*arrows*) due to inflow effects

In most cases we want to separate the arteries from the veins in order to avoid overlap. Saturation pulses irradiate the blood outside the imaging field and exhaust its signal capacity before arrival in the region of interest (Fig. 103).

It is cumbersome to trace mentally the continuity of the vessels from slice to slice in a large stack of MRA images. Useful formats should create a three-dimensional impression of the vessels from any viewing angle we wish. The most common post-processing algorithm relies on the principle of maximum intensity projection (MIP). Imagine rays emanating from the eye of the viewer that pierce the volume of interest. Along the path of each ray we pick the brightest pixel and assign that value to the corresponding pixel of the final projection image (Figs. 104–106). The MIP method is also used in phase contrast MRA and in contrast-enhanced MRA. Please note that in data processing there is a loss of information. For example, small or "faint" aneurysms or hypoplastic segments may not show up in MIP. Thus, the source images should always be studied meticulously, in conjunction with the reconstructions.

Artifactual signal loss in TOF MRA can be due to:

1. Turbulent jets (in vessel bends/bifurcations or post-stenotic vortices)
2. Saturation, due to sluggish flow or in-plane flow or thick slab (Fig. 107)
3. Magnetic susceptibility (e.g., at the skull base entrance of the internal carotid arteries in the petrous canals)

This type of artifact may result in the overestimation of stenoses, faint depiction of aneurysms, or underestimation of the vessel lumen. In extreme cases, vessels appear discontinuous.

Another inconvenient artifact is the "shine through" of structures with short T1 values. Even though the inflow sequences are heavily weighted toward T1 there is variable success in background suppression. Let us consider some examples in the head. The scalp and orbital fat diminish the overall visibility of vessels, especially in the orbits. Following contrast injection the normal, enhanced pituitary and cavernous sinuses may obscure the carotid siphons.

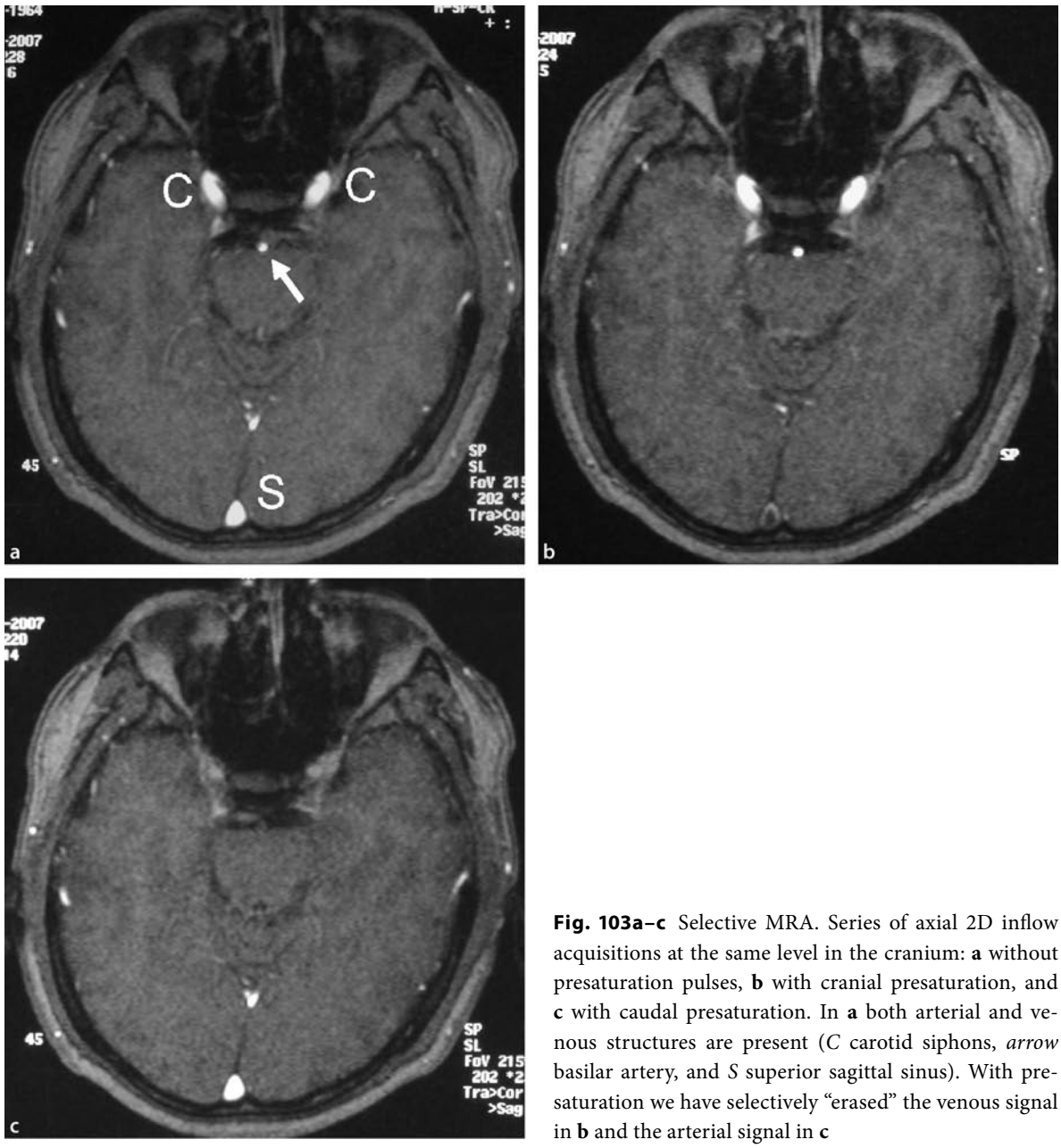

Fig. 103a–c Selective MRA. Series of axial 2D inflow acquisitions at the same level in the cranium: **a** without presaturation pulses, **b** with cranial presaturation, and **c** with caudal presaturation. In **a** both arterial and venous structures are present (*C* carotid siphons, *arrow* basilar artery, and *S* superior sagittal sinus). With presaturation we have selectively "erased" the venous signal in **b** and the arterial signal in **c**

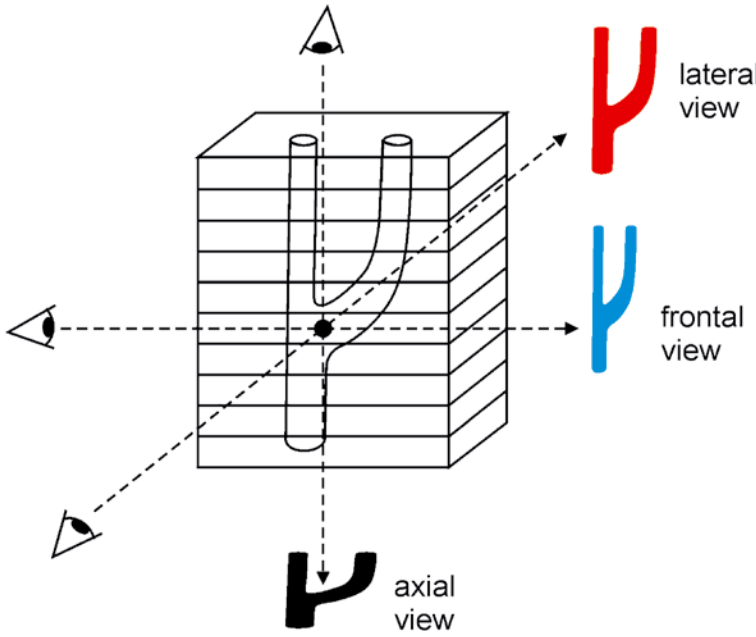

Fig. 104 Maximum intensity projection (MIP) algorithm. Let us take a carotid bifurcation as an example, imaged transversely. With the MIP algorithm we can "walk" around the stack of slices and view the data as projections from different angles

Some hematomas can hide the underlying source of bleeding, e.g., if a ruptured aneurysm is surrounded completely by hyperintense thrombus.

Phase contrast (PC) MRA has several unique features compared with TOF MRA, rendering the two techniques complementary. Let us look at the peculiarities of PC MRA:

1. There is complete suppression of the background, due to the subtraction algorithm, at the expense of increased scan time (Figs. 108, 109).
2. The need for velocity encoding (VENC). We choose a value and the machine searches for flow velocity within a narrow range around the VENC. The brightness of flow depends on the match of the actual velocity to the preselected VENC (Fig. 108). Great mismatch results in signal drop-out, necessitating multiple VENC steps to ensure or exclude vascular occlusion.
3. A complete 3D angiogram requires velocity encoding in three orthogonal directions, thus multiplying the total acquisition time. High resolution (3D) PC MRA is very time-consuming. On the contrary, a projection (2D) PC angiogram is quite fast, albeit of limited spatial resolution.

In contrast-enhanced MRA we use gadolinium that lowers the T1 rate of blood, resulting in:

1. The apparent augmentation of inflow phenomena, which compete with saturation, wash-out, and dephasing forces. The final appearance of a vessel depends on the specific pulse sequence, vessel geometry, and flow dynamics (Figs. 110, 111).
2. The propagation of luminal signal deeper into the imaging volume. In other words, with gadolinium we can combat saturation phenomena. This property is very convenient for the coverage of long vascular segments, such as the thoracic or abdominal aorta.

The concepts of contrast-enhanced MRA are similar to those of CT or catheter angiography. We want to create a "dense" cast of the vessels without arterio-venous overlap. Careful timing of contrast administration to data acquisition is crucial in order to "catch" the bolus in the first "pass", before recirculation effects (Figs. 112, 113). By necessity these sequences are brief (less than 20 s acquisition time) and can be conducted during breath-holding.

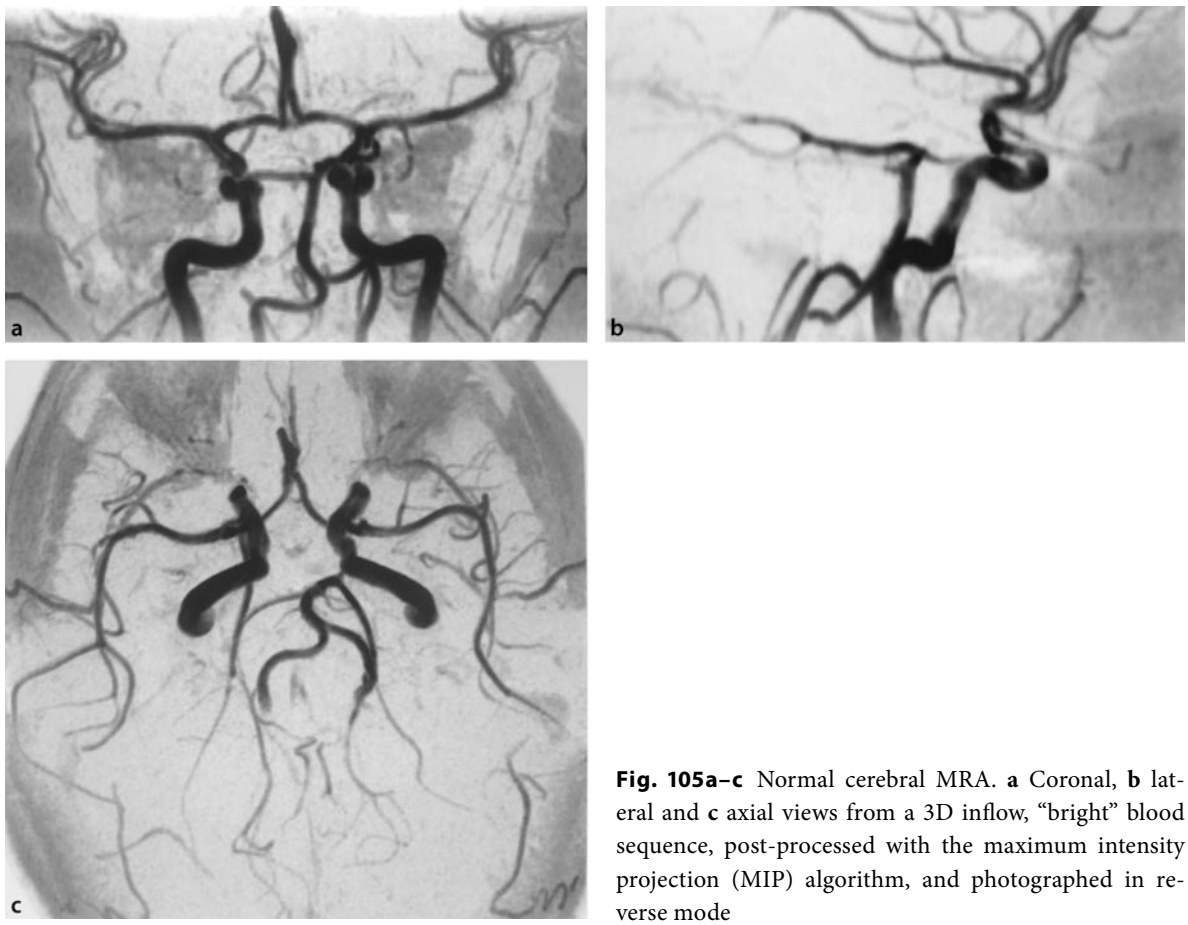

Fig. 105a–c Normal cerebral MRA. **a** Coronal, **b** lateral and **c** axial views from a 3D inflow, "bright" blood sequence, post-processed with the maximum intensity projection (MIP) algorithm, and photographed in reverse mode

► **Fig. 106a–e** Correlation of black and bright blood angiographic methods. A 72-year-old woman with an episode of amaurosis fugax. **a**, **b** Axial T2w images and **c–e** reconstructions from a 3D inflow acquisition (TR/TE/θ 37/9.6/20). **c** Parasagittal 2D slice, **d** "lateral" 3D view targeted about the midline (excluding the middle cerebral arteries), and **e** coronal 3D view. The patient harbors two small lobulated aneurysms in the right anterior cerebral artery (*arrows*) without a neck or thrombus (lumen diameter 8 mm proximally and 6 mm distally). The larger of the aneurysms appears "faint" in **d** and **e** due to turbulent or recirculating flow in the core, resulting in loss of signal. Also, note the atherosclerotic irregularity of the distal basilar artery (*B*) and the poor flow/stenosis of the right middle cerebral artery (*M*).

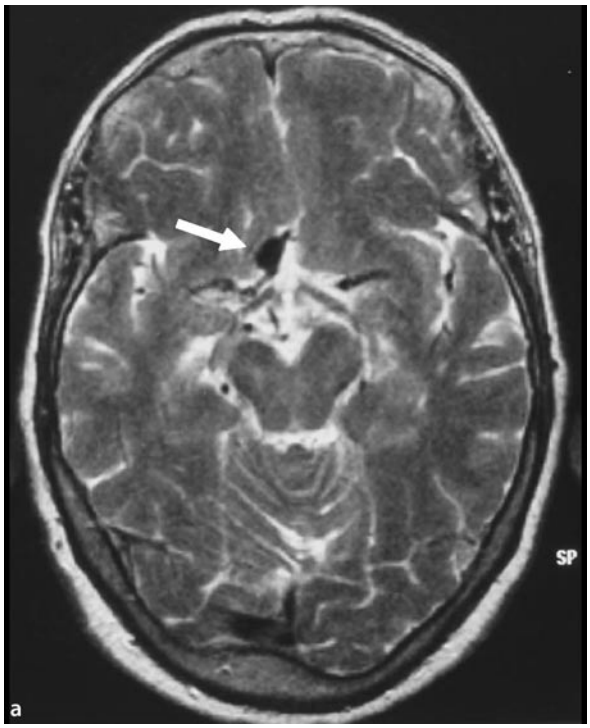
SP
a

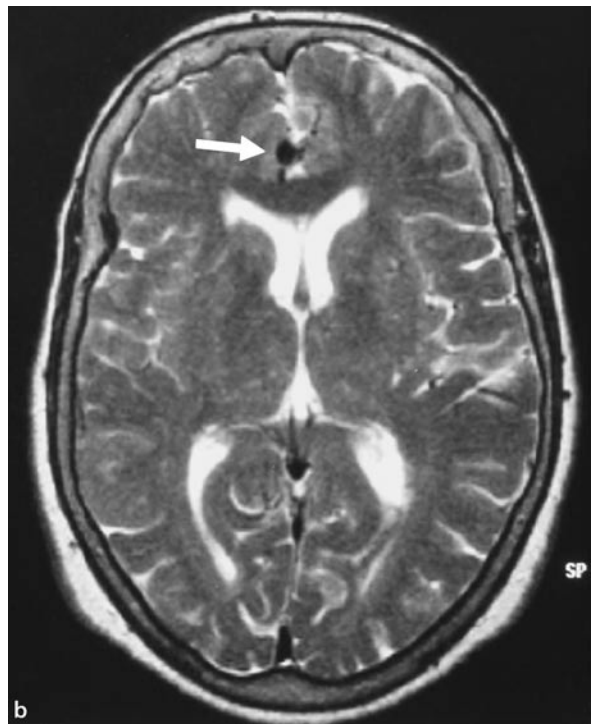
SP
b

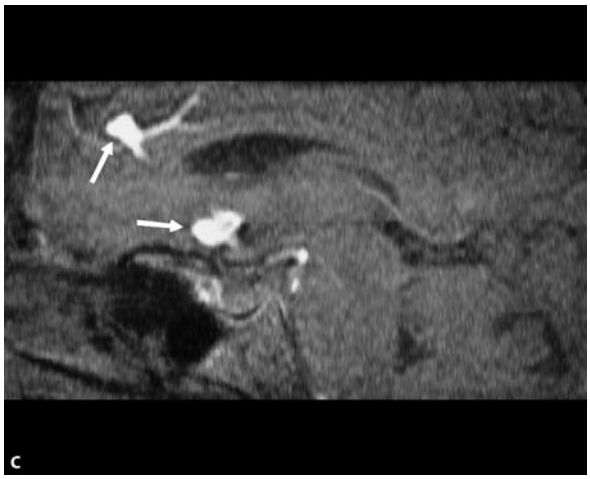
c

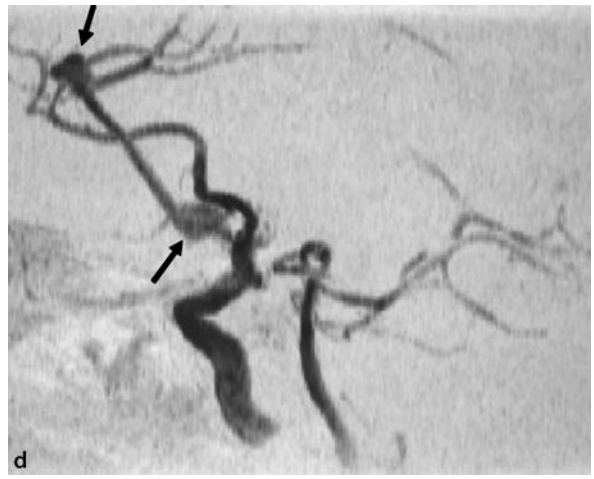
d

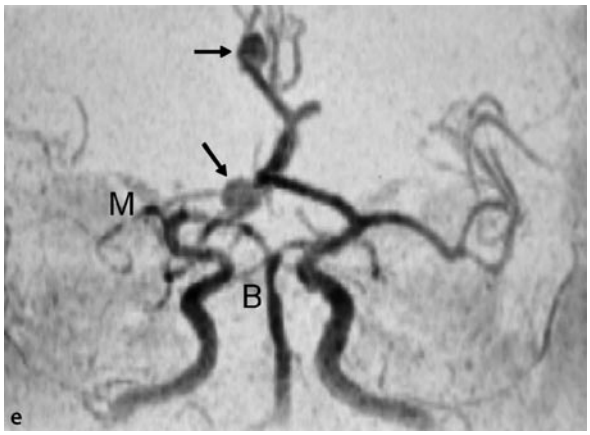
M
B
e

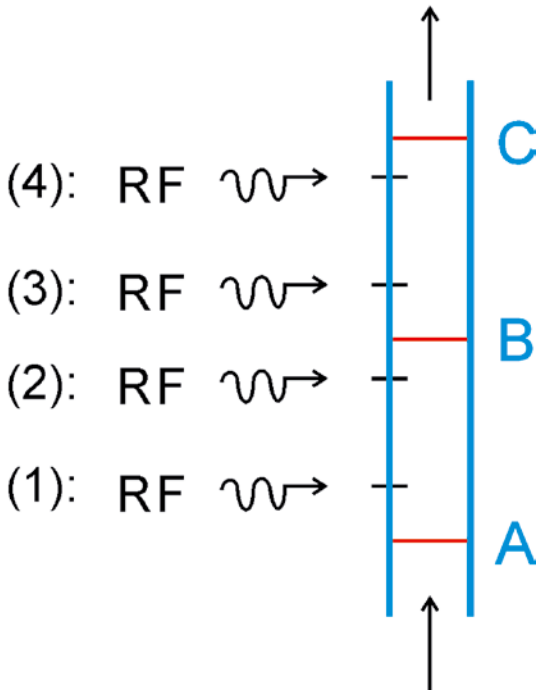

Fig. 107 Saturation. Here, blood is shown to flow at constant velocity, in a straight path, and perpendicular to the imaging volume, entering at level *A*. The head of the moving blood column experiences a greater number of RF excitatory pulses than does the tail. Thus, saturation of blood occurs to a greater degree in the leading front than in the trailing edge

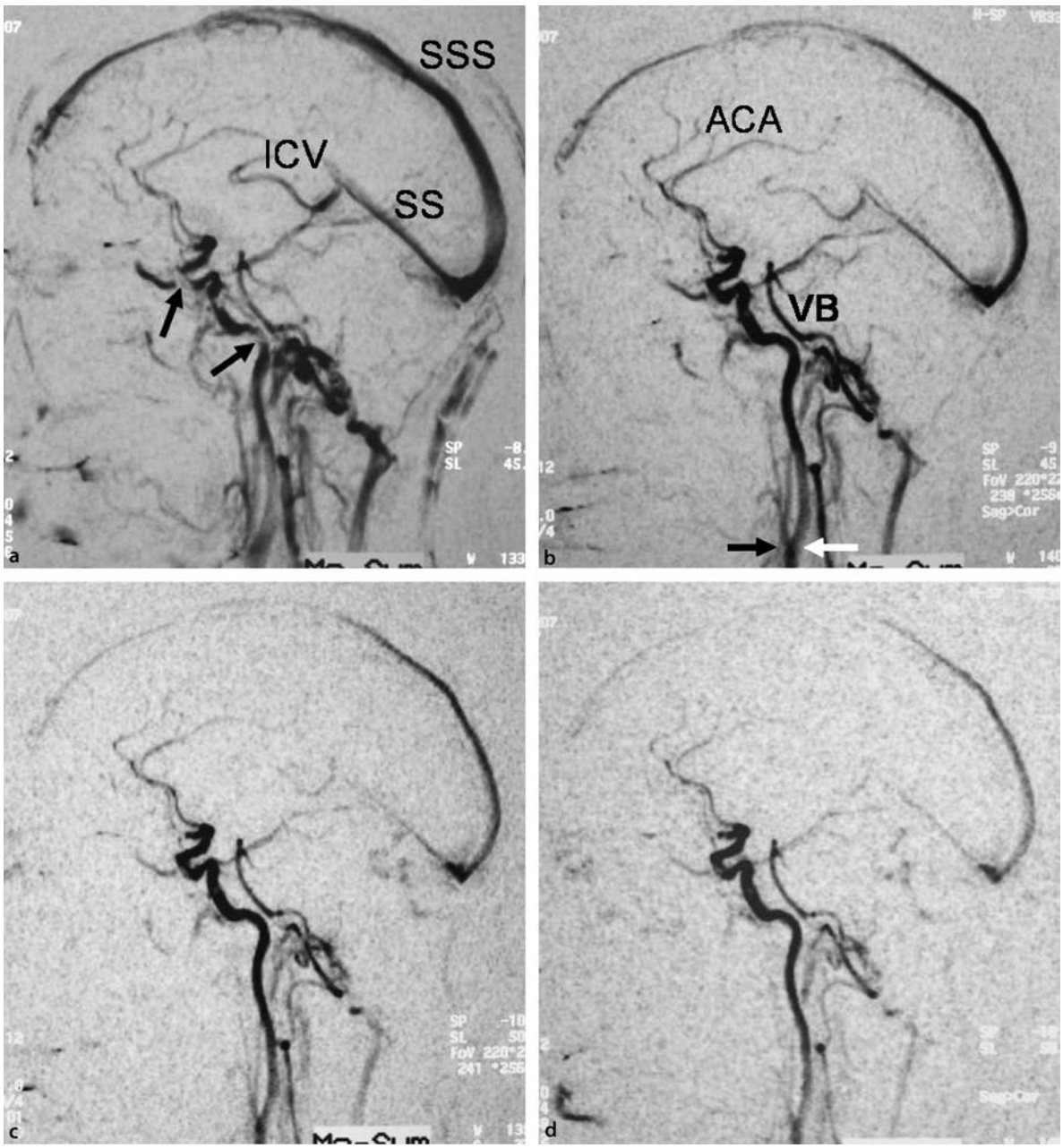

Fig. 108a–d Velocity encoding (VENC): manipulation of contrast (vessel visibility) in phase contrast MRA (normal 40-year-old volunteer). Midsagittal (45-mm thick slab) PC angiograms with different VENC: **a** 10 cm/s, **b** 30 cm/s, **c** 45 cm/s, **d** 60 cm/s. A low VENC (**a**) is suited for depiction of the deep and superficial venous system. At this VENC (10 cm/s) the carotid bends appear artifactually discontinuous (*arrows*, compare with the other images). As VENC increases, there is progressive "drop-out" of venous structures as well as small arterial branches. In this particular example, a VENC of 30 cm/s (**b**) is optimal for the depiction of the carotid bulb (*arrow*), vertebrobasilar system (*VB*) and the distal anterior cerebral arteries (*ACA*). *ICV* internal cerebral veins, *SS* straight sinus, *SSS* superior sagittal sinus

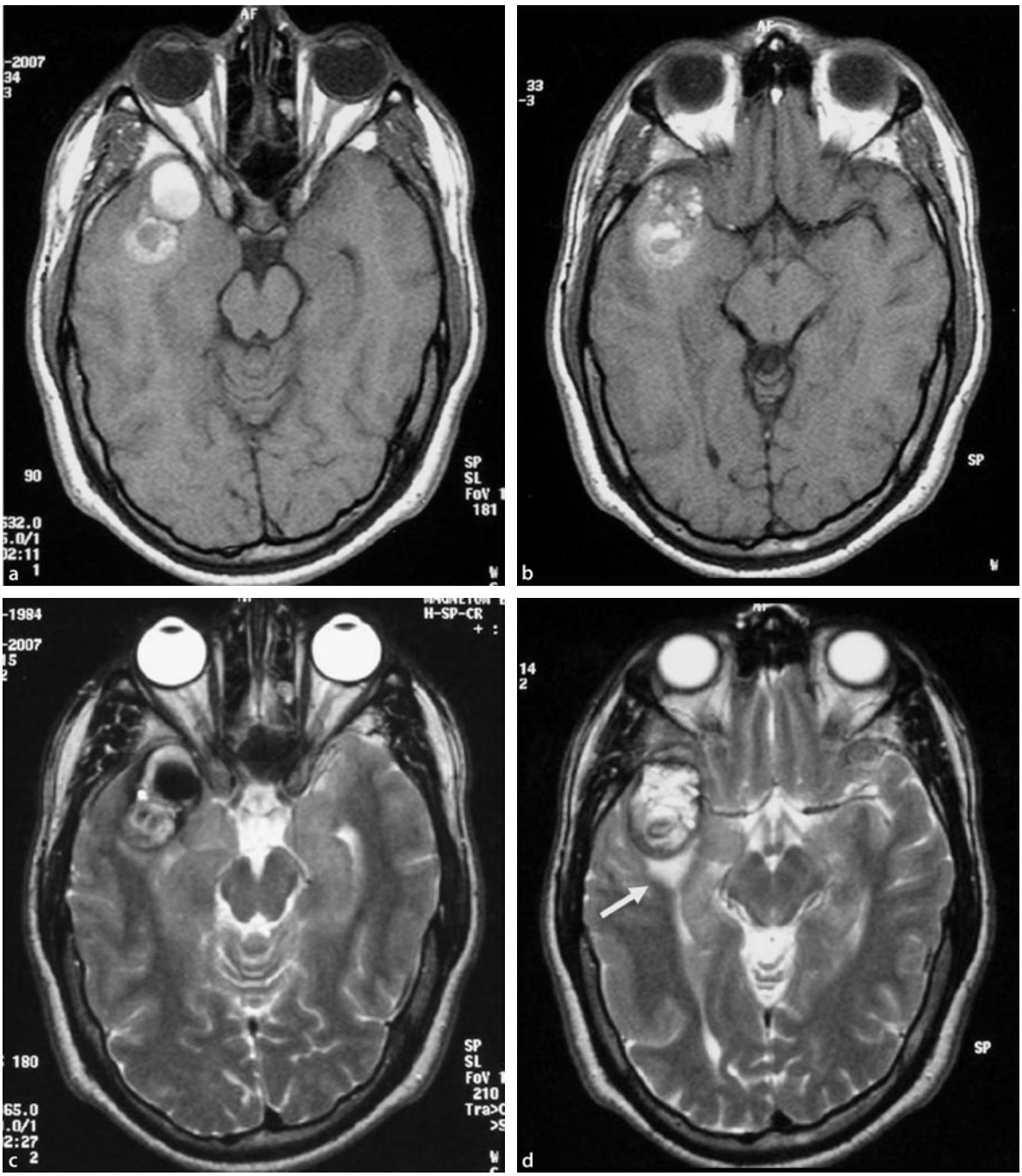

Fig. 109a–j Correlation of TOF and PC MR angiographic methods. A 23-year-old with acute onset headaches and an epileptic crisis. **a**,**b** Two consecutive transverse T1w SE (532/15) images. **c**,**d** Corresponding T2w TSE (4,465/112) slices. **e**–**j** *see next page*

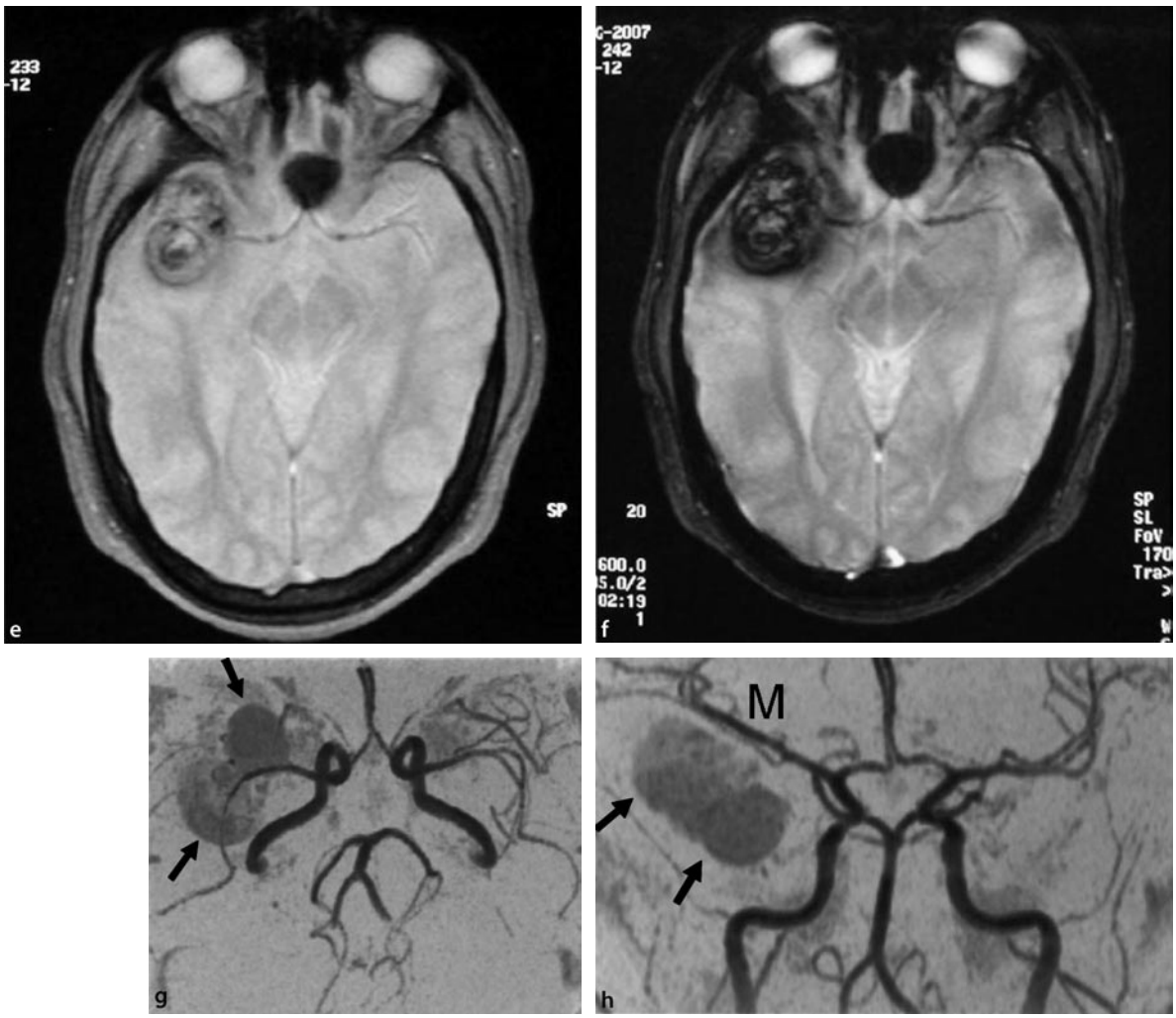

Fig. 109a–j *(continued)* **e**,**f** Dual echo/gradient echo (600/15; 35/20°) images corresponding to **b** and **d**. Bilobed right temporal lobe lesion with bizarre, mixed T1 and T2 signal intensity, and marked "blooming" artifact. There is also slight edema posteriorly (*arrow*). **g**,**h** Transaxial and coronal MIP views from a TOF 3D angiographic scan (37/9.6/20°). The lesion "shines" through (*arrows*) and elevates the middle cerebral artery (*M*). **i, j** *see next page*

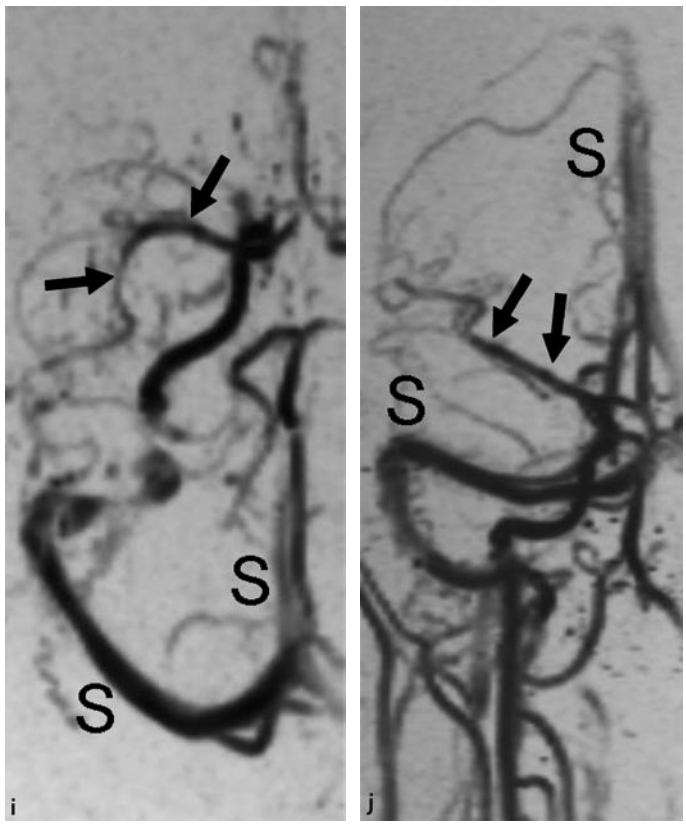

Fig. 109a–j *(continued)* **i** and **j** Corresponding MIP reconstructions from a phase contrast sequence (VENC 30, post-contrast infusion). The lesion has been "subtracted" out. The *arrows* point to the right middle cerebral artery. Dural sinuses (*S*) are also visible in addition to arteries. The mass was resected and the diagnosis was cavernoma with fresh and old hemorrhage

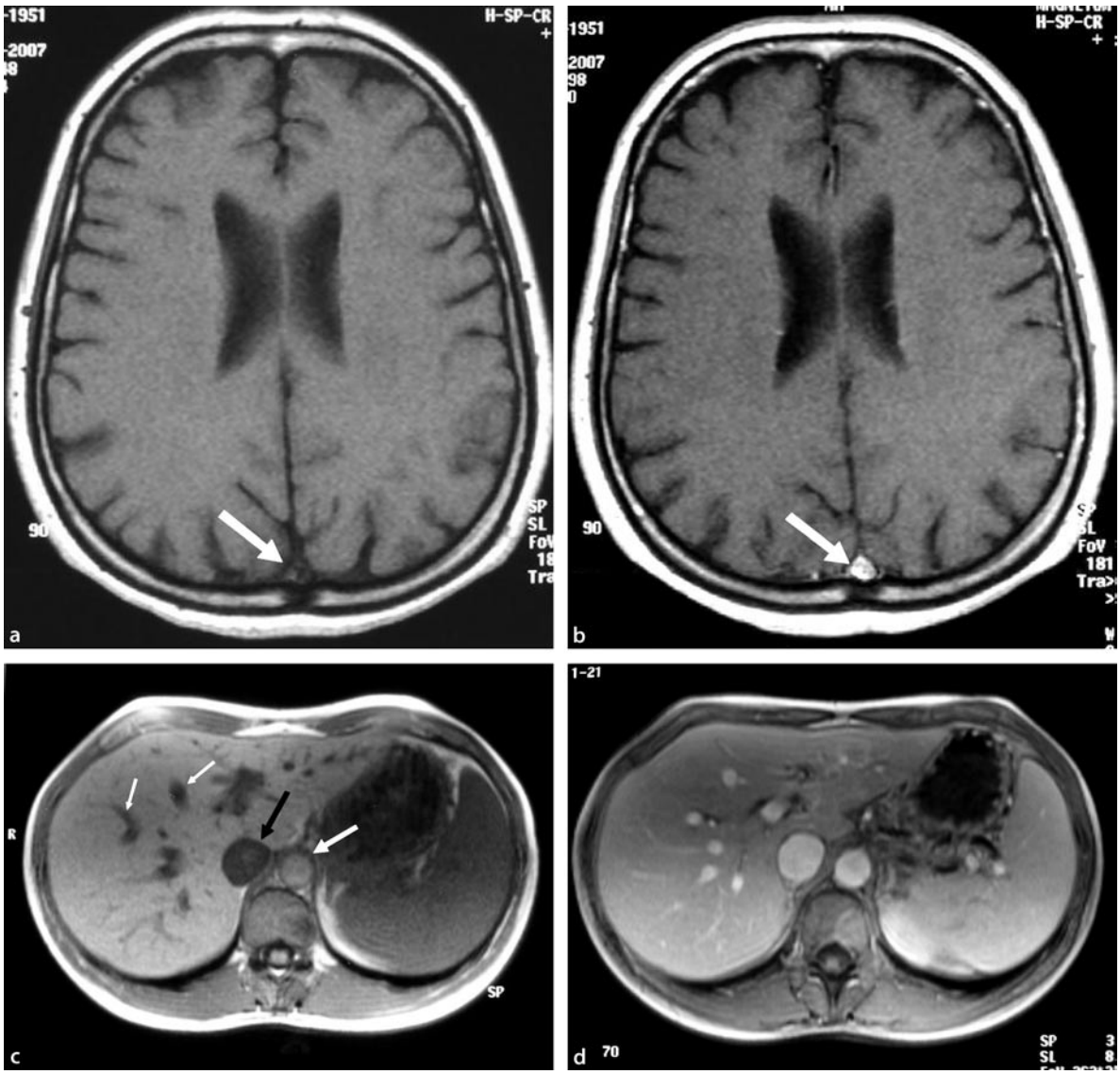

Fig. 110a–d Reduction of T1 of flowing blood due to enrichment with gadolinium. **a**,**b** T1w SE (532/15) images before and after intravenous gadolinium administration. Note enhancement of the lumen of the superior sagittal sinus (*arrows*). **c**,**d** T1w gradient echo sequences (150/6/70°) before and after injection of gadolinium, portal venous phase. Marked enhancement of the aorta (*large white arrow*), inferior vena cava (*black arrow*), and intrahepatic veins (*small white arrows*)

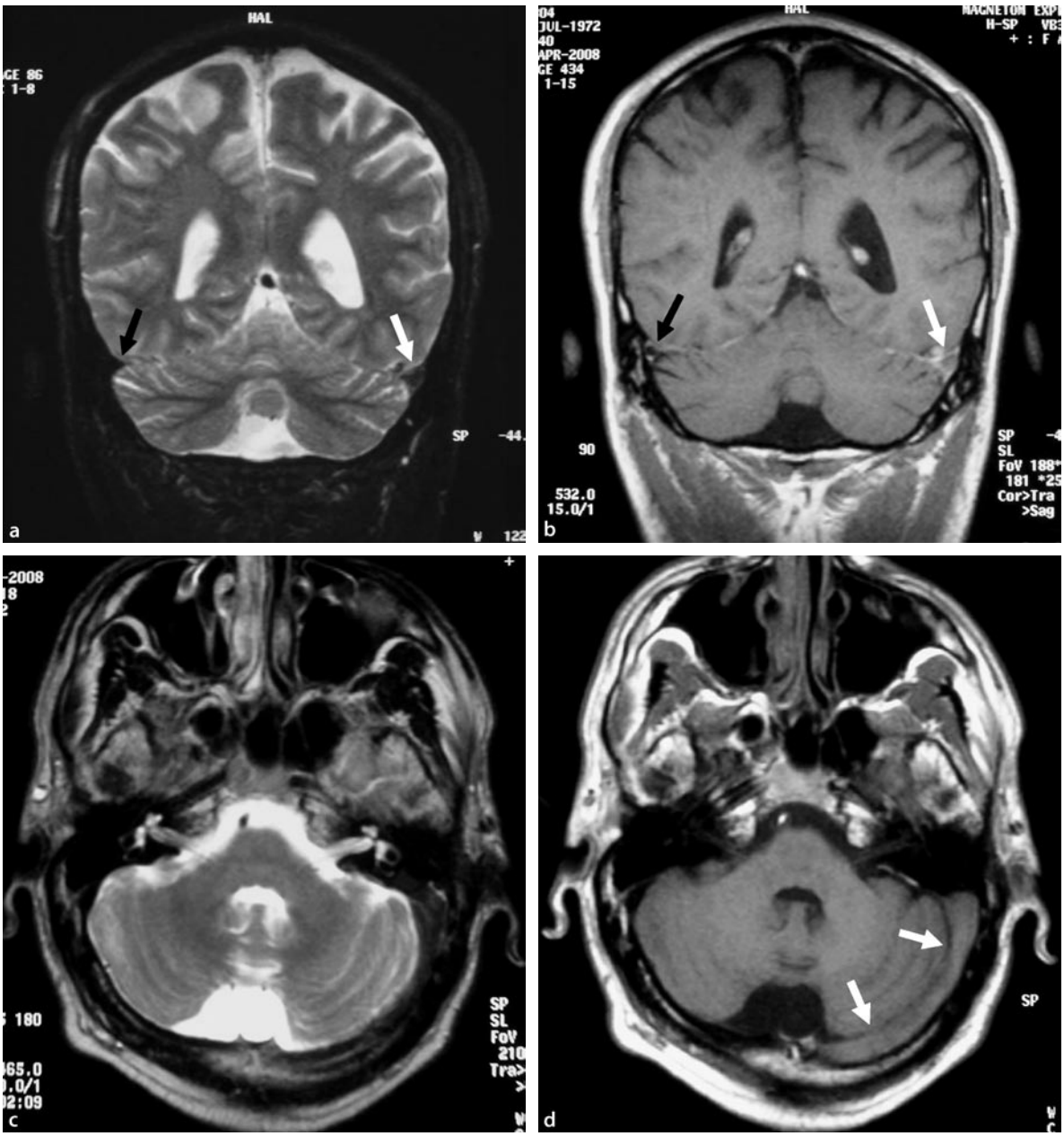

Fig. 111a–f Evaluation of cerebral dural sinuses before and after intravenous contrast administration. A 26-year-old with acute severe headache. Non-contrast CT scan was interpreted as normal (not shown). The patient was referred for an MRI scan. No parenchymal or extra-parenchymal abnormalities were seen. **a**,**b** Coronal STIR (5400/T1 120/30) and post-contrast T1w SE (532/15) images. The left transverse sinus appears "gray" with enhancement of its walls (*white arrows*). Normal situation on the right with signal void (*black arrows*). **c** Transverse T2w TSE (4465/120), **d** T1w SE (532/15), and **e** post-contrast images. **e**,**f** *see next page*

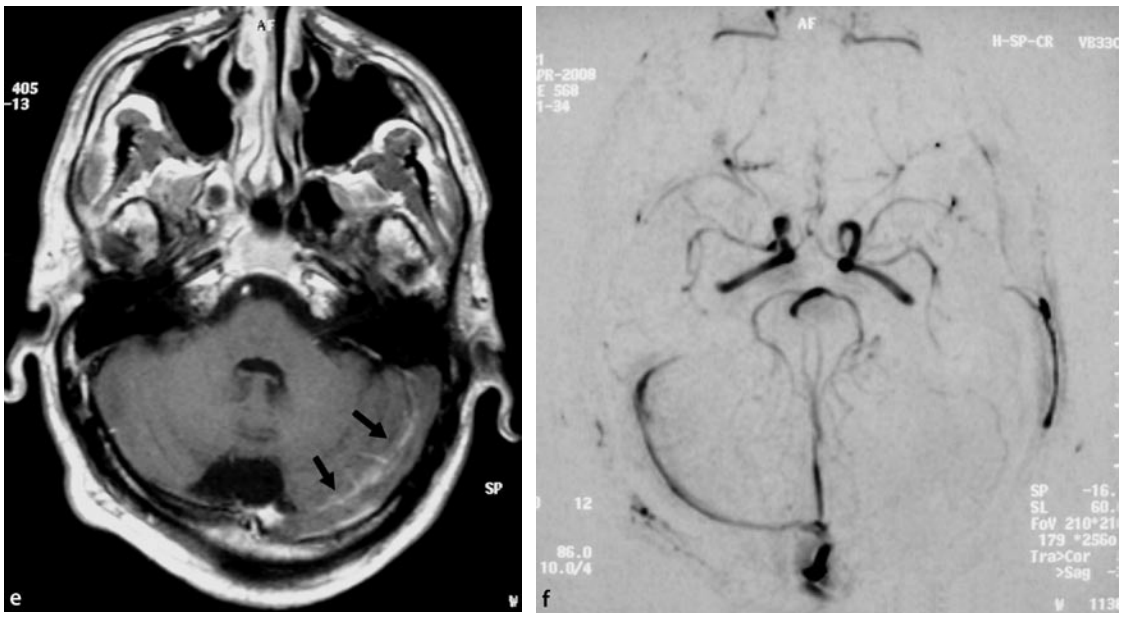

Fig. 111a–f *(continued)* **e** The thrombus is isointense to the parenchyma (*arrows*), fills the lumen of the sinus, and is outlined by the enhancing walls (*black arrows*). **f** Axial 2D phase contrast MR angiogram (VENC 30, post-contrast): absence of flow in the left transverse sinus

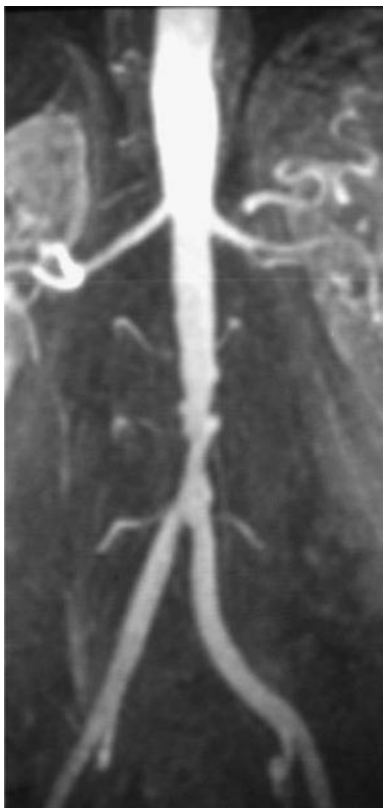

Fig. 112 Abdominal aortic atherosclerosis. A 58-year-old diabetic hypertensive patient. Contrast-enhanced MR aortography (5.7/2.2/30°), coronal MIP view. Atherosclerotic irregularity and stenosis of the distal aorta

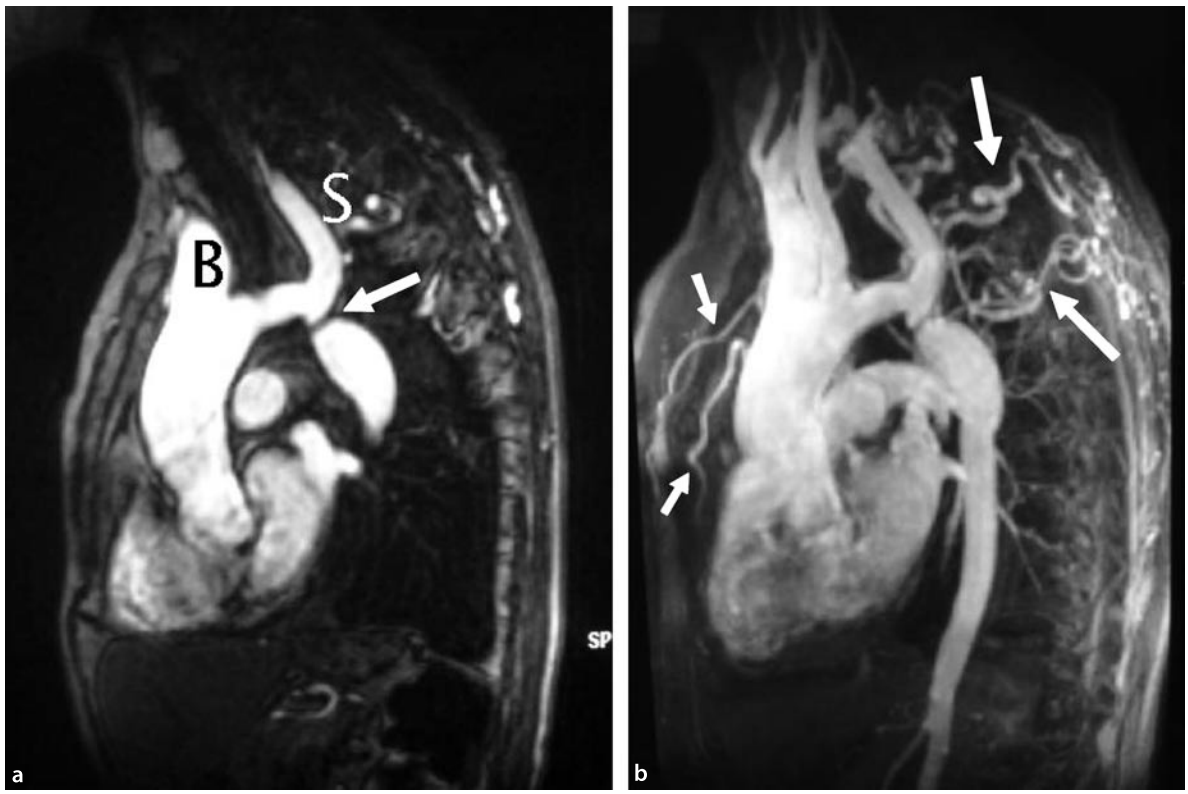

Fig. 113a,b Aortic coarctation. A 52-year-old thin woman of short stature with a difference in arterial pressure in the upper extremities. Contrast-enhanced MR arteriography (5.7/2.2/30°), **a** source image and **b** oblique sagittal MIP view. **a** Aortic arch stenosis beyond the brachiocephalic (*B*) take-off and complete interruption (*arrow*) just distal to the origin of the subclavian artery (*S*). **b** Reconstitution of the descending aorta occurs through hypertrophied intercostal branches (*large arrows*). Note dilatation of the internal mammary arteries (*small arrows*) as part of the collateral network. There is also dilatation of the aortic arch branches

Basics of MR Examinations and Interpretation

31

Now we are ready to attack the practical considerations of the performance and interpretation of MRI, many of which are of course applicable to any type of radiologic study. Some of the remarks are personal thoughts and preferences of the author.

Proper planning of the MR study depends on the relevant anatomy and pathology. For example, knee ligaments and menisci are evaluated to advantage in the sagittal and coronal planes. Evaluation of the pituitary gland requires higher resolution than brain examinations. Remember, though, that we cannot have everything: there is always a trade-off among resolution, acquisition time, and SNR.

Several protocols have been tried and established for any type of MR study, the basic premise being three planes and at least T1–T2 weighting. Additional sequences (e.g., fat saturation) and additional planes (obliques) are recruited as needed, in order to fully address the clinical question.

A multiplicity of sequences and a variety of planes increase the likelihood of lesion detection and lesion characterization (at the expense of longer scan times).

Correlation in three planes affords optimal evaluation of the gross anatomic extent of the abnormality (Fig. 114). The availability of three planes is also convenient, to confirm a suspicion as a true finding, or to dismiss a suspicion as an artifact.

A combination of sequences is necessary for lesion characterization, or for prediction of histopathology. Now is the appropriate time to summarize the anatomic correlates of various signal patterns, keeping in mind that MRI "looks" at mobile protons, mostly in water and lipids. The nonmobile protons are invisible due to extremely rapid T2 decay (e.g., collagen).

On the T1 scale, the most intense structures are fat and some hematomas (Fig. 115). Moderate to marked T1 hyperintensity can be achieved by intravascular flow, blood clots, and melanin (Fig. 116). On the T2 scale, extreme intensity is achieved by fluids/cysts, mucoid/myxoid material (Fig. 117), and some hematomas. Hematomas may behave in a bizarre way, depending on their age, location, sequestration, and other factors (Figs. 53, 115). However, a detailed discussion of hemorrhage is beyond the scope of this book.

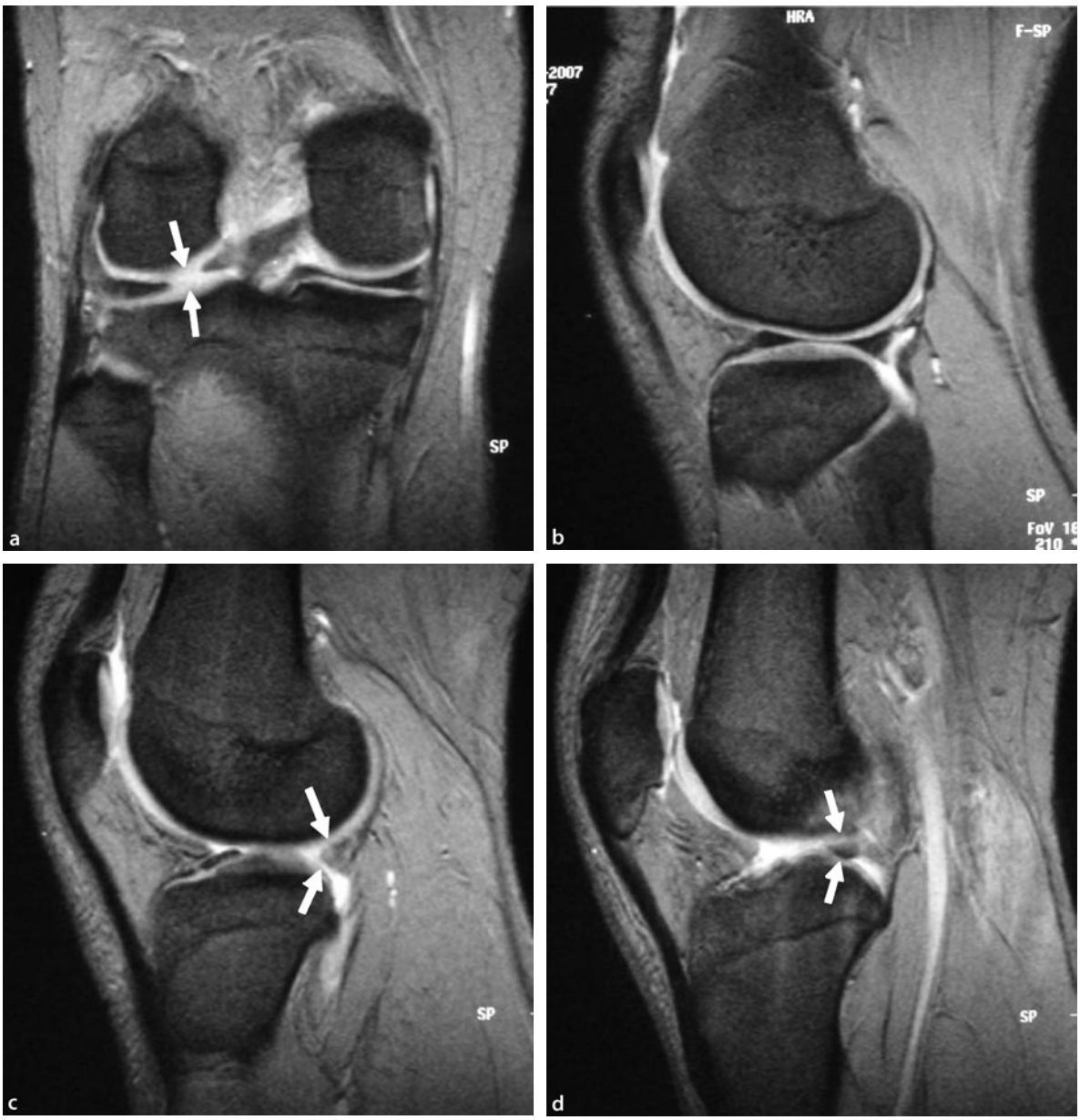

Fig. 114a–f Three-plane correlation of findings. A 23-year-old with knee pain and locking 2 months post trauma. **a** Coronal T2* (817/23/35°) section depicts a defect of the free edge of the posterior horn of the lateral meniscus (*arrows*). **b–d** Sagittal T2* (817/23/35°) images. **b** Both meniscal horns appear normal in a far lateral slice. **c** Two steps toward the midline: there is bright signal in the posterior horn and truncation of its free edge (*arrows*). **d** Moving closer to the center of the joint we see a normal root of the posterior horn (*arrow*). From images **a–d** we cannot ascertain with confidence the extent of the tear. **e**, **f** *see next page*

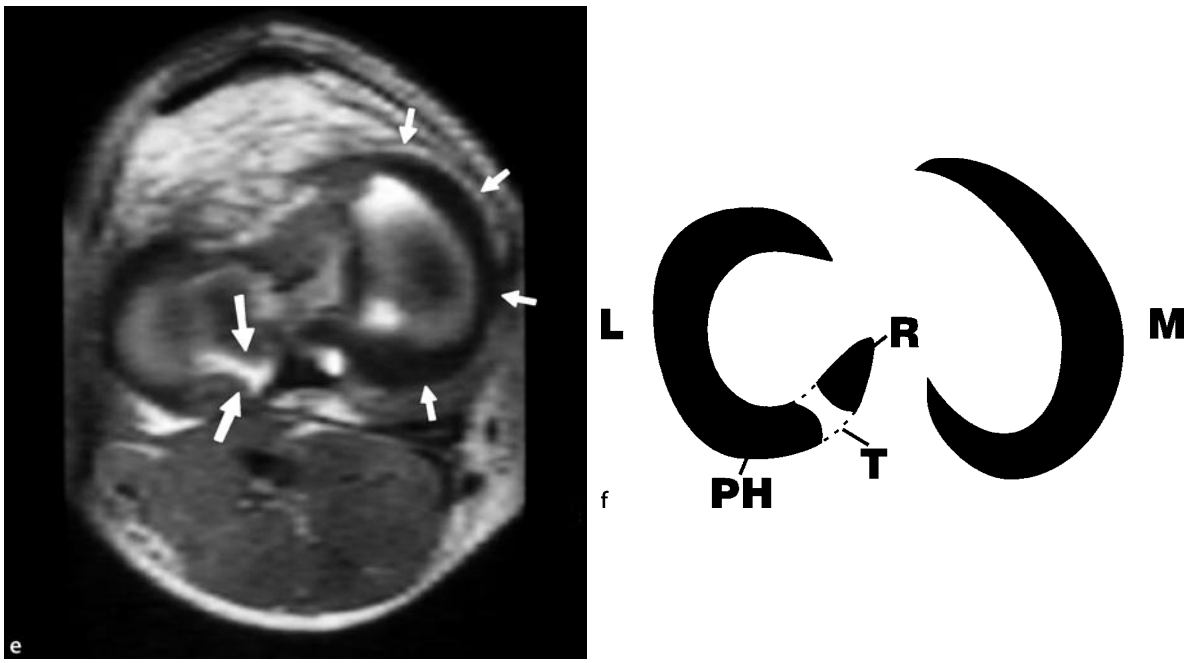

Fig. 114 *(continued)* **e** Axial reconstruction from a 3D gradient echo acquisition: hyperintense joint fluid outlines the gap between the meniscal fragments (*large arrows*). The gap measures up to 0.4 cm and is close to the root of the posterior horn. There is disruption of the entire radial thickness of the meniscus (free margin to capsular surface). The *small arrows* outline the medial meniscus. **f** Schematic representation of slice **e**. The tear's oblique orientation explains its confusing appearance in the sagittal and coronal imaging planes. *L* lateral meniscus, *PH* posterior horn, *R* root of the PH, *M* medial meniscus, *T* radial, full thickness tear

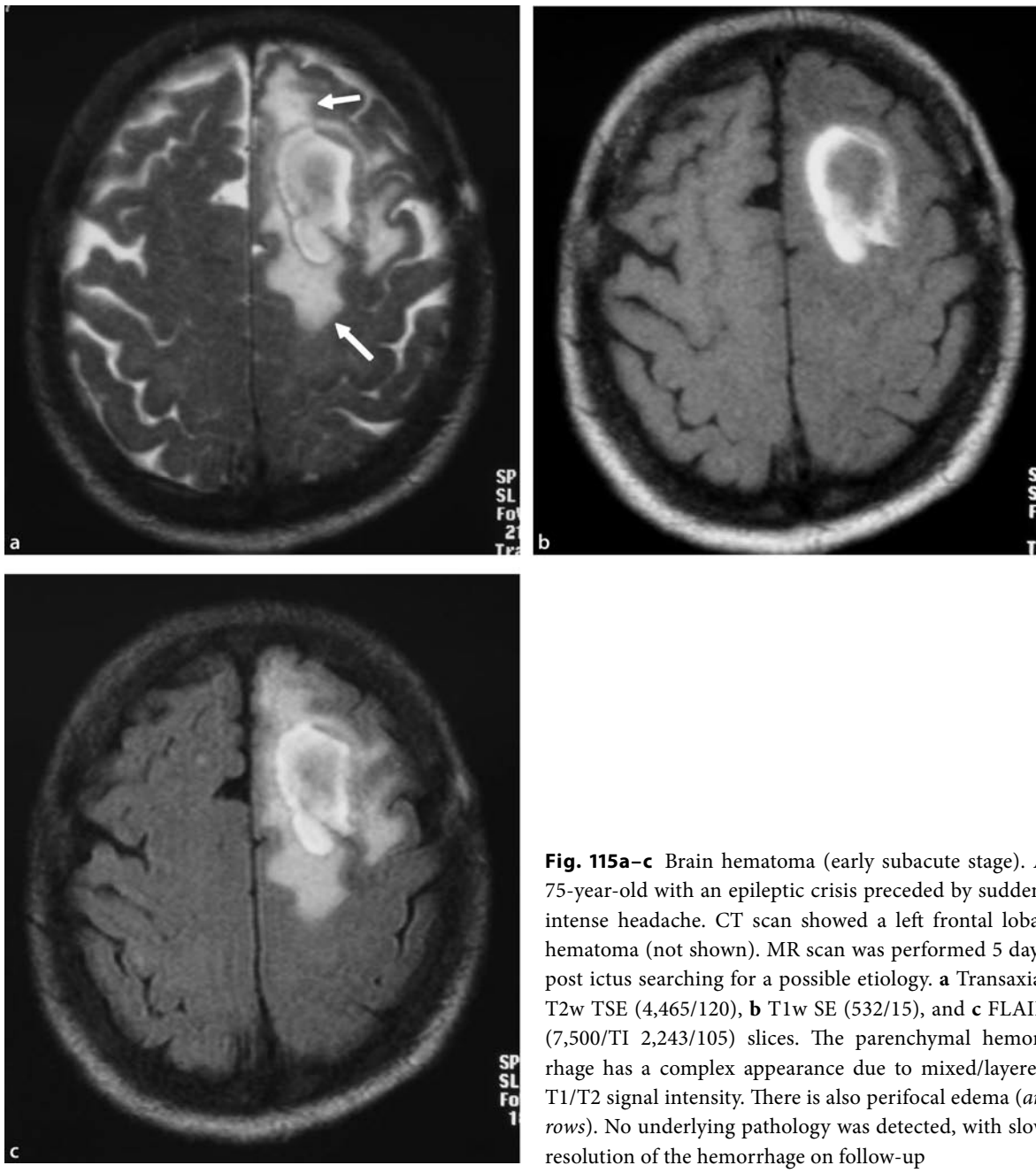

Fig. 115a–c Brain hematoma (early subacute stage). A 75-year-old with an epileptic crisis preceded by sudden, intense headache. CT scan showed a left frontal lobar hematoma (not shown). MR scan was performed 5 days post ictus searching for a possible etiology. **a** Transaxial T2w TSE (4,465/120), **b** T1w SE (532/15), and **c** FLAIR (7,500/TI 2,243/105) slices. The parenchymal hemorrhage has a complex appearance due to mixed/layered T1/T2 signal intensity. There is also perifocal edema (*arrows*). No underlying pathology was detected, with slow resolution of the hemorrhage on follow-up

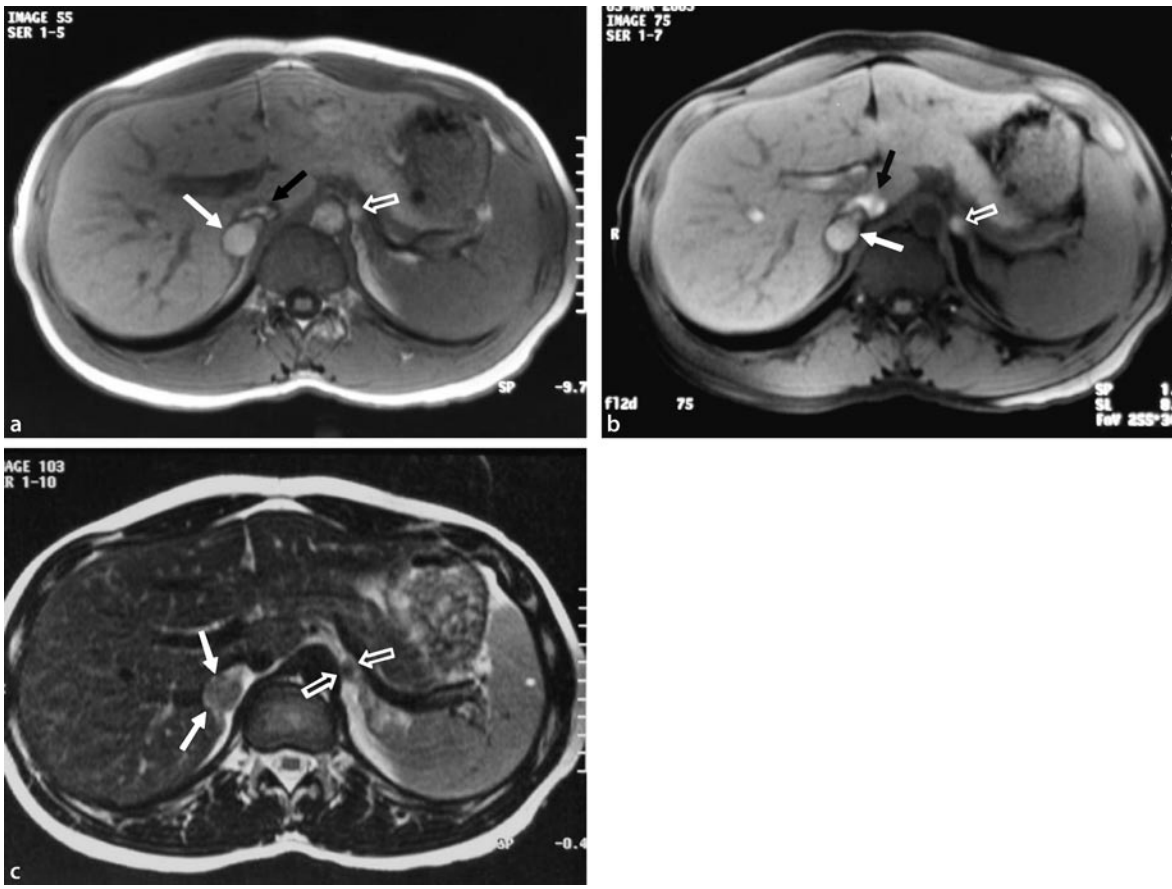

Fig. 116a–c Metastatic melanoma. A 24-year-old with multiple pulmonary nodules undergoing a search for the primary site. Abdominal MRI study in a transverse orientation: **a** T1w gradient echo (GE, 156/6/70°), **b** fat-suppressed T1w GE (163/4.8/75°), and **c** T2w TSE (3,135/138) images, all with breath-holding. A well-defined 2.3-cm mass in the right adrenal (*solid white arrows*) is hyperintense in **a** with signal intensity similar to peritoneal and retroperitoneal fat. The mass stays bright after fat suppression **b**. It has intermediate T2 signal intensity, similar to spleen and brighter than liver in **c**. The inferior vena cava (*black arrows*) is deformed and compressed by the mass. Note the similar, much smaller lesion in the contralateral adrenal (*open arrows*). Diagnosis: metastatic melanoma, biopsy-proven. No skin lesions were detected. Melanin, as a paramagnetic agent, is responsible for this signal pattern, which is not specific; it can also occur in some hematomas (early subacute stages). Incidentally, the vena cava appears very bright on the T1w images, due to inflow phenomena (Chap. 29)

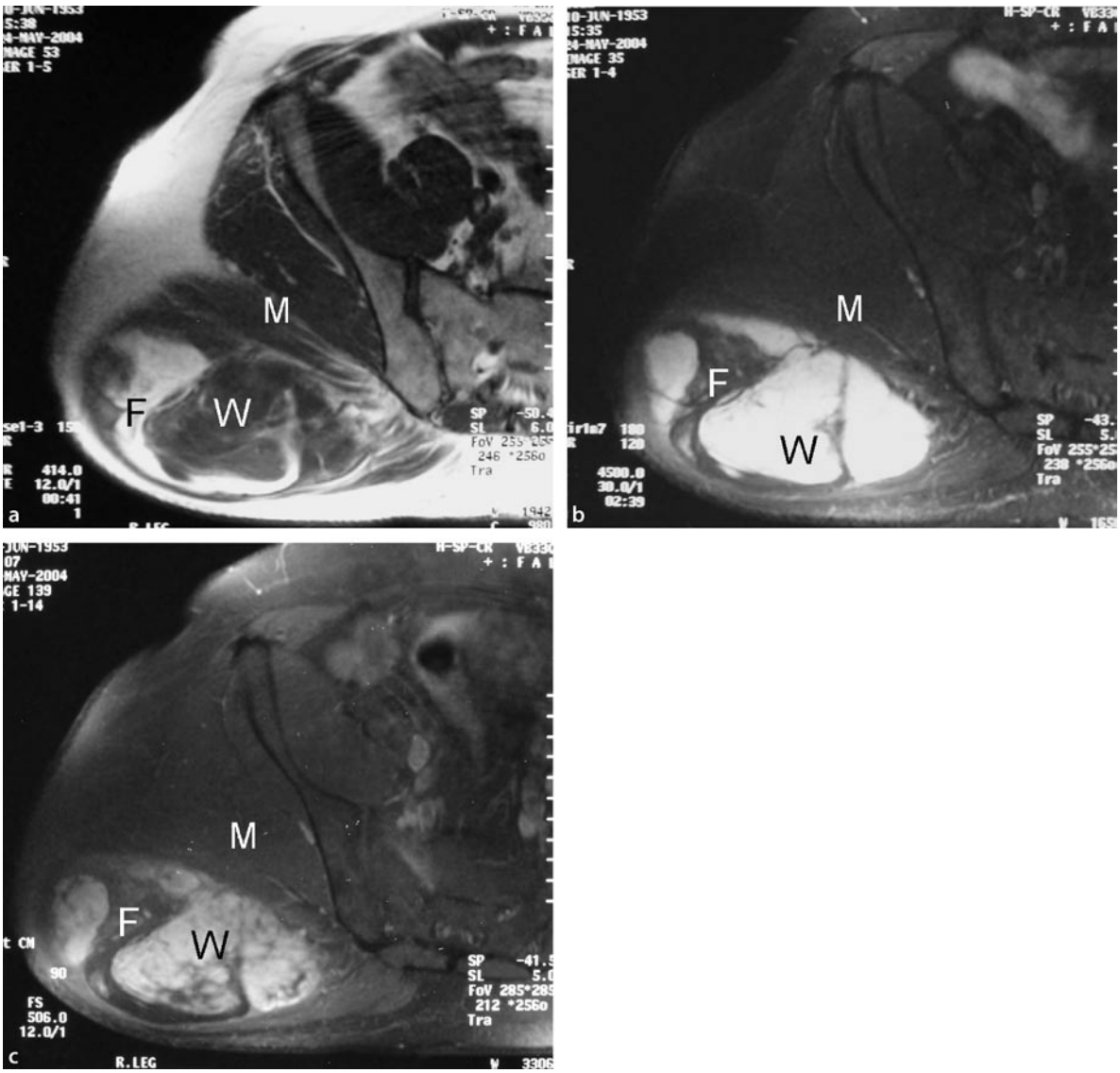

Fig. 117a–c Fluid mimic. A 50-year-old with an enlarging mass in the right buttock. Axial **a** T1w SE (414/12), **b** STIR (4,500/TI 120/30), and **c** fat-suppressed/contrast-enhanced T1w (506/12) images. A large (15-cm) inhomogeneous mass is embedded in the superficial buttock musculature (*M*). Let us look at the noncontrast images first. The mass has two components: one behaves like fat (*F*) and sends septa to the water-like constituent (*W*). Now let us turn to image **c**, which is from a selective fat suppression sequence: we become certain that *F* is fat (since its signal is abolished). Note the avid enhancement of *W*. Thus, *W* is not water or some other type of fluid[1]. The mass was resected surgically and *W* corresponded to a myxoid matrix. Diagnosis: myxoid liposarcoma

[1] There are two exceptions to this statement: cystic or necrotic parts of tumors may trap contrast in delayed images due to passive diffusion from enhancing solid components, and contrast administered intravenously may accumulate in joint fluid via passage through the synovial lining, especially when leaky or inflamed.

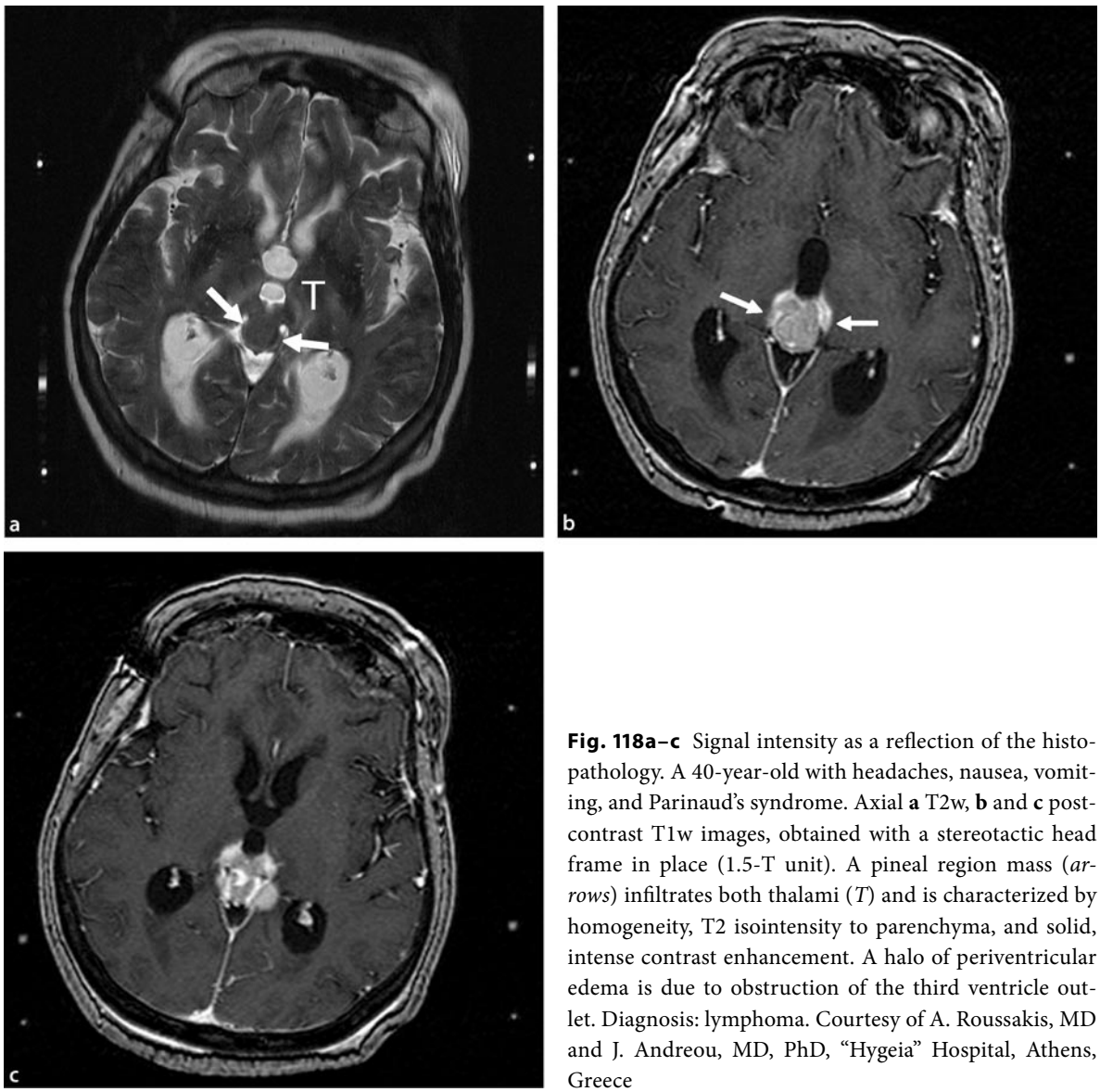

Fig. 118a–c Signal intensity as a reflection of the histopathology. A 40-year-old with headaches, nausea, vomiting, and Parinaud's syndrome. Axial **a** T2w, **b** and **c** postcontrast T1w images, obtained with a stereotactic head frame in place (1.5-T unit). A pineal region mass (*arrows*) infiltrates both thalami (*T*) and is characterized by homogeneity, T2 isointensity to parenchyma, and solid, intense contrast enhancement. A halo of periventricular edema is due to obstruction of the third ventricle outlet. Diagnosis: lymphoma. Courtesy of A. Roussakis, MD and J. Andreou, MD, PhD, "Hygeia" Hospital, Athens, Greece

On T2 TSE sequences fat remains bright while melanin with a short T2 turns "dark". Simple cysts and fluid collections are of low T1 and of high to very high T2 signal intensity, depending on the specific TR/TE values we have chosen. Inflammation increases the free water of tissues, prolonging both T1 and T2.

Most solid neoplasms exhibit mild to moderate T1 hypo T2 hyper-intensity with regard to normal parenchyma (excluding hemorrhagic, melanotic or calcified parts). The exceptions to this rule reflect histopathologic peculiarities and provide relative MR specificity. For example, primitive neuroectodermal tumors are organized in dense nests of small cells with narrow interstitial spaces and a paucity of stroma or matrix. This architecture can support only a low content of free water, and theory would predict T2 iso- or hypointensity relative to healthy parenchyma. This group of neoplasms includes lymphoma, medulloblastoma, neuroblastoma, rhabdomyosarcoma, and Ewing's sarcoma (Fig. 118). Densely fibrous tumors remain quite hypointense in any pulse sequence due to the presence of nonmobile protons. Benign fatty tumors follow the signal of subcutaneous fat.

Signal void is a hallmark of inherently low density of protons or mobile protons (such as dense calcifica-

tions, air, cortical bone) or of intense artifacts (e.g., rapid/turbulent flow).

Image Interpretation

The remainder of the discussion is designed to create a reading room "atmosphere" and will be most useful to budding radiologists.

Please be careful, as there are a variety of errors in radiology. Unfortunately, this topic has not received the attention it deserves (Renfrew et al. 1992; Samuel et al. 1995). First of all we match the requisition to the MR study (including the films and the film jackets, if applicable) to ensure that they belong to the same patient. Then we assess the technical adequacy of the scan with regard to the clinical problem and note any factors limiting the diagnostic value of the examination. If necessary, the patient returns to the Department for supplementary sequences. Then we are free to practice the purely diagnostic aspect of our work that consists of two arms: analysis and synthesis. Analysis is the "dissection" of the images into their constituents with the goal of detecting and describing any abnormality. Synthesis is the integration of the MRI information with the available clinical, laboratory, and imaging data in order to formulate a meaningful diagnosis. The mature radiologist moves with ease back and forth between these two steps until satisfaction of the search and until completion of his/her mental algorithms.

With MRI we recognize two broad categories of pathology: distortion of normal anatomy and distortion of normal signal intensity. For any deviations we should first exclude anatomic variations and pseudolesions (artifacts). Normal variants should be mentioned because they may be of clinical significance or they may be confused with pathology. Artifacts, whether subtle or gross, may mislead the referring physician and occasionally need to be included in our report.

No matter how easy or how difficult a case, we should take our time and follow faithfully the routine we have established for any type of MR examination. This rule is mandatory for the correct interpretation of the case and formulation of either a specific diagnosis or a short differential list. Do not underestimate the clinical information or be restricted by it: the MR scan may reveal unsuspected key findings or the patient may harbor more than one disease, which had been unknown to the referring physician.

Our description should be meticulous and thorough. I like to start with the anatomic coordinates and the anatomic origin of the abnormality. Then I proceed with what I call the primary and secondary features that arise when we "isolate" the lesion from the rest of the image contents. This separation is of course artificial, but it helps to organize our thought patterns. Let us take a close look at these.

First, we need to pinpoint the site and source of the lesion. In many cases multiplanar imaging gives us the luxury of appreciating the exact location and origin of the lesion as well as its full extent. We should be as specific as possible, e.g., an osseous abnormality might be superficial (periosteum, cortex) or deep (in the medullary canal) or it might involve both compartments.Sometimes we cannot be certain of the origin or the vector of growth due to size extremes (either very small or very large). It is then fitting to use terms such as the epicenter, or the base of the lesion, or the host space. Spaces can be real or potential. A real space is easily seen, filled or distended by a tissue, such as the fatty peri- and pararenal compartments. Potential spaces are normally collapsed, such as the pleural cavity.

Primary Elements

Imagine that we "carve" out the lesion and neglect temporarily the rest of the image. We are then left with the inherent features of the abnormality, which include size, shape, borders (smoothness/lobulation, poor or sharp definition), homogeneity, T1/T2 signature, presence/type of contrast enhancement and vascularity (obviously multiple or enlarged vessels within the lesion). If there is inhomogeneity we try to separate the various constituents and identify them as a solid part, cysts, necrosis, calcium, hemorrhage. Cystic components are examined for septations, mural nodules, wall thickness, and completeness of capsule. Multiplicity of foci calls for evaluation of distribution, uni- or bilaterality, symmetry, and uniformity. These are the primary characteristics.

Secondary Elements

The secondary elements refer to the rest of the image (ignoring the lesion) and complement the primary characteristics. We can prepare three categories: lo-

cal, distant, and pseudodistant. These distinctions of course are not always pure or applicable. Some offenders cannot be separated securely from reactive changes, e.g., high grade gliomas may blend in imperceptibly with the vasogenic edema they have incited. An abnormal position of a normal structure cannot be appreciated in vacuo, e.g., a low-lying, tethered spinal cord.

The local events against the neighboring structures can be direct, such as displacement, infiltration, and erosion, or indirect (reactive changes) such as edema, periostitis, and enlarged afferent/efferent vessels. Some of the local features help us predict the nature of the lesion. For example:

1. Expansion, remodeling or smooth erosion of bone testify to a long standing process or slow growth (Figs. 92, 119).
2. Conformity to the available space is an indication of a soft or malleable nature of the lesion (Fig. 120).
3. Violation of natural barriers (fascia, bone) suggests a lesion with aggressive behavior.

An aggressive appearance, however, should not be equated with malignancy. The reverse is also true: a benign picture is not equivalent to benign histology. For example, some carcinomas and sarcomas may appear homogeneous and have smooth, well-defined borders. The thin delimiting capsule may be true (fibrous) or it may be a pseudocapsule due to compressed parenchyma.

Metastases fall in the category of distant lesions, since by definition they are separate from the primary culprit. Metastases can be confused with multifocal or synchronous tumors that develop in the same organ without anatomic connections (e.g., primary lung carcinomas).

With regard to pseudodistant lesions, I can think only of a single situation for this category. In multicentric tumors (e.g., gliomas) macro- or microscopic bridges of neoplastic cells connect the seemingly independent tumorous islands.

Next, I would like to draw your attention to certain situations that can be especially difficult for beginners. The overlap you will encounter emphasizes the fact that we may afford more than one diagnostic approach to certain lesions.

The appearance of cysts and cyst-like lesions depends on their etiology and the nature of their contents. At first it seems easy to diagnose simple cystic lesions without risking false-positive or false-negative diagnoses. This statement is true, provided that we have images post-intravenous contrast and/or specialized pulse sequences (e.g., diffusion; Figs. 71, 121, 122).

Complex fluids/cysts may produce confusing signal patterns (Fig. 123). Inflammatory or hemorrhagic debris, mucin or a high protein content may lower one or both relaxation rates (T1, T2). Thus, we may encounter the reverse pattern of the expected, i.e., T1 hyperintensity with T2 hypointensity. In some cases hyperintensity persists in all pulse sequences.

Some general rules apply when entertaining the diagnosis of a cystic lesion. The borders are smooth and well defined and the contents are homogeneous or nearly so. The wall is thin or imperceptible and it may or may not enhance (Fig. 92). There may be septations and/or mural nodules. Reactive changes (edema, hyperemia), if present, may reach modest proportions (Fig. 123). Beware of the exceptions, as the above statements are not foolproof for cysts (Fig. 124). Thick or corrugated walls with intense enhancement suggest superinfection of the cyst or a liquefactive/necrotic process (Fig. 125).

To conclude, we can be certain that a complex lesion (or a component of a lesion) is cystic only when we see a fluid level (fluid–fluid, fat–fluid, sediment–fluid or air–fluid; Fig. 126).

The inclusion cysts deserve separate mention because of their unique properties, due to their solid or semisolid composition. They can be congenital or post-traumatic in etiology, classified as epidermoid (or cholesteatoma) or dermoid types. They are lined with squamous epithelium with or without skin appendages. The contents can be a mixture of water, desquamated keratin, cholesterol, and debris (Fig. 127). The inclusion cysts should not be confused with the ovarian dermoids, which are tumors (derived from germ cells). As developmental anomalies they result from the arrest and growth of ectoderm in aberrant locations. Acquired epidermoids may result from penetrating trauma with deep implantation of epidermis deep along the wound and subsequent growth through exfoliation. A similar process may occur in the middle ear cavity following tympanic membrane perforation.

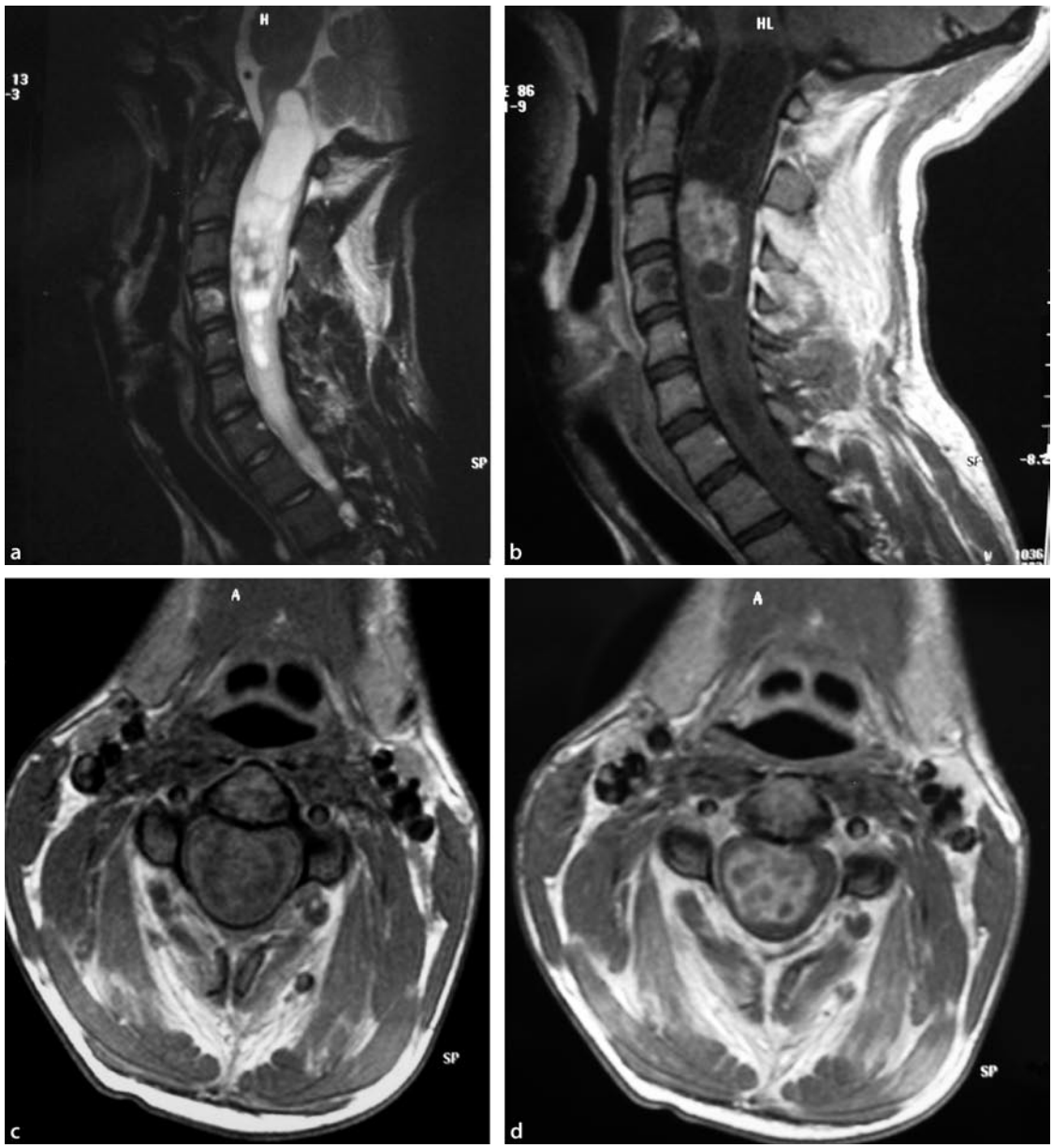

Fig. 119a–d Bony remodeling due to long-standing pressure. A 22-year-old sought medical attention after a minor vehicle accident while on vacation. He gave a long history of tingling in all four extremities that had worsened significantly after the accident. He also complained of neck pain. Plain radiographs and CT of the cervical spine were remarkable for marked widening of the spinal canal (not shown). An MR study was requested. Sagittal **a** T2w TSE and **b** post-contrast T1w TSE images. **c**, **d** Axial T1w SE images, before and after contrast at the C3 level. An extensive inhomogeneous, infiltrative and space-occupying process has caused marked expansion of the cord and secondary osseous remodeling. The lesion has solid and "cystic" components. Neoplastic "cysts" show rim enhancement. Reactive "cysts" or hydromyelic cavities bulge upward into the medulla and push downward to the lower cervical region. Cord infiltration continues below the visualized segments. Foci of low T2 signal about the C3–C4 interspace were attributed to calcifications or hemorrhage. Diagnosis: astrocytoma/glioma (presumed). The patient was lost to follow-up

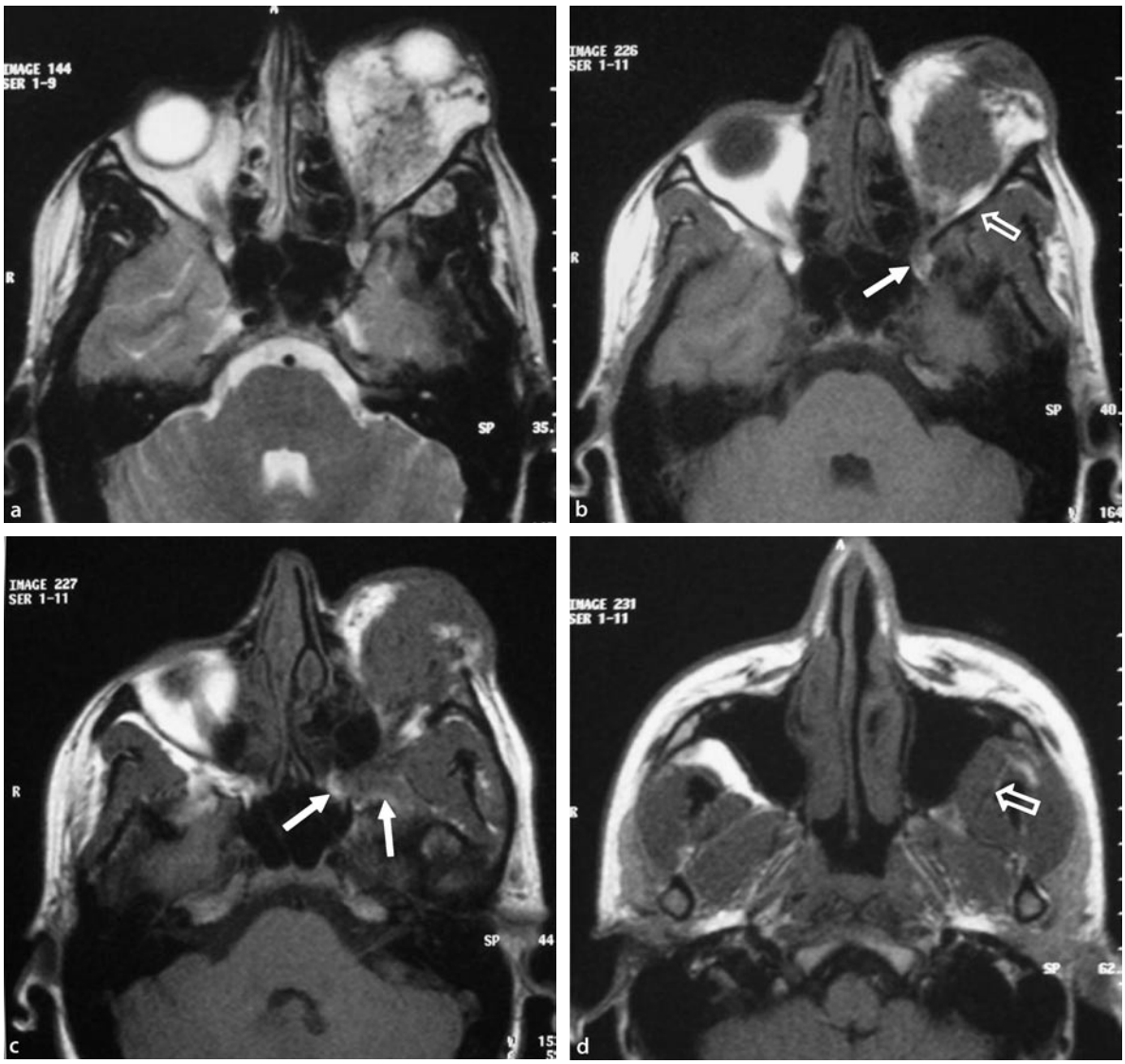

Fig. 120a–h Unusual configuration and pattern of the spread of a lesion. A 26-year-old woman with insidious, slowly progressive left exophthalmos. Axial **a** T2w TSE (4,465/120) and **b** T1w SE (532/15) images at the same level. **c**, **d** Axial T1w SE slices moving caudally. **e**, **f** Post-contrast T1w SE (532/15) images corresponding to **b** and **d**. **g** and **h** Coronal T1w SE (532/15) and fat-suppressed, post-contrast T1w SE (640/15) slices. **a–d** The exophthalmos is due to a soft tissue mass (4.5 cm in length) that occupies the floor of the orbit and extends to the lower eyelid. Note numerous internal flow voids. The lesion has escaped through the inferior orbital fissure (*single solid arrow*) and spills into the pterygopalatine fossa (PF, *two solid arrows*). Compare with a normal right PF, filled with fat. From the PF the mass follows the path of least resistance, extending downward (for 7.5 cm) behind the maxillary antrum to finally exit into the fatty tissues of the cheek (not shown). There is a second, small extraorbital component behind the outer wall of the orbit. Note effacement of the fat layers behind the orbit and maxillary sinus (*open arrows*). **e–h** *see next page*

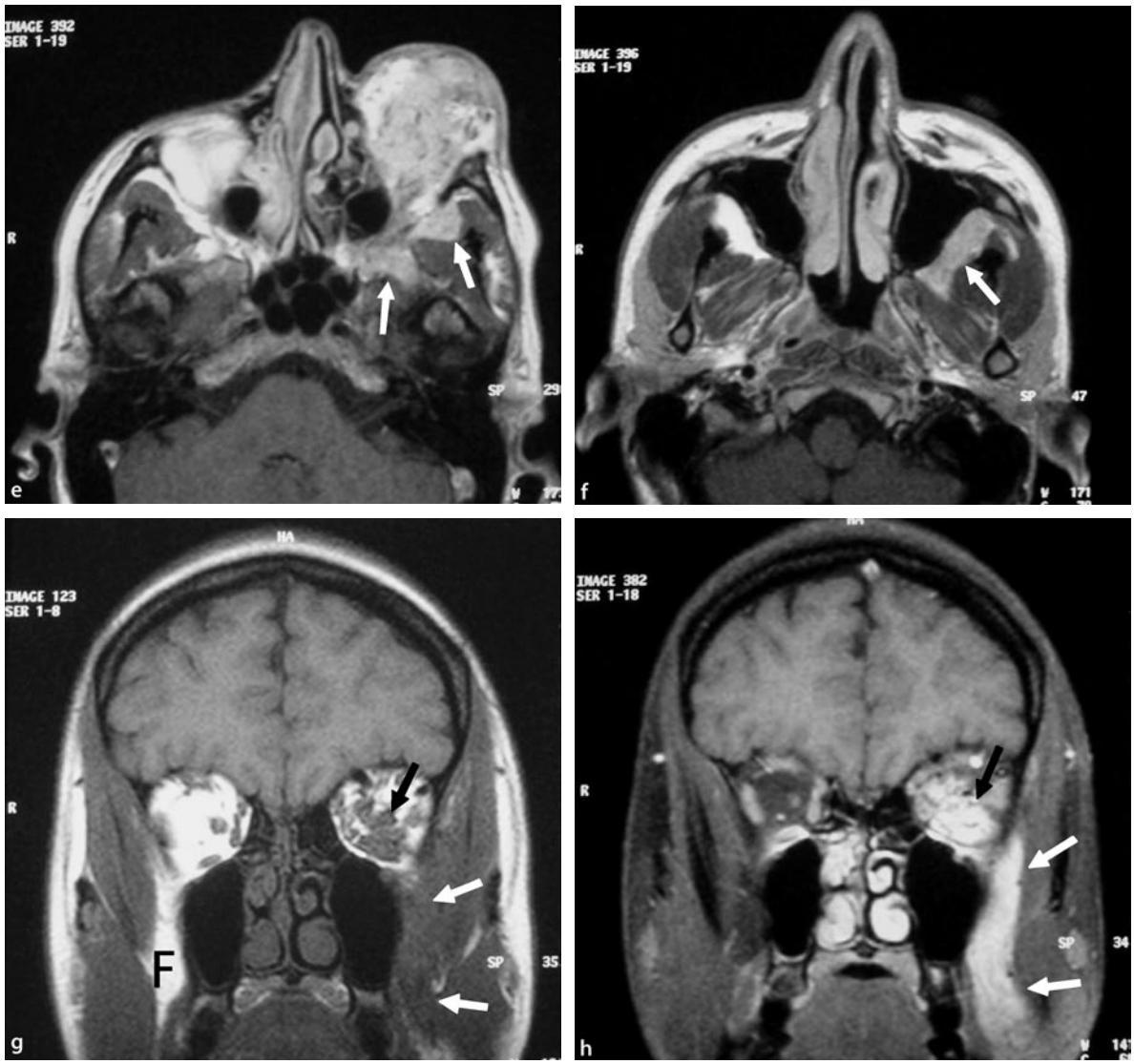

Fig. 120a–h *(continued)* **e**,**f** Note avid enhancement and flow voids. The *arrows* point to the retro- and infraorbital extension of the lesion. **g** and **h** afford a continuous view of the retromaxillary portion of the mass (*white arrows*); compare with the normal contralateral fat stripe (*F*). The *black arrows* point to the orbital portion of the abnormality. I was impressed by the unusual shape of the lesion with constriction and abrupt bending at the inferior orbital fissure. Despite its large size and presence in several compartments there is no muscle infiltration, bony destruction or entry into the cranium. It is notable that the lesion has grown by replacing/displacing fatty filled spaces. Diagnosis: recurrent vascular malformation. Eight years prior to this study the patient had been diagnosed with a vascular malformation confined to the orbit. She underwent embolization and subtotal surgical resection of the malformation (most of the inferior rectus muscle had to be sacrificed). Subsequent to this MR study the patient underwent a major combined procedure of embolization and surgical extirpation of the malformation

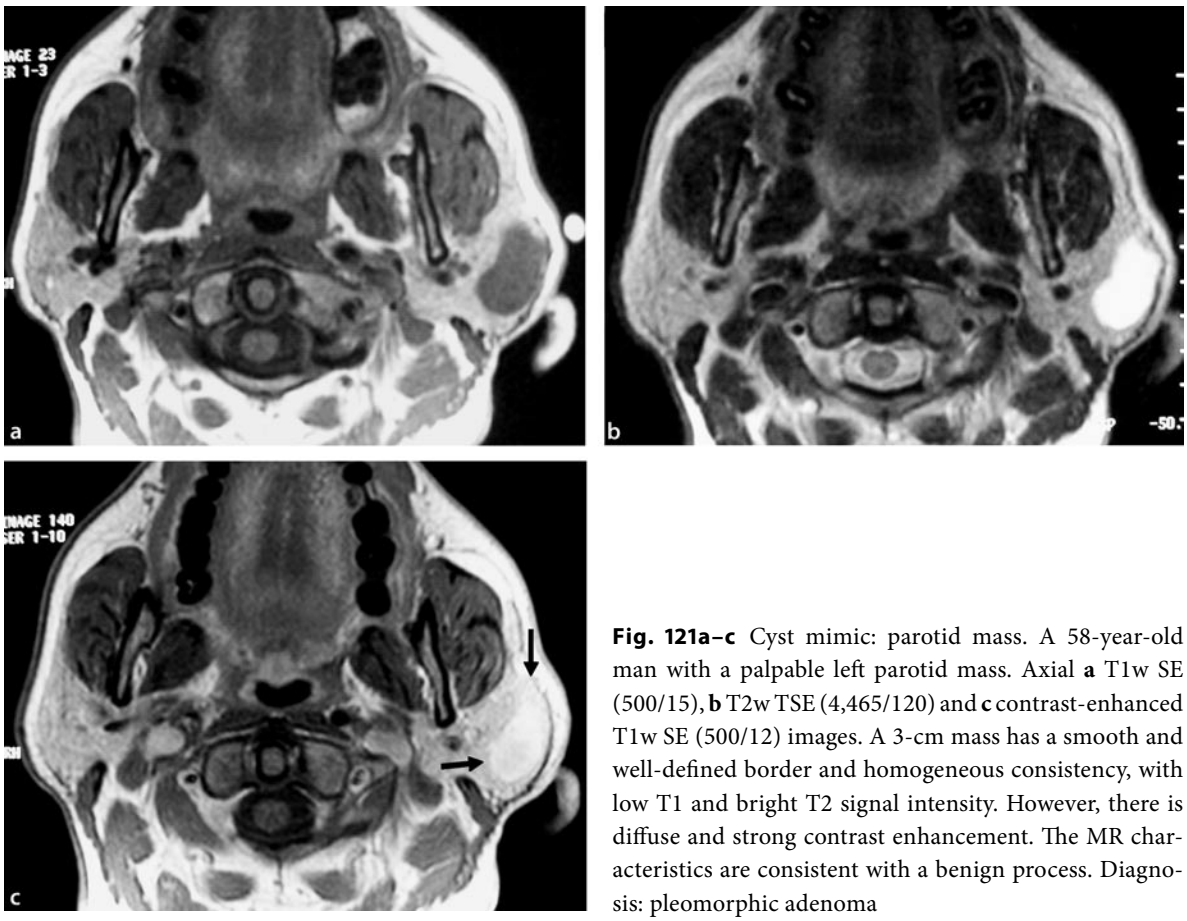

Fig. 121a–c Cyst mimic: parotid mass. A 58-year-old man with a palpable left parotid mass. Axial **a** T1w SE (500/15), **b** T2w TSE (4,465/120) and **c** contrast-enhanced T1w SE (500/12) images. A 3-cm mass has a smooth and well-defined border and homogeneous consistency, with low T1 and bright T2 signal intensity. However, there is diffuse and strong contrast enhancement. The MR characteristics are consistent with a benign process. Diagnosis: pleomorphic adenoma

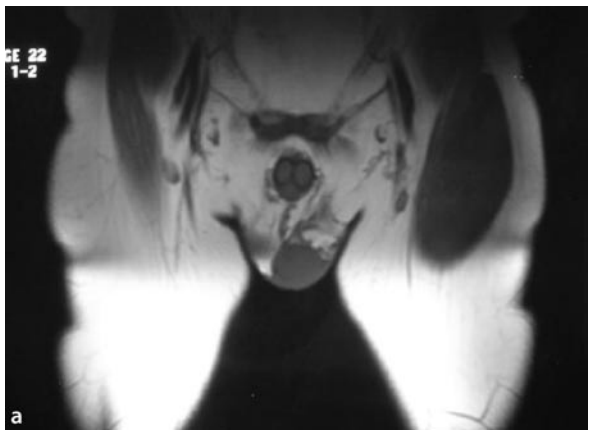
a

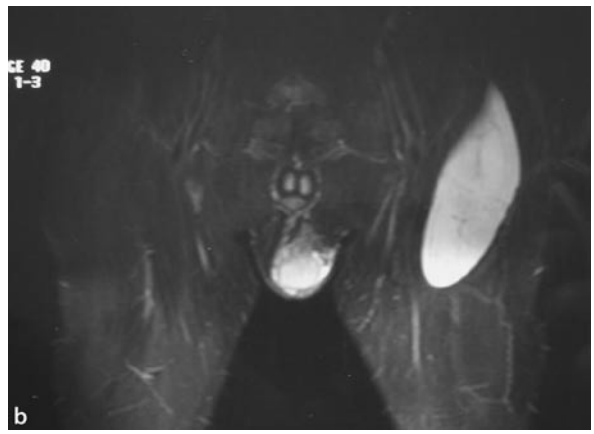
b

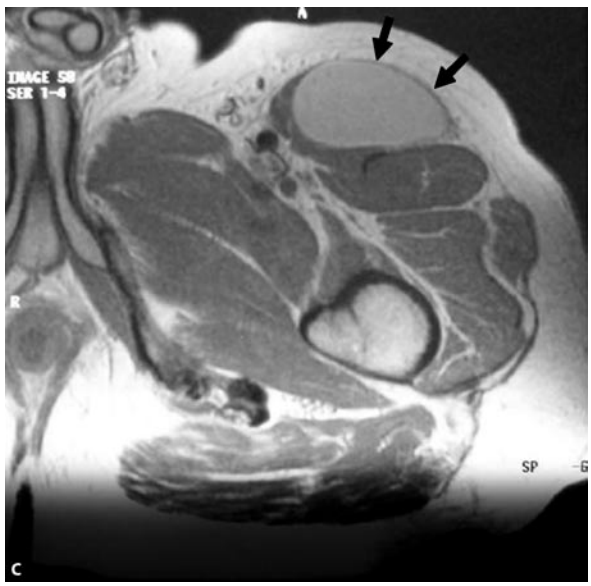
c

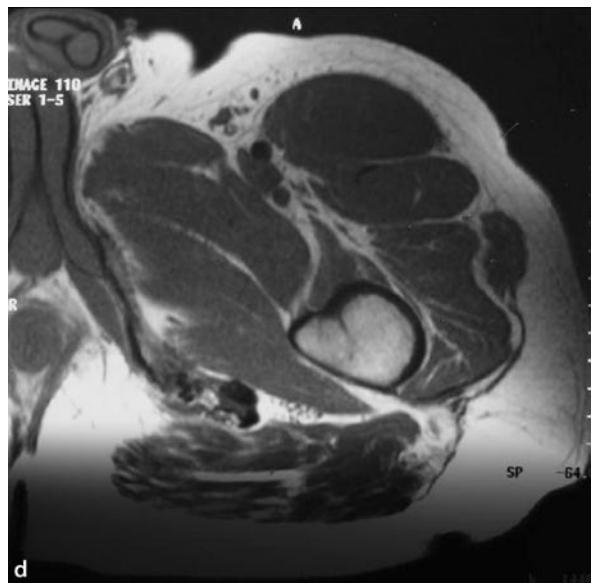
d

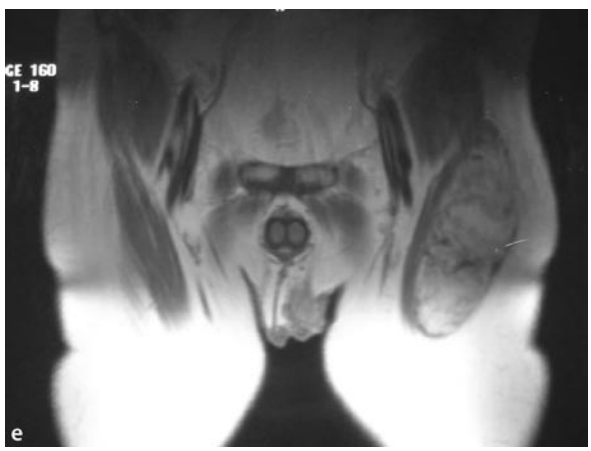
e

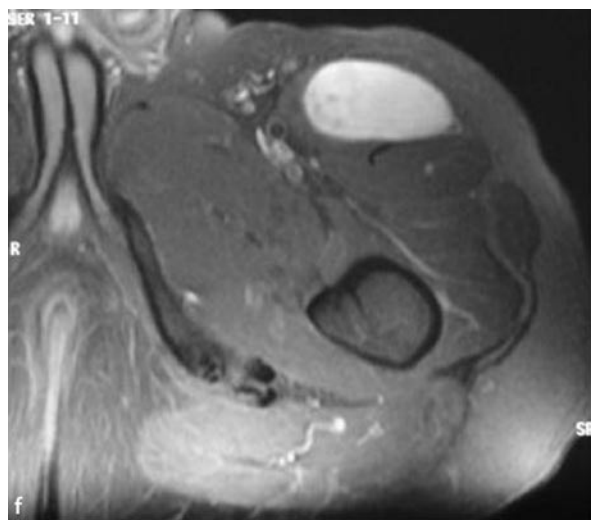
f

◂ **Fig. 122a–f** Cyst mimic: thigh mass. A 58-year-old with a slowly enlarging anterior thigh mass. Coronal **a** T1w SE (456/14) and **b** STIR (5,814/TI 130/60) images. Axial **c** PDw TSE (3,300/16) and **d** T1w SE (624/14) images. A well-defined mass looks embedded within the superficial musculature (*M*). It is sausage-shaped (13 cm in maximal diameter) and nearly homogeneous, with low T1 and high T2 signal intensity. A thin rim anteriorly may be a capsule or a slip of compressed muscle (*arrows*). **e** The coronal T1w SE sequence was repeated after contrast administration. **f** The last sequence was obtained with fat suppression (800/14) in the axial plane. There is intense and nearly homogeneous contrast enhancement. Despite the benignity of several MR features the mass was malignant. Diagnosis: sarcoma

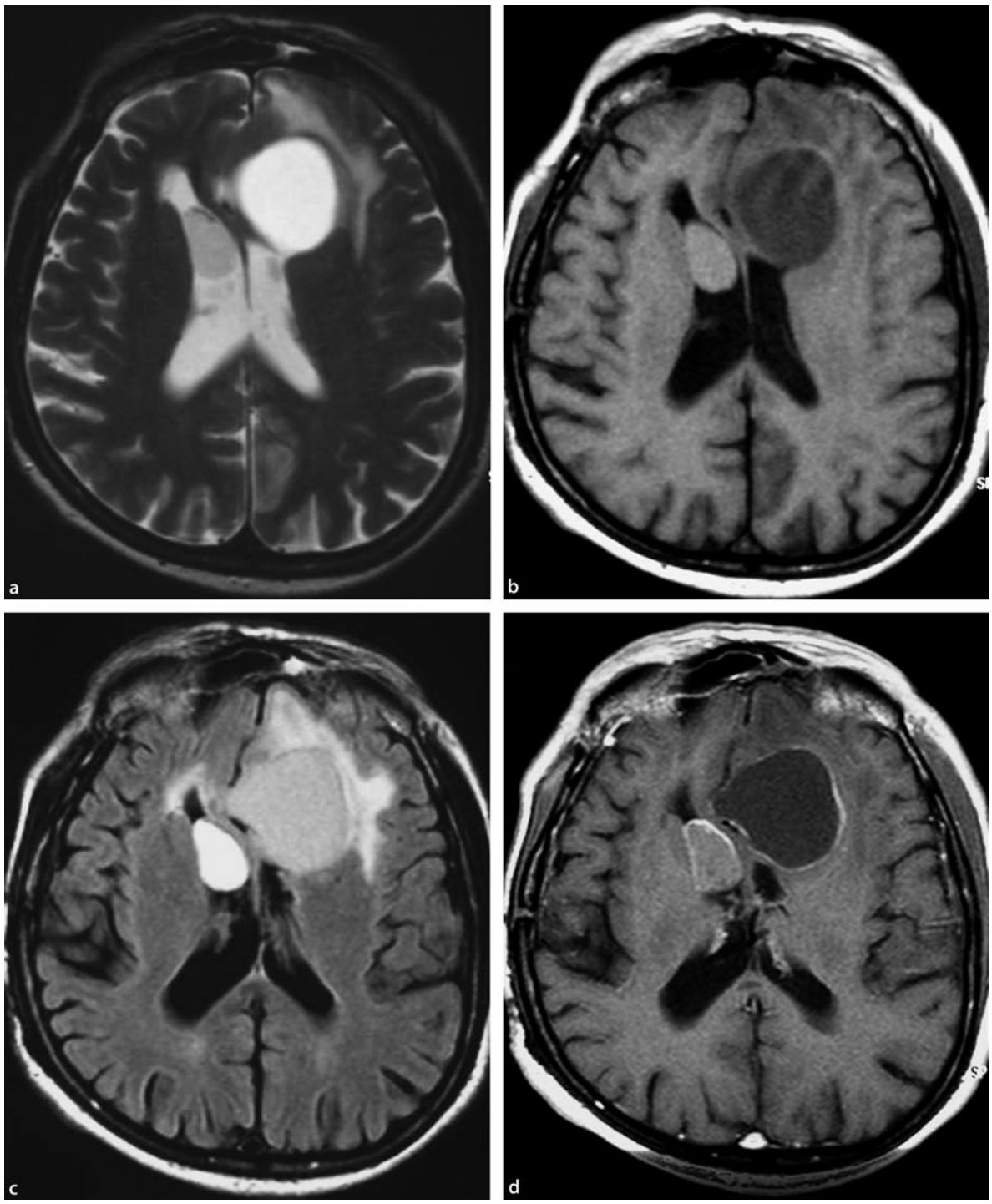
a
b
c
d

◂ **Fig. 123a–d** Intracranial tumoral cysts. A 58-year-old man presenting with headaches and visual disturbances, due to a craniopharyngioma of mixed consistency. A small (1.5-cm) solid component was seated within the sella attached to multiple supra- and parasellar cysts, ranging in size from 1.2 to 3.8 cm. The cysts recurred, necessitating multiple operations. Transaxial **a** T2w TSE (4,465/120), **b** T1w SE (532/15), **c** FLAIR (7,500/TI 2,243/105), and **d** post-contrast T1w (532/15) images. We see two suprasellar cysts impressing upon the frontal horns of the lateral ventricles. The cysts appear markedly different from CSF and display strong enhancement of their thin wall. Note edema in the left frontal lobe adjacent to the left cyst. Aspiration of the cysts yielded slightly turbid and slightly viscous fluid, of yellow–green color

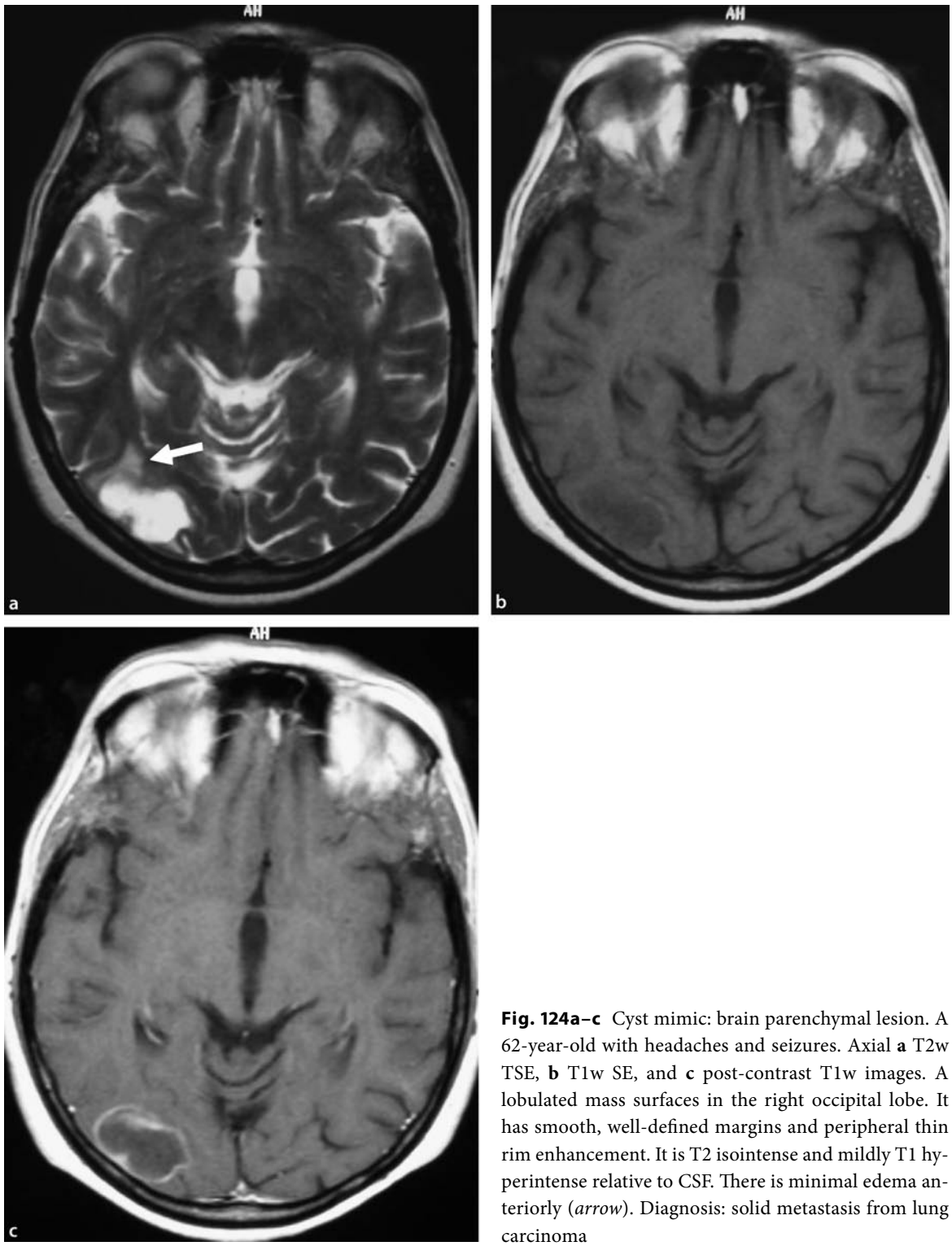

Fig. 124a–c Cyst mimic: brain parenchymal lesion. A 62-year-old with headaches and seizures. Axial **a** T2w TSE, **b** T1w SE, and **c** post-contrast T1w images. A lobulated mass surfaces in the right occipital lobe. It has smooth, well-defined margins and peripheral thin rim enhancement. It is T2 isointense and mildly T1 hyperintense relative to CSF. There is minimal edema anteriorly (*arrow*). Diagnosis: solid metastasis from lung carcinoma

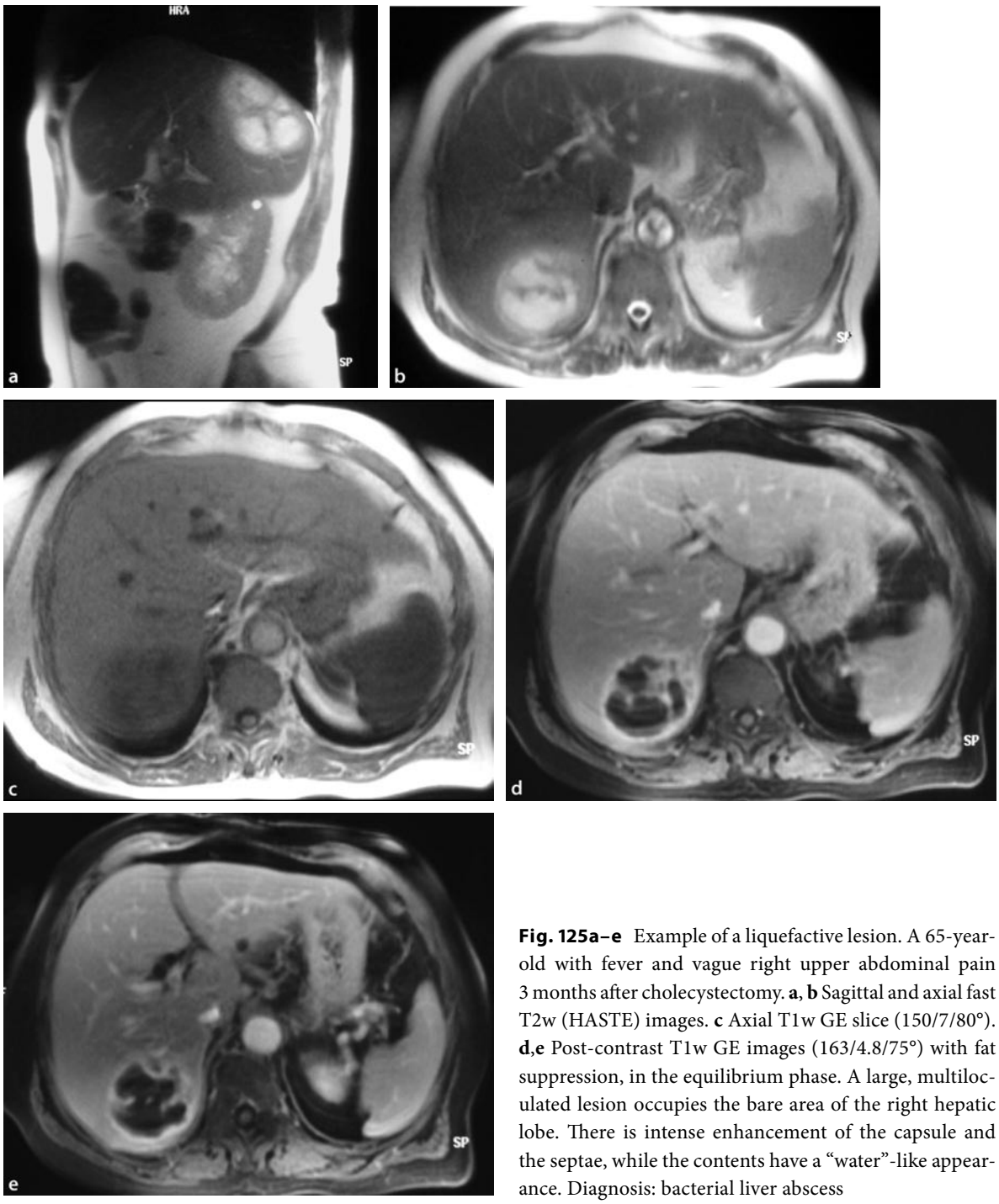

Fig. 125a–e Example of a liquefactive lesion. A 65-year-old with fever and vague right upper abdominal pain 3 months after cholecystectomy. **a**, **b** Sagittal and axial fast T2w (HASTE) images. **c** Axial T1w GE slice (150/7/80°). **d**,**e** Post-contrast T1w GE images (163/4.8/75°) with fat suppression, in the equilibrium phase. A large, multiloculated lesion occupies the bare area of the right hepatic lobe. There is intense enhancement of the capsule and the septae, while the contents have a "water"-like appearance. Diagnosis: bacterial liver abscess

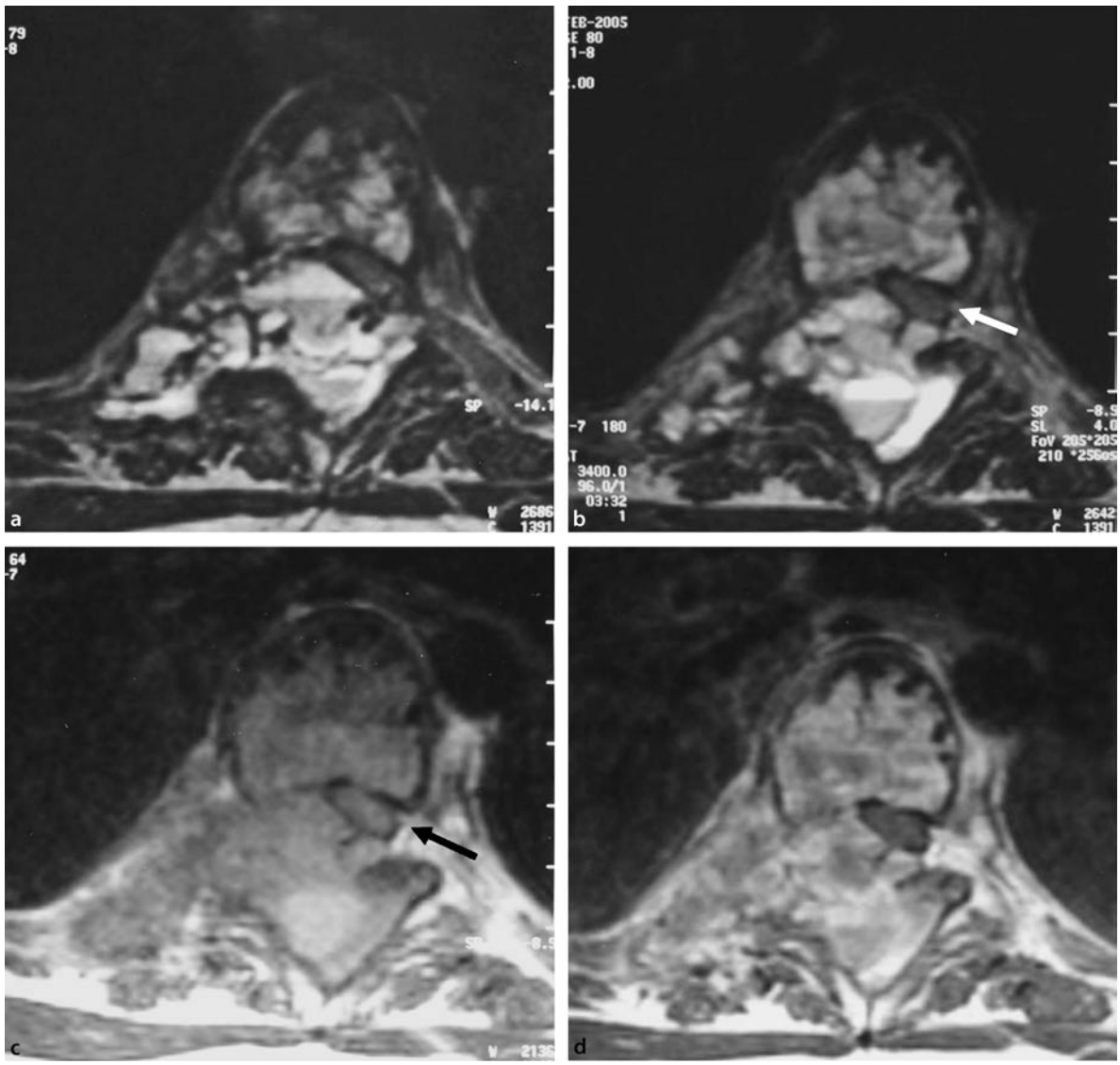

Fig. 126a–d Fluid–fluid levels in a cystic mass. A 14-year-old girl with dorsal ache and disturbances of both lower extremities (motor and sensory). MRI of the thoracic spine was performed. **a**,**b** Consecutive axial T2w TSE (3,400/96) images. **c**,**d** T1w SE (800/12) images before and after intravenous application of gadolinium, corresponding to **a**. There is a lobulated, expansile osseous mass in the mid-thoracic spine involving the T6 body and neural arch. The internal architecture is notable for the presence of multiple fluid–fluid levels. The water-like "compartments" display strong and homogeneous enhancement. The spinal cord is compressed and displaced forward and leftward (*arrows*). Diagnosis: aneurysmal bone cyst (ABC). Macroscopically and histologically, ABCs are cavernous lakes filled with blood. Their lining is a thin fibrous capsule. The fluid–fluid levels are due to blood and sediment. Contrast material easily reaches the interior of an ABC. Once there, it becomes "trapped" due to slow refreshment of the contents, explaining the marked and protracted contrast enhancement

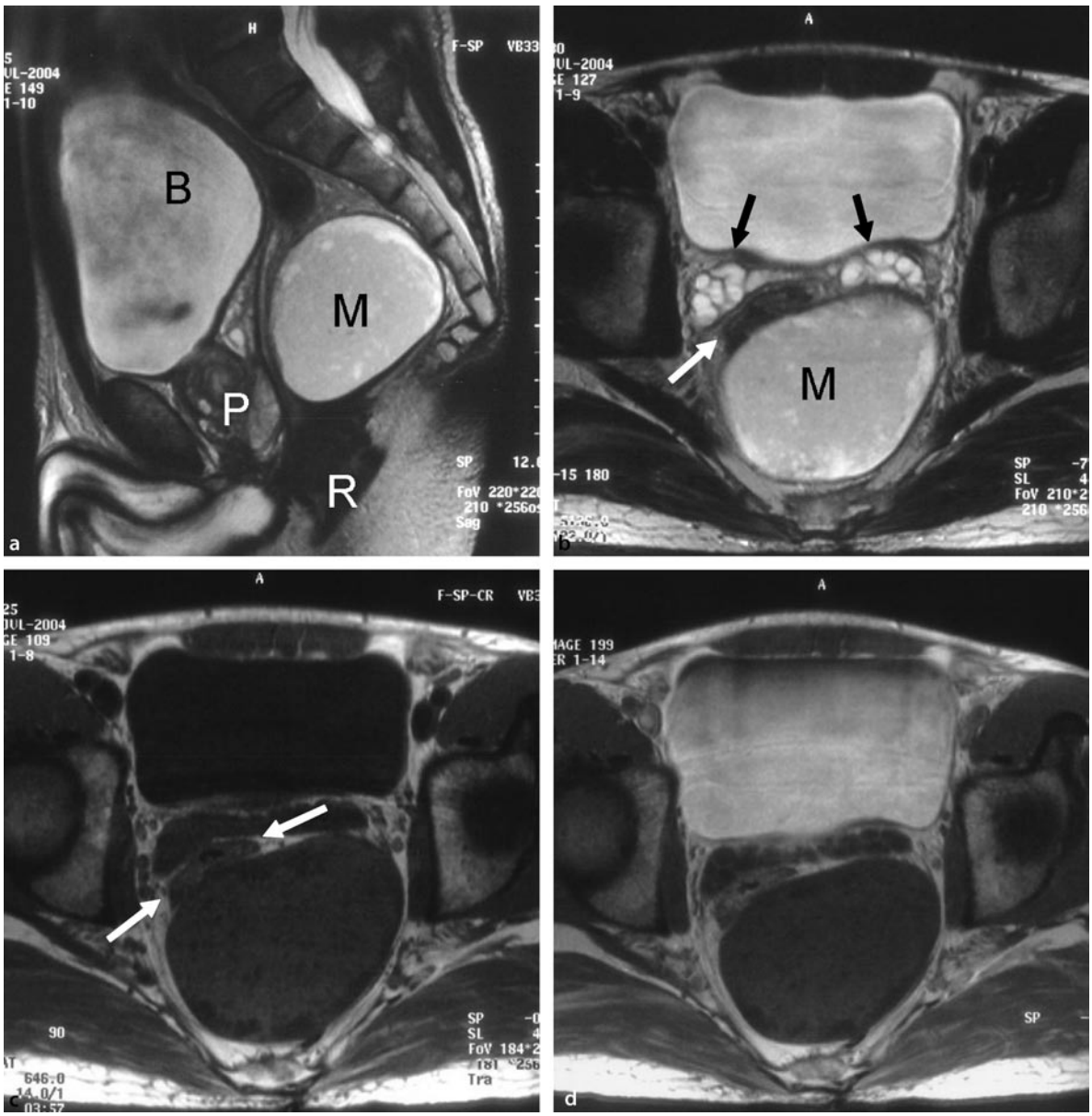

Fig. 127a–d Inclusion cyst. A 54-year-old man with symptoms suggestive of benign prostatic hypertrophy. Sonography revealed a presacral mass. **a** Sagittal and **b** axial T2-oriented TSE (5,000/136) images. **c**,**d** Axial T1-oriented SE images (646/14) before and after contrast injection. A well-defined 7.7-cm mass (*M*) is seated among the rectum (*R*), prostate (*P*), sacrum, and coccyx. A hypointense capsule is apparent in **a** and **b**. The contents are inhomogeneous, mostly T1 iso- and T2 hypo-intense with regard to muscle. Note T1 hypo- and T2 hyperintense material scattered centrally as "droplets" and forming a thick rind beneath the capsule. There is no contrast enhancement. The sacrum and coccyx appear intact. The sigmoid is compressed and displaced anteriorly (*white arrows*). The *black arrows* point to the seminal vesicles. Diagnosis: dermoid inclusion cyst, surgically resected, containing mostly sebum and a small amount of saliva. The wall was composed of hyperkeratotic squamous epithelium with skin appendages. *B* urinary bladder

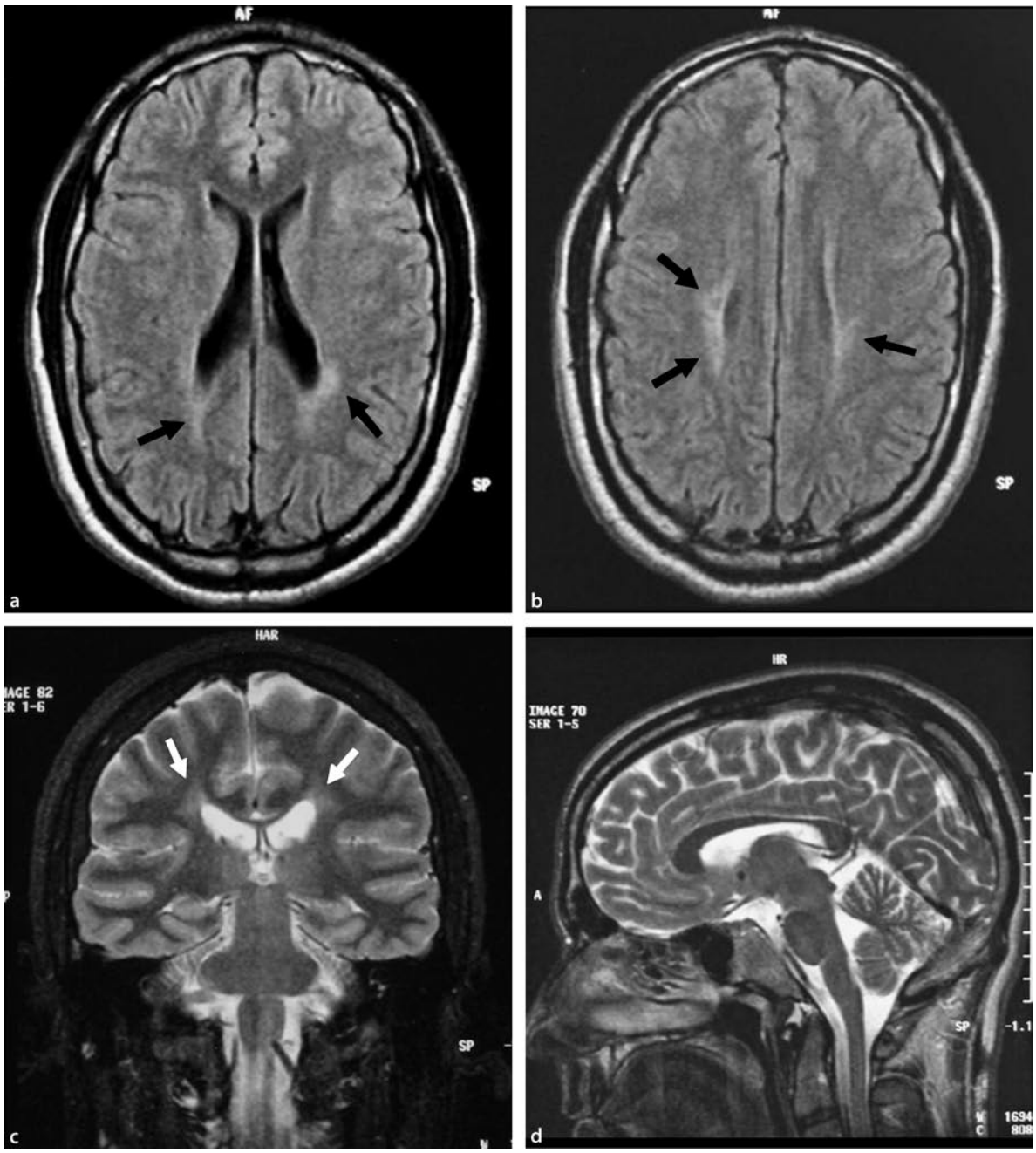

Fig. 128a–d Symmetric parenchymal pathology. A 23-year-old patient with headaches. **a**,**b** Axial FLAIR (7,500/TI 2,243/105) images. **c** Coronal STIR (4,000/TI 120/30) image. Periventricular hyperintensities fan out from the roofs of the lateral ventricles (*arrows*). **d** Sagittal T2w TSE (4,465/120) slice: focal thinning of the posterior body of the corpus callosum. This finding is due to white matter loss at an early age. Diagnosis: periventricular leukomalacia; to be distinguished from areas of terminal myelination, which is a normal variant and found more dorsally. Additional inquiry of the patient revealed a history of premature birth with perinatal hypoxia

Pitfalls

Some structures posses inherent symmetry (e.g., the brain in axial and coronal sections) and can be afflicted by diffuse or multifocal processes. By fortuitous chance the lesions may be distributed symmetrically about the midline and thus be neglected on first inspection (Figs. 128–132).

We should be wary of the iso-/hypointensity pitfall. Usually we start our search biased toward T1 hypointense/T2 hyperintense lesions. Iso- or hypointense disorders may go unnoticed, whether centrally, peripherally or at interfaces (Figs. 133–137). Convoluted pathways are especially difficult to follow, such as the intestinal tract or the cortical ribbon of brain. It is a matter of discipline and patience to "sweep" all borders and junctions looking for distortion, thickening, or loss of sharpness.

Our impulse is to detect the lesion(s), in other words find "something" that does not belong in the image. It is equally important to find "everything" that should be there. Examples include normal variants, post-traumatic or degenerative conditions, and congenital disorders (Figs. 138, 139).

Our attention is directed by the clinical history to certain structures and we may underestimate the rest of the contents of the image. If we have a narrow focus we may miss the relevant pathology. If our initial evaluation is non-productive we should intensify our search to structures that are "nearby" the suspicious ones (Figs. 140, 141).

The topic of incidentalomas overlaps slightly with that of the previous paragraph. Our job is not finished until we have examined every "corner" of the image. The patient may have harbor unsuspected findings that can be innocent or of grave importance (Figs. 142, 143).

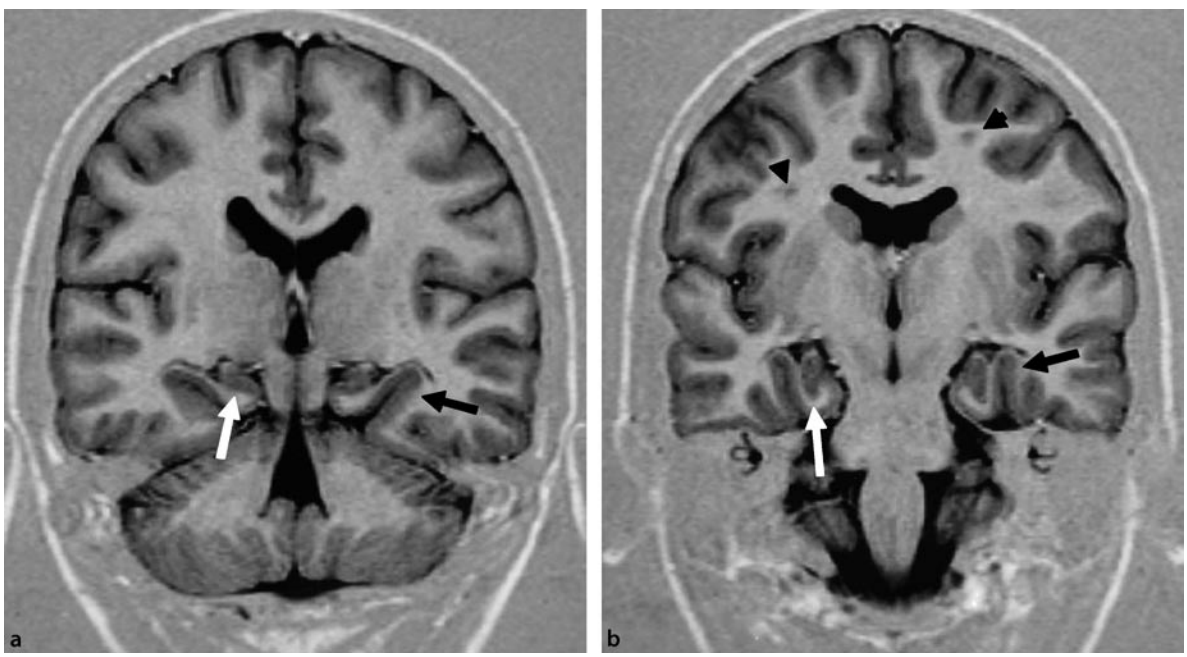

Fig. 129a,b Symmetric parenchymal malformation. A 6-year-old with a 4-year history of epilepsy. **a**,**b** Oblique coronal T1w inversion recovery (7,000/TI 300/60) images through the temporal lobes. The hippocampi (*white arrows*) are of normal signal intensity, but are malformed: note vertical orientation in **b**. Their position is relatively close to the midline. The collateral sulci are also vertical (*black arrows*). The temporal horns are dysplastic, wing-like, and extend beyond the collateral sulci. A few small islands of heterotopic gray matter are present at supraventricular levels (*arrowheads*). Diagnosis: bilateral hippocampal malformation. Compare this case with the Figs. 130 and 131

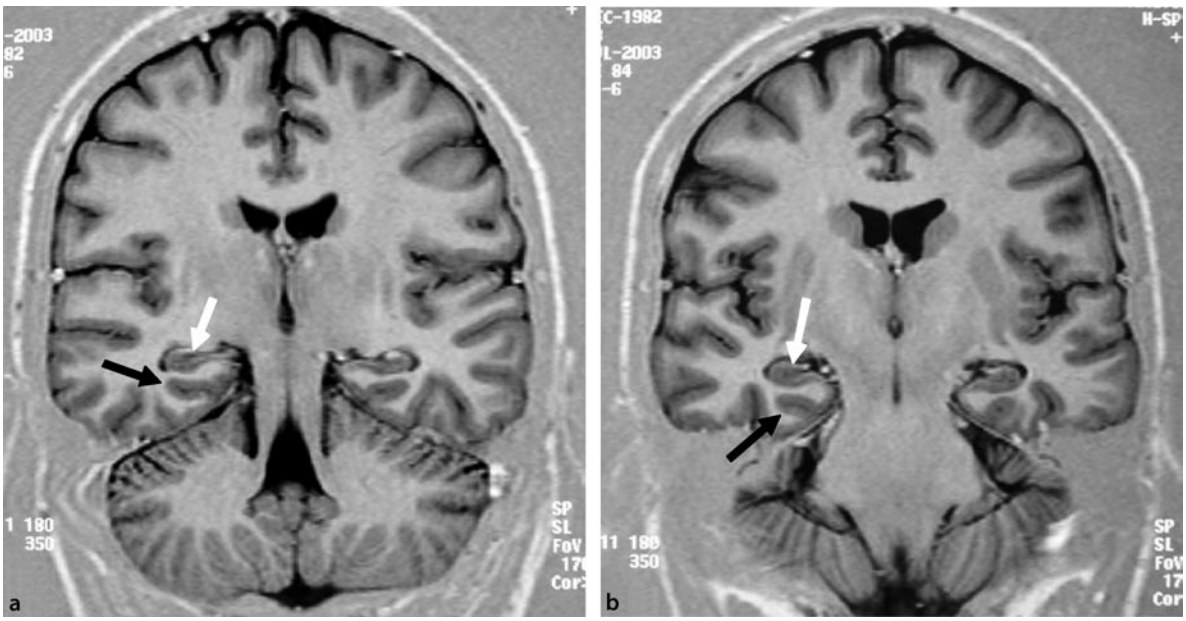

Fig. 130a,b Normal hippocampi for comparison with Fig. 129. A 32-year-old healthy volunteer. **a**,**b** T1w IR (7,000/TI 300/60) oblique coronal sections. The hippocampi (*arrows*) have an ovoid shape with the long axis oriented transversely. They are further from the midline compared with the case depicted in Fig. 129 and are completely "covered" by the temporal horns (*white arrows*). The collateral sulci are nearly horizontal (*black arrows*)

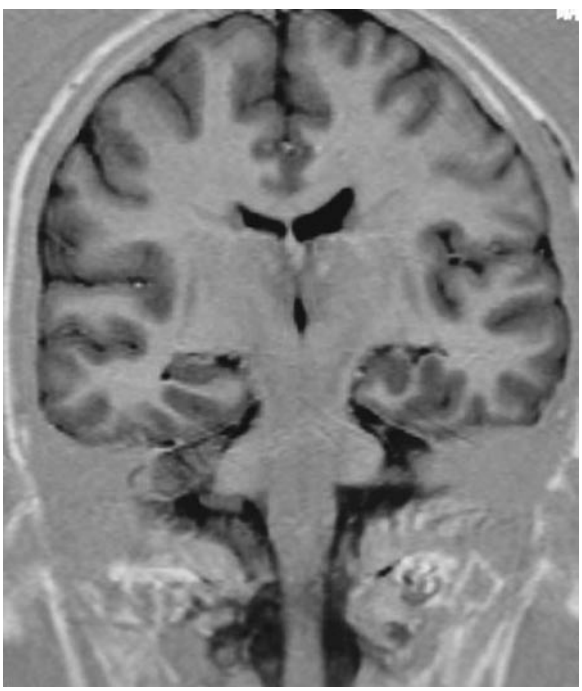

Fig. 131 Unilateral hippocampal malformation for comparison with Fig. 129. A 13-year-old with a long-standing history of epilepsy, since early childhood. T1w IR (7,000/TI 300/60) oblique coronal image. In this instance, it is easy to spot the asymmetric morphology of the hippocampi. Since the malformed left side retains normal signal intensity we have to be careful which side we call abnormal

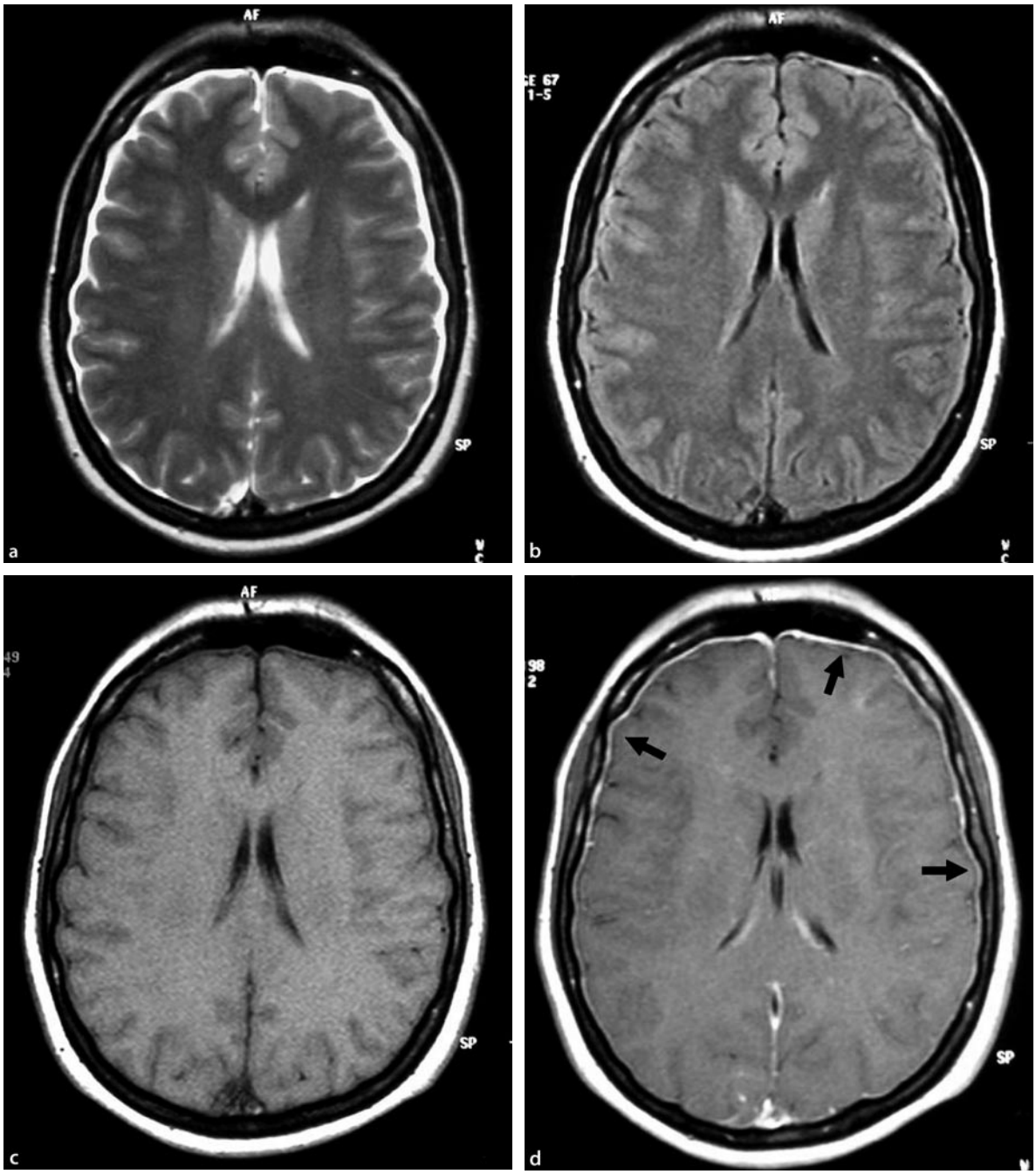

Fig. 132a–f Extraparenchymal symmetric pathology. A 28-year-old with severe headaches. Axial **a** T2w TSE (4,465/120), **b** FLAIR (7,500/TI 2,243/105), and **c** T1w SE (532/15) images. The gyri do not reach the skull and the cortical veins (flow voids) are closely applied to the surface of the brain. Superficially, it looks like dilatation of the subarachnoid spaces. However, the extraparenchymal "material" is of high signal in FLAIR and the lateral ventricles seem compressed. **d–f e, f** *see next page*

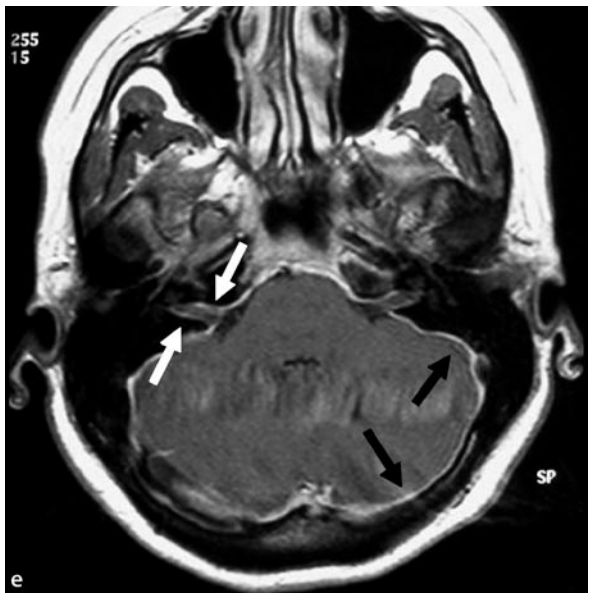

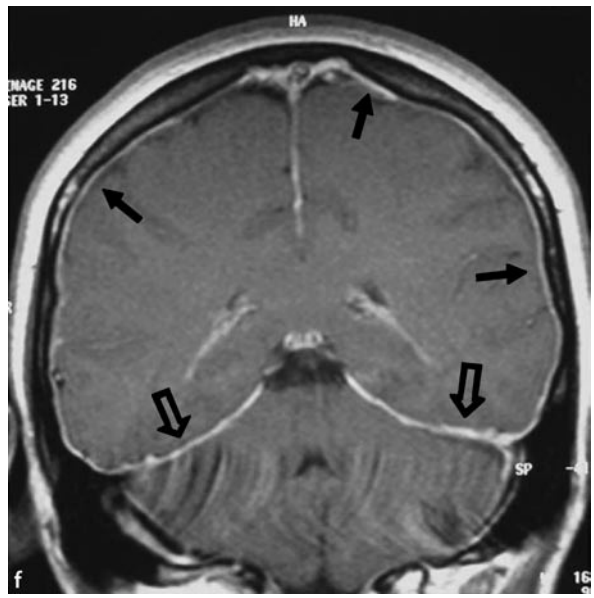

Fig. 132a–f *(continued)* **e,f** After contrast infusion we recognize diffuse thickening and hyperemia of the dura (*solid black arrows*), including the tentorium (*open arrows*), and the lining of the internal auditory canals (*white arrows*). Diagnosis: spontaneous intracranial hypotension

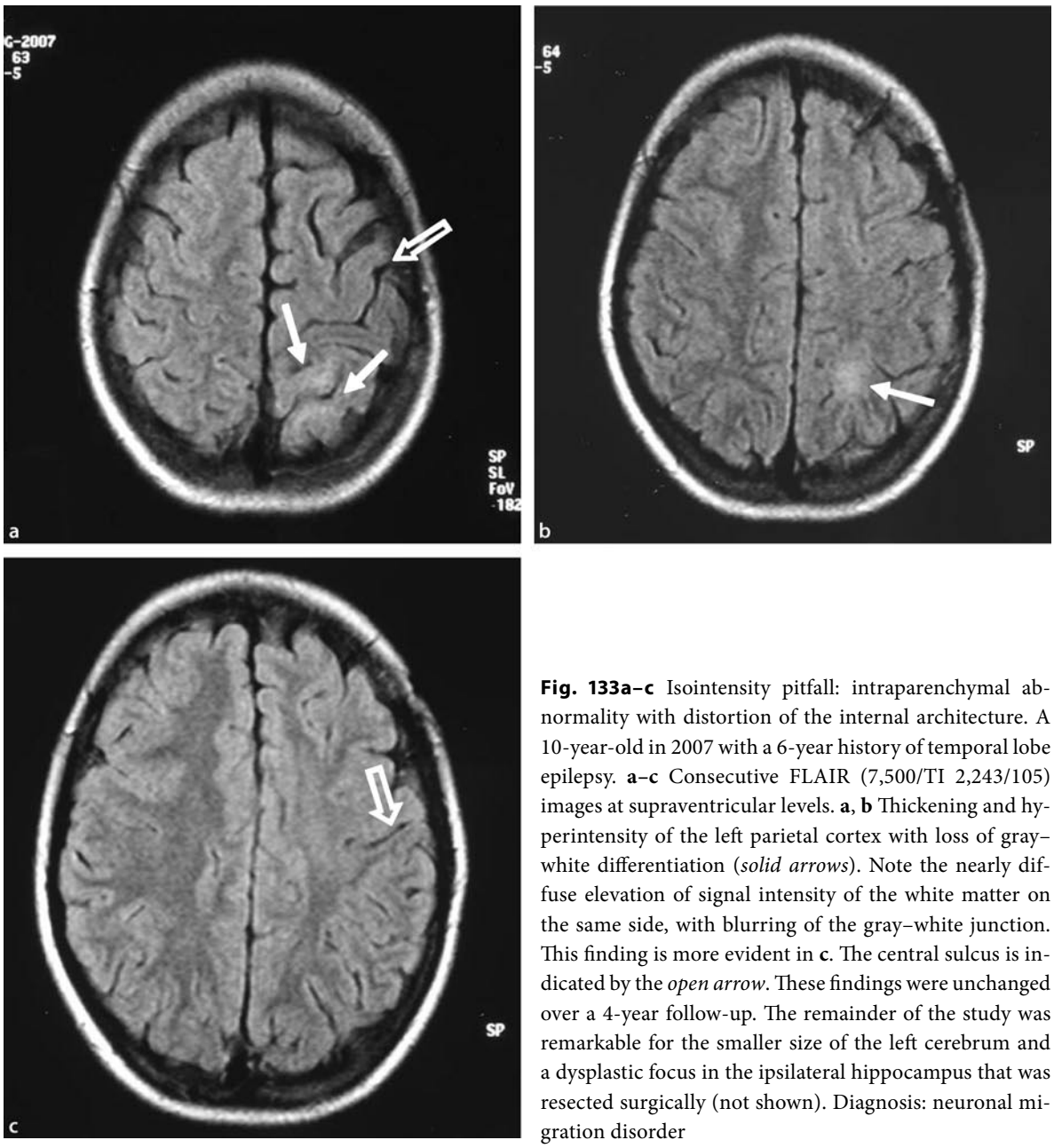

Fig. 133a–c Isointensity pitfall: intraparenchymal abnormality with distortion of the internal architecture. A 10-year-old in 2007 with a 6-year history of temporal lobe epilepsy. **a–c** Consecutive FLAIR (7,500/TI 2,243/105) images at supraventricular levels. **a**, **b** Thickening and hyperintensity of the left parietal cortex with loss of gray–white differentiation (*solid arrows*). Note the nearly diffuse elevation of signal intensity of the white matter on the same side, with blurring of the gray–white junction. This finding is more evident in **c**. The central sulcus is indicated by the *open arrow*. These findings were unchanged over a 4-year follow-up. The remainder of the study was remarkable for the smaller size of the left cerebrum and a dysplastic focus in the ipsilateral hippocampus that was resected surgically (not shown). Diagnosis: neuronal migration disorder

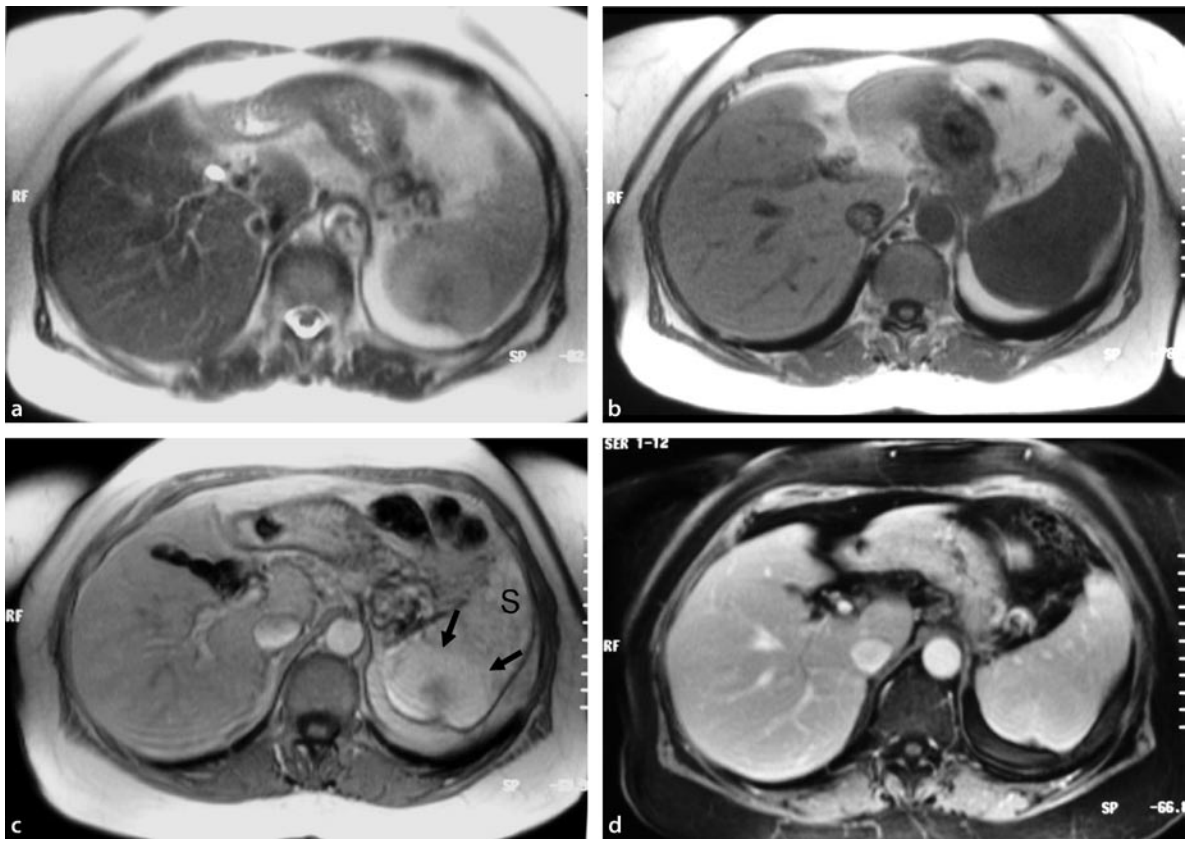

Fig. 134a–d Isointensity pitfall: parenchymal abnormality – lobulation of borders. A 74-year-old with "fullness" in the upper left quadrant. Fast **a** T2w (HASTE) and **b** T1w GE (150/7/80°) images are notable for a bulbous posterior margin of the spleen. This finding could be a normal variant, but should alert us to a possible abnormality. There is also mild signal inhomogeneity of the spleen in **a**. **c** T1w GE image (150/7/80°) after an intravenous bolus of gadolinium, in the late arterial phase. There is strong, nearly diffuse enhancement of the posterior half of the spleen (*arrows*), except for a central "scar". In this phase we expect the normal splenic parenchyma (*S*) to have a mottled appearance. **d** This image was obtained in the equilibration phase, with fat suppression (147/4.8/75°). Note the uniform distribution of contrast in the spleen and the mass, including the central "scar". In retrospect, the central "scar" is hypointense in **a** and isointense in **b**. Diagnosis: cavernous hemangioma of the spleen (presumed). The appearance has remained stable over a 4.5-year follow-up

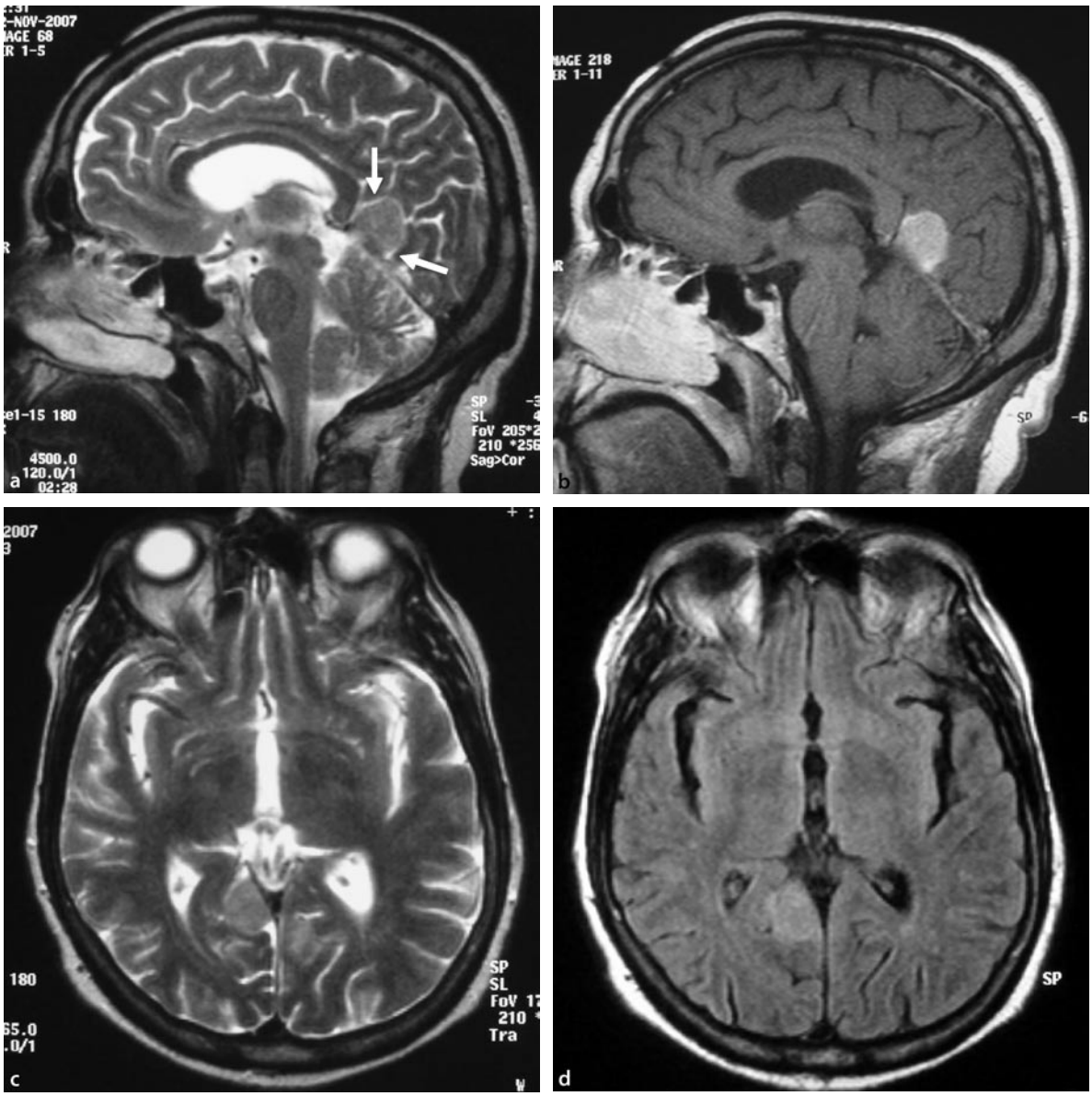

Fig. 135a–f Isointensity pitfall: extraparenchymal lesion. A 59-year-old woman with headaches. **a** Paramidline sagittal T2w TSE (4,465/120) and **b** post-contrast T1w (532/15) views. Axial **c** T2w TSE (4,465/120), **d** FLAIR (7,500/TI 2,243/105). **e,f** *see next page*

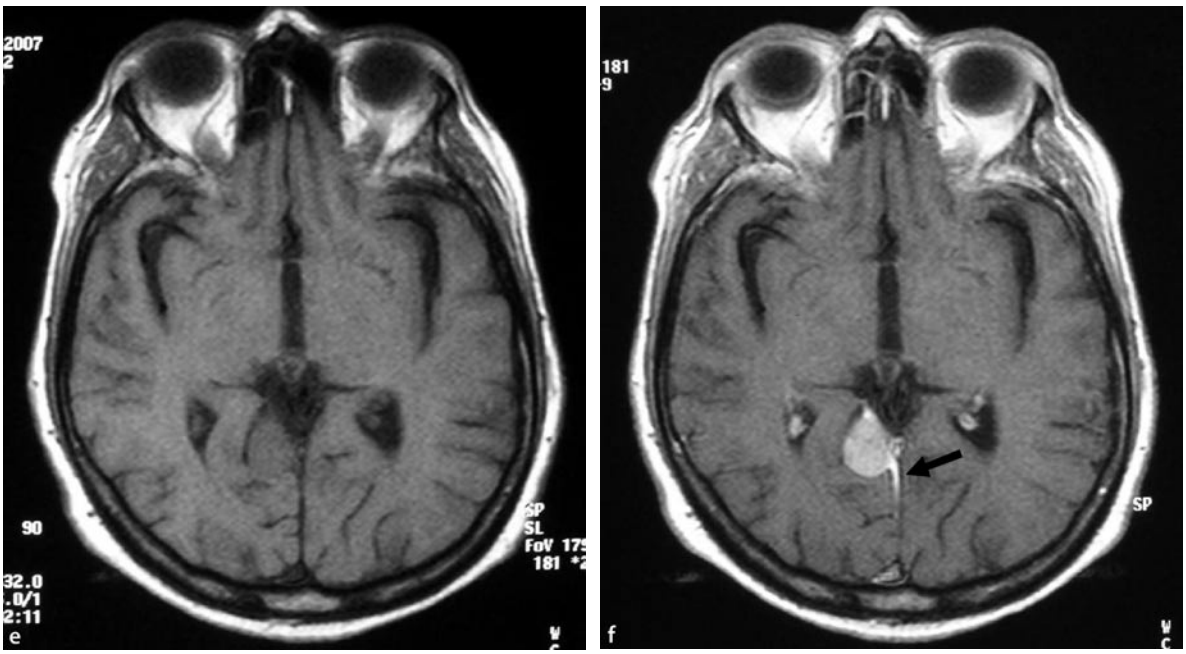

Fig. 135a–f *(continued)* **e** T1w SE (532/15), and **f** gadolinium-assisted T1w (532/15) images. There is a subtle, isointense extra-axial mass behind the splenium of the corpus callosum with a broad base against the tentorium, 2 cm in size. The lesion invaginates into the parenchyma. Note the thin rim of CSF around the free edge of the mass (*white arrows*). There is strong and homogeneous enhancement and thickening of the adjacent dural margin (*black arrow*), known as the "dural tail" sign. Diagnosis: meningioma

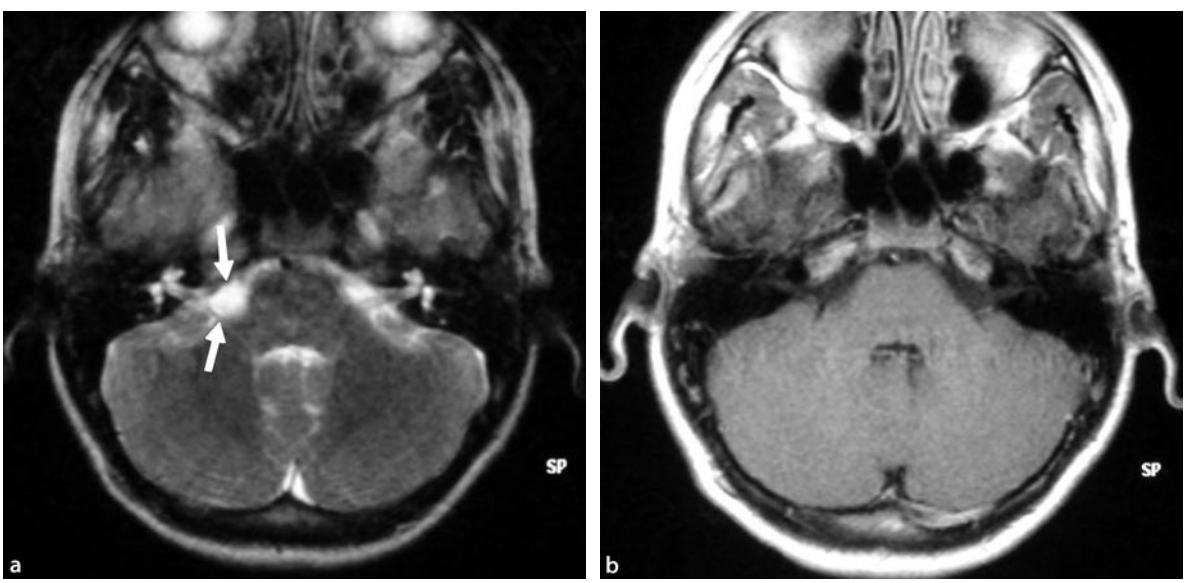

Fig. 136a–h Isointensity pitfall: value of specialized pulse sequences. Intracranial extra-axial cyst similar to CSF in conventional sequences. A 13-year-old boy with dizziness, vertigo, and headaches. Axial **a** T2w TSE (4,465/120) and **b** post-contrast T1w SE (532/15) images at the level of the internal auditory canals. **c–h** *see next page*

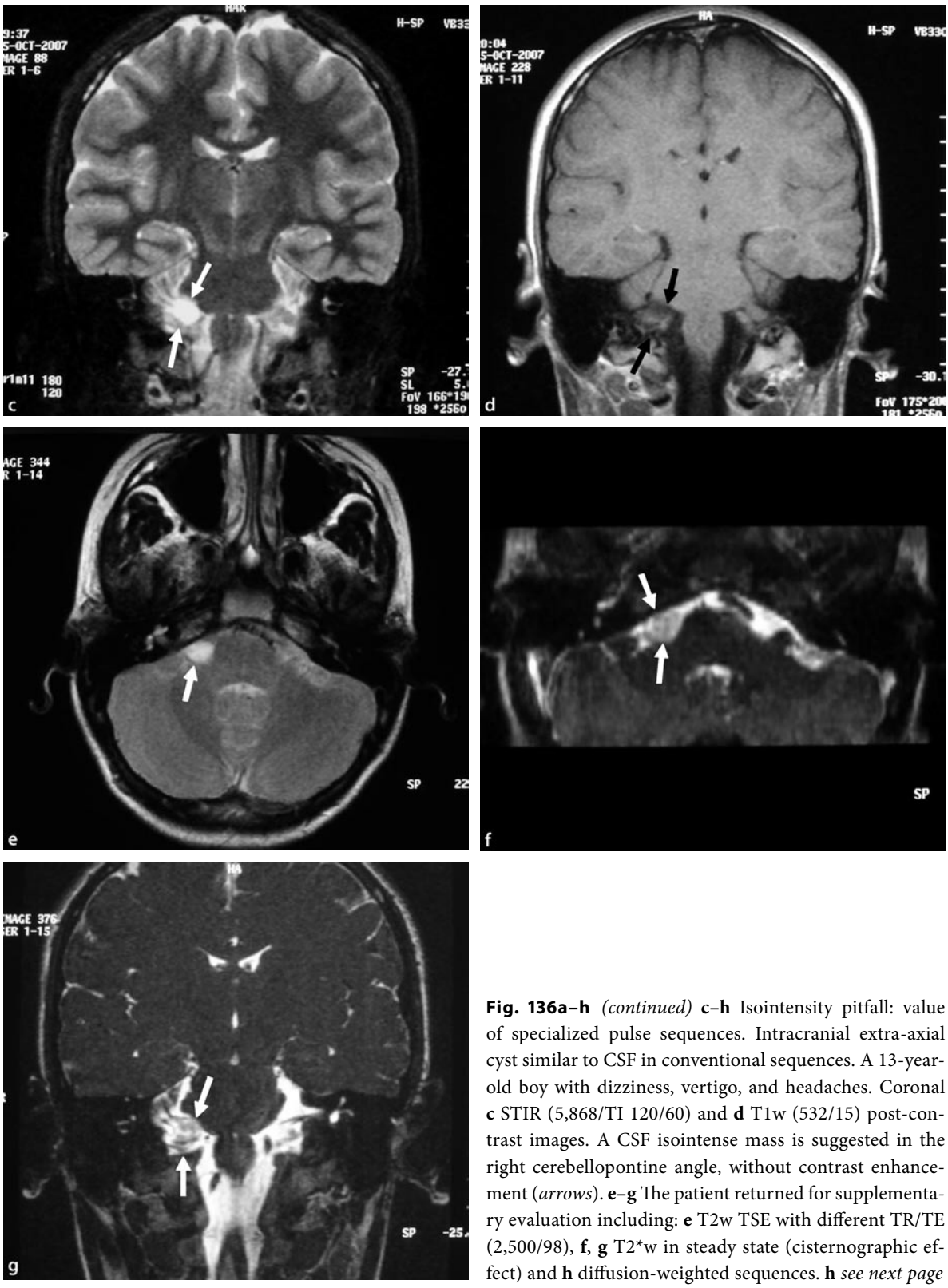

Fig. 136a–h *(continued)* **c–h** Isointensity pitfall: value of specialized pulse sequences. Intracranial extra-axial cyst similar to CSF in conventional sequences. A 13-year-old boy with dizziness, vertigo, and headaches. Coronal **c** STIR (5,868/TI 120/60) and **d** T1w (532/15) post-contrast images. A CSF isointense mass is suggested in the right cerebellopontine angle, without contrast enhancement (*arrows*). **e–g** The patient returned for supplementary evaluation including: **e** T2w TSE with different TR/TE (2,500/98), **f**, **g** T2*w in steady state (cisternographic effect) and **h** diffusion-weighted sequences. **h** *see next page*

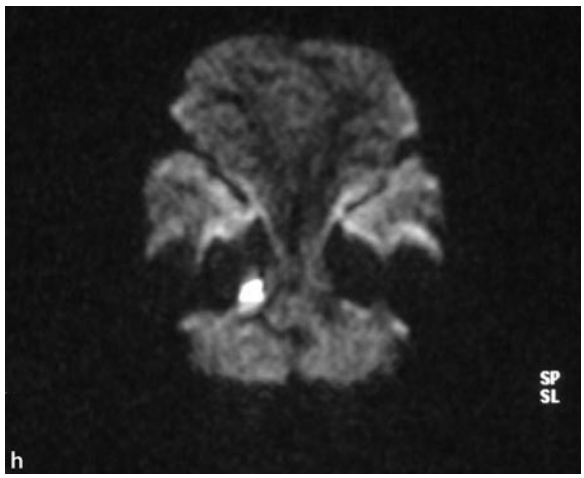

Fig. 136a–h *(continued)* **h** The lesion is now separated from the CSF, appearing slightly hyperintense in **e**, inhomogeneous with a low signal rim in **f** and **g**, (*arrows*) and very bright in **h**. Diagnosis: epidermoid (inclusion) cyst, presumed

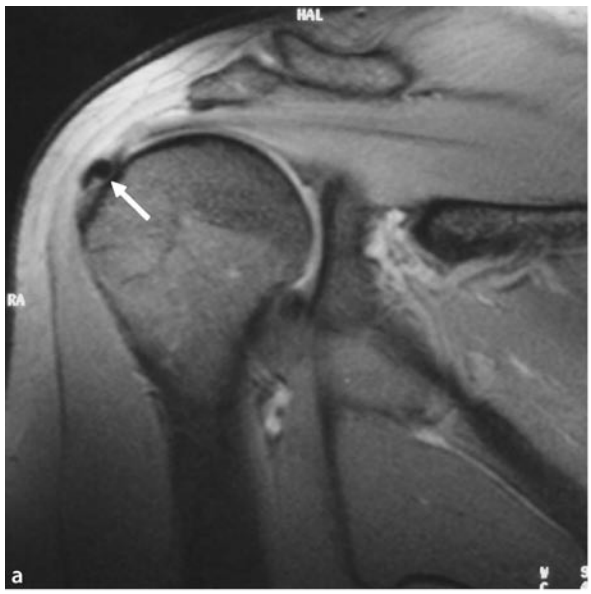

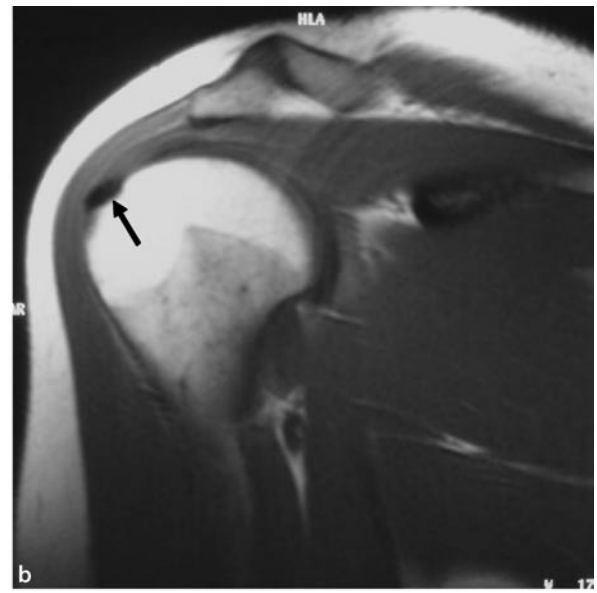

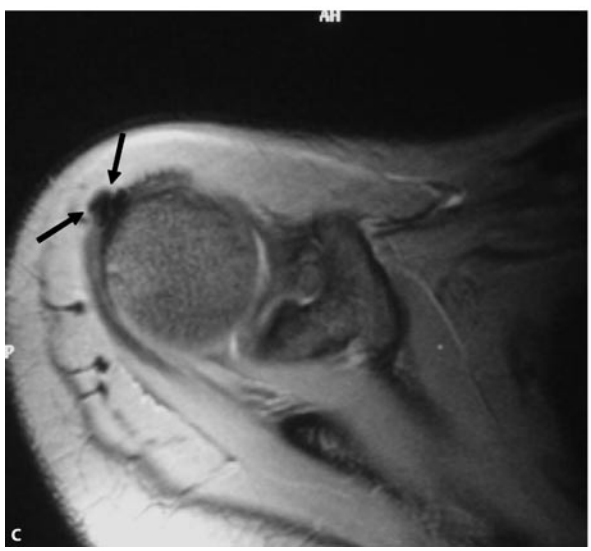

Fig. 137a–c Hypointensity pitfall. A 33-year-old with shoulder pain and difficulty in arm raising. Oblique coronal **a** T2*w (980/23/35°) and **b** T1w (415/12) images. **c** Axial T2*w slice. A focus of signal void lies in the course of the distal supraspinatus tendon (*arrows*). It represents a globular deposit of calcium, confirmed by plain radiography (not shown). Normal tendons have very low signal intensity, albeit higher than dense calcifications. Additional findings in the coronal image were thinning and hyperintensity of the tendon both proximally and distally to the calcification due to partial tearing

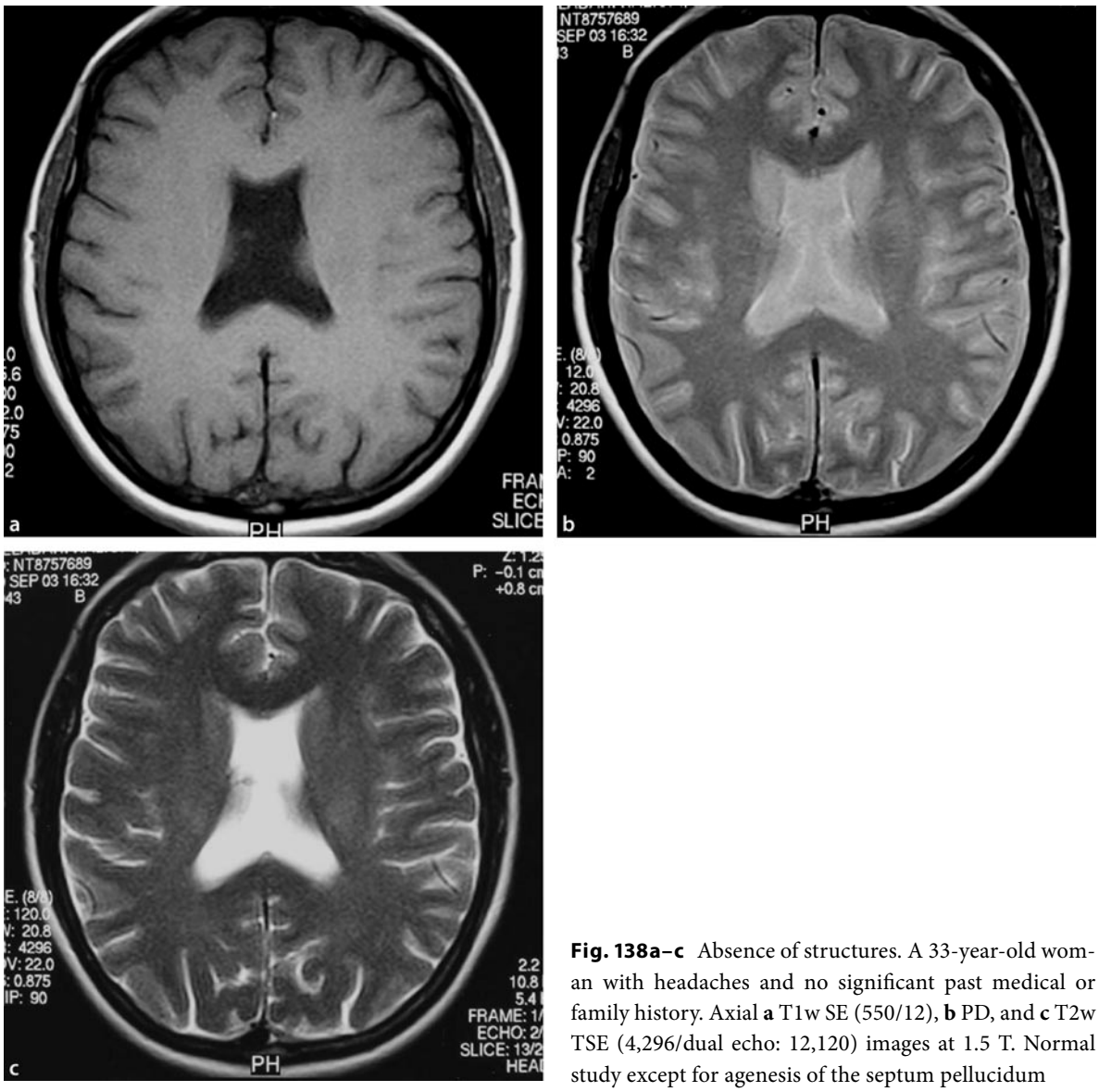

Fig. 138a–c Absence of structures. A 33-year-old woman with headaches and no significant past medical or family history. Axial **a** T1w SE (550/12), **b** PD, and **c** T2w TSE (4,296/dual echo: 12,120) images at 1.5 T. Normal study except for agenesis of the septum pellucidum

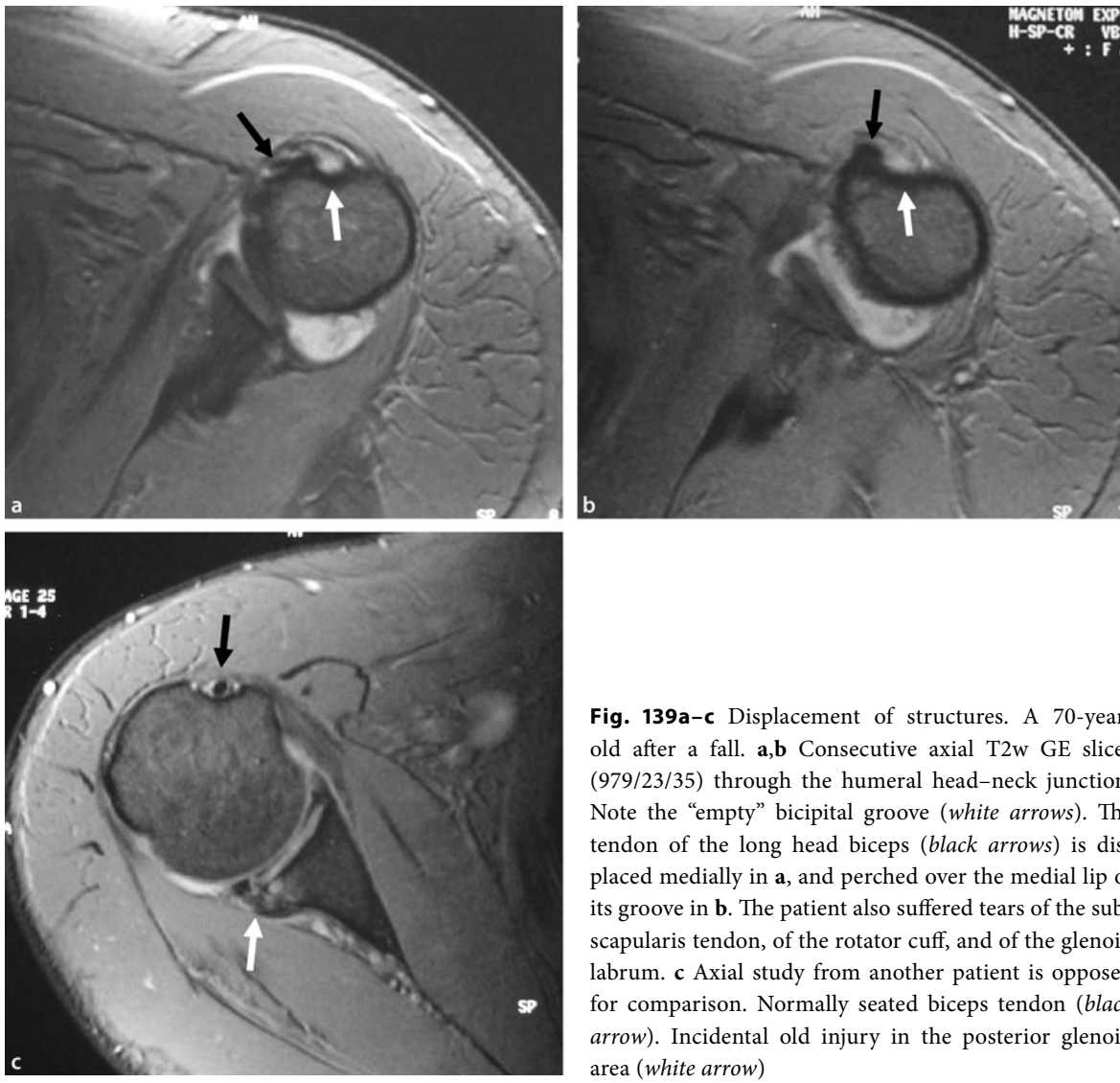

Fig. 139a–c Displacement of structures. A 70-year-old after a fall. **a**,**b** Consecutive axial T2w GE slices (979/23/35) through the humeral head–neck junction. Note the "empty" bicipital groove (*white arrows*). The tendon of the long head biceps (*black arrows*) is displaced medially in **a**, and perched over the medial lip of its groove in **b**. The patient also suffered tears of the subscapularis tendon, of the rotator cuff, and of the glenoid labrum. **c** Axial study from another patient is opposed for comparison. Normally seated biceps tendon (*black arrow*). Incidental old injury in the posterior glenoid area (*white arrow*)

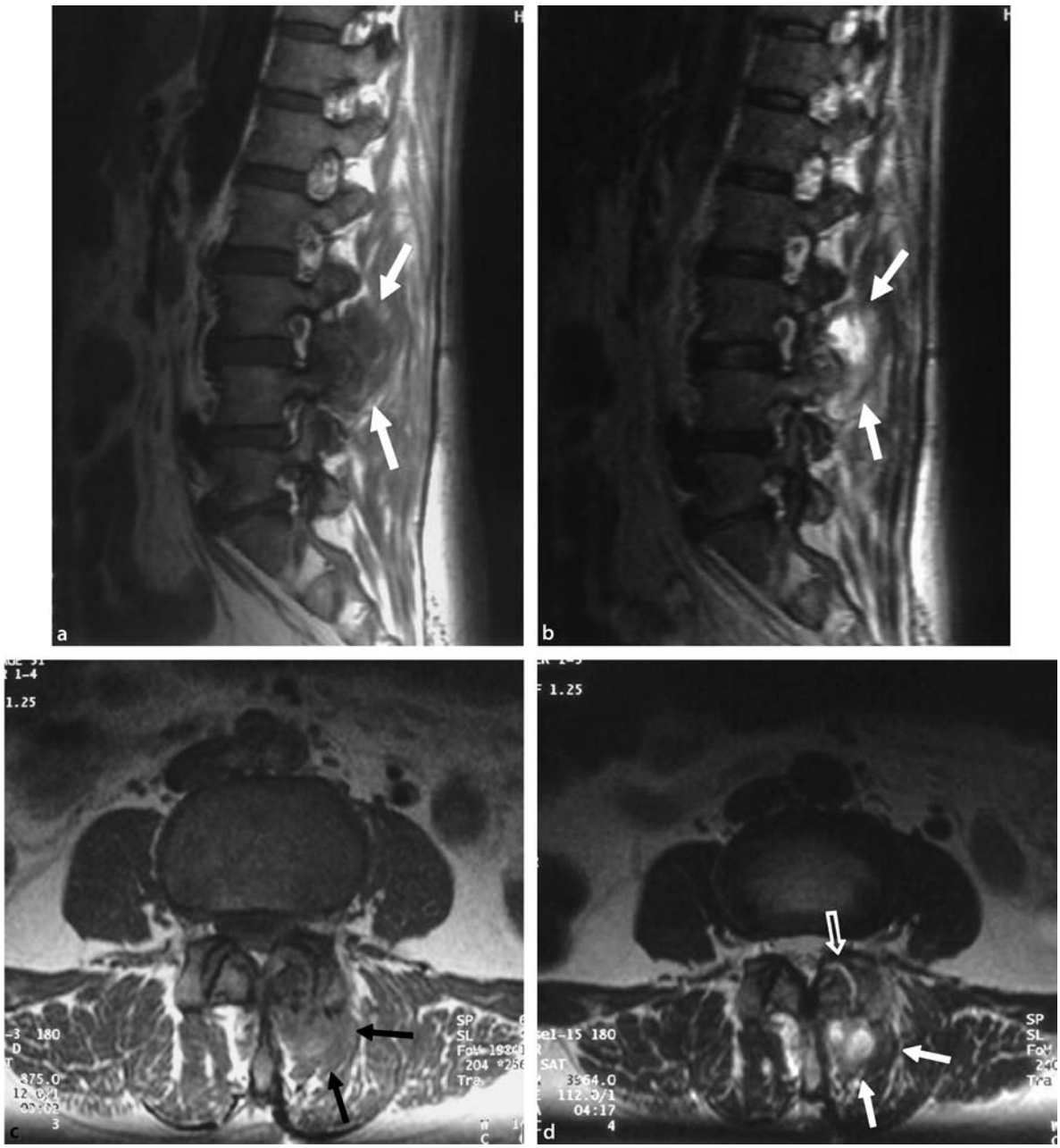

Fig. 140a–d "Nearby" lesion: first example. A 52-year-old woman with diffuse low back pain 3 years post L4–L5 and L5–S1 diskectomy via laminectomy. Lateral sagittal sections **a** T1w TSE (700/12) and **b** T2w TSE (3,946/112). The fat planes around the L3–L4 facet joint have been obliterated by a T1 iso- and T2 hyperintense lesion (*arrows*). Axial sections were then prescribed through the L3–L4 level. **c** T1w TSE (875/12) and **d** T2w TSE (4,342/112). The abnormality is attached to the left apophyseal joint and represents a loculated fluid collection with thick walls (*solid arrows*). Note fluid within the left apophyseal joint (*open arrow*). There is also bone marrow edema in the left L3 facet and loss of definition in its cortex. Contrast was not administered due to history of anaphylactic shock to iodinated contrast medium. Final diagnosis: septic (bacterial) arthritis of the apophyseal joint

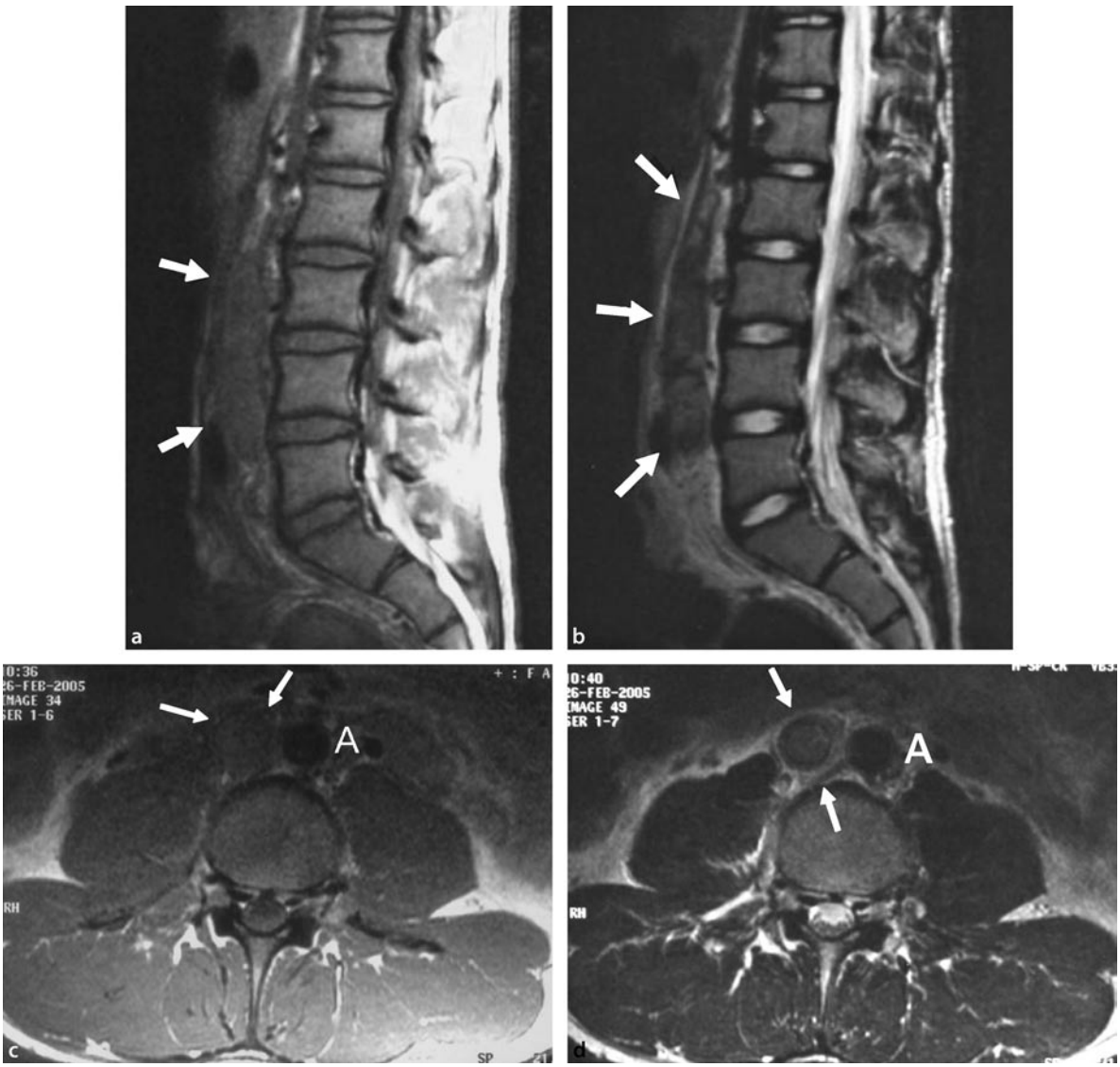

Fig. 141a–d "Nearby" lesion: second example. A 13-year-old boy with relatively rapid onset of a constant dull ache in the lumbar area. Right paramidline **a** T1w TSE (740/12) and **b** T2w TSE (4,324/112) slices. Axial **c** T1w TSE (800/12) and **d** T2w TSE (3,400/96) sections. **a**, **b** An elongated "mass" in the prespinal soft tissues (*arrows*) extends over several vertebral segments to the right of the aorta (*A*). Its T1 signal intensity is intermediate and homogeneous. In the T2w images we discern a central circle of low signal intensity that represents the occluded vascular lumen. A collar of edematous inflammatory tissue has obliterated the surrounding fat planes. Diagnosis: massive thrombosis of the inferior vena cava; confirmed by CT and triplex/color sonography. The thrombus also occluded the iliac veins bilaterally (not shown). Further evaluation revealed coagulopathy due to protein C deficiency

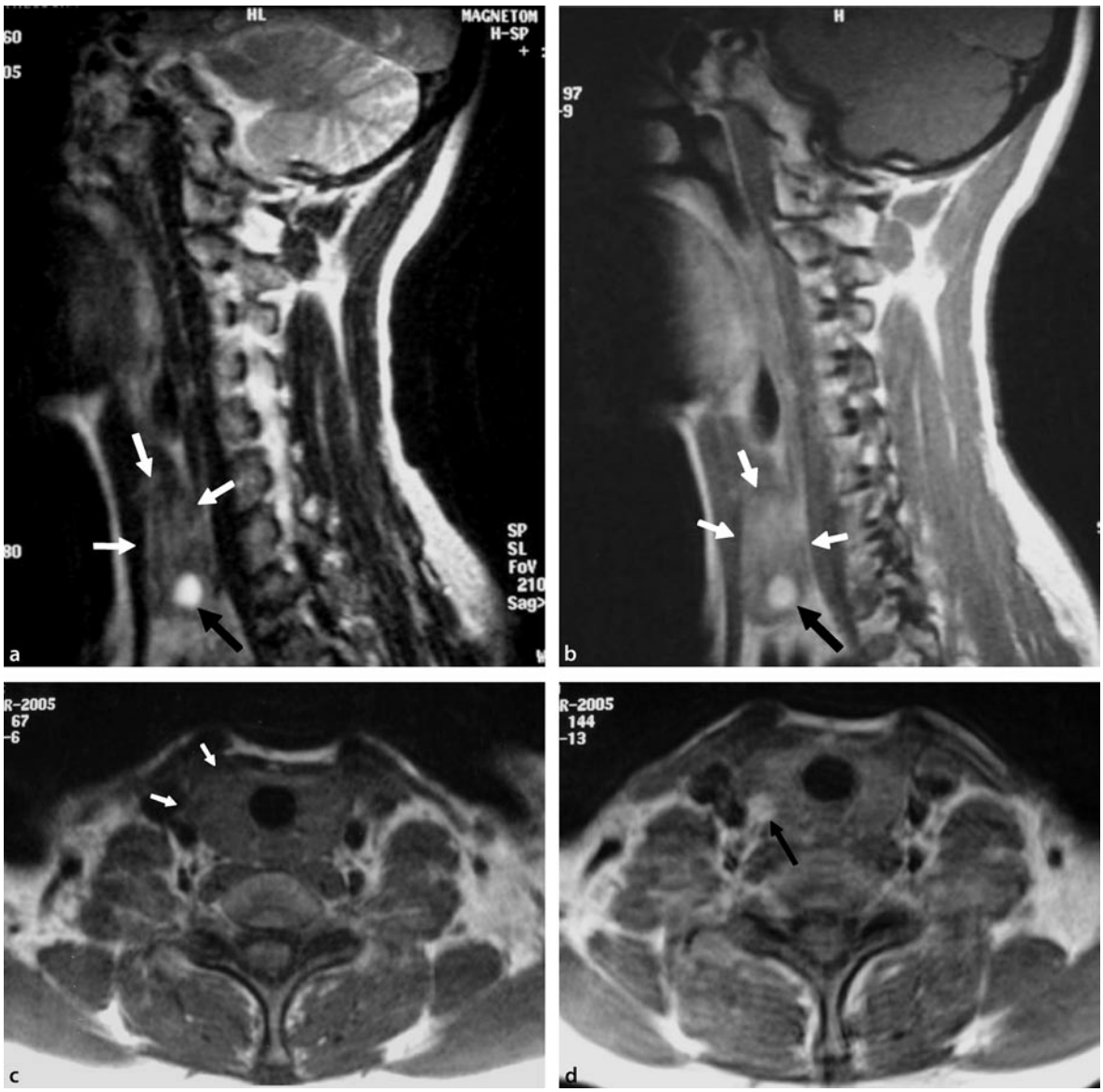

Fig. 142a–d Incidentaloma in a cervical spine MRI. A 45-year-old woman with a clinical picture of myelopathy. Lateral **a** T2w TSE (4,324/112) and **b** post-contrast T1w TSE (650/12) images. **c**,**d** Axial T1w SE (450/12) images pre- and post-gadolinium. There is a well-defined, 8 mm nodule (*black arrows*) in the inferior pole of the right thyroid lobe (*white arrows*). The enhancement is strong and homogeneous. Diagnosis: parathyroid adenoma

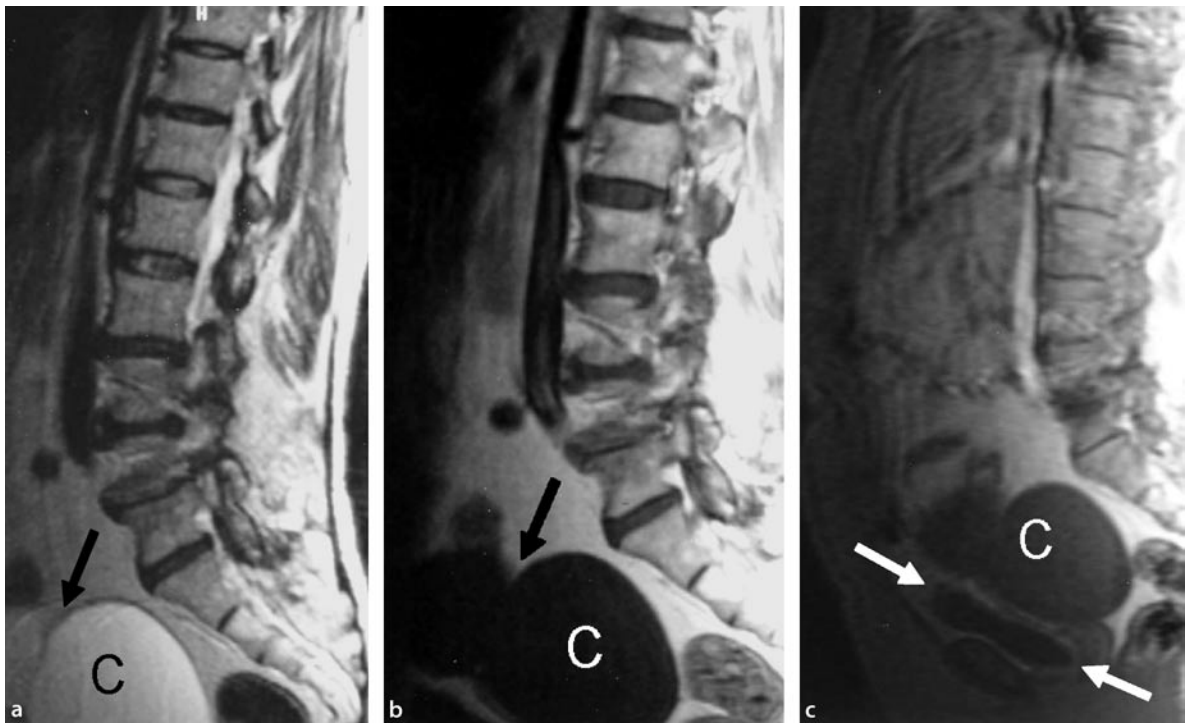

Fig. 143a–c Incidentaloma on a lumbar spine MRI scan. A 70-year-old woman with low back pain and radiculitis. Sagittal **a** T2w TSE (4,324/112) and **b** T1w TSE (700/12) images. A cyst-like structure (*C*) looks like the urinary bladder in full distention. However, there is suggestion of lobulation with a thin septum anterosuperiorly (*arrows*). The scout T1w image (**c**) was retrieved and reviewed: the urinary bladder (*arrows*) appears compressed and is definitely separate from the "cyst" (*C*). Final diagnosis: ovarian cystadenoma (10 cm in size)

Contrast Enhancement

Regarding the assessment of contrast enhancement, the reaction of a lesion to the administration of contrast can be complex since it depends on multiple factors, including the number and type of efferent and afferent vessels, the density and leakiness of the capillaries, the size of the interstitium, and the specifics of the host tissue or organ. Please keep in mind the following:

1. Contrast may travel rapidly from one compartment to another, and in some cases we have to "chase" it with fast sequences fired in rapid succession. For example, scans in the arterial, portal venous, and equilibrium phases are necessary for a thorough evaluation of the liver, pancreas, and spleen (Figs. 144, 145).
2. Contrast enhancement by itself is a nonspecific finding. For example, some solid tumors show weak, partial or no enhancement (Fig. 124). On the contrary, intense contrast uptake may be seen in reactive changes such as bone marrow edema or hyperemia.
3. Contrast enhancement does not always mark the margins of the lesion. Thus, there is a danger of over- or under-estimating the size/extent of a lesion if we rely too heavily upon the area that enhances (Fig. 146).
4. The type, degree, extent, and time course of contrast enhancement are features that should be integrated with the rest of the information we have gathered (from the plain images; Fig. 146).

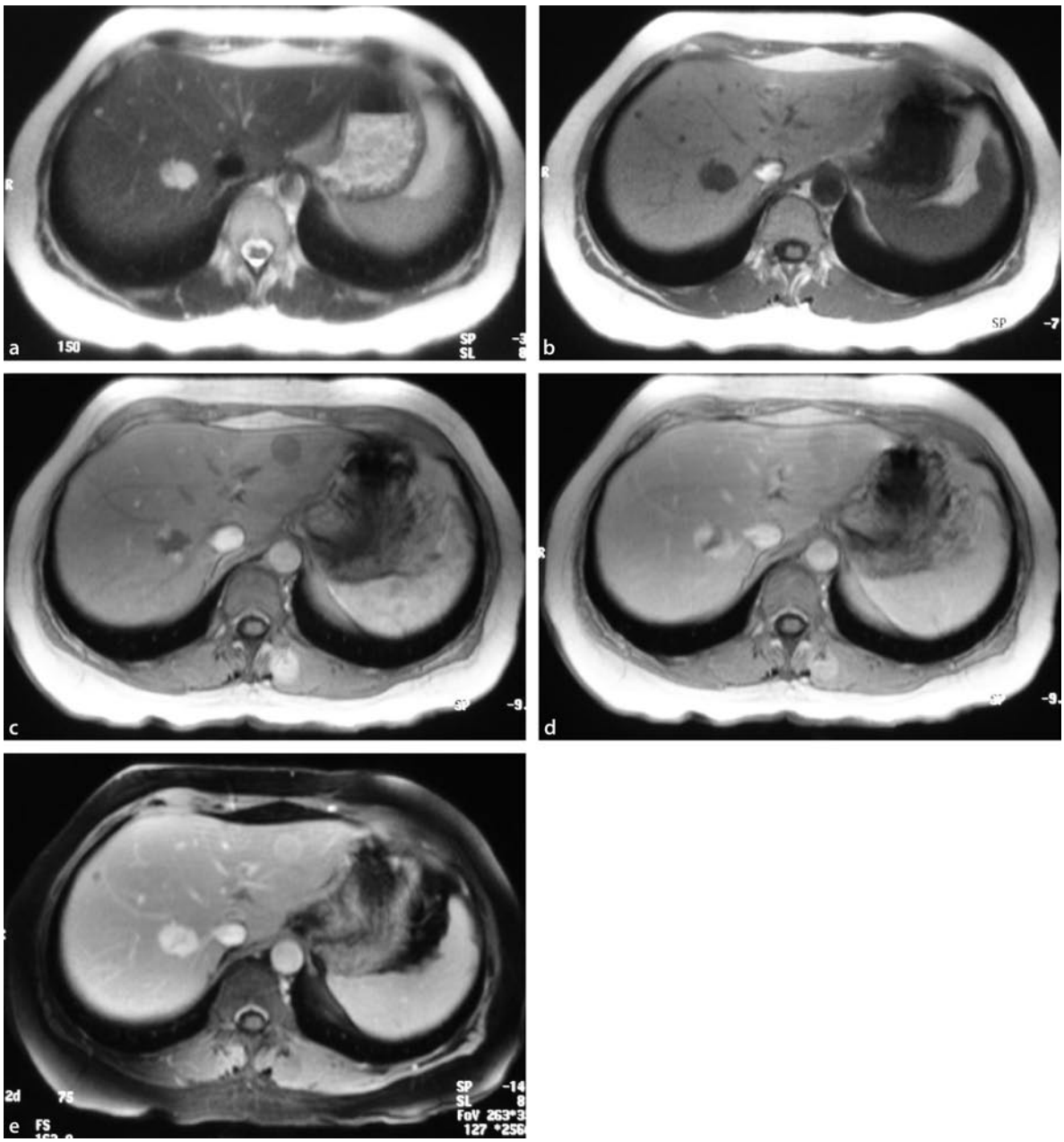

Fig. 144a–e Progressive, centripetal contrast enhancement. A 54-year-old woman with right upper quadrant pain. Sonography revealed a liver nodule in the right lobe and an MR scan was requested. A series of axial **a** fast T2w (HASTE) and **b** T1w gradient echo (127/7/80°) slices. A well-defined, homogeneous and lobulated mass has elevated T2 and low T1 signal intensity. **c–e** following bolus injection of contrast the T1w GE sequence was repeated in the arterial, portal venous, and equilibrium phases, with fat suppression in the last image. Early on we note globular peripheral enhancement (**a**), that progresses to an incomplete rim (**b**), and finally reaches the center of the "mass" (**e**). The progressive accumulation of contrast renders the lesion considerably more intense than the parenchyma. Diagnosis: cavernous hemangioma

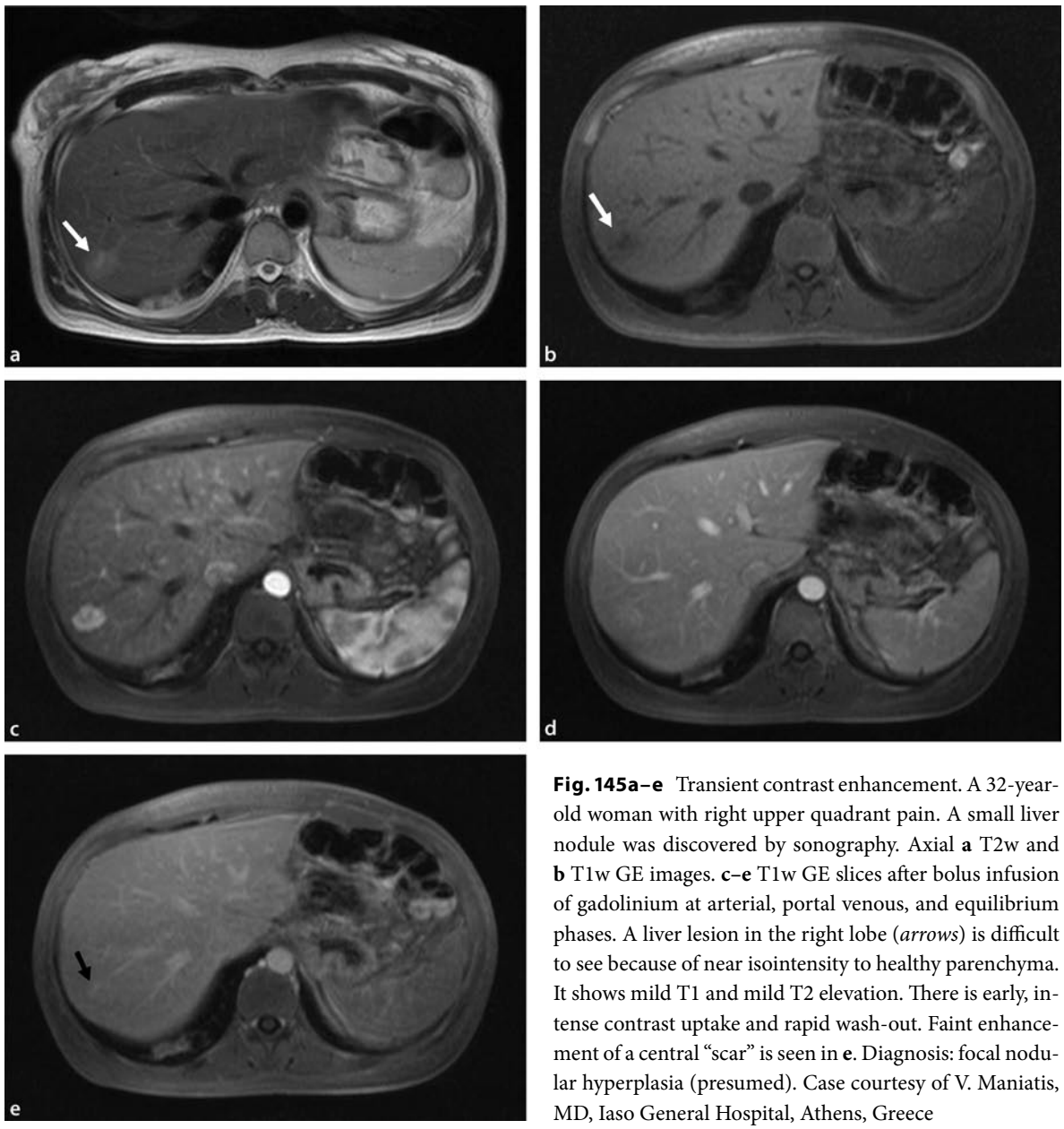

Fig. 145a–e Transient contrast enhancement. A 32-year-old woman with right upper quadrant pain. A small liver nodule was discovered by sonography. Axial **a** T2w and **b** T1w GE images. **c–e** T1w GE slices after bolus infusion of gadolinium at arterial, portal venous, and equilibrium phases. A liver lesion in the right lobe (*arrows*) is difficult to see because of near isointensity to healthy parenchyma. It shows mild T1 and mild T2 elevation. There is early, intense contrast uptake and rapid wash-out. Faint enhancement of a central "scar" is seen in **e**. Diagnosis: focal nodular hyperplasia (presumed). Case courtesy of V. Maniatis, MD, Iaso General Hospital, Athens, Greece

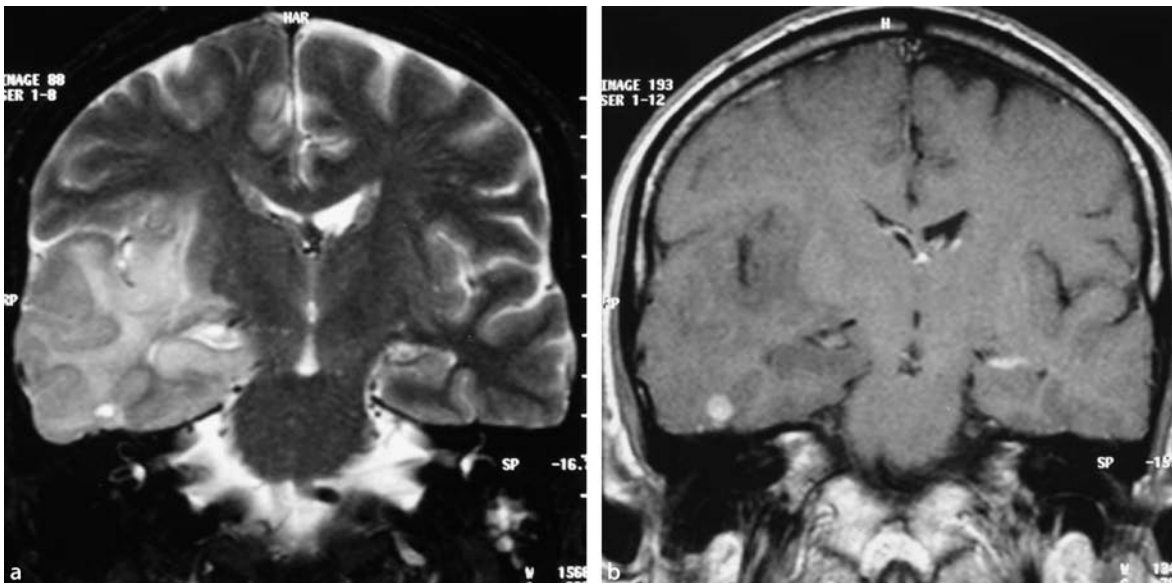

Fig. 146a–d Integration of pre- and post-contrast scans. A 52-year-old, without prior medical history, presents with progressive headaches and a generalized seizure. Coronal **a** STIR (5,624/TI 120/60) and **b** post-contrast T1w SE images (532/15). Grossly abnormal signal extends over a large part of the right cerebral hemisphere, including the temporal lobe, insula, and hippocampus. Both gray and white matter structures are involved. Contrast enhancement is limited to a tiny nodule in the inferior temporal region. Could this be an abscess with perifocal edema? There are two objections to this possibility. First, the volume of "edema" is disproportionate to the size of the enhancing focus. Second, there is equal involvement of gray and white matter by the "edema." Note the thickening of the cortex and blunting of the gray–white border. **c,d** *see next page*

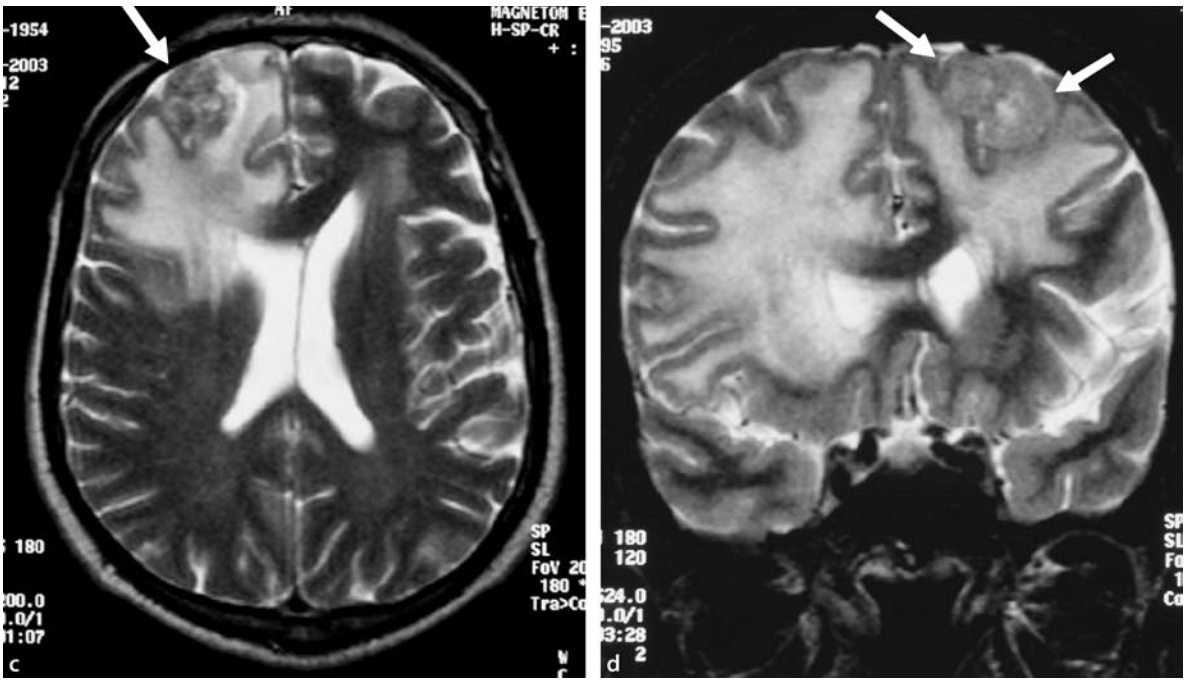

Fig. 146a–d *(continued)* Compare with **c** and **d**, which are from a different patient with a known lung malignancy, who complains of headaches, nausea, and vomiting. **c**, **d** Axial T2w TSE (4,465/120) and coronal STIR (5,624/TI 120/60) slices. Bifrontal superficial metastases (*arrows*) have incited extensive edema in the white matter. Note how the edema seems to stop at the gray–white junction. The cortex is flattened and appears thinned. Thus, the gray–white interface is accentuated and sharpened. These imaging features are quite different from what we see in **a** and **b**. Let us return to the case depicted in **a** and **b** and look at the diagnosis: glioma with extensive infiltration; the enhancing nodule represented an anaplastic focus. How can we reconcile this apparent discrepancy? The answer lies in the blood–brain barrier (BBB). Contrast leakage in the brain marks the site(s) of active BBB disruption and does not always indicate the margins of primary brain tumors. Indeed some gliomas infiltrate beyond the area of contrast enhancement, at a considerable distance. In such cases conventional MRI cannot separate the tumor from reactive edema. This differentiation can be achieved safely with MR perfusion or MR spectroscopy maps

Pertinent Findings

A discussion of associated and pertinent findings could be entitled "what the clinician needs to know": In straightforward cases we need only describe the abnormality (e.g., acute complete tear of a knee ligament). Other times we need to stretch our abilities to arrive at a specific diagnosis or at a short differential list that satisfies the clinical picture. An effort should be made to uncover the etiology, estimate the age of the lesion and warn about possible complications (where applicable). Thus, any significant/relevant piece of data should be communicated as present or absent. Let me provide some examples.

A hemorrhagic brain infarction can be caused either by arterial occlusion or by venous thrombosis. Thus, we should check for the patency of both the arterial and venous sides of the afflicted territory. In a case of aggressive or neglected otomastoiditis we should look again for signs of extra-axial or parenchymal sepsis or venous sinus thrombosis. When we detect a knee osteochondral defect we should "hunt" for a loose body that represents the "missing" piece. In other words, some situations call for a mental feedback loop, requiring intensification of the search for additional, related lesions (Figs. 147, 148).

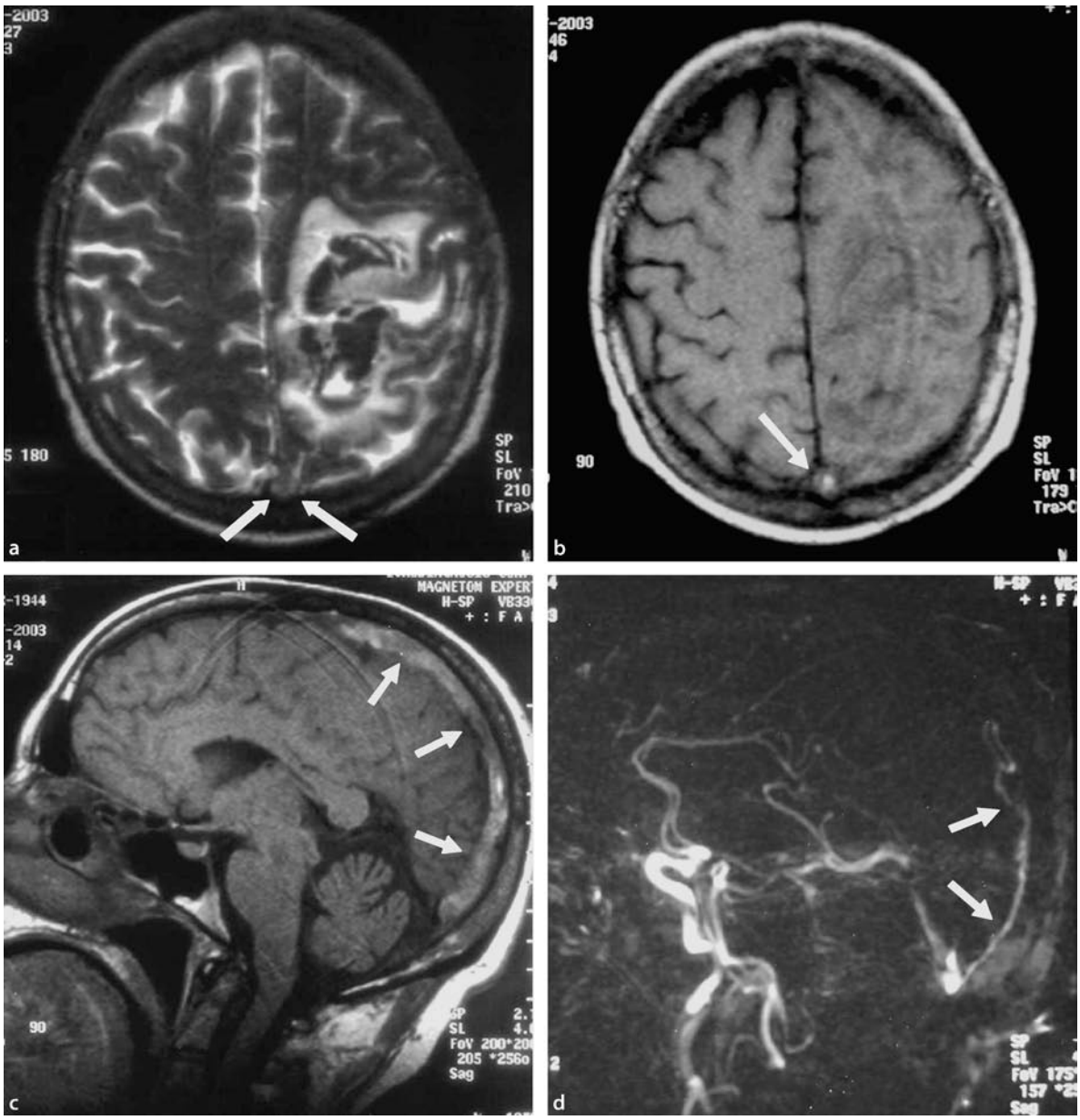

Fig. 147a–d What the clinician needs to know: example of a neurological case. A 59-year-old woman undergoing systemic chemotherapy for ovarian carcinoma, presenting with a focal clonic seizure of the right extremities. A CT scan within 2 h (not shown) revealed parenchymal edema and hemorrhage in the high left frontoparietal area. An MR scan was obtained 2 days later with axial **a** T2w TSE (4,465/120) and **b** T1w SE (532/15), and sagittal **c** T1w SE (532/15) and **d** phase contrast MRA (VENC 20) sequences. **a**,**b** The acute hemorrhage is markedly T2 hypointense and contrasts sharply with the surrounding hyperintense edema. The hematoma cannot be distinguished from edema with confidence in **b**. The superior sagittal sinus (*SSS*, *arrows*) displays signal intensity higher than expected in both **a** and **b**. The midline T1w slice (**c**) demonstrates a hyperintense clot filling the SSS (*arrows*). The MR "venogram" (**d**) demonstrates a small residual channel in the vertical segment of the SSS ("string" sign, *arrows*). The remainder of the sinus is occluded (compare with Fig. 108) Diagnosis: hemorrhagic infarction due to thrombosis of the SSS. The thrombosis was attributed to the dehydration of the patient due to extensive vomiting as a side effect of chemotherapy. Follow-up MR scans revealed near complete sinus recanalization and slow resolution of the parenchymal abnormalities, without evidence of intracranial metastatic disease

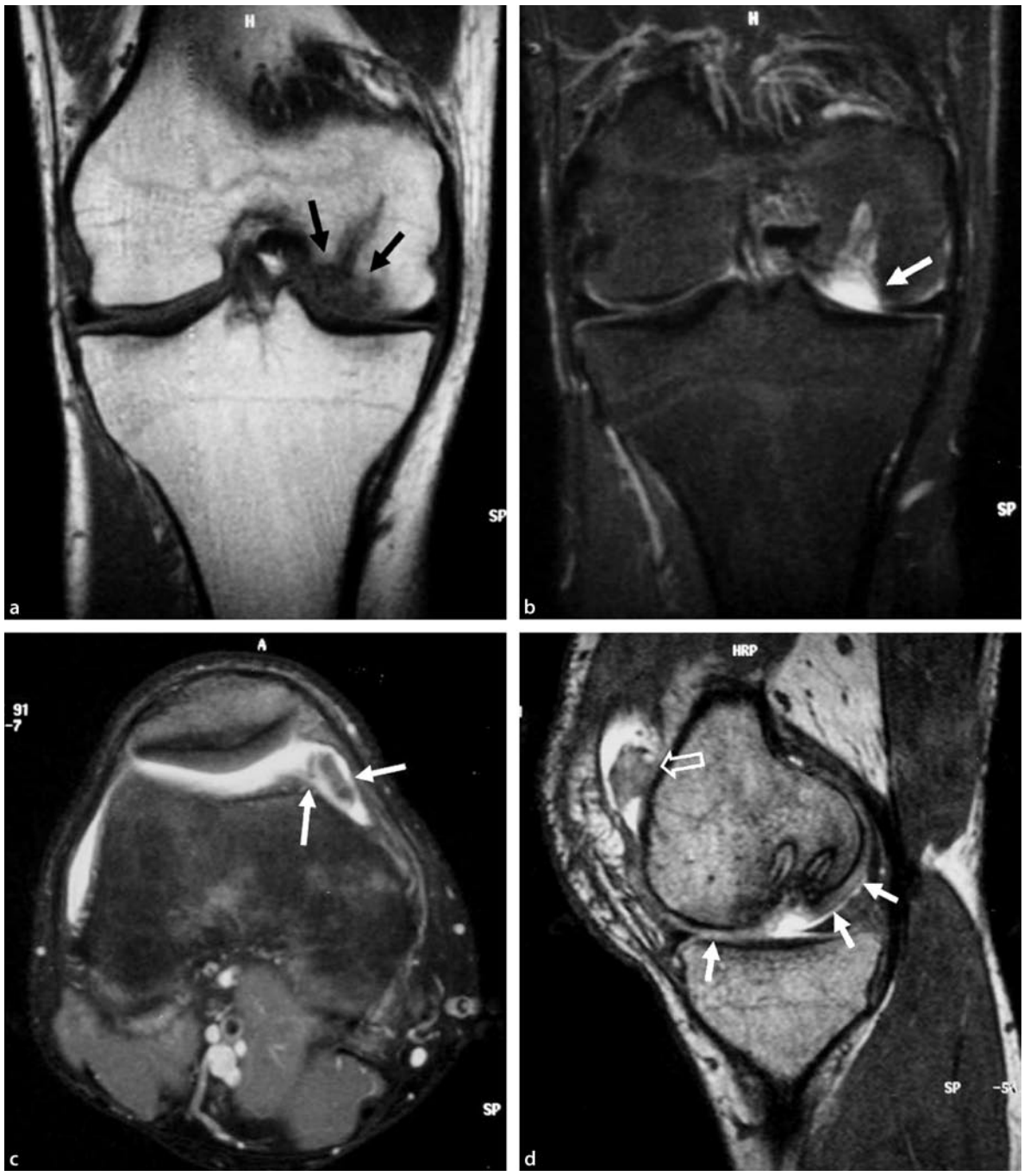

Differential Diagnosis

Arriving at a sound differential diagnosis is like piecing together a jigsaw puzzle. After a full description of the examination we group together all related findings and stratify them in order of importance.

Keep in mind that associated or secondary findings may be more obvious than the primary or inciting lesion (Figs. 149, 150).

It is to our advantage to keep a broad perspective, compose at first a wide differential list and then narrow it by eliminating the unlikely possibilities.

◂ **Fig. 148a–d** What the clinician needs to know: example of an orthopedic case. An 18-year-old with osteochondritis dissecans of the medial femoral condyle. The patient underwent pinning of autologous chondral implants. An MR scan was requested because of new pain and locking. **a** T1w SE (450/12) and **b** STIR (4,230/TI 120/30) images in a coronal orientation: a large osteochondral defect of the medial femoral condyle (*arrows*) is outlined by joint fluid. **c** Axial fat-suppressed PDw (3,000/33) image: the chondral grafts have disengaged from the surgical bed and float "free" in the joint, close to the patella (the *arrows* point to two adjacent loose bodies). **d** Sagittal slice from a T2* 3D acquisition: this type of sequence is excellent for depicting articular cartilage. Healthy cartilage (*solid arrows*) contrasts sharply against the dark cortical rim and the bright joint fluid. It is easy to ascertain the margins of the "crater" and the extent of the missing components (i.e., articular cartilage, cortex, and subchondral marrow). The *open arrow* points to a large loose body, also seen in **c**

A convenient and useful classification scheme of diseases is the following: congenital, neoplastic, pseudotumors, infectious, inflammatory (noninfectious), vascular, traumatic, and toxic/metabolic.

If in doubt or in trouble, we can recruit the following three "pearls":

1. List the anatomic contents in the space for the origin of the lesion (Figs. 151, 152). For example let us consider the presacral/precoccygeal space. What do we find there? Gut (rectum), spine, and embryonic remnants, which can give rise to:
   - Cysts (enteric, neurenteric, inclusion; Fig. 127)
   - Pseudocysts (anterior sacral meningocele)
   - Tumors (rectal leiomyosarcoma, spinal chordoma, and sacrococcygeal teratoma)
   - Inflammatory conditions (pyogenic abscess)

2. Remember that unusual manifestations of common diseases are more frequent than common manifestations of rare diseases. The "uncommonness" can be either in appearance or in place (Figs. 71, 153).
3. Keep in mind two great mimics: lymphoma and tuberculosis. Both can have protean manifestations at a single site or at multiple sites. They can involve any tissue, structure, solid organ, or system (Fig. 154). Tuberculosis, furthermore, can also destroy joints and disk spaces (osteomyelitis, synovitis, and erosive arthritis).

Let us return to the differential diagnosis list provided above. I would like to add the category "complications", which has a dual interpretation. The obvious one refers to the undesirable side effects of trauma, inflammation or any therapeutic manipulation (either immediate or delayed). The other possibility refers to a breakdown of the steady state of the disease as part of its natural history.

Such events can be sudden or insidious. In the first case we have to think of:

- Hemorrhage
- Thrombosis/rupture of a vessel, a vascular malformation or a tumor (Fig. 147)
- A stress or pathologic fracture
- Torsion of a cyst or a mass

Slow onset complications point to malignant degeneration of a low grade or a chronic disease. Examples include the following

- Sarcomas developing in Pagetic bone
- Carcinomas arising in fistulous tracts
- The dedifferentiation of gliomas from low to high grade varities
- The sarcomatous transformation of benign tumors (Fig. 155)

Superinfection of pre-existing pathology can present either acutely or insidiously.

Radiologic Report

Finally, I would like to devote a few words about the report of our findings: it is the distillation of our labor and it reflects both our diagnostic and our communication skills. Anyone reading it should have no difficulty in mentally replicating the MR examination. The standard format of the report consists of three sections: technique, findings, and conclusion or impression. The last paragraph should be a "translation" of the findings into an explicit answer to the clinical question.

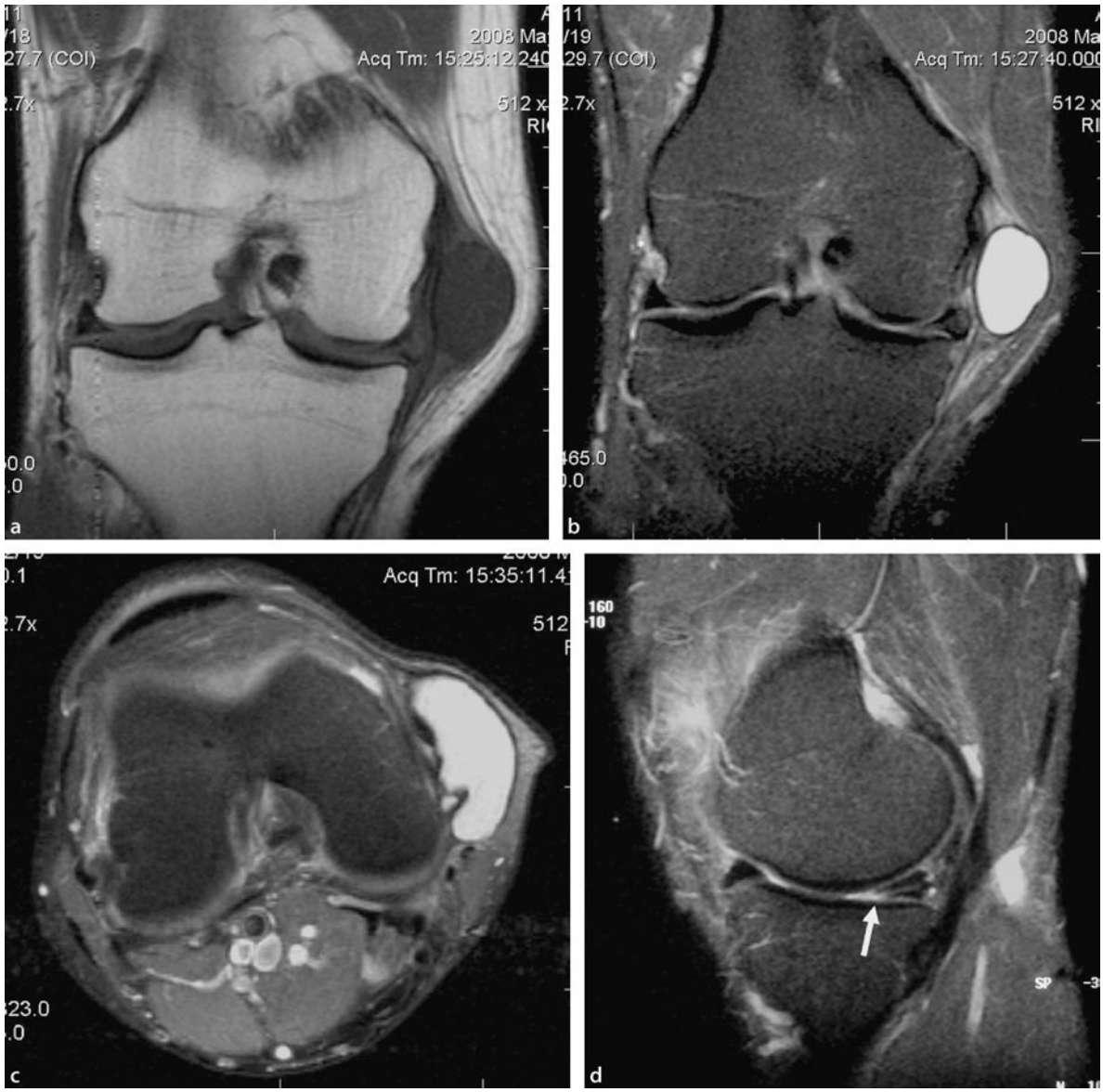

Fig. 149a–d Secondary finding that is more obvious than the primary lesion. A 25-year-old with a fluctuant "mass" in the medial aspect of the right knee and a remote history of knee trauma for which he did not seek medical advice. Coronal **a** T1w SE (475/15) and **b** STIR (4,465/TI 120/30) images, **c** axial fat suppressed PD (2,823/33) slice. The "mass" is a cyst closely apposed to the medial collateral ligament and the joint capsule. Note also the diffuse alteration of the meniscal signal ipsilaterally. **d** Sagittal STIR section through the medial condyles shows a longitudinal tear of the meniscus with violation of the free edge of the posterior horn (*arrow*). The cyst looks impressive compared with the small meniscal tear. These two entities have a cause and effect relationship: through the meniscal tear, joint fluid can escape outside the strict confines of the capsule. Accumulation of fluid within or beyond the meniscus results in the formation of an intra- or parameniscal cyst. Definitive treatment of the cyst requires treatment of the meniscal tear first

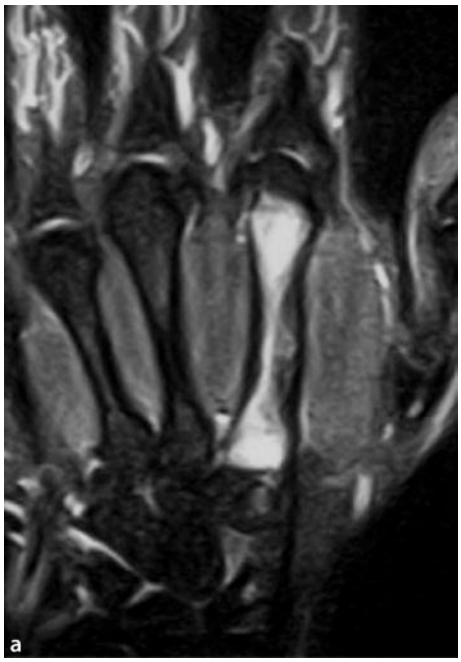

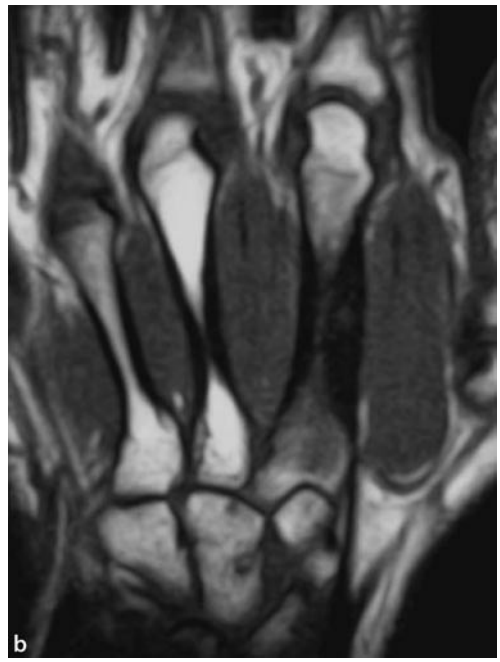

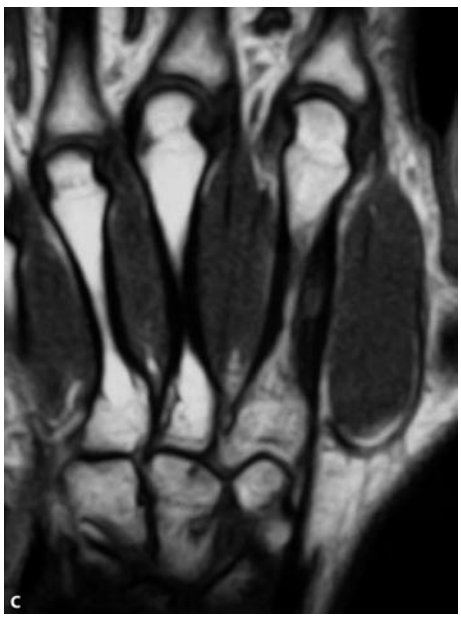

Fig. 150a–f Secondary findings that are more obvious than the primary lesion. A 23-year-old with pain and swelling of the left hand, in the region of the first metacarpal (*MC*). **a–c** Coronal STIR (4,500/130/60), T1w SE (480/12), and T1w SE (480/12) after contrast infusion slices. The striking feature is the abnormal signal and the intense contrast enhancement in the medullary canal of the first MC. The pattern is consistent with bone marrow edema. Thus, we have to look for underlying pathology, and we next notice solid thickening of the medial cortex. **d–f** *see next page*

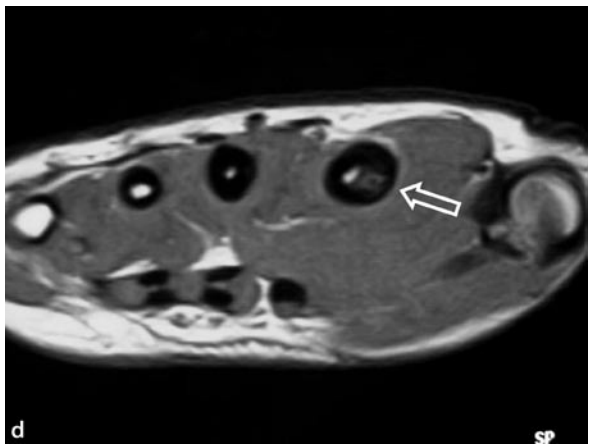

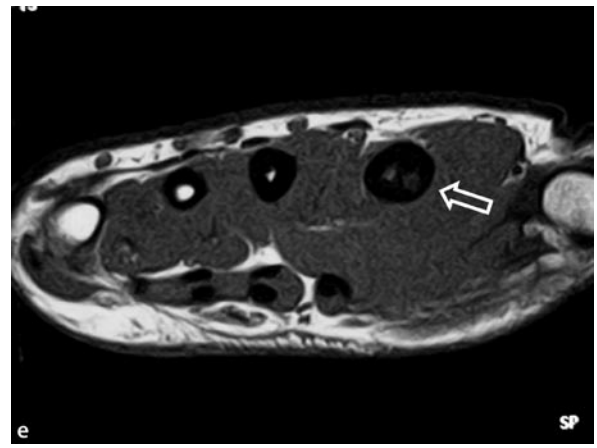

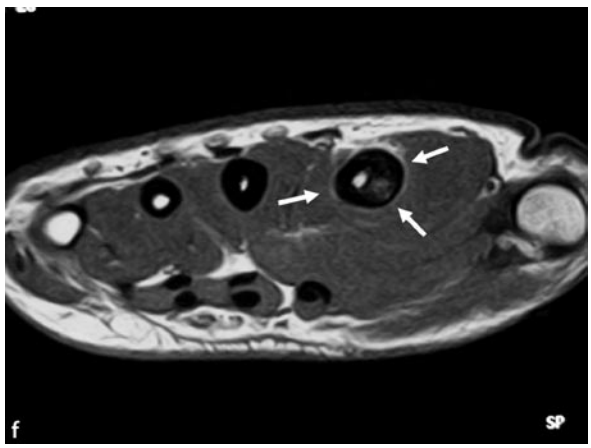

Fig. 150a–f *(continued)* Let us narrow our focus of attention a little more and switch to the transverse plane: **d–f** PD TSE (300/16) and T1w SE (480/12) pre- and post-contrast images. Right in the middle of the thickened cortex there is a soft tissue area, which in turn carries a mineralized focus right in the center (*open arrows*). The soft tissue material takes up the contrast. Note also the thin collar of enhancement around the first MC due to mild reactive changes (*solid arrows*). Diagnosis: osteoid osteoma

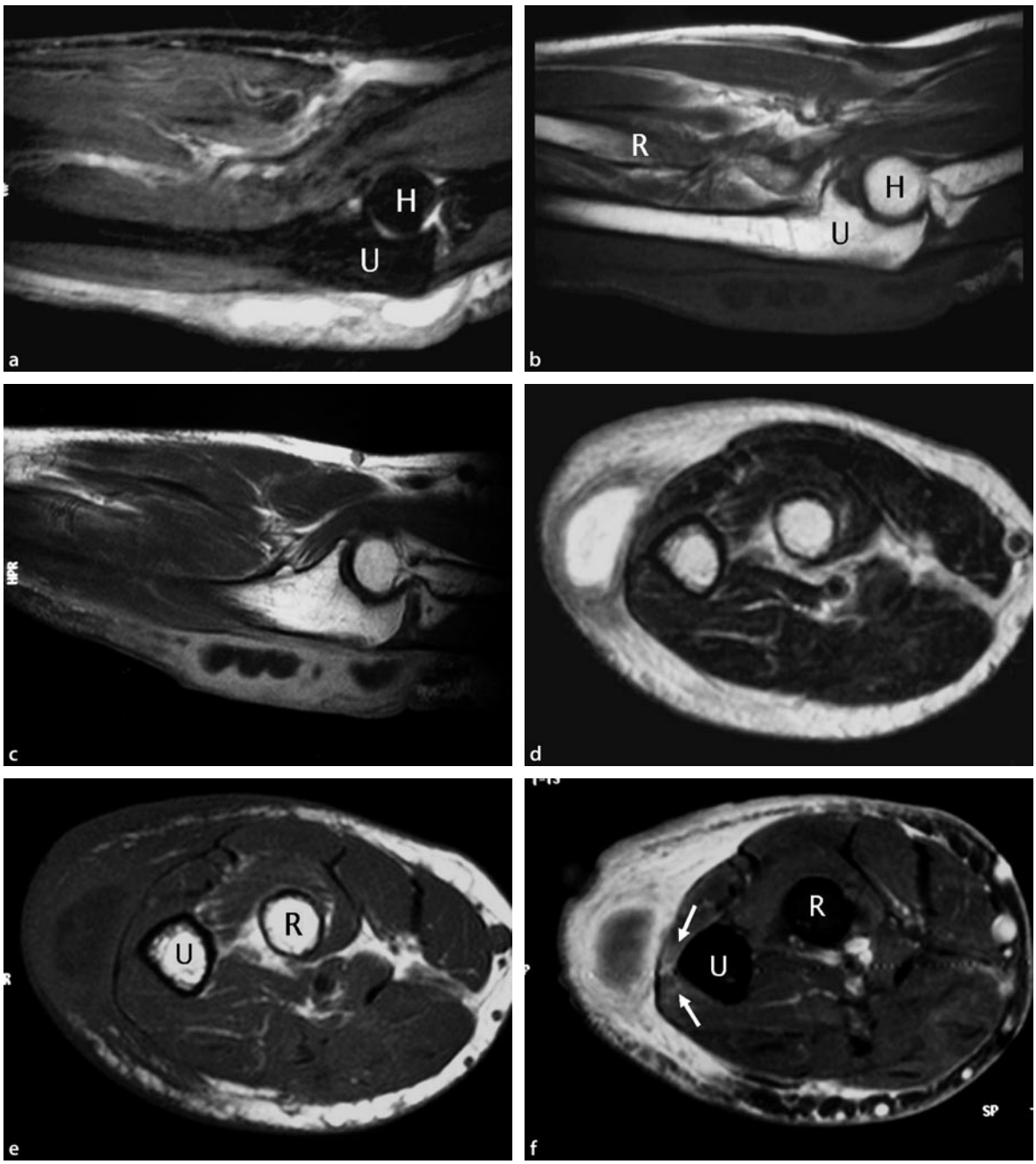

Fig. 151a–f Anatomic contents of a particular space. A 54-year-old with fever and pain with swelling in the elbow. Sagittal **a–c** STIR (4,000/TI 120/30), T1w SE (500/12), and post-contrast T1w SE (500/12). **d–f** Transverse T1w SE (450/15), T2w TSE (3,500/96), and fat-suppressed, contrast-enhanced (715/20) images through the distended part of the lesion (proximal forearm). An oblong lesion occupies the dorsal subcutaneous soft tissues and is centered on the elbow joint. It has a thick, irregular, enhancing wall and water-like contents (low T1 and very high T2 signal). Note the "rosary bead" appearance with loculation/compartmentalization. There is also marked thickening, inflammation and enhancement of the fat around the lesion. Minimal contrast enhancement proceeds deep to the barrier of the muscular fascia (*arrow*), close to the dorsal surface of the ulna (*U*). What lies dorsal to the olecranon process of the ulna? Diagnosis: septic olecranon bursitis. *R* radius, *H* humerus

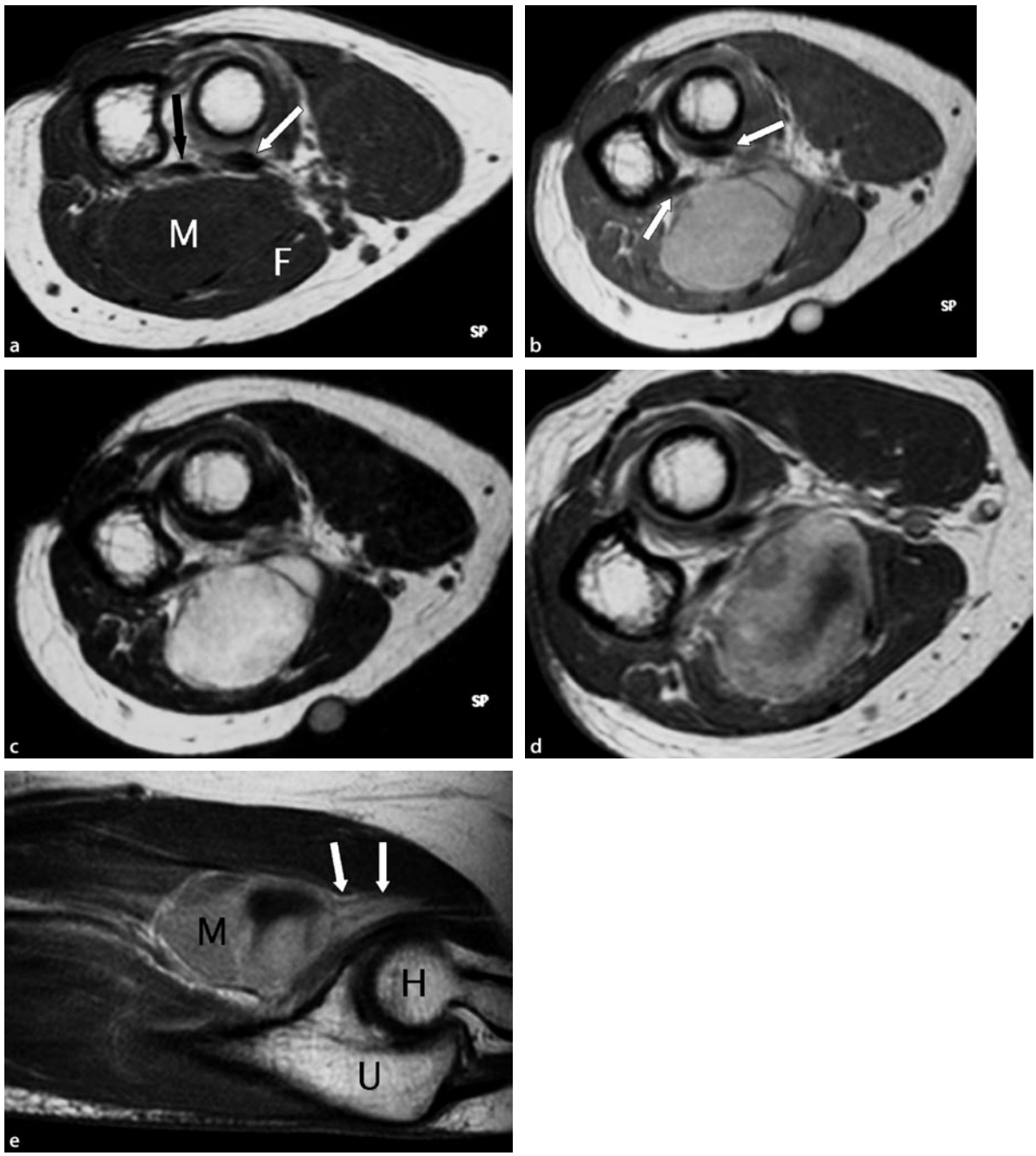

Fig. 152a–e Anatomic contents of a particular space. A 59-year-old woman with a slowly enlarging cubital mass. **a** Transverse T1w SE (500/12) section through the upper forearm. The mass (*M*) cannot be differentiated from the overlying flexor musculature (*F*). **b**, **c** axial PD/T2w TSE image pair (3,500/16; 96): the tumor stands out clearly, with progressive elevation in signal intensity. Its borders are smooth and well defined and a thin septum is present distally. **d** T1w SE image post intravenous contrast. There is strong, inhomogeneous enhancement. In all images the tendons that reside in the cubital fossa (*arrows*) are clearly separate from the mass. What else resides in the cubital fossa? **e** Hint: longitudinal T1w slice after contrast. Note the tapered proximal edge of the lesion (*arrows*). Diagnosis: malignant peripheral nerve sheath tumor (median nerve). *U* ulna, *H* humerus

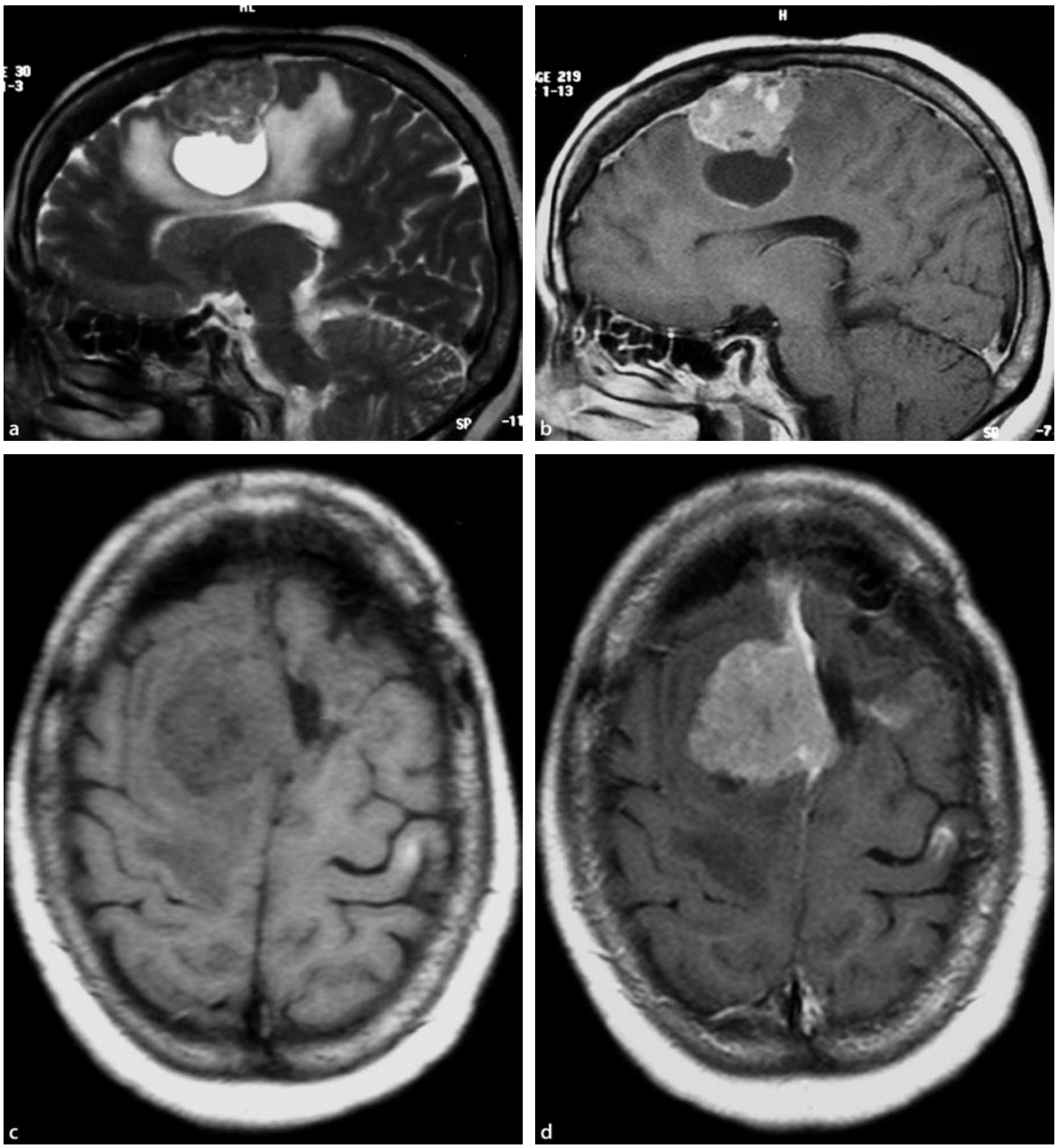

Fig. 153a–f Atypical presentation of a common disorder. Sagittal **a** T2w TSE (4,465/112) and **b** post-contrast T1w SE (532/15) images. An inhomogeneous tumor has a solid and a cystic component. **c–f** Axial T1w SE (532/15) slices through the cranial and caudal parts of the mass, before and after contrast administration. The solid part (3.8 cm in size) has a broad base against the inner skull base and the falx and looks similar to the parenchyma in terms of signal intensity. Contrast uptake is strong and inhomogeneous. A thin-walled cyst of similar size arises from the lower aspect of the mass and invaginates deep into the parenchyma. The cyst wall is also enhancing. There is moderate perilesional edema. Note also the dural "tail" anterior and posterior to the mass (**b**, **d**). Let us ignore the cyst for a moment. Does the solid part remind you of anything? Diagnosis: cystic meningioma, or more appropriately, meningioma with a peripheral cyst **e, f** *see next page*

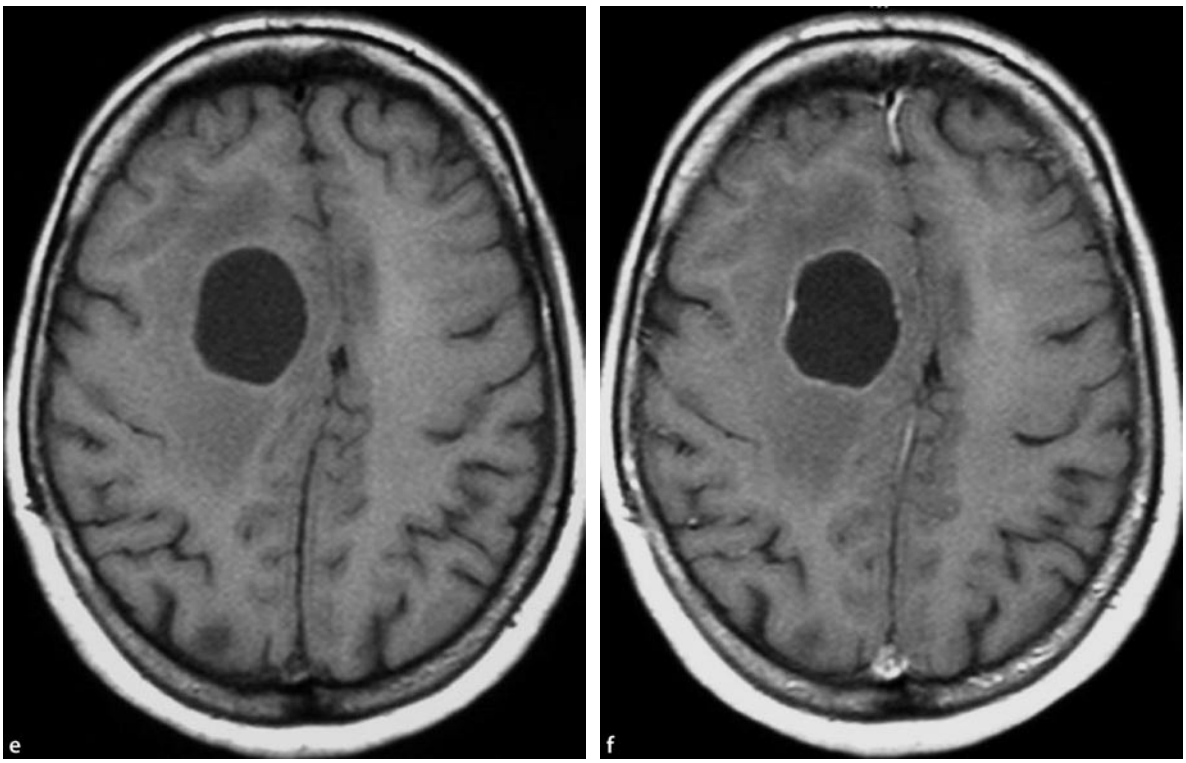

Fig. 153a–f *(continued)* **e,f**

► **Fig. 154a–f** Lymphoma: osseous involvement as the initial presentation. A 46-year-old woman with left trigeminal neuralgia. Axial **a** T1w (532/15), **b** T2w TSE (4,000/112), and coronal **c** T1w SE (500/15) and **d** STIR (4,000/TI 120/30) images. **e** T1w image after contrast administration. **f** Fat-suppressed, post-contrast T1w (500/12) slice. In the left ramus of the mandible there is infiltration of the marrow and cortical thinning. Surface breakthrough has occurred in the region of the mental foramen with minimal thickening/involvement of the overlying soft tissues (*solid arrows*). The enhancement is moderate and uniform. The lesion is poorly seen by the T2w TSE method. The soft tissue involvement is seen to advantage in the fat-suppressed sequences (*open arrows*). Diagnosis: non-Hodgkin's lymphoma, by open biopsy. No additional foci of disease were detected by subsequent extensive staging

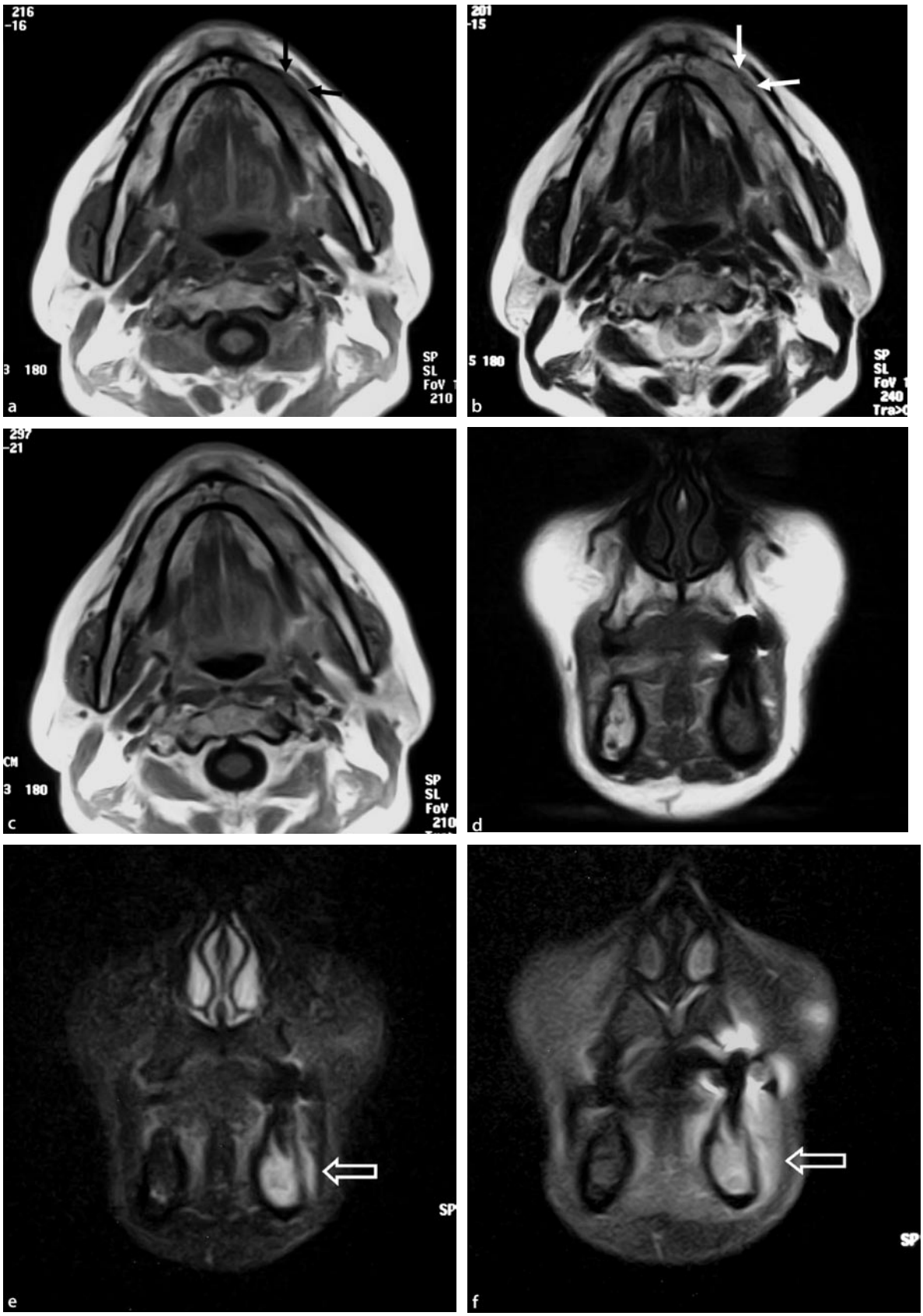
216
-16
SP
SL
FoV
210
a
201
-15
SP
SL
FoV
240
b
297
-21
SP
SL
FoV
210
c
d
SP
e
SP
f

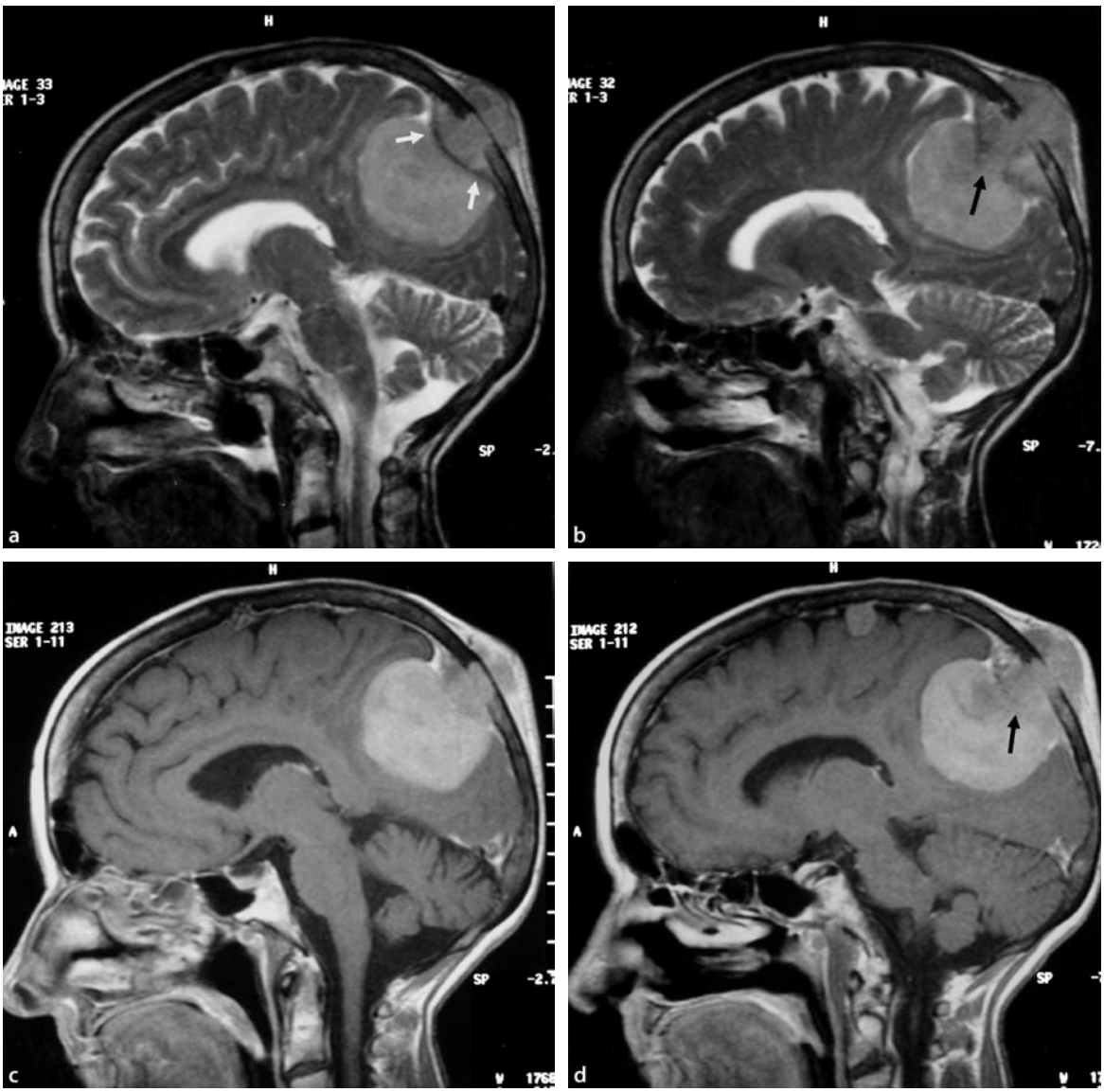

Fig. 155a–g Example of a "complication". A 69-year-old woman with recurrence of a resected meningioma. **a–d** Sagittal pairs of T2w TSE (4,465/112) and post-contrast T1w SE (532/15) sections. **e–g** *see next page*

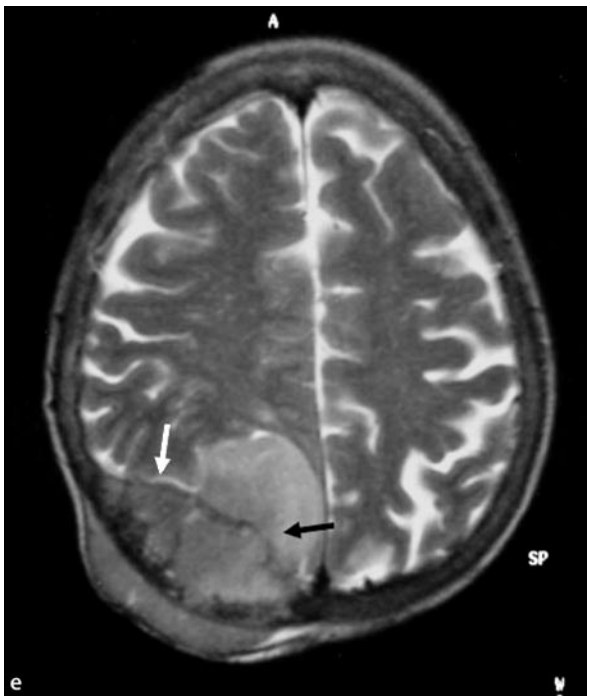

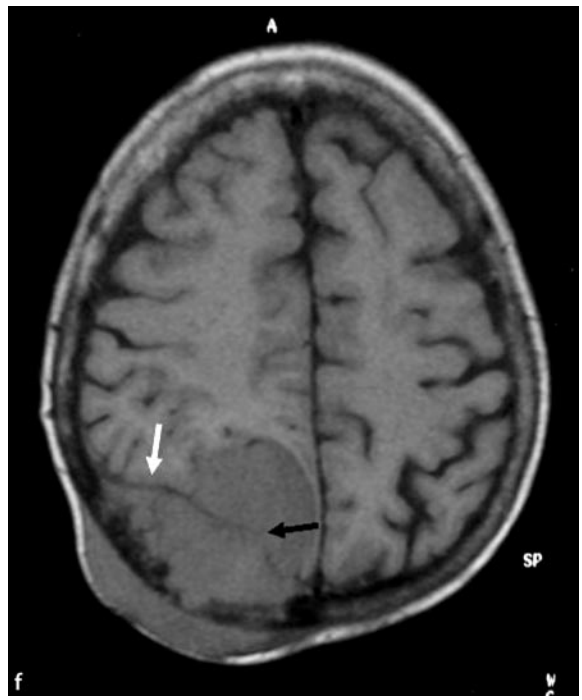

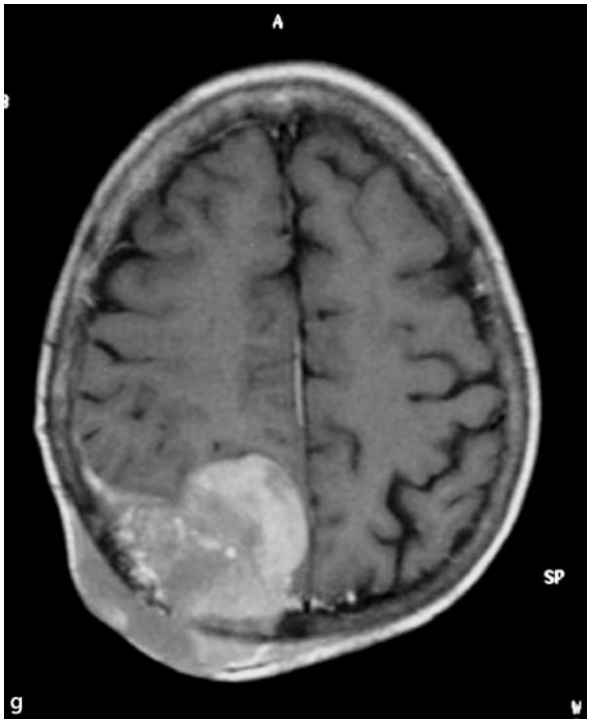

Fig. 155a–g *(continued)* **e–g** Transverse T2w TSE (4,465/112), T1w SE (532/15), and T1w SE (532/15) post-contrast images. There is a large, bilobed, inhomogeneous, extra-axial mass in the posterior parietal area. The two lobes are separated by a thin dark band that represents the dura (*white arrows*). The deep part invaginates extensively into the parenchyma and has stronger contrast uptake. The superficial component seems to invade the deep lobe through the dural defect (*black arrows*). There is also erosion and infiltration of bone at the prior craniotomy site, extending into the soft tissues of the scalp. Diagnosis: malignant transformation into meningeal sarcoma. Incidentally, note the second small meningioma at the vertex in the sagittal images (**b,d**)

Conclusion

Even the simplest MR study contains an extraordinary amount of information. The student of MRI needs a firm clinical background and a systematic approach, whilst being fluent in anatomy and MR physics. In the beginning it is certainly a complex and difficult task, but do not get discouraged! With time, patience, and persistence, one can master the nuances of MRI and the appearance of various diseases. Speed and critical thought develop hand in hand with feedback from clinical colleagues.

I would like to close by paraphrasing the following quote by Jim Horning and Barry LePatner:

Good judgment comes from experience (and knowledge), and experience comes from bad judgment (and thinking about it).

Good luck!

References

Amirsys (various) The Pocket Radiologist Series. Saunders, Philadelphia

Amirsys (various) The Diagnostic Imaging Series. Saunders, Philadelphia

Atlas SW (ed) (2001) Magnetic resonance imaging of the brain and spine, 3rd edn. Lippincott, Williams & Wilkins, Philadelphia

Berquist TM (2005) MRI of the musculoskeletal system, 5th edn. Lippincott Williams & Wilkins, Philadelphia

Fischbein NJ, Dillon WP, Barkovich AJ (2000) Teaching atlas of brain imaging. Thieme, Stuttgart

Haacke EM (1999) Magnetic resonance imaging: physical principles and sequence design. Wiley-Liss, New York

Hashemi R, Bradley WG, Lisanti CJ (2004) MRI: the basics, 2nd edn. Lippincott, Williams & Wilkins, Philadelphia

McRobbie DW, Moore EA, Graves MJ, Prince MR (2003) MRI: from picture to proton. Cambridge University Press, New York

Mitchell DG, Cohen MS (2004) MRI principles, 2nd edn. Saunders, Philadelphia

Renfrew DL, Franken EA Jr, Berbaum KS, Weigelt FH, Abu-Yousef MM (1992) Error in radiology: classification and lessons in 182 cases presented at a problem case conference. Radiology 183:145–150

Ros PR, Mortele KJ, Lee S, Pelsser V (2006) CT and MRI of the abdomen and pelvis. A teaching file. Lippincott Williams & Wilkins, Philadelphia

Runge VM (2005) The physics of clinical MR taught through images. Thieme, Stuttgart

Samuel S, Kundel HL, Nodine CF, Toto LC (1995) Mechanism of satisfaction of search: eye position recordings in the reading of chest radiographs. Radiology 194:895–902

Sprawls P (1987) Physical principles of medical imaging. Aspen, Maryland

Weishaupt D, Koechli VD, Marincek B (2006) How does MRI work? An introduction to the physics and function of magnetic resonance imaging, 2nd edn. Springer, Heidelberg

Westbrook C (2002) MRI at a glance. Blackwell Science, Oxford

Yock DH Jr (2002) Magnetic resonance imaging of CNS diseases. A teaching file, 2nd edn. Mosby, St. Louis

Glossary

Aliasing: an artifact also called fold-over or wrap-around. It occurs in the phase encoding direction when the chosen field of view (FOV) is small relative to the area under investigation. The radiofrequency pulses and the gradients affect all the tissues in a particular slice/slab, whether the tissues fit in the FOV or "spill" outside. Nevertheless, the anatomic parts "excluded" from the FOV "enter" the image as though the anatomic area is folded or wrapped in an improper location and may obscure the relevant anatomy.

Bulk: a term denoting a large number, e.g., of spins, water molecules, vectors, etc.

Chemical shift: the difference (shift) in the resonance (Larmor) frequency of a particular spin when found in different chemical environments, such as the hydrogen nucleus (proton) in different molecules. In clinical MRI we are interested in the proton chemical shift in water relative to lipids.

Chemical shift artifact: the artifact that results from the chemical shift phenomenon, described above. It can be exploited for diagnostic purposes.

Coherence: the synchronized motion of spins, specifically of their transverse magnetization. Rotation in the transverse plane is coherent or in phase when the magnetization vectors stay together and point in the same direction. In this case the vector sum, and thus the MR signal, is maximal.

Diamagnetism: a magnetic property of a tissue or a substance that becomes apparent upon application of an external magnetic field (B). This type of tissue or substance acquires magnetization opposite to B, resulting in a reduction of the local magnetic field.

Diffusion: the random motion of molecules (not spins) with frequent changes in the direction and speed of motion. These individual events cannot be measured; thus, the phenomenon of diffusion is treated as a statistical process.

Echo: the MR signal appearing after refocusing the spins, to be contrasted with the free induction decay signal, or the raw MR signal. Refocusing can be accomplished either with radiofrequency pulses or with gradients, resulting in spin echoes or gradient echoes respectively.

Echo planar imaging (EPI): an ultrafast pulse sequence, suitable for diffusion imaging.

Echo time (TE): the time interval from the application of the excitatory pulse to the formation of the echo.

Electromagnetic radiation or waves: a form of energy.

Equilibrium: a stable condition that is maintained on its own. Perturbation of this state requires the addition of energy.

Excitation: the transition of spins from a lower to a higher energy level. It requires the addition of energy and the ability of the spins to absorb it. Upon satisfaction of stringent conditions, absorption of the energy supplied is possible, resulting in a condition called resonance.

Fast spin echo imaging: a pulse sequence that generates multiple spin echoes, each with a different phase value, per TR cycle. Thus, multiple phase steps are completed in each TR cycle. The result is acceleration of data acquisition and reduction of the scan time.

Ferromagnetism: a property of a tissue or substance that allows retention of its magnetism even after withdrawal of the external magnetic field.

Field of view: the area that we wish to depict in our images. It can be square (symmetric) or rectangular (asymmetric) and usually ranges from 10 to 45 cm.

Fold-over artifact: *see* Aliasing artifact.

Fourier transform: a mathematical process for extracting spatial information from the MR signal.

Free induction decay: the raw MR signal that results from the return of excited spins to their ground or steady state.

Frequency: the number of repetitions of a process per unit of time.

Frequency encoding: the encryption of spatial coordinates in frequency information. It is performed with magnetic field gradients

Gadolinium: the metal with the strongest paramagnetic properties. It serves as the active agent in several MR contrast media.

Gating: the collection of data is performed during only a fraction of a repetitive process (e.g., in the diastole of the cardiac cycle). It is like opening a gate to signal reception for a specific time interval.

Ghost artifact: replica(s) of the moving tissue or structure. This type of artifact always occurs along the phase encoding direction.

Gradient: more properly called a magnetic field gradient. It is a static (i.e., nonrotating) magnetic field that increases in amplitude in a linear fashion along a specified direction in space.

Gradient echo: the echo that is produced with gradients, to be contrasted with spin echoes, which are produced with radiofrequency pulses.

Gradient echo imaging: MR technique in which the echo signal is formed with gradients (and not with radiofrequency pulses, as occurs in spin echo imaging).

Gyromagnetic ratio: a constant for each spin that enters the Larmor equation.

HASTE (half Fourier single-shot turbo spin echo): a very fast T2-weighted pulse sequence suitable for abdominal imaging.

Inversion recovery: an MR imaging method that starts with an inversion pulse, i.e., by rotating the longitudinal magnetization 180°. In this way the longitudinal recovery curve starts from negative values and has to cross the zero point before it completes its ascent (into positive values).

Inversion time: the time from the inversion pulse to the excitation pulse.

Larmor equation: the mathematical relation of the resonant frequency of a particular spin to the strength of the main static magnetic field.

Larmor frequency: synonymous with resonant frequency, which is the intrinsic oscillation frequency of the spins. When the frequency of the stimulating radiation matches the resonant frequency of the spins, there is efficient absorption of energy and maximization of the spin oscillation amplitude.

Lattice: the physicochemical environment that supports the process of longitudinal relaxation.

Longitudinal magnetization: the component of magnetization that is parallel to the direction of the main static magnetic field.

Longitudinal relaxation: the return to equilibrium on the longitudinal axis, i.e., the regrowth of longitudinal magnetization after its perturbation by an excitatory pulse.

Longitudinal relaxation rate: a constant for each spin and tissue. It is a measure of the rapidity of longitudinal relaxation. Specifically, it is the time required for the longitudinal magnetization vector to regain 63% of its maximal value.

Magnetic dipole: a magnetically active substance or structure with two ends of opposing signs, e.g., a needle compass with a positive and a negative pole.

Magnetic field: lines of magnetic force that emanate from a magnet and spread out for a variable distance in space.

Magnetic moment: a vector useful for describing the interaction of magnetic dipoles with externally applied magnetic fields, i.e., how the dipole moves in response to the external field.

Magnetic resonance: resonance of magnetically active nuclei due to absorption of electromagnetic radiation. In clinical MRI we are interested in the hydrogen nucleus, which consists of a single particle, a proton.

Magnetic susceptibility: the degree and orientation of the magnetization of a substance or tissue when exposed to an exogenous magnetic field.

Magnetization: the vector sum of the magnetization moments of a group of spins.

Matrix: the lattice formed by the columns and rows that divide the image into pixels. The number of rows and columns represent the number of phase and frequency encoding steps. It can be symmetric or asymmetric (square, e.g., 256 × 256, or rectangular, e.g., 192 × 256). Increasing the matrix improves the (in-plane) spatial resolution.

Maximum intensity projection (MIP) algorithm: a reconstruction algorithm that picks the pixel with the highest signal intensity along the projection line. It is widely used in MR angiography and MR cholangiography.

Mxy: equivalent term to transverse magnetization.

Mz: term representing longitudinal magnetization.

Null point: the point in time in which the inversion recovery curve crosses the zero (null) value.

NEX: the number of repetitions of the complete (entire) process of image acquisition. The purpose is to improve image quality by increasing the signal-to-noise ratio.

NSA: number of signals averaged, *see* NEX.

Paramagnetism: a property of certain magnetically active structures that results in local reinforcement of an externally applied magnetic field.

Partial saturation: a state of spins in which their longitudinal magnetization is kept low, by closely spaced excitation pulses (preventing full longitudinal relaxation).

Phase: the feature of a vector that describes its orientation in space. In MRI we are interested in the phase of the transverse component of magnetization (Mxy), i.e., its spatial relation to the x- and y-axes.

Phase contrast: type of tissue contrast based upon differences in phase, useful for studying motion/flow.

Phase encoding: the process of transcribing spatial position into phase information. It is performed with magnetic field gradients.

Pixel or picture element: the smallest division of the image. The pixel size depends on the size of the field of view and the size of the matrix. The smaller the pixel, the higher the in-plane spatial resolution.

Precession: the rotatory motion of the spins or of their transverse magnetization vector around the z-axis.

Precession frequency: the speed of rotation of the spins around the z-axis. It is equivalent to the Larmor or resonance frequency.

Presaturation: the magnetic disabling of moving or "unwanted" tissues, e.g., blood. The saturation pulses are applied outside the region of interest. The purpose is to prevent these tissues from producing signal or artifacts within the area under investigation.

Proton density: the number of protons in a pixel or voxel. The higher the proton density, the stronger the

MR signal, if we allow full longitudinal relaxation and no transverse relaxation.

Proton density weighted: the type of tissue contrast that is due to differences in proton density.

Pulse: a burst of energy. Also used in place of the term "radiofrequency pulse."

Pulse sequence: a specific arrangement of radiofrequency pulses and gradients, including the intervening time delays.

Radiofrequency (RF) pulses: rotating (i.e., nonstatic) magnetic fields.

Radiofrequency range: part of the continuous spectrum of electromagnetic radiation. The pulses used in MRI fall within the radiowave frequencies; thus, these pulses are also called radiofrequency pulses.

Reconstruction: the processing of images as composite projections of the same or different viewing angles. It is useful in studies with a large number of source images, such as MR angiograms, MR cholangiograms, etc.

Recovery: synonymous term for the growth of the longitudinal magnetization vector.

Relaxation: the process of returning to equilibrium or steady state, either through loss of energy or loss of phase coherence (longitudinal and transverse relaxation respectively).

Relaxation curve: the graphic representation of the relaxation processes, i.e., the time course of the strength (or amplitude) of the magnetization vector(s).

Repetition time (TR): the time elapsed between successive excitation pulses.

Resonance: the phenomenon in which a free oscillator executes forced motion of maximal amplitude, provided that the frequency of action of the causative agent matches the natural frequency of the oscillator.

Resonance frequency: *see* Larmor frequency.

Resolution: the ability to distinguish two points in space or time as separate entities.

Rewinding gradient: designed to rephase (rewind) the transverse magnetization (Mxy) after the echo read-out. The purpose is to establish and maintain a steady state of Mxy over successive TR cycles, when TR is very short. The benefit is strong T2 contrast with gradient echo sequences (similar to spin echo with a long TE).

Saturation: the suppression of longitudinal magnetization with closely spaced radiofrequency (saturation) pulses.

Signal averaging: *see* NEX.

Signal-to-noise ratio: an index of the strength or adequacy of the MR signal.

Signal void: absence of signal, either due to artifacts or to very low spin density.

Spin density: equivalent term to proton density, since in clinical MR we are looking at protons and not other magnetically active nuclei.

Spin density weighted: equivalent term to proton density weighted.

Spin echo: the MR signal produced after the application of refocusing pulses; to be contrasted with gradient echoes that form with gradients.

Spin lattice relaxation: *see* Longitudinal relaxation

Spin lattice relaxation rate: *see* Longitudinal relaxation rate.

SPIR (spectral presaturation with inversion recovery): technique for selective fat saturation.

Spoiled gradient echo sequence: a standard gradient echo sequence with the addition of a spoiler gradient after the echo read-out.

Spoiler gradient: magnetic field gradient whose purpose is to destroy (spoil) any residual transverse magnetization before a new TR cycle is started. It is

used in very short TR sequences that do not allow enough time for completion of the T2 decay process. Thus, there is a build-up of transverse magnetization over successive TR cycles, altering the desired type of contrast.

Steady state: *see* Equilibrium.

Steady-state gradient echo sequence: a standard gradient echo sequence with the addition of a rewinding (rephrasing) gradient after the echo read-out.

STIR (short TI inversion recovery): an inversion recovery sequence with a short TI (around 130 ms at 1.0 T) aimed at nulling the fat signal.

TE: *see* Echo time

TI: *see* Inversion time.

TR: *see* Repetition time

Time to echo: *see* Echo time

Transverse magnetization: the transverse component of magnetization (i.e., perpendicular to the longitudinal component). It is the magnetization component that gives rise to the MR signal.

Transverse plane: the plane perpendicular to the axis of the main magnetic field. It hosts the transverse component of magnetization.

Transverse relaxation: the relaxation process of the transverse component of magnetization. It starts immediately after cessation of the excitatory pulse and is due to phase coherence of the precessing spins because of spin–spin interactions.

Transverse relaxation rate: a constant for each type of spin or each tissue. It is a measure of the duration of the transverse relaxation process. Specifically, T2 is equal to the time required for Mxy to fall to 37% of its initial value.

Triggering: a mechanism whereby the acquisition or manipulation of data is linked to specific time events, i.e., to the cardiac systole or diastole, guided by the patient's electrocardiogram.

Turbo spin echo: *see* Fast spin echo imaging.

T1 relaxation: *see* Longitudinal relaxation.

T1 relaxation rate: *see* Longitudinal relaxation rate.

T2 relaxation: *see* Transverse relaxation.

T2 relaxation rate: *see* Transverse relaxation rate.

T2* relaxation rate: the rate of decay of the FID (free induction decay) signal

T1 weighting: the type of contrast between tissues that is determined primarily by the differences in T1 rates. This is achieved through the appropriate selection of the machine parameters TR, TE, and flip angle.

T2 weighting: the type of tissue contrast governed mostly by differences in T2 rates. Accomplished through the appropriate choice of machine variables TR, TE, and flip angle.

T2* weighting: the type of tissue contrast emphasizing differences in T2* rates, which incorporate the inhomogeneities of the main magnetic field. Thus, spin refocusing is accomplished with gradients and not radiofrequency pulses.

Vector: a mathematical quantity with two characteristics: size (or amplitude) and orientation (or direction in space).

Voxel or volume element: the smallest cube into which the structure or patient has been partitioned. This number is given by the pixel multiplied by the slice thickness

Wrap-around artifact: *see* Aliasing artifact.

Z-axis: by convention the axis of the main magnetic field and the axis of the longitudinal magnetization vector.

Subject Index

G

H

I

L

M

N

O

P

V

W